RECOVERY AND RECRYSTALLIZATION IN FCC METALS AFTER HIGH TEMPERATURE DEFORMATION

by

R.A. PETKOVIC-LUTON

A thesis submitted to the Faculty of Graduate Studies and Research
in partial fulfilment of the requirements for the degree of
Doctor of Philosophy

Department of Mining and Metallurgical Engineering
McGill University
Montreal, Canada

[illegible]

RECOVERY AND RECRYSTALLIZATION AFTER HOT WORKING OF FCC METALS Ph.D. R.A. Petkovic-Luton

ABSTRACT

Interrupted compression tests were used to study the static softening of a 0.06% C low carbon steel, a 0.07% C+Nb-bearing steel and tough pitch copper. The tests were carried out at temperatures from 450 to 1040°C and prior strains were applied at strain rates in the range 10^{-3} to $10^{-1}s^{-1}$. Quantitative metallography was carried out on samples of the tough pitch copper quenched to room temperature after increasing amounts of prestrain and delay time. The grain size distributions obtained in this way were used to follow the progress of static recyrstallization

The results indicate that a critical strain is required for the initiation of static, i.e. classical recrystallization after prior hot deformation. For strains inferior to this critical amount, recrystallization does not occur at all, and softening takes place instead entirely by static recovery. Evidence is presented for the existence of a second critical strain, about twice as large as the first, which corresponds to a point just before the peak in the flow curve. This is the critical strain for the initiation of post-dynamic (metadynamic) recrystallization.

The results are interpreted in terms of a three-mechanism softening model in which there is a recovery stage and two recrystallization stages. The first recrystallization process, like recovery, is a 'no-delay' process, while the second one involves a distinct incubation time. The dependence of the three softening mechanisms on prestrain, strain rate and temperature is described and the kinetics of the processes are considered in some detail. Some attention is also given to the influence of alloying elements on softening rates in austenite.

It is shown that the progress of softening can be described by simple empirical relationships which can be used in the design of industrial rolling schedules.

RESUME

L'adoucissement statique d'un acier à bas carbone (0.06%C), d'un acier au niobium contenant 0.07%C et de cuivre de pureté commerciale a été étudié par des essais de compression avec interruptions. Les essais ont été réalisés dans un domaine de températures allant de 450°C à 1040°C, et dans une gamme de vitesses vraies de déformation s'étendant de 10^{-3} à $10^{-1}s^{-1}$. La distribution des tailles de grains dans des échantillons de cuivre commercial trempés a été déterminée quantitativement par métallographie. L'évolution de cette distribution pour des déformations avant interruption et des temps d'interruption croissants a permis de suivre le progrès de la recristallisation statique.

Les résultats montrent que pour des déformations avant interruption inférieures à une valeur critique, l'adoucissement se fait entièrement par restauration statique. Par contre, au delà de la valeur critique, la recristallisation statique, c'est à dire classique, se produit. Les résultats mettent en évidence l'existence d'une seconde valeur critique de la déformation, environ le double de la première, qui amorce une recristallisation post-dynamique (métadynamique). Cette seconde valeur critique correspond à une déformation légèrement inférieure à celle pour laquelle la contrainte dans la courbe effort déformation est maximale.

Les résultats sont interprétés à l'aide d'un modèle faisant agir trois mécanismes d'adoucissement: un de restauration et <u>deux</u> de recristallisation. Le premier processus de recristallisation est, comme la restauration, un processus "instantané", tandis que le second requiert un temps d'incubation. Les effets de la déformation avant interruption, de la vitesse de déformation et de la température sur la cinétique de ces mécanismes sont présentés en détail. L'influence des éléments d'alliage sur la cinétique de l'adoucissement dans l'austénite est discutée.

L'évolution de l'adoucissement peut être décrite par des relations empiriques simples qui peuvent être appliquées à la mise au point des programmes de laminage dans les conditions industrielles.

КРАТАК ПРЕГЛЕД

Цилиндрични узорци од ниско угленичног челика са 0.06%C, ниско угленичног челика третираног са 0.07% ниобиума и бакра, били су изложени испитивању на притисак са меджу растеретеньем, у температурном подручју од 450 до 1040^{o} C и при брзинама деформациа од 10^{-3} до 10^{-1} c^{-1}.

Узорци су такодже били подвргнути квантитативно металогравском испитивању, са намером да се одреди дистрибуциа величине зрна. Распоред величине зрна, добиен овом методом,користио се да прати статичку рекристализациу после деформацие на високим температурама.

Резултати су показали да за статичку односно класичну рекристализациу да се одигра, после деформацие на високим температурама, потребно је превазитји критични степен деформацие за статичку рекристализациу.За сва напрезања испод критичног степена деформациа, рекристализациа се не одиграва и једини оперативни процес је отпуштање.Евиденциа постои, такодје, оегзистенции још једне критичне брзине деформацие,отприлике два пута ветје од предходне, која је потребно да се превазидје да би се метадинамичка рекристализациа одиграла.

Резултати су интерпретирани у виду модела који се састои од три процеса: процес отпуштања и два процеса рекристализацие, Први рекристализациони процес исто као и отпуштање нема инкубациони период, док други има веома динстинктив инкубациони период.Утицај брзине и степена деформациа и температуре на три процеса, као и њихова кинетика детаљно је анализирана у приложеном раду.

Показано је да једноставна емпиричка једначина може да се примени за одредјивање кинетике поменутих процеса и употреби за пројектовање распореда ваљања у индустриским размерама.

ACKNOWLEDGEMENTS

The author would like to express her sincere appreciation and gratitude to Dr. J.J. Jonas, director of this research, for his invaluable guidance and encouragement. Particular thanks are also expressed to Dr. M.J. Luton, who contributed significantly through many stimulating discussions and suggestions.

The author wishes to extend her marked appreciation to Dr. H.J. McQueen and to Dr. D.H. Sastry for their help and guidance. Thanks are also due to her fellow graduate students for their interest and support at all stages of the work.

Special recognition must be given to Mr. L.J. Vroomen and Dr. P.J. Zsombor-Murray for helping with the extensive computerization undertaken in this research. Thanks are also expressed to Messrs. G. Dedic, O. Muehling and M. Knoepfel for assistance with construction of the equipment and the preparation of specimens.

The author would also like to express her gratitude to the Steel Company of Canada Ltd., and the Olin Corporation for provision of some of the experimental materials. In particular, special thanks are due to Mr. D. McCutcheon and Dr. R. Jamieson (STELCO) and to Dr. E. Shapiro (OLIN) for their encouragement and support. Thanks are due to the McConnell Foundation for the award of a Postgraduate Fellowship.

LIST OF FIGURES

page

LIST OF TABLES

INTRODUCTION

The development of inexpensive, strong, tough and easily weldable steels for structural and line pipe applications has been one of the most attractive areas of development in the steel industry over the past ten years. All the advances associated with these developments have depended to some extent on the control of recovery and recrystallization rates in the metastable austenite. These are, unfortunately, very difficult to study because of the breakdown of the unstable γ-phase on cooling. The processes are nevertheless important as the final properties of the hot worked product are dependent on their detailed interaction. The plastic properties, such as yield and ultimate strength, elongation, reduction of area, and hardness are clearly in this category, as are the fracture properties, such as impact strength and the ductile-brittle transition temperature.

Recently a promising mechanical technique was developed which permits study of the static softening processes in austenite following high temperature deformation. The technique involves the use of a "Gleeble" testing machine and is based on the principle of interrupted mechanical testing. A sample is work hardened at a typical hot working temperature; the deformation is interrupted for a series of increasing delay times; the test is then resumed until fracture occurs. The process of softening during the delay is followed in terms of the decrease in load from that carried prior to interruption to that occurring on ultimate failure.

Although the Gleeble technique can be considered as a useful one, it has a number of inherent limitations. These are largely attributable to the use of "load" rather than "true stress" as an experimental variable and to the difficulty of producing a constant true strain rate with the equipment.

The method employed in the present work is based on the Gleeble method, but makes use of the technique of hot compression instead. The latter lends itself to the production of constant true strain rates, as well as to the determination of yield stresses, and to the calculation of the true stresses developed during deformation. By eliminating the disadvantages of the earlier technique, it has permitted a more detailed understanding of recrystallization kinetics to be attained. It has also led to the formulation of the three-stage softening model that is described below.

The preliminary results obtained by this technique were presented by the author in her Master's thesis. The observations were restricted to plain carbon steels, and the microstructural interpretations advanced were open to the criticism that they were speculative and unverified. It was the main purpose of the present work to carry out tests on a material which behaved like carbon steel, but which did not undergo a change on cooling to room temperature. Tests on such a material would therefore be suitable for the detailed metallographic studies required to verify or reject the earlier interpretations. The model material selected was tough pitch copper, which has the required susceptibility for dynamic recrystallization, while retaining a microstructural stability appropriate to an industrial material. Some nine-hundred experiments were carried out on these samples, which enabled the progress of the softening mechanisms to be followed in detail. It will be for the reader to judge the extent to which these results can be considered to apply to carbon steels.

Before proceeding with an account of the present work, some of the literature associated with deformation and softening at high temperatures will first be reviewed. The development of the present technique to its current level of sophistication will then be outlined, and a full description of the results obtained will be presented. Finally, the significance of the results will be considered in some detail, and some conclusions will be drawn concerning the kinetics of softening under diverse experimental conditions.

CHAPTER 1

FUNDAMENTAL ASPECTS OF STATIC SOFTENING AFTER HIGH TEMPERATURE DEFORMATION

1.1 INTRODUCTION

Hot working refers to that category of high temperature deformation which takes place at relatively high strain rates (e.g. 10^{-2} to 10^3 s^{-1}) and at temperatures above ~0.6 T_m. (Here T_m is the melting temperature in degrees Kelvin)(1-4). The flow stresses under hot working conditions tend to be considerably lower than at room temperature. Furthermore, as enhanced ductilities are usually observed at high temperatures, hot working operations are generally carried out to large strains.

In one type of hot working operation (e.g. extrusion or planetary rolling) continuous, nearly isothermal deformation conditions exist. That is, the total strain is applied in one step and at roughly constant temperature. But large numbers of metals and alloys are hot deformed under interrupted, non-isothermal conditions. In forging or rolling, for example, the total strain is applied in increments at generally decreasing temperatures. This involves a complicated interaction between the dynamic and static softening processes, which makes it difficult to interpret the final microstructures produced by these means. It is the main purpose of the present chapter to consider the micro-structural changes occurring both during and after hot working and to describe the influence of these changes on the mechanical properties of the worked material. Although our attention is primarily focussed on softening processes at high temperatures, some aspects of flow behaviour will also be covered because of the close link between these two types of phenomena.

1.2 RESTORATION PROCESSES DURING HIGH TEMPERATURE DEFORMATION

For a long time, the principal restoration process under hot working conditions was considered to be dynamic recrystallization(5). This was concluded from metallographic examinations at room temperature, which almost always indicated the presence of recrystallized structures. More recently, it was established, by Tegart(6,7), Rossard(8) and McQueen et al(9) that recrystallization does not generally take place <u>during</u> deformation, but that it usually occurs statically, after complete forming and before cooling down to room temperature. Their results, obtained by means of rapid quenching after deformation, also clarified the role of recovery and polygonization in the restoration processes associated with hot working.

The principal factor that determines whether recovery or recrystallization will be the main restoration process during working seems to be the stacking fault energy. If the common metals are now listed in the order of decreasing tendency to recrystallize during creep:

e.g. Pb, Ag, Ni, Cu, γ-Fe, Zn, Mg, Cd, α-Fe, Al, Sn

it can be seen that the stacking fault energy increases from Pb to Sn. Thus it appears that the lower the stacking fault energy, the greater is the tendency for dynamic recrystallization to occur in a material.

The evidence for the order of materials listed above was gathered from creep experiments. It can be expected to apply to hot working only to the extent that hot working is a valid equivalent of creep deformation at considerably higher rates of strain. This has not been generally accepted in recent years and, as conclusive evidence for dynamic recrystallization was very difficult to produce under hot working conditions, there has been considerable controversy about whether it occurs at all at high strain rates(10,11).

In Table 1.1 are introduced the high temperature softening processes operating under both hot working and creep conditions in a number of metals and alloys. At high temperatures, most materials undergo an initial stage of transient deformation which eventually leads to a "steady state", in which work hardening is balanced by recovery. In creep tests (constant stress), this appears as secondary or steady state creep, whereas in constant strain rate tests, it appears as a regime of constant flow stress. It is now evident that the steady state mechanical and structural properties, whether determined under constant strain rate or creep conditions, are equivalent(1,12). However, the present study was carried out under hot working conditions only, and further discussion will therefore be largely restricted to this mode of deformation.

TABLE 1.1 High Temperature Softening Processes

	Dynamic Softening Processes		Static Softening Processes	
Metals	At Small Strains	At Large Strains	At Small Strains	At Large Strains
Ni, Ni base super alloys, Cu, γFe, austenitic alloys, brass	**Recovery**	Recovery and Recrystallization[†]	Recovery followed by Classical Recrystallization	Recovery and Metadynamic Recrystallization followed by Classical Recrystallization
Al, αFe, ferritic alloys, bcc refractory metals, Zr alloys, hcp **metals**	**Recovery**	Recovery	Recovery followed by Classical Recrystallization	Recovery followed by Classical Recrystallization

[†] **Under creep conditions,** at very low strain rates (i.e. low stresses), dynamic recrystallization may **not occur at all.**

1.3 DYNAMIC RECOVERY

The characteristic flow curve of a material undergoing dynamic recovery during hot working is illustrated schematically in Figure 1.1. The flow curve can be divided into three distinct regimes of behaviour: a microstrain regime, a transient or work hardening regime, and a steady state one. During the microstrain regime, the plastic strain rate in the material increases from zero to approximately the applied rate of the test. There are limited data available on the behaviour of the material in this interval. However, it has been reported recently(13) that some dislocation multiplication takes place during this interval, causing an increase in dislocation density of about one order of magnitude by the commencement of macroscopic flow.

The transient or work hardening region begins at the macroscopic yield stress and is characterized by a gradual decrease in the net work hardening rate. The net rate of work hardening is zero when the deformation parameters of stress, temperature and strain rate remain constant.

At high strain rates and at temperatures below $\sim 0.6\ T_m$, the subgrains may become somewhat elongated, but are always equiaxed above $\sim 0.6\ T_m$, even after very large strains.

Many workers have observed a correlation between the steady state subgrain size and the applied stress(1,14,15) and have established that the mean subgrain size $\overline{d}$ is a function of the stress σ, as represented by:

$$\overline{d} = k\sigma^{-M} \tag{1.1}$$

Here k and M are constants which depend on the material, the method of measurement and the purity. Bird et al(14) have reported that, for a large amount of creep data, $M \simeq 1$ and $k = 20b\mu$, where b is the Burgers vector and μ is the shear modulus.

A considerable amount of work has been carried out to determine the density of dislocations within subgrains by using etch pitting techniques and electron microscopy. Bird et al(14) have assembled most of the available data and found that the familiar relationship between

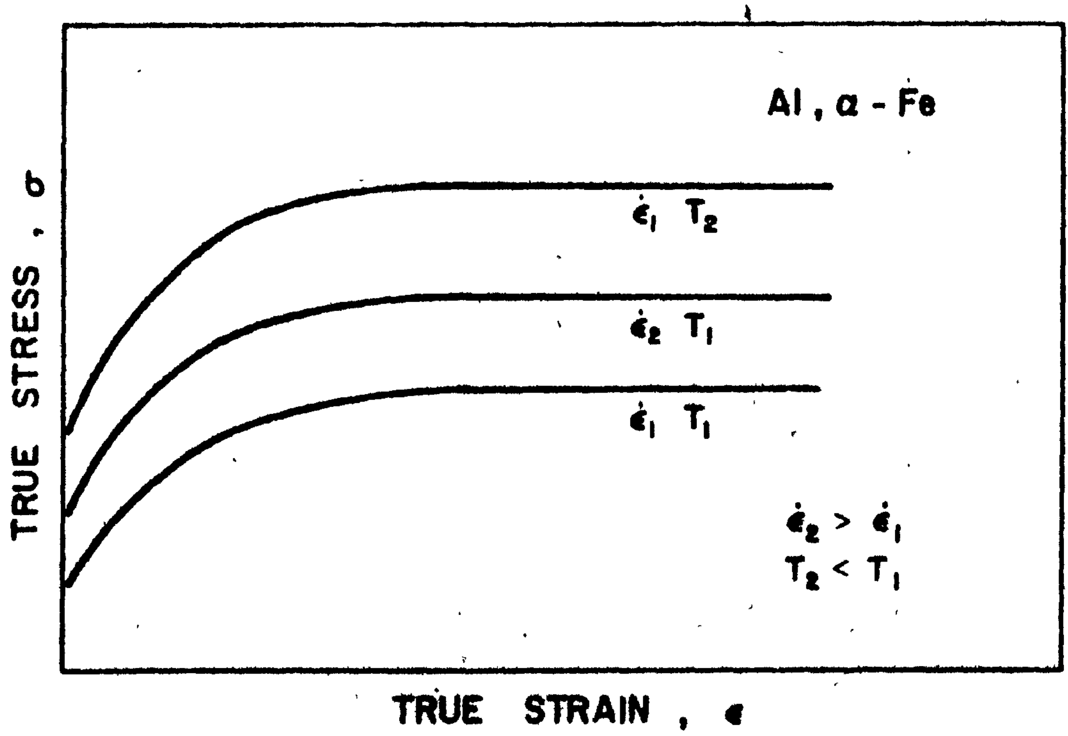

Figure 1.1 Schematic representation of the flow curve of metals that recover dynamically

applied stress and dislocation density established for low temperature deformation, is also followed at elevated temperatures; that is, that:

$$\sigma = \alpha \mu b \sqrt{\rho} \tag{1.2}$$

Here ρ is the dislocation density and α is a constant which takes a value of about 1.2 at high temperatures, in contrast to the low temperature value of ∼1.

Several models have been proposed in recent years in attempts to explain high temperature experimental data and these will now be reviewed briefly. The first model, the jogged screw-dislocation model, is open to some doubt since it cannot explain the effect of changes in stacking fault energy(16) or the effect of alloying additions(16). The climb model suffers from the same limitations and is also unable to account for the effect of instantaneous stress changes(16,17).

It is of interest that recent investigations(18,19) have shown that most dislocations within the subgrains in deformed molybdenum and copper single crystals are edge in character, an observation which favours the climb mechanism as the rate controlling process. Such a mechanism requires the presence of pile-ups, but they have never been observed. Dorn has argued that the absence of piled-up arrays cannot be used to refute the applicability of climb models since these arrays are inherently unstable. Davies et al(20) have also suggested that the rapid runback of dislocations may be responsible for the absence of the arrays.

The hypothesis that piled-up arrays are present during high temperature deformation could be tested by quenching a sample under load, so as to preserve the deformation substructure, and then irradiating at a low temperature. The glide dislocations pinned by the radiation defects that are produced would then be made available for examination by transmission electron microscopy. Such a technique, however, has not yet been applied to metals deformed under creep or hot working conditions.

The recovery model of McLean(21,22) and Carvalinhos(23) is more realistic than the climb or cross-slip models, inasmuch as it is based on the experimentally observed three-dimensional network of dislocations. In this theory, the creep rate is governed by the ratio of the rate of network coarsening (recovery) to the rate of network refinement (work hardening). According to various workers, the hardening rate (h), as given by

$$h = (\partial\sigma/\partial\varepsilon)_{time} \tag{1.4}$$

has been found to be largely independent of stress and temperature. By contrast, the recovery rate (r), as given by

$$r = (\partial\sigma/\partial t)_{\varepsilon} \tag{1.5}$$

is constant only during steady-state deformation and is highly stress and temperature dependent. The combined effect of strain hardening and recovery during steady state deformation is given by:

$$\dot{\varepsilon}_s = r/h \tag{1.6}$$

whereas the transient strain rate $\dot{\varepsilon}$ is given by:

$$\dot{\varepsilon} = \dot{\varepsilon}_0 \exp\{-v(h\varepsilon-rt)/kT\} \tag{1.7}$$

Here v is an activation volume, and the term $\{h\varepsilon-rt\}$, was introduced by Jonas et al(16) as a back stress that builds up during primary deformation so as to decrease the strain rate to its steady state value. The incorporation of a back stress term in the theory helped to remove some of the difficulties inherent in the two earlier models, but the theory is still not completely satisfactory. Particular problems arise in the experimental determination of the parameters r and h, and of structural factors such as the activation volume, which are affected by sudden changes in applied stress and temperature.

The Stüwe theory(10,24) for high temperature flow under conditions of dynamic recovery, also introduced recently, is qualitatively satisfactory but cannot account for the observation that the subgrain size remains constant during steady state flow nor can it easily be represented in the form of a strain rate equation. In this theory, dislocations are generated within the subgrains and glide to the sub-boundaries. Here the screw dislocations cross-slip and the edge dislocations climb into the boundaries to annihilate with dislocations from the adjacent subgrains. The vacancies needed for the rate controlling climb process are provided by the intersection of moving screw dislocations.

McQueen et al(2) argue, on the other hand, that dynamic recovery occurs by a process whereby the sub-boundaries are continuously breaking up and reforming during steady state deformation. This dynamic process of regeneration has been termed repolygonization. The balance between the hardening and recovery rates exists, as in Stüwe's model, but the regeneration process explains the absence of distorted subgrains even after very large strains. There is evidence in the literature(2,25-27) concerning the processes by which the sub-boundaries disintegrate; this has been attributed to a decrease in the stability of the sub-boundaries when they become heavily jogged through interaction with mobile dislocations. The dislocations emanating from the disintegrated networks rearrange themselves into new sub-boundaries. The recent observations of Hasegawa et al (28), for example, lend support to these views.

1.4 DYNAMIC RECRYSTALLIZATION

In the past, it has been common for investigators to consider dynamic recrystallization as a process which occurs only at low strain rates. However, the work in copper(6), nickel(6) and austenitic alloys(29) carried out at high temperatures and strain rates, in which the original grains were replaced by nearly equiaxed recrystallized grains, led Hardwick and Tegart(6) to conclude that dynamic recrystallization is the operative softening process in these cases as well. This conclusion has been further substantiated by activation energy measurements(1), as well as by the observation(11,29) of regular oscillations in flow stress at low strain rates. The latter are analogous to the periodic cycles in strain rate resulting from recrystallization during creep in these metals(30,31).

It is of interest that Stüwe(10,24) disagreed with the suggestion that dynamic recrystallization was taking place under hot working conditions and argued that similar flow behaviour could result when recovery alone occurs. However, numerous workers(32-37) in the past few years have demonstrated that the original conclusions of Hardwick and Tegart (6) and of Rossard(29) were correct, so that there is little doubt today concerning the existence of dynamic recrystallization.

Some typical flow curves for a material which recrystallizes dynamically during constant strain rate deformation are shown in Figure 1.2. Two important features of the stress-strain curves are: (i) the sharp peak in flow stress at the higher strain rate and (ii) the oscillations in flow stress at the lower strain rate. In addition, three points along the flow curve that characterize the structural changes taking place during flow should also be distinguished. These are: the critical strain to initiate dynamic recrystallization ε_c, the strain to the peak ε_r, and the minimum steady state strain ε_s.

The critical strain to initiate recrystallization was first observed in studies of recrystallization during creep(30,38), which showed that ε_c is a function of stress, temperature and purity(30,38). Reports based on hot working studies(34,36,39-41) also indicated that new grains appear in the region of the grain boundaries in the neighbourhood of the peak stress. Thus, the strain to the peak flow stress can be expected to be closely related to the critical strain for recrystallization. Although the relation between the peak strain and the critical strain is not known exactly, Rossard(41) has suggested that the latter is about 5/6ths of the strain to the peak.

The most detailed study of the critical strain for the initiation of dynamic recrystallization was that of Luton and Sellars(40). They found that the strain to the peak flow stress ε_r varies with stress. In the creep of nickel, the time (t_x) for a large constant fraction of recrystallization to occur varies with stress as $t_x \propto \sigma^{-3}$, and since the strain rate $\dot{\varepsilon}$ is proportional to the fifth power of the stress(16), ε_x depends on stress according to $\varepsilon_x \propto \sigma^2$. From Figure 1.3 it can be seen that below the crossover of the two curves, recrystallization will be complete before the critical strain to initiate the next cycle of recrystallization is reached. Above the crossover, which indicates a critical stress, the successive cycles of recrystallization are initiated before the previous recrystallization is complete. The model of Luton and Sellars thus requires the stress oscillation to disappear with an increase

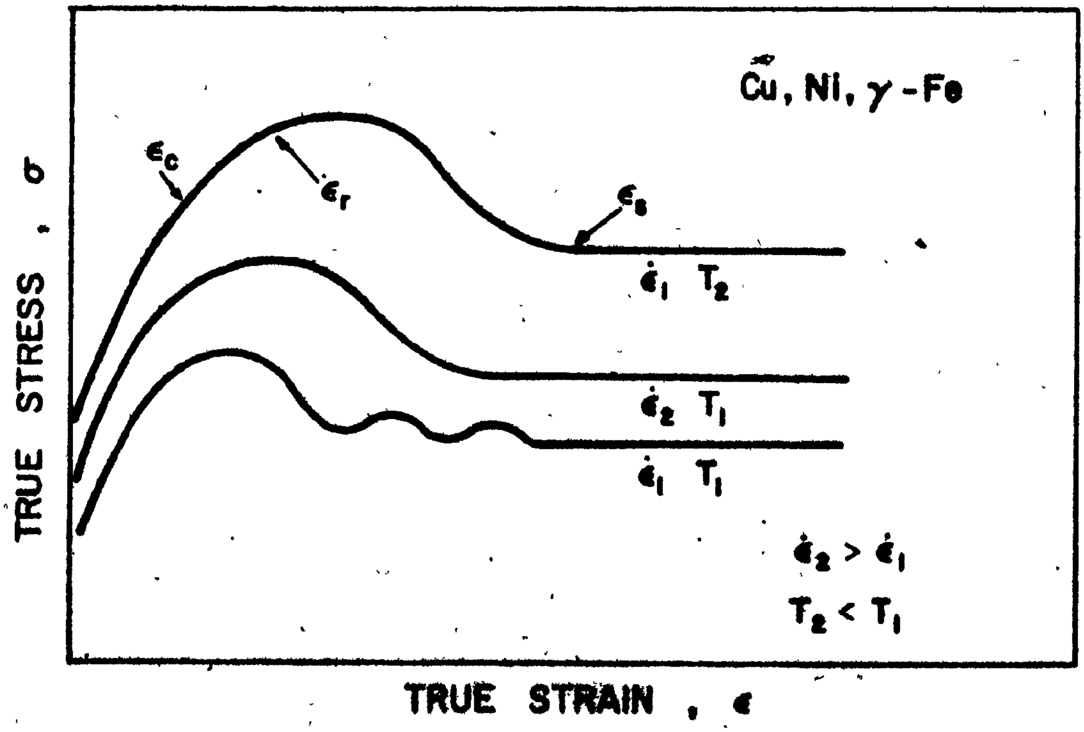

Figure 1.2 Schematic representation of the flow curves for dynamic recrystallization at high and low strain rates

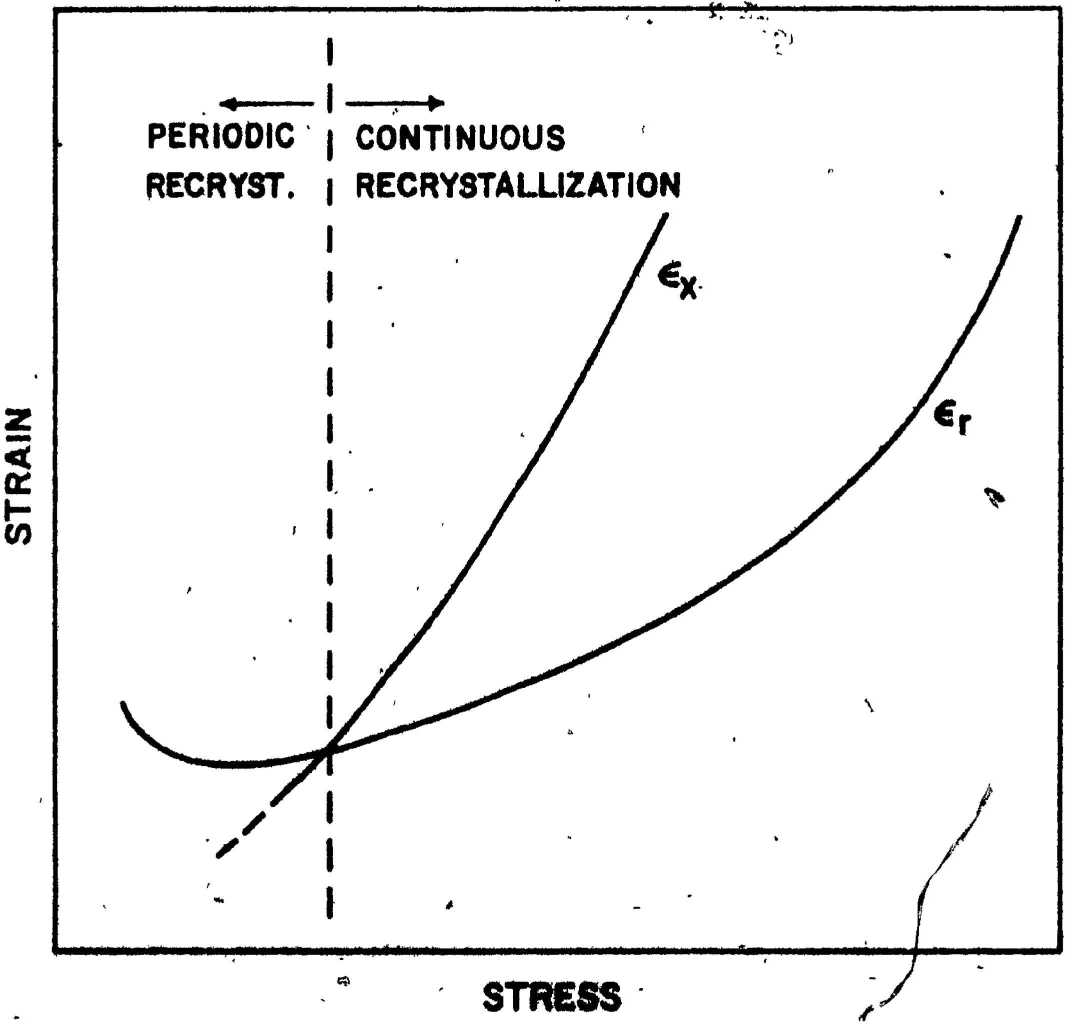

Figure 1.3 Schematic representation of the stress-dependence of the strain to the peak flow stress (after Jonas, Sellars and Tegart, Ref. [illegible])

in stress. It should be noted that there have been earlier models (42,43) concerned with dynamic recrystallization. Gifkins (42) proposed a model for recrystallization during creep which is based on the nucleation of recrystallizing grains by subgrain growth. It shows qualitative agreement with the refinement of the dynamically recrystallized grain size with increasing stress. Richardson, Sellars and Tegart (43), also developed a model for dynamic recrystallization based on experiments in creep. Their results indicate that recrystallization during the creep of nickel occurs by the localized migration of portions of the original grain boundaries, rather than by the coalescence and growth of subgrains. They therefore suggested that a mechanism similar to that proposed by Bailey and Hirsch (44) for recrystallization after cold work applied in their material. However, Luton and Sellars (40) concluded that, on the basis of their data, it is difficult to distinguish between the two possible nucleation mechanisms of recrystallization (i.e. between the coalescence and growth of subgrains on the one hand, and localized migration of the original grain boundaries on the other), since both mechanisms were shown to lead to similar relationships between the dynamically recrystallized grain size and the high temperature flow stress.

1.4.1 Structural Features Associated with Dynamic Recrystallization

For dynamic recrystallization to occur, there are two basic requirements that have to be satisfied:

1. Conditions that are conducive to the formation of nuclei, such as well-defined subgrains and sub-boundaries, must be present.
2. Sufficient energy density must be built up to provide a driving force for the growth of nuclei once germinated.

In addition, Sandström and Lagneborg (35) have suggested that the diameter of the critical nucleus d_n must be less than a characteristic distance x_{cr}. The length x_{cr} is the width of a band of material behind the moving boundary that is relatively free of dislocations. As straining continues, the boundary advances, taking with it this zone of low dislocation density. This effect arises because work hardening takes place in the just recrystallized material until the dislocation density reaches the level ρ_d present in front of the migrating boundary. Sandström and

Lagneborg have shown that x_{cr} is a function of strain rate as follows:

$$x_{cr} = \frac{b\ell_d}{\dot{\varepsilon}}\{\rho_d^{o}\}^{2} m\tau \qquad (1.2)$$

Here b is the burgers vector, $\dot{\varepsilon}$ is the strain rate, m is the mobility of the boundary, τ is the dislocation energy per unit length and ℓ_d is the mean free path of the dislocation. It can be seen from Equation 1.2 that at low strain rates x_{cr} is likely to be large, so that the condition $x_{cr} > d_n$ is easily satisfied and recrystallization can take place. By contrast, at very high strain rates, it may be possible to suppress nucleation completely.

The Sandström and Lagneborg model will be discussed in more detail later in the light of the present results.

1.4.2 Dynamic Recrystallization and Grain Size

When the mechanism for the nucleation of dynamic recrystallization is the bulging of local regions(30,36,38,40,46) and is therefore associated with the pinning of grain boundaries at their extremities by sub-boundaries, the number of potential sites for nucleation per unit volume is proportional to $3/d_g d^2$. Here d_g is the mean grain size and d is the mean subgrain size. The resulting recrystallized grain size is then expected to be related to the subgrain size through the relation(40)

$$1/d_g^3 = 3P/d_g d^2 \qquad (1.3)$$

where P is the probability of a site being activated. A similar relationship is obtained if a model for nucleation by subgrain coalescence is assumed.

Several workers(36,40,46) have reported that under most conditions, the recrystallized grain size is a unique function of the developed stress (σ_s), independent of temperature, and that a relationship of the form

$$\sigma_s = \sigma_0 + k_1 d_g^{-m} \qquad (1.4)$$

is obeyed. Here σ_0, k_1 and m are constants. The value of m was found to be about 0.75 in Ni and Ni-Fe alloys(40), zone refined α-Fe(36) and Cu-Al alloys(46), one in Cu and Ni(36), and in these cases $\sigma_0 \approx 0$. An equally good correlation is obtained with $m = 1/2$, but then $\sigma_0 \neq 0$.

The most recent report(34) on the relation between flow stress and recrystallized grain size shows that the relation is independent of temperature, strain and strain rate, as reported previously(36,40). The interesting feature of this report(34) is that the steady state grain sizes and stresses are the same for a particular strain rate and temperature, irrespective of the starting grain size and irrespective of how many recrystallization cycles have occurred. This is interpreted as signifying that recrystallization occurs by the continuous nucleation of new grains, forming colonies. Growth of the new grains stops soon after their formation, due to the concurrent work-hardening taking place behind the migrating boundaries. The limiting size of the new grains seems to depend only on the imposed strain rate and temperature (i.e. on the work-hardening conditions) and not on the initial grain size.

Returning to Equation 1.4, it is of interest that the form of this equation is similar to that used to relate subgrain size and stress in a number of materials which undergo dynamic recovery only(42,47-49). In these cases, $\sigma_0 \approx 0$ again, but $m = 1 - 1.5$. Because of the similarity in the algebraic form of the stress dependences of recrystallized grain size and subgrain size, we can express the flow stress in the steady state as the following sum:

$$\sigma_s = \sigma^* + \alpha\mu b\sqrt{\rho_s} + k_2 d^{-1} + k_3 d_g^{-\frac{1}{2}} \qquad (1.5)$$

For $\sqrt{\rho_s} \propto \frac{1}{d}$ and $d_g \approx d$, Equation 1.5 becomes

$$\sigma_s = \sigma^* + k_4 d_g^{-1} + k_3 d_g^{-\frac{1}{2}} \qquad (1.6)$$

where, σ^* is the effective stress

$\alpha\mu b\sqrt{\rho}$ is the hardening or internal stress contribution of the dislocations,

$\sigma_i = k_2 d^{-1}$ is the sub-boundary contribution to the internal stress,

$k_3 d_g^{-\frac{1}{2}}$ is the Hall-Petch strengthening contribution of the grain boundaries, and

$k_4 d_g^{-1}$ is the component of substructure strengthening expressed in terms of d_g.

The values of $m = 0.75$ and 1.0(36,40,46) obtained experimentally are closer to 1 than to 1/2, indicating that the component of substructure strengthening $k_4 d_g^{-1}$ is likely to be greater than the Hall-Petch contribution of the grain boundaries $k_3 d_g^{-\frac{1}{2}}$(50).

Returning to Equation 1.4, when $\sigma_o = 0$ we can write:

$$\sigma_s = k_1 d_g^{-m} \tag{1.7}$$

In view of the above discussion, this empirical relation can be regarded as evidence that under conditions of dynamic recrystallization the flow stress is causally related, through the grain size and the nucleus density, to the subgrain size, rather than being directly linked to the grain size itself.

Although, in writing Equation 1.5, the Hall-Petch relation was assumed to be valid at high temperatures, this dependence has not been established with any certainty. Some recent reports(51,52) give qualitative support to the view that above grain sizes of 20 μm, the high temperature yield strength increases with decreasing grain size. This is an important question to which we will return later when some experimental results pertaining to the influence of grain size on the high temperature yield stress are presented and discussed.

1.4.3 Effect of Alloy Additions on Dynamic Recrystallization

It has been observed that the addition of solutes to alloys affects the conditions of recrystallization in two ways. First, it reduces the ability of the metal to recover and in that way increases the driving force, and therefore the tendency to dynamic recrystallization. This may arise through the influence of solute concentration on the stacking fault energy. Second, it may retard the migration rate of grain boundaries and consequently the rate of dynamic recrystallization. The second effect is exemplified by work on brass(53), plain carbon and stainless steels(8), monel(54) and nickel-base superalloys(55), which showed that the addition of alloying elements retards recrystallization or even prevents it altogether.

In Ni-Fe alloys(40), as the iron concentration is increased to 20%, the stresses at the peak and in the steady state region gradually increase. Increasing the iron content decreases the value of k_1 in Equation 1.4, from 10 $MPa/mm^{0.75}$ for pure Ni to 5.65 $MPa/mm^{0.75}$ for 20% Fe. This indicates that, for a given flow stress, the grain size of the alloy is finer as the Fe concentration is increased, because the dissolved iron increases the probability of nucleation and decreases the rate of boundary migration.

In alloys of copper in which the aluminum content varies between 1 to 8%(56), the flow stress at a constant value of the temperature corrected strain rate increases with the addition of up to 4% Al, but shows little further change with 8% Al. These changes in flow stress arise as a result of an increased work hardening rate and a decreased recovery rate caused by the decrease in stacking fault energy with alloying.

When the solid solubility is exceeded and a second phase is present, the presence of such dispersed particles tends to stabilize the deformation substructure and to prevent or restrain grain boundary migration. Such inhibition or retardation of dynamic recrystallization has been observed in austenite containing NbC(57) and in Udimet 700 with γ' precipitate(58). This effect is of considerable importance in the commercial process of controlled rolling.

1.4.4 Effect of Interruptions in Straining on the Microstructure

The interruption of deformation during mechanical testing has the same effect on the structure of the material as does the interval between passes during rolling. As the steel passes through the rolls, the deformation is applied in increments (5-15%), with intervals of holding time between the successive increases in strain. On the second and subsequent passes, the initial structure of the material is determined by the prior deformation schedule. In this respect, the interpass times are as important as the deformation produced by each pass because they determine the extent to which the grain structure can change between passes.

At high temperatures, and in relatively pure metals, the structure will begin to recrystallize *dynamically* during the second or third pass. After this pass, the material will recrystallize *statically*, partially or completely, depending on the length of the interruption before restraining. The more severely strained regions can be expected to recrystallize first, so that the flow stress in a subsequent pass will be less than for uninterrupted rolling.

At lower temperatures, or in the presence of particular alloying elements, dynamic recrystallization does not occur during deformation, although static recrystallization may still take place during subsequent holding. In torsion testing, if partial recrystallization takes place during the interruption, on restraining, the strain to the peak stress, as well as the peak height are reduced. On the other hand, if recrystallization goes to completion during the interruption, then the flow curve upon restraining resembles that of the previous cycle.

It is clear from the above that the effect of the holding interval on the parameters of subsequent deformation are fairly complex. The microstructural changes taking place during the delay play an important role in determining the properties of the hot finished material. Because of the importance of these changes, we will review in turn the various processes taking place during the holding interval, and their effects on the structure and properties of hot worked materials.

1.5 STATIC SOFTENING PROCESSES AFTER HIGH TEMPERATURE DEFORMATION

In the previous sections, attention was focussed on the softening processes occurring *during* high temperature deformation. In the discussion to come, the static softening processes that take place *after* high temperature deformation or between intervals of hot working will be reviewed and discussed in turn. These processes can be divided into the following categories:

a) the recovery processes, which involve the annihilation of dislocations in individual events,

b) the classical recrystallization process, in which dislocations are simultaneously eliminated in large numbers as a result of the motion of high angle boundaries; this generally takes place in regions which have been softened previously by dynamic recovery and involves a distinct nucleation event,

c) the process of metadynamic recrystallization, which only occurs after previous dynamic recrystallization and which does not require any static nucleation.

1.6 THEORETICAL ASPECTS OF STATIC RECOVERY

The term recovery has been used to cover processes which do not result in the replacement of deformed grains by new grains, but which nevertheless lead to structural changes on a fine scale within the existing grains. The mechanisms of recovery after high temperature deformation are similar to those occurring after cold deformation and, as there are few published data concerning the former, the factors affecting the latter will be reviewed briefly. The driving force for both processes is the reduction in strain energy achieved by the removal of excess point defects and dislocations.

The progress of static recovery can be studied by structural methods, such as the techniques of x-ray diffraction, and optical and electron microscopy. It can also be followed mechanically by determining the change in properties with time during recovery. An example of the latter approach is the classical work of Drouard et al(59) in which the recovery rate in deformed zinc single crystals was investigated using flow stress measurements. In this study, the single crystals were first deformed plastically in pure shear at -50°C to some maximum shear stress, σ_m. Each crystal was then given an isothermal recovery anneal at a particular elevated temperature T; after this it was returned to the shear apparatus, brought back to -50°C and reloaded in plastic shear. The value of the yield stress in shear σ on reloading was generally less than σ_m and the amount of recovery X was expressed as

$$X = \frac{\sigma_m - \sigma}{\sigma_m - \sigma_o} \times 100$$

Here σ_o is the value of the initial yield stress. Since X can run from 0 to 100%, the amount of retained strain hardening is given by (100-X). From these data, activation energies for the recovery process can be obtained. It must first be assumed that $\sigma_m - \sigma$ is proportional to the number of unspecified defects which are causing the recovery. Then an equation of the following type can be written:

$$\frac{d(\sigma_m - \sigma)}{dt} = K(\sigma_m - \sigma)^{\alpha} e^{-(\frac{Q}{RT})} \quad (1.8)$$

Here α is an integer which represents the order of the reaction, Q is an activation energy, R is the gas constant, T is the absolute temperature and K is the rate constant.

By rearranging Equation 1.8, the following expression is obtained:

$$\int \frac{d(\sigma_m - \sigma)}{(\sigma_m - \sigma)^{\alpha}} = \int K e^{-(\frac{Q}{RT})} dt \quad (1.9)$$

If the left side is now represented by some function f of $(\sigma_m - \sigma)$, Equation 1.9 can be rewritten as:

$$f(\sigma_m - \sigma) = Kte^{-(\frac{Q}{RT})} \quad (1.10)$$

The value of Q can be found by plotting the residual strain hardening (100-X) versus annealing time for a series of temperatures. For this purpose, Equation 1.10 is rearranged to give:

$$t = 1/Kfe(\frac{Q}{RT}) \quad (1.11)$$

or, in log form:

$$\ln t = -\ln K + \ln f + \frac{Q}{R}(\frac{1}{T}) \quad (1.12)$$

Thus, from a series of values for t and T at constant (100-X), Q can be calculated.

In this way Drouard defined the activation energy for the recovery of zinc to be 84 kJ/mol (20 kcal/mol), which is about equal to the activation energy for self-diffusion in zinc. There are also reports in the literature that the activation energy increases during recovery(39,60,61). Kuhlmann-Wilsdorf(60) explained this by suggesting that the most deformed regions, in which the stored energy is highest and the activation energy lowest, recover first. Similar findings were also reported by Michalak and Paxton(61) for zone-refined iron strained 5% in tension at 0°C. They found that the activation energy increased continuously during recovery. In zone-refined iron, the activation energy Q was 92 kJ/mol (22 kcal/mol) at the start of recovery and increased to 282 kJ/mol (67.4 kcal/mol) at the end of recovery.

They proposed that two mechanisms operate during recovery. To begin with, there is an excess of vacancies present and simple vacancy migration is rate controlling. As recovery proceeds, the excess vacancy concentration decreases and the activation energy approaches that for self-diffusion. The results obtained in plain carbon steel(39) appear to follow a similar pattern of behaviour, the activation energy increasing from 84 to 155 kJ/mol (20 to 37 kcal/mol). Higher values were not obtained, presumably because the other softening processes took over at longer delay times.

The increase in the activation energy for recovery with annealing time can also be given an interpretation in terms of the theory of thermally activated glide. According to this view, recovery is a stress dependent process and therefore one in which the activation energy decreases with increasing stress. The stresses driving static recovery are, of course, the internal stresses, and these decrease with annealing time. The decrease in internal stress will, in terms of this theory, lead to an increase in the experimental activation energy.

1.6.1 Recovery Kinetics

Static recovery is expected to follow first order kinetics(60, 62), as given by:

$$\frac{dx}{dt} - kx \qquad (1.13)$$

Here x is some property of the work hardened state and $x = \sigma_m - \sigma_0$ when x is a maximum. Furthermore k is a rate constant which represents the probability that a given amount of softening occurs in unit time. The latter is in turn given by:

$$k = K \exp(-Q/RT) \qquad (1.14)$$

so that

$$\frac{dx}{x} = -K \exp(-Q/RT)dt \qquad (1.15)$$

Equation 1.15 can be integrated to give:

$$\int_{x_0}^{x} d \ln x = -K \exp(-Q/RT)\int_{0}^{t} dt \qquad (1.16)$$

where $x = x_0$ at $t = 0$.
Thus

$$\ln x_0/x = Kt \exp(-Q/RT) \qquad (1.17)$$

The above relation can also be expressed in terms of X, the fractional softening, by noting that $x/x_0 = (1-X)$. Equation 1.17 can therefore be rewritten as

$$\ln(1-X) = -K\, t \exp(-Q/RT) \qquad (1.18)$$

or as:

$$\log(1/1-X) = 0.4343\, Kt \exp(-Q/RT) \qquad (1.19)$$

An alternative way of analyzing recovery behaviour is based on the assumption that recovery follows zero order kinetics, that is, that:

$$dx/dt = -K \qquad (1.20)$$

$$\int_{x_0}^{x} dx = -k\int_{0}^{t} dt \qquad (1.21)$$

or

$$x_0 - x = K\,t\,\exp(-Q/RT) \qquad (1.22)$$

Equation 1.22 can again be expressed in terms of the fractional softening X

$$1-X = \frac{K}{x_0}\,t\,\exp(-Q/RT) \qquad (1.23)$$

According to Equation 1.23, the slopes of the curves should depend on the initial work hardened state, x_0, which is different for each set of test conditions.

1.6.2 Effect of Experimental Variables on the Rate of Static Recovery

The most important experimental variables that effect the recovery rate after high temperature deformation are the temperature, prior strain, strain rate and composition. In the report(39) concerned with the first part of the present investigation, it was shown that the recovery rate increases with temperature, strain and strain rate. The effect of temperature on recovery rate is not as evident as it is on recrystallization rate, probably because the amount of stored energy driving the recovery process decreases as the deformation temperature is increased. Because of the different driving forces at different deformation temperatures, it is difficult to determine the activation energy of the process(39).

Increases in the prior strain lead to increases in the recovery rate until steady state flow is reached. This can be attributed to the attendant increase in dislocation density, and therefore driving force, with strain until dynamic equilibrium is achieved.

The strain rate of prior working affects the recovery rate in a similar way. With an increase in strain rate at a fixed temperature, the recovery rate increases(39). The effect of solute or alloying additions on the rate of static recovery is one of the subjects of the present thesis and will be considered in more detail below.

1.7 METADYNAMIC RECRYSTALLIZATION

In some of the studies concerned with dynamic recrystallization (31,33,40,63), it was reported that under certain conditions, deformed materials can recrystallize statically very rapidly during the quenching period. The rates of recrystallization were unusually high, but experiments carried out by means of metallographic techniques did not lead to a full explanation of the unusual behaviour. More recently, several metallographic studies of hot deformed materials have produced further evidence concerning some unusual features of the softening processes occurring after high temperature deformation. These studies have included investigations of the behaviour of hot-forged austenitic steel(64,65), α-iron(66), stainless steel(67), HSLA steel(67), pure copper(68) and aluminum bronze(68).

For example, the work of Pluhar, Zuna and associates(64,65) involved measurements of average grain size and dislocation density as a function of delay time before quenching. Their measurements indicated that two cycles of recrystallization were involved. The first one, which occurred "very rapidly", resulted in a dislocation density which was much higher ($\sim 10^9/cm^2$) than that of annealed material and which was "very unevenly distributed". The second cycle of recrystallization occurred by the "clear-cut nucleation and growth of new grains" and was followed by a decrease in the dislocation density to a uniformly lower level, as expected for the mechanism of classical recrystallization.

The suggestion that three distinct softening processes took place after high temperature deformation was first introduced by Petkovic-Djaic and Jonas(69,70). They based their three-process concept on data obtained from interrupted compression tests on various steels deformed in the austenite phase. According to their model, the very rapid recrystallization cycle, christened metadynamic (or post-dynamic) recrystallization, is a type of static softening process that can occur only after previous dynamic recrystallization (i.e. recrystallization concurrent with deformation). According to this view(69,70), the recrystallization centres nucleated <u>during</u> deformation will, on interruption, continue to grow into the surrounding deformed material. This process is only completed when all the nuclei formed during deformation are exhausted. As this type of recrystallization does not require a nucleation interval, it proceeds very rapidly upon the termination of deformation. Nevertheless, nucleation for static recrystallization can still take place in regions which do not contain dynamic nuclei, thus accounting for the second cycle of recrystallization observed by Pluhar and Zuna(64,65).

Although the model of Petkovic-Djaic and Jonas(69,70), based on mechanical tests, was in excellent circumstantial agreement with the results of Pluhar and Zuna, which were obtained by metallographic means, it was open to an important criticism. Because of the γ-α transformation, a metallographic investigation was not carried out in parallel with the interrupted tests. Thus the agreement referred to above could have been fortuitous. In addition, whilst the model may have applied to the results of Pluhar and Zuna, its applicability might have been limited to a few special materials and so could have been of only limited utility. These doubts concerning the model were among the principal motivating factors for the present study and will be dealt with in detail later when the results of this investigation are presented and discussed.

1.8 THEORETICAL ASPECTS OF STATIC RECRYSTALLIZATION

The literature shows that the mechanism of classical recrystallization after hot deformation is similar to that occurring after cold deformation. We will therefore begin this section by reviewing some theoretical aspects of annealing after cold working. The reason for the similarity is that both processes take place by nucleation and growth.

1.8.1 Recrystallization Kinetics

1.8.1.1 Formal theory

Recrystallization, like many true phase changes, can be treated as a nucleation and growth process. Thus the fundamental quantities of interest are N, the rate of nucleation and G, the rate of growth of the recrystallization nuclei. Many theoretical treatments of nucleation have been reported in attempts to define a relationship for the fraction recrystallized in a given time in terms of N and G.

The formal theory of recrystallization developed by Johnson and Mehl(71) was based on four simplifying assumptions. Firstly, the nuclei are assumed to form randomly within the unrecrystallized material.

Secondly, the nucleation rate N and thirdly, the growth rate G are invariant with time. The nucleation rate is defined as the number of nuclei that form in unit volume in the unrecrystallized material in unit time. G is the increase in radius of the recrystallizing grain per unit time. Finally, the nuclei are assumed to be spherical and this shape is considered to be maintained until the growing spheres impinge on one another.

The amount of deformed matrix absorbed as a function of time can then be determined by a formal theoretical treatment(71-73), which leads to the expression:

$$f(t) = 1-e^{-(\pi/3)NG^3t^4} \tag{1.24}$$

where f(t) is the fraction transformed in a given time t. Equation (1.24), when plotted on semi-logarithmic paper, leads to curves of the general form shown in Figure 1.4. The shape of this curve changes somewhat with different values of N and G, but remains fixed when the expression $\sqrt[4]{NG^3}$ is constant. Thus, the amount of material transformed depends on the value of this expression, rather than on the separate values of N and G.

1.8.1.2 The Avrami theory

Avrami(74,75) took the formal theory of Johnson and Mehl a step further by examining the effect of a possible change in the rate of nucleation N with time. It was assumed that prior to transformation, there are N_0 preferred sites for nucleation, each of which has a nucleation frequency γ. These are gradually used up during recrystallization so that the nucleation rate N decreases exponentially. Thus $N = N_0\gamma e^{-\gamma t}$ in the Avrami analysis, whereas in the Johnson-Mehl treatment $N = N_0\gamma$. When this expression is introduced into the theory, two expressions for the fraction recrystallized are obtained, depending on the magnitude of γt.

When γt is large

$$f(t) = 1-e^{-kG^3Nt^3}$$

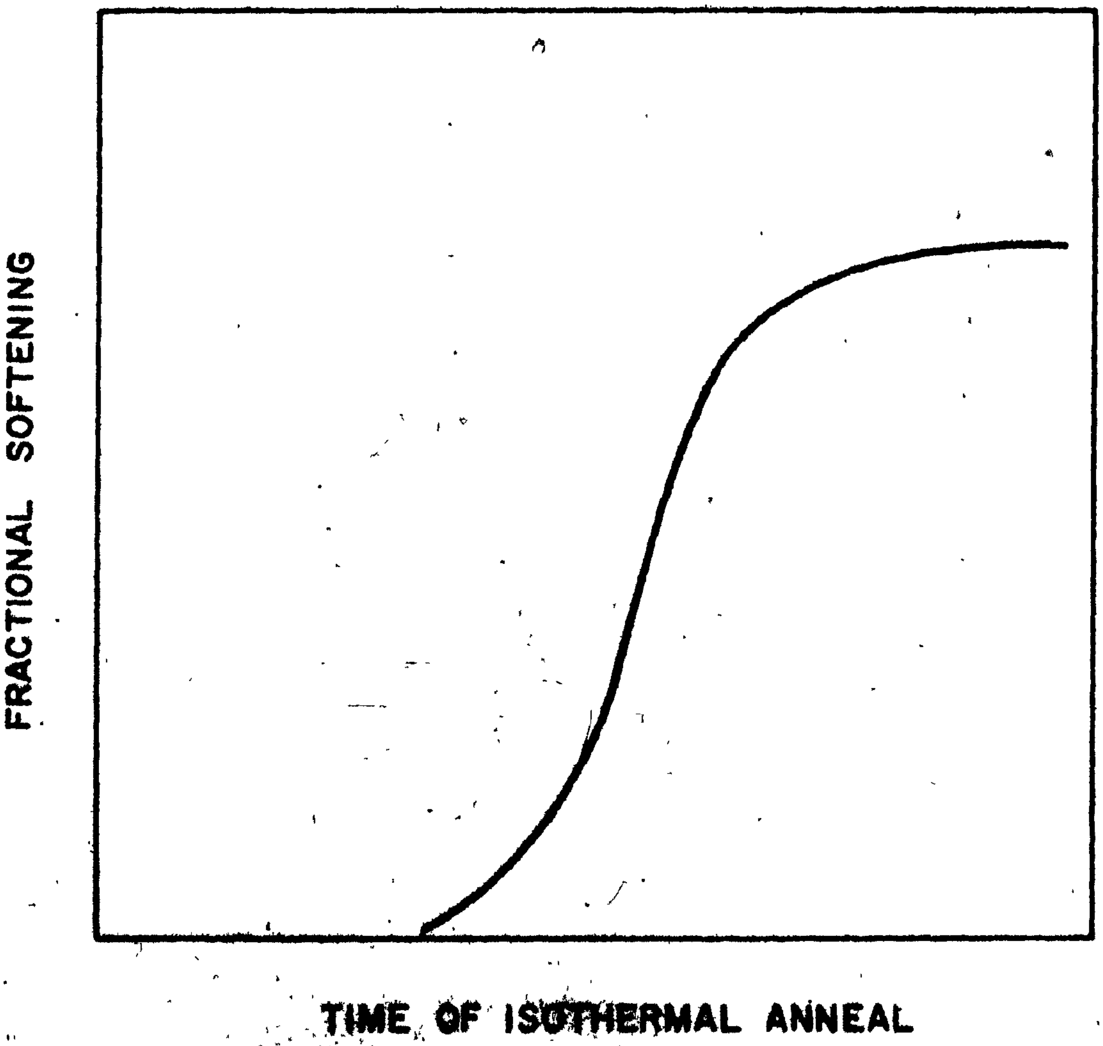

Figure 1.4 The progress of isothermal annealing after cold deformation

but when $\gamma t \to 0$, an equation similar to that of Johnson and Mehl is obtained,

$$f(t) = 1-e^{(-kG^3Nt^4)/4}$$

Since the Avrami formulation has received general acceptance, we will consider the derivation of the above expressions in more detail below.

Avrami(74,75) assumed that, after an incubation period τ, nuclei of strain-free grains begin to grow from a number of sites in the cold-worked matrix. If D is the diameter of such a growing grain, then she considered that D varies with time t as described by

$$D = G(t-\tau) \qquad (1.25)$$

Here the nucleation time τ is inversely proportional to the nucleation rate N. To obtain the expression for fraction recrystallized as a function of time, relation (1.25) can be extended in three directions (x, y and z). Then the volume v of a particular recrystallized grain at time t can be expressed as:

$$v = f\, G_x G_y G_z (t-\tau)^3 \qquad (1.26)$$

Here f is a shape factor, and G_x, G_y and G_z are the linear growth rates in the three directions x, y and z, which are assumed to be independent of time.

In the earlier treatments of nucleation, the number of nuclei originating in the time interval dt was written as $dn' = Ndt$. However, Avrami felt that this was incorrect, because it included the number of "phantom" grains that would have appeared in the recrystallized volume X had this particular volume not already been filled with recrystallized grains. To correct for this quantity, Avrami redefined the number of nuclei dn originating in the time interval dt as

$$dn = N(1-X)dt = dn'-NXdt \qquad (1.27)$$

where NXdt is the number of these "phantom" grains.

The "extended" volume fraction X_{ex}, which includes the phantom grains, was defined by Avrami(74) as

$$X_{ex} = \int_0^t v dn' \tag{1.28}$$

Substitution of Equations 1.26 and 1.27 into 1.28 leads to the expression:

$$X_{ex} = f\, G_x G_y G_z \int_0^t (t-\tau)^3 N dt \tag{1.29}$$

The ratio of the extended volume fraction to the real volume fraction is given by the relation

$$dX/dX_{ex} = (1-X) \tag{1.30}$$

Thus

$$\int_0^X dX_{ex} = \int_0^X dX/(1-X) = X_{ex} = -\ln(1-X) \tag{1.31}$$

and, using this equivalence in Equation 1.29, we obtain

$$-\ln(1-X) = f\, G_x G_y G_z \int_0^t (t-\tau)^3 N dt \tag{1.32}$$

or

$$X = 1-\exp\{-f\, G_x G_y G_z \int_0^t (t-\tau)^3 N dt\} \tag{1.33}$$

In the Johnson and Mehl approach, where the nucleation and growth rates were taken to be constant, and the values of τ were considered to be negligibly small, Equation 1.33 can be written as:

$$X = 1-\exp\{-f(G_x G_y G_z N t^4/4)\} \tag{1.34}$$

The time exponent n derived in this manner has the value 4, which has been observed to hold for the formation of pearlite from austenite(71), for example, the process for which the equation was derived.

In the more general category of isothermal reaction kinetics, however, the exponent n has been observed to vary from 0.5 to 2.5 and range as high as 6 occasionally(76). Thus the Johnson and Mehl equation does not apply to these data in its original form. In the form of Equation 1.33 proposed by Avrami, on the other hand, this discrepancy has been overcome, as will be shown below. Avrami took $N = N(t)$ and $\tau \not\approx 0$ in her analysis. The assumption that $\tau \sim 0$ is very useful because it is very difficult to establish the reaction "start" time. In any event, the assumption that $\tau \sim 0$ introduces negligible error(76). The assumption that $N = N(t)$ is a more useful one. When a value for N of A/t^v, for example, is substituted in Equation 1.33, the following relation is obtained:

$$X = 1-\exp\{-f\, G_x G_y G_z \int_0^t t^3 A/t^v dt\} \tag{1.35}$$

or

$$X = 1-\exp\{-f\, G_x G_y G_z A \int_0^t t^{3-v} dt\} \tag{1.36}$$

It can be seen that Equation 1.36 leads, on integration, to

$$X = 1-\exp(-\beta t^k) \tag{1.37}$$

where $k = 4-v$.

From the above it is evident that it is the relaxation of the invariance of N which permits the time exponent k to adopt values which differ from 4, and are therefore in better agreement with experimental data.

The above theory applies only if nucleation is taken to be a random process. This is one of the weak points of the theory, because nucleation during recrystallization is not completely random, as nuclei do form at favoured sites such as grain boundaries, phase interfaces, twins, deformation bands and the surface of the material. These sites can often be characterized as regions of heavy distortion or of high dislocation density, because they are generally located in the vicinity of marked changes in orientation.

1.8.2 Recent Theoretical Developments Concerning Nucleation Mechanisms

Recent investigators have distinguished three main nucleation mechanisms:

A. the bulge model of nucleation,
B. the subgrain growth model, and
C. the subgrain coalescence model.

These will now be discussed in turn.

1.8.2A Bulge nucleation model

Bailey and Hirsch(74) derived a theory describing the progress of recrystallization, not in terms of N and G, but in terms of the changes in surface energy and strain energy which occur during the growth of nuclei. They developed an expression for the rate of growth of recrystallized grains using a model where a length of boundary 2L bulges out to form a spherical cap of radius R and then migrates, as shown in Figure 1.5. The driving force is assumed to be the difference in strain energy (i.e. dislocation density) across the boundary. Grain A (Figure 1.5) is taken to have a larger dislocation density than grain B. This difference provides the driving force for the grain boundary to bulge between pinning points 1 and 2, as shown in the illustration. If ΔE is the stored energy difference per unit volume across the migrating boundary, γ is the surface energy and A is the surface area of the bulge, the rate of growth of the bulge can be given as:

$$dV/dt = Abf\{\Delta E-\gamma(dA/dV)\} \qquad (1.38)$$

Here b^3 is the volume occupied by one atom, and f is the jump frequency(77).

For growth to occur, $dV/dt > 0$ and therefore $\{E-\gamma(dA/dV)\}$ must be positive. If the rate of growth of the recrystallizing grain is expressed in terms of α:

$$d\alpha/dt = (2bf/L)\{\Delta E-(2\gamma/L)\sin\alpha\}(1+\cos\alpha) \qquad (1.39)$$

and it follows that the condition for growth to occur is:

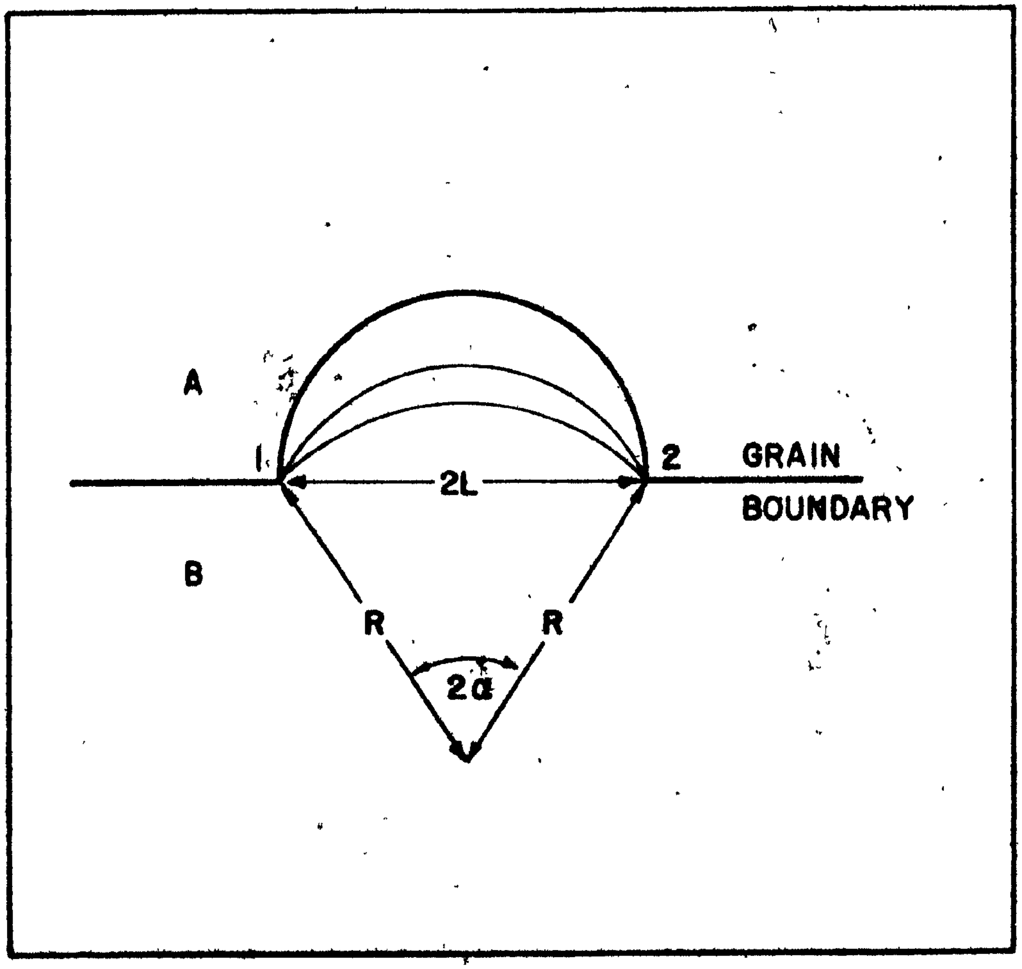

Figure 1.5 Model for the growth of a recrystallization nucleus

$$L > 2\gamma/\Delta E \tag{1.40}$$

for all values of α.

The model of Bailey and Hirsch(44) is compatible with the usual kinetics of the recrystallization process and is in broad agreement with the Avrami equation.

It is of interest that in a recent study of the recrystallization phenomenon in pure copper and aluminum bronze(68), no evidence for bulge nucleation was detected. These experiments were conducted continuously in a photoemission electron microscope, and the bulging out of an existing grain boundary to initiate recrystallization was never observed in any of the specimens studied. Nevertheless, there seems to be no doubt that the bulge nucleation mechanism is an important one and commonly occurs in moderately deformed metals(44). Even in heavily deformed materials, in which the grain boundaries are difficult to observe and therefore active bulges are difficult to detect, it is still possible that the bulge mechanism operates(44).

1.8.2B Subgrain growth model

The concept that a recrystallized grain may be formed by gradual subgrain growth was introduced by Cahn(78). According to his theory, the highly curved regions in a deformed crystal become relatively strain free by polygonization(62,79). A given polygonized subgrain then grows at the expense of its neighbours, developing into a recrystallization nucleus.

Cottrell(80) extended Cahn's theory by including another condition for nucleation, that of the presence of a high-angle boundary, since only these boundaries have the necessary kinematic freedom for motion in arbitrary directions. This condition immediately restricts nucleation sites to regions of strong curvature. At first, while the angles between polygonized subgrains are still small, growth takes place rapidly, because of the relatively high mobility of sub-boundaries of very small angle. In the rapid phase, the dislocations within the cells are attracted into the cell walls and the redundant dislocations in the cell walls annihilate each other, leaving neat dislocation networks separating the polygonal crystallites(81,82). The formation of a cellular substructure in cold worked materials and of subgrains in hot worked materials is illustrated schematically in Figure 1.6.

Eventually, when the angles approach the range of a few degrees, growth becomes much slower. Finally, one of the subgrains reaches the critical size necessary for rapid growth and then becomes recognizable as a new unstrained grain separated from the neighbouring subgrains by a high-angle boundary(83,84).

1.8.2C Subgrain coalescence model

The coalescence of subgrains(85) may be explained by the movement of dislocations from a disappearing boundary into the adjoining boundaries around the subgrains. A schematic representation was given by Li(86) at about the time that Hu(83) reported his extensive electron micrographic observations of recrystallization in silicon-iron single crystals. The latter's thin-foil electron micrographs showed that some subgrains grow preferentially in the microband regions by a coalescence process, during which certain sub-boundaries disappear without migration. It has been proposed that coalescence is achieved by the rotation of one or more adjacent subgrains, until the disorientation is removed(86). Subsequently the large coalesced subgrains become recrystallization nuclei.

McQueen and Jonas(50) in their recent review have suggested that the actual mechanism of nucleation depends on the SFE (and therefore the metal) as well as on the strain, Figure 1.7. The subgrain coalescence mechanism can be expected to occur easily in metals of high stacking fault energy, leading to the establishment of regions of low internal dislocation content surrounded by boundaries of high misorientation capable of migrating(87), Figure 1.7(a). In metals of lower stacking fault energy, severe straining creates localized high densities of dislocations which transform into high angle boundaries upon annealing(44), Figure 1.7(b). When the amount of prior straining is reduced, then the mechanism of grain boundary bulging takes place. This process entails the bulging out of a short segment of an existing high angle boundary into a region of higher density, Figure 1.7(c).

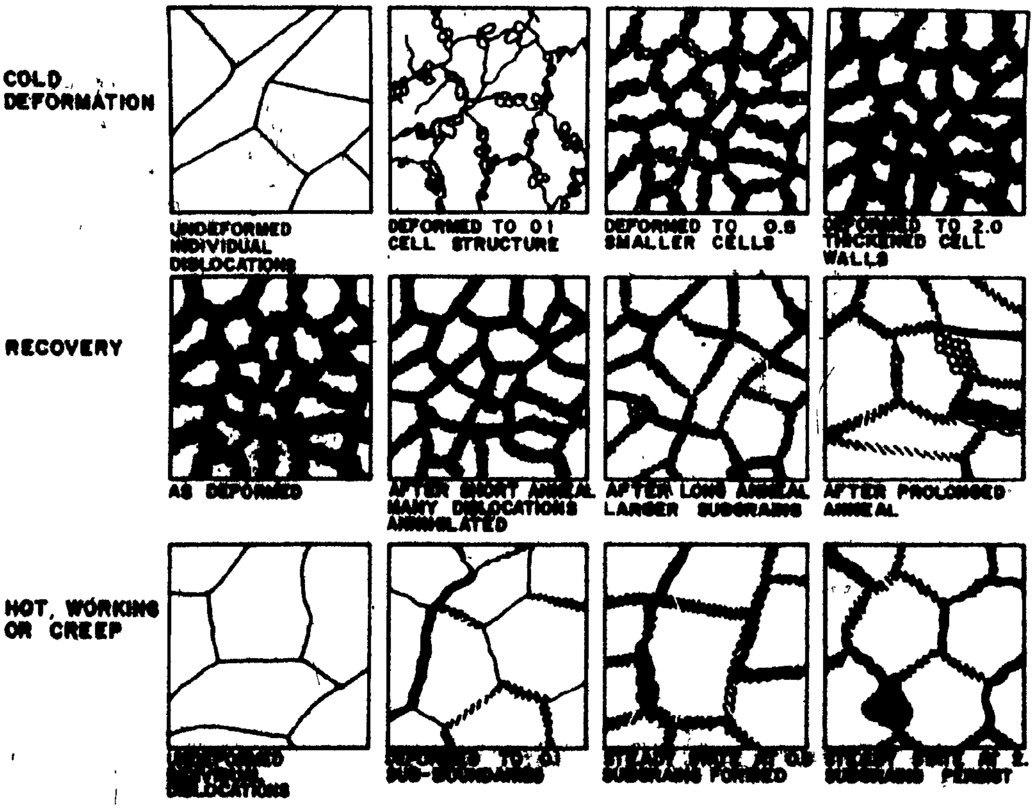

Figure 1.6 Schematic illustration of subgrain formation following cold or hot working (after McQueen and Jonas, Ref. 50)

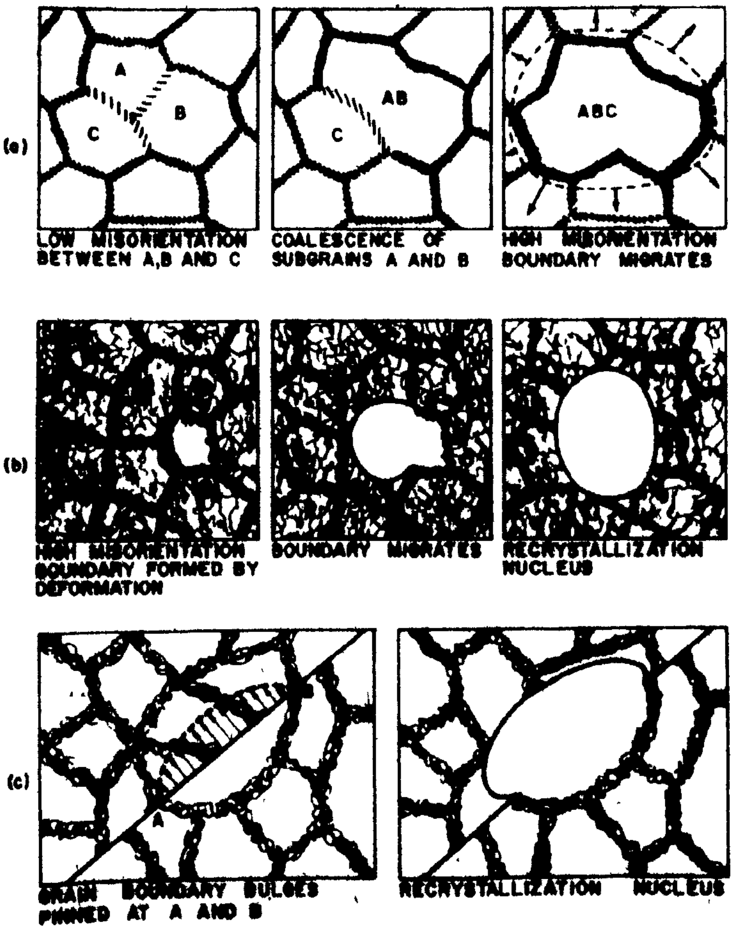

Figure 1.7 Schematic illustration of the mechanism of nucleation of recrystallized grains as a function of SFE and strain (after McQueen and Jonas, Ref. 50)

1.9 STATIC RECRYSTALLIZATION AFTER HOT WORKING

The occurrence of static recrystallization after the hot working of steel is very difficult to study quantitatively. This is because its progress is not readily followed by means of optical metallography and also because the intervention of metadynamic recrystallization tends to obscure such results as are obtained. For example, laboratory investigations carried out by several workers have shown that low alloy steels recrystallize rapidly after deformation in the austenite range(88-90). On this basis, it was concluded(91) that complete recrystallization probably occurs between rolling passes at almost all hot working temperatures. Such a simple picture does not, however, allow for the complex effect of the various experimental variables involved in hot working, such as the prior strain, strain rate, temperature, holding time and concentration of alloying elements. It will be an aim of the present work to consider the influence of these variables in some detail in selected materials. Before turning to the results of this investigation, we will first review some of the published information concerning static recrystallization after hot working.

1.9.1 Recrystallization Kinetics

A general expression describing a nucleation and growth process is the Avrami equation (1.37), already introduced in Section 1.8.1, in which the parameter k is a constant governed by the time-dependence of the nucleation and growth rates. This equation was used to fit the experimental data in a recent study by Glover and Sellars(66) dealing with recrystallization kinetics after hot working. They found that, for vacuum-melted and zone-refined iron, k varied from ~ 1 to ~ 2, depending on the prior structure. After previous dynamic recovery (i.e. for classical recrystallization), $k = \sim 2$, and after previous dynamic recrystallization (i.e. for metadynamic recrystallization) $k = \sim 1$. Similarly, in an earlier study by the present worker(39), the value of k in plain carbon steel was also observed to depend, albeit more weakly, on the nature of the prior softening mechanism, varying in the range 1.2 - 1.6.

By comparison, Michalak and Hibbard(92) found that for OFHC copper, k ranged from 1.1 to 1.5, depending on the annealing temperature.

For the same material and similar conditions, Gordon(93) observed that k ranged from 3.1 to 3.9, whereas Decker and Harker(94) reported that k fell between 2.1 and 3.2, depending on the recrystallization temperature. Thus we see that values for k ranging from 1 to 2 have been reported for recrystallization after high temperature deformation, whereas the wider range of 1 to 4 has been quoted for annealing following cold working.

Decker and Harker(94) have suggested that differences in the exponent k following cold working also depend on the amount of concurrent recovery, with small values of k indicating that considerable recovery has taken place prior to or during recrystallization.

In a more recent investigation, Hayes and Shyne(95) studied the influence of ultrasound on the kinetics of recrystallization in cold rolled copper. It is of interest that, although concurrent irradiation increased recrystallization rates by factors of 30 to 100, the values of k for both irradiated and non-irradiated samples were in the range 1.1 to 1.2. Since the value for k was not appreciably changed by the action of ultrasound during recrystallization, they concluded that the superposition of acoustic vibration did not alter the form of the time dependence of the nucleation and growth rates for recrystallization.

Finally it should be noted that in the work on aluminum bronze and pure copper described earlier, in which recrystallization was observed by means of photoemission electron microscopy, the authors concluded(68) that an equation of the Avrami type could not be used. They considered that the kinetics of recrystallization after hot working were not amenable to analysis by the means described here because two different recrystallization processes were interacting simultaneously during the cooling interval.

1.9.2 Experimental Variables Affecting Recrystallization

1.9.2A Effect of inclusions and precipitates on recrystallization

Inclusions and precipitates have similar effects on recrystallization. Nucleation can be retarded or accelerated, depending on the particle size and interparticle spacing. If the particles are large and the spacing is coarse, then nucleation is accelerated(62,96). Such acceleration has been attributed to the high dislocation densities produced in the neighbourhood of the particles by the previous deformation. But if the precipitates interfere with the growth of subgrains during the nucleation stage, then they act as barriers, preventing many of the cells from growing and in that way retarding nucleation.

It has been reported that Nb additions retard recrystallization (90,97,98). For example, Cordea and Hook(90) have reported that the recrystallization of austenite in the temperature range from 870°C to 1040°C was retarded when as little as 0.02% Nb was added to a 0.10%C steel. A similar effect is observed in the case of V additions, but the effect is weaker than for Nb(90,97). Kozasu and Kubota(97) also found that Al additions accelerated recrystallization, as did the presence of N. A similar study was conducted on a 0.06% steel by Herrnstein et al(99), in which they observed that additions of 0.24% Ti retarded softening after hot deformation at 870°C and 950°C.

The exact mechanisms by which the various additions retard austenite recrystallization is not clear. There is some evidence to indicate that deformation promotes precipitation in the austenite. The precipitation can be expected to occur on sub-boundaries and in that way to retard the subgrain growth mechanism(97,100). Another possible explanation(90) is that precipitated alloy carbides interact strongly with dislocations and stacking faults during deformation, thereby retarding recovery and subsequent nucleation by one of the other mechanisms. However, the higher stored energy of deformation in the structure would then be expected to promote faster growth rates.

1.9.2B Effect of solutes on recrystallization

The retardation of grain boundary migration by solute impurities has been discussed by several investigators. Lücke and Detert(101), for example, assumed that impurity atoms in solid solution tend to segregate to grain boundaries because of an interaction between the solute atoms and the boundaries. When a grain boundary loaded with impurity atoms is forced to move, the dragging motion of the impurity atmosphere is the source of a drag force on the boundary. At low boundary velocities, the impurities diffuse behind the boundary and consequently its velocity is governed by the diffusion coefficient of the solute in the matrix. At high boundary velocities, the boundary breaks away from its solute atmosphere and boundary motion becomes solute independent. Thus at low boundary velocities, Q_G is equal to the activation energy for the diffusion of solute in the matrix. At high velocities, the activation energy is equal to Q_B (the activation energy for boundary self diffusion).

Cahn(102) and Lücke and Stüwe(103), have attempted a more rigorous formulation of the effect of impurity drag on moving grain boundaries. As in the theory of Lücke and Detert, two limiting conditions of motion are found, impurity-controlled migration at low drag forces and large solute contents ($Q_G > Q_B$), and impurity-independent migration at high driving forces and low solute contents ($Q_G \simeq Q_B$).

1.9.2C Effect of strain and prior recovery on recrystallization

Bailey and Hirsch(44) found that, after previous cold working, nucleation and growth rates both increase with strain. But because the nucleation rate increases faster than the growth rate, increasing strain restricts the growth of recrystallized grains and leads to the production of finer recrystallized grain sizes. This effect has been attributed by Anderson and Mehl(72) to a decrease in the activation energies for nucleation and growth with strain. The results of these workers(44,72) lead to the conclusion that the rates of nucleation and growth should decrease with the amount of prior recovery. The extent of retardation due to recovery can be expected to depend on the material, its purity, the temperature, the grain size, the orientation of the grains with respect to the strain, and the amount and mode of deformation. The retardation should be more pronounced at lower temperatures, since recovery processes proceed with lower activation energies than those for static recrystallization.

When it comes to behaviour in the hot working range, several recent investigations are of interest. These have been concerned with the influence of the amount of prior strain on the rate of recrystallization and on the recrystallized grain size, and were carried out on bcc silicon iron(66,104), fcc austenitic stainless steel(105,106) and plain carbon steel in the austenite range(69,107-109).

Some of these data are collected(69) and illustrated in Figure 1.8. Here it can be seen that the time for 50% softening by recrystallization decreases by as much as two orders of magnitude with increasing strain, finally levelling out when the steady state is reached. For deformation between the critical strains for static† and dynamic recrystallization, the increase in rate can be attributed to the increased driving force. When the strain is greater than the critical strain for dynamic recrystallization, the increase in recrystallization rate with strain is accompanied by a decrease in recrystallized grain size. The grain size becomes independent of strain when steady state flow is reached.

1.10 THE INTER-RELATION BETWEEN THE THREE PROCESSES OF STATIC SOFTENING

Detailed analyses of softening behaviour after hot working were very difficult to achieve in the past, due in part to the limitations of the testing techniques employed. Furthermore, these restoration processes occur very rapidly and are frequently completed in one second, or in a small fraction of a second. It is, therefore, readily understood why only limited data can be found in the literature on this subject. Much insight has, however, been gained through the use of a new experimental method employing interrupted mechanical tests. This technique which will be described in detail later, has been employed successfully over the past few years by a number of researchers(39,57,67,69,70,89,90,104,107, 110,111) who have been able to distinguish the time dependence of the various restoration processes that take place after hot working.

The principal feature of the softening curves obtained by interrupted testing that had not been observed during the annealing of cold worked material was the presence of multiple softening plateaus or arrests along the curves. Several workers(39,67,69,70,89,90) have reported that the softening curves after hot working exhibit one or two arrests along the curve, depending on the strain rate, temperature and interruption strain. The first plateau was associated, by these workers, with the completion of static recovery, and the associated delay in softening until the rate of static recrystallization becomes appreciable.

---

†The critical strain for static recrystallization was found to be of the order of 10%.

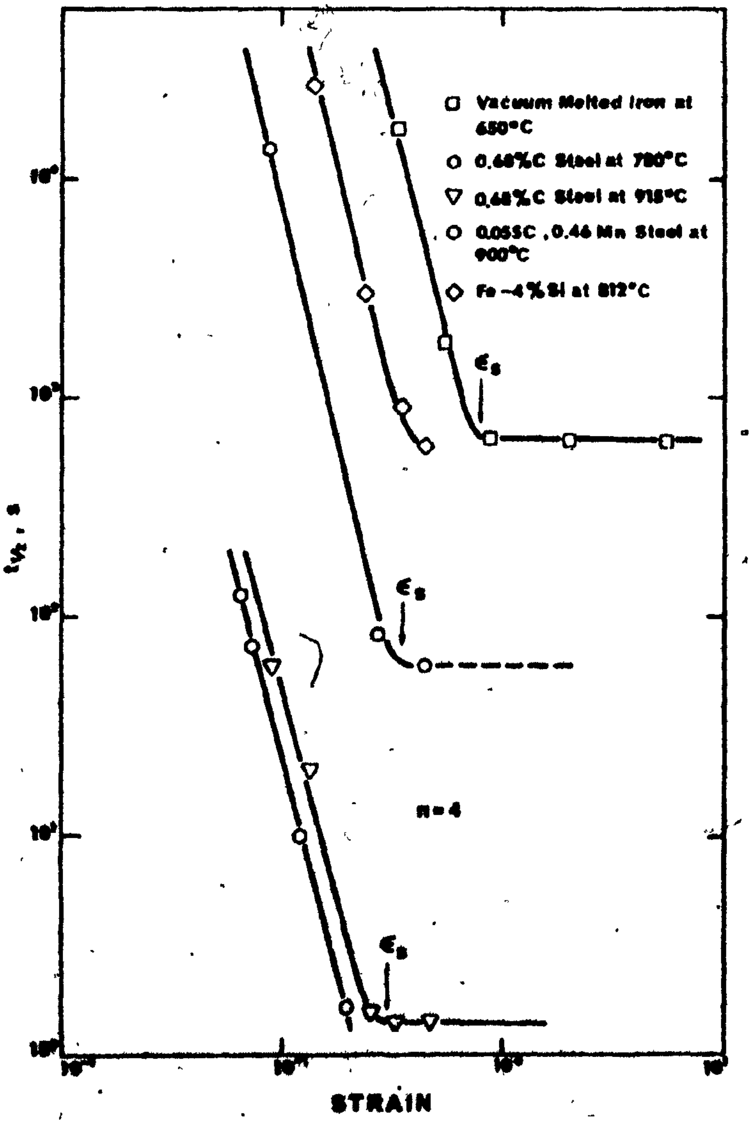

Figure 1.8 The effect of strain on the time for 50% softening for several ferrous alloys in both the ferritic and austenitic conditions

The cause of the second arrest, when present, has not however been attributed to a unique source. For example, Capeletti et al(67) explained the first plateau as being due to the saturation of recovery, but gave two different explanations for the presence of the second plateau in the two materials. In the HSLA steel, they suggested that NbC precipitation caused the second plateau to appear, whereas in 304 stainless steel, they concluded that thermal microtwinning was the relevant softening mechanism. These explanations are not completely convincing, however, as the appearance and duration of the plateaus vary in a similar way with increases in strain in the two materials. It is at least possible, therefore, that the same softening mechanism is responsible for the presence of the additional plateau in both materials.

Extensive investigation of the softening behaviour of low and medium carbon steels by Petkovic (previously Djaic) and Jonas(39,69,70) has enabled an alternative hypothesis concerning the static mechanisms of softening to be formulated. This hypothesis is based on three distinct softening mechanisms. The operating ranges and interrelationships between the three softening mechanisms are delineated in Figure 1.9, in which the effect of strain on the softening proportions attributable to each of the processes is illustrated. The region identified as I on the diagram represents softening by static recovery; similarly regions II and III represent softening by metadynamic and by classical recrystallization, respectively. The region ABCD is a "forbidden zone", which cannot be entered under normal experimental conditions. The diagram indicates that at strains below the critical strain for static recrystallization (an arbitrary 8 pct was used in the construction of the diagram), the only restoration process that operates is static recovery. When the strain exceeds 8 pct, but is less than 16 pct, static recovery is followed by static recrystallization, the proportion of softening produced by the two mechanisms being given by the vertical distances above and below BF. When the interruption strain exceeds the strain required to reach the peak of the flow curve (arbitrarily selected as 16 pct in the construction of the diagram), the dynamic recrystallization nuclei formed during straining are free to serve as nuclei for the ensuing restoration, which has been termed metadynamic recrystallization. As the prior strain

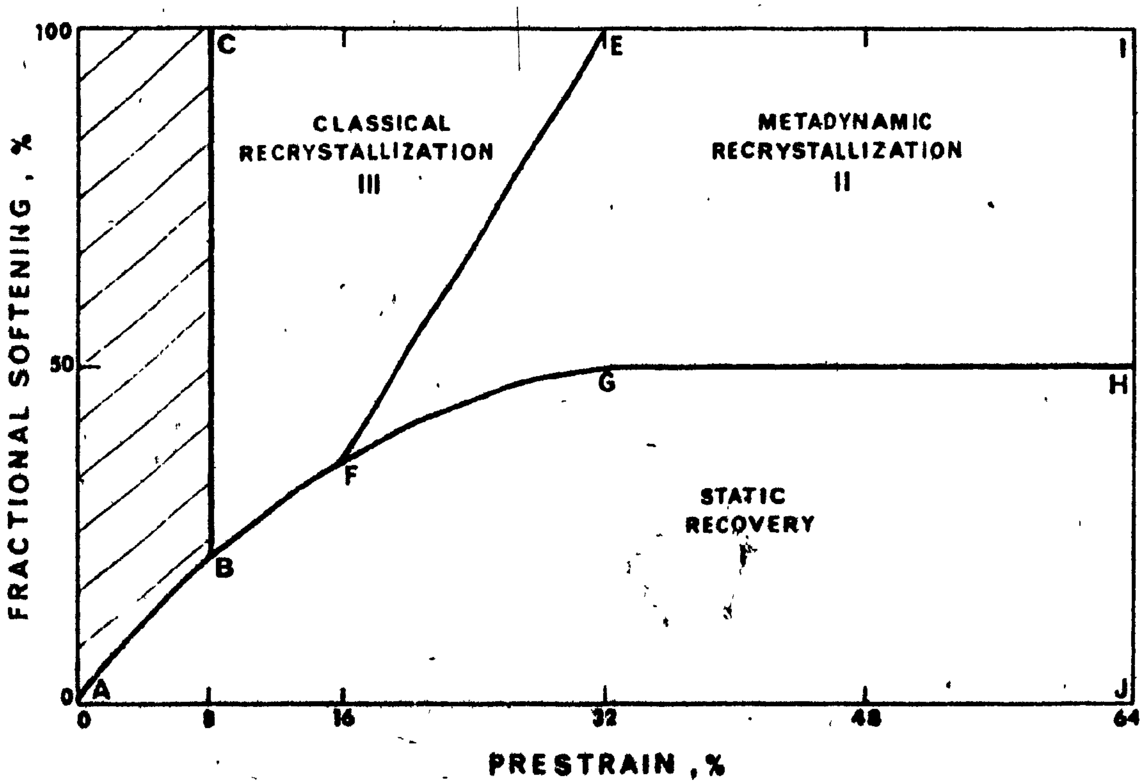

Figure 1.9 Schematic representation of the interrelation between the three softening mechanisms (after R. Petkovic-Djaic and J.J. Jonas, Ref. 69)

is increased from the peak (16 pct) to the steady-state strain (32 pct), the interruption flow stress drops as a result of the increasing contribution of dynamic recrystallization to the dynamic softening processes. It can be inferred from the above that the density of dynamic recrystallization nuclei increases with strain between 16 and 32 pct. The increasing nucleus density, in turn, leads to the decreasing importance of classical recrystallization indicated by the line FE in Figure 1.9.

Unfortunately, a supporting metallographic investigation was not carried out on the samples produced by the interrupted tests(69,70). This was partly because of the difficulties introduced by the γ to α transformation, and also because of a lack of the time required. Thus the conflict between the interpretation of Capeletti et al(67) and the present author could not be resolved. This conflict provided one of the motivating factors for the study described below; it will be for the reader to decide whether the results obtained are sufficient for a consensus concerning the controversy to be attained.

CHAPTER 2

EXPERIMENTAL MATERIALS AND PROCEDURE

The purpose of the research described in this thesis was to investigate the influence of various deformation and delay conditions on the kinetics of static recovery and recrystallization following hot deformation. This aim was achieved by the development of a quantitative method for the investigation of softening behaviour based on mechanical measurements at the deformation temperature(39). Although several investigators(67,89,90,107,111) have tried to achieve this end using other test methods, e.g. tension(67,89,107), torsion(112) and cam plastometry(111), for a reason that will become apparent below, the compression test was selected as being the most suitable for the purpose of the investigation.

2.1 THE INTERRUPTED COMPRESSION TEST

The method developed in the present work to examine the softening behaviour of a variety of materials is illustrated in Figure 2.1. The test method is based on the principle that the yield stress at high temperatures is a sensitive measure of the structural state of the material. Samples are loaded at a constant true strain rate to some prescribed strain and then unloaded and held at zero load for increasing time intervals. The samples are subsequently reloaded at the same strain rate as before. The magnitude of the yield stress on reloading is governed by the degree of structural change that has occurred during the holding interval, and can therefore be taken as a measure of the progress of the static softening processes. After a short holding time, t_1 in Figure 2.1, the flow stress on reloading rises rapidly to a stress level comparable with the unloading stress. On the other hand, after a long delay, t_6, the stress-strain behaviour on reloading approaches that observed during initial loading of the annealed material. It is evident from the foregoing description of the test that precise measurements of yield stress are essential to this type of testing procedure.

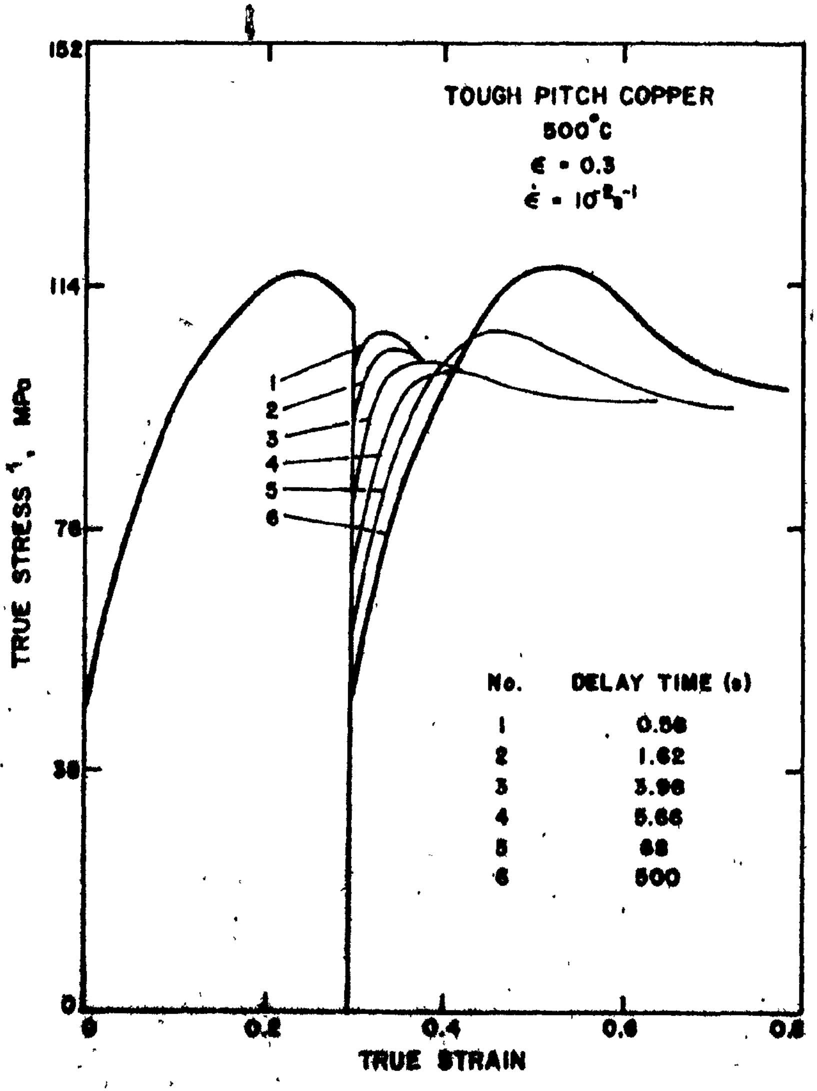

Figure 2.1 Effect of increasing delay time on the interrupted flow curve

The earliest investigations of this type utilized the tension test(67,89,90,107). The tension test, however, has many inherent limitations when used in the present context at high temperatures. For example, the true strain rate is not, in general, held fixed, and constant crosshead velocities are used instead(6,8,24,89,113,114). This is, unfortunately, particularly inappropriate at high temperatures, where the rate sensitivity tends to be rather high. A constant true strain rate tension test is difficult to achieve because of the onset of necking (the necking strain is typically ∼0.2 - 0.3 for many steels). Furthermore, the onset of necking precludes the metallographic examination of material behaviour at high strains. The latter limitation also leads to difficulties where interrupted tests are concerned, since reloading may be carried out on previously necked samples, thus rendering the yield "stress" on reloading ambiguous.

Although the torsion testing of solid bar specimens can eliminate the problems associated with necking in tension, and high strains can therefore be achieved, the strain, strain rate and stress gradients along the radius of torsion samples again make yield stress measurements rather dubious(7,31,112,115-133).

Somewhat better results can be obtained with the aid of interrupted compression tests using cam plastometers(111). The major advantage of these machines is that strain rates comparable to those found in industrial hot working practice can be readily produced. Here the constant true strain rate is achieved by driving the compression tooling with a specially profiled cam. During an interrupted test, the strain to interruption is determined by the design of the cam. Consequently, for each interruption strain, a different cam is generally required. The technique is therefore rather inflexible and expensive.

The present test method uses an Instron testing machine and has the advantage of flexibility in both the interruption strains as well as the delay times. A disadvantage is that the velocity limitations of the Instron drive system constrain the testing range to strain rates below 0.5 s^{-1} (that is about one and a half orders of magnitude slower than those typically found in plate mill practice). The technique itself, however, can be used in electro-hydraulic machines (e.g. an MTS system), where this upper limit of strain rate can be raised to about 5 s^{-1}. The details of the testing system and the control of the experimental variables are described below, after the materials and sample geometry are outlined.

2.2 EXPERIMENTAL MATERIALS

The stimulus for the present study arose from the results obtained on the softening behaviour of a series of plain carbon austenites (39,69,70). Interpretation of the previous results was restricted, however, because metallographic analysis of the developed austenitic structures was prevented by the γ to α transformation. It was proposed, therefore, that a model material should be selected in which no such transformation occurs. The initial choice was type 304 stainless steel. Unfortunately, this material did not exhibit dynamic recrystallization at temperatures below 1100°C. Consequently, as an apparatus was not available for testing and subsequently quenching at these temperatures, the type 304 could not be taken as a model for plain carbon austenite. Subsequently, a series of tests was carried out on high purity copper, but in this case dynamic and static recrystallization were so rapid, that the progress of static softening could not be easily followed with the present equipment. To assist with this problem, a series of copper-based solid solution alloys were specially prepared by the Olin Corporation.† Some of these alloys exhibited suitable stress-strain and static softening behaviour, but the small experimental melts resulted in significant segregation, which led to a lack of reproducibility in the test samples.

Finally, commercial tough pitch copper was selected as the model material. The test samples were all prepared from one 6-meter length of cold drawn, 9 mm diameter round bar. Such a large quantity of the material was required because of the large number of tests envisioned (~700 tests).

In addition to the experiments on copper, two other series of tests were carried out to compare the softening behaviour of a HSLA

---

† By courtesy of Dr. E. Shapiro.

(high strength low alloy) steel containing Nb(Cb) and that of a plain carbon steel of similar chemistry. The HSLA steel was supplied by the Steel Company of Canada Ltd. and the plain carbon steel by the Sivaco Wire and Nail Company. The analyses of the three main experimental materials are given in Table 2.1.

2.2.1 Specimen Preparation

The compression samples were machined from the available rods into right cylinders 11.4 mm in height and 7.6 mm in diameter, as shown in Figure 2.2. The dimensions selected were based on the load capacity and crosshead speed range of the Instron and on previous experience with the equipment(39,134-137). The end faces of the samples were grooved (39,104,134,136,138) in order to retain the glass lubricants used in high temperature deformation. The choice of groove geometry was based on the work of Luton(134). He found that the best results were obtained with flat bottomed grooves, where the grooves are wider at their bases than are the ridges between them. The modified 2 teeth/mm thread chaser used to produce the required flat-bottomed grooves is shown in Figure 2.2.

In order to minimize differences in the initial structure of the samples to be tested at different temperatures, all tough pitch copper specimens were strain-annealed as follows. The samples were first prestrained in compression between two polished platens using an MTS testing machine. The strained samples were then annealed for 16h at 900°C(139). The resulting mean grain size was 0.6 mm. Prior to straining, a layer of teflon tape was placed at the ends of each specimen to act as a lubricant and to help prevent collapse of the grooves. In this way no apparent barreling occurred. Pilot tests were used to determine the prior strain required for a recrystallized grain size of 0.6 mm; this was 0.02, which was found to be insufficient to damage the sample grooves.

Prior to annealing, the samples were degreased carefully in carbon tetrachloride, using ultrasonic scrubbing, rinsed in methanol and dried. The samples were then placed into Sen-Pak† stainless steel

---

† Registered trade mark of the Sentry Co., Foxboro, Mass..

TABLE 2.1 Chemical Composition in wt% of the Materials Tested

	Pb	Ni	O_2	Ag	Bi	As
Tough Pitch Copper	.09	<.05	0.015	<.005	.04	<3ppm

	C	Mn	Si	P	S	Cr	Ni	Mo	Cu	Al	Sn	Nb
Niobium bearing steel	.07	1.18	.57	.008	.002	.114	.073	.032	.064	.064	.005	.074
0.06%C low carbon steel	.06	.41	.10	.02	.031	.02	<.01	<.01	.02	<.01	<.01	---

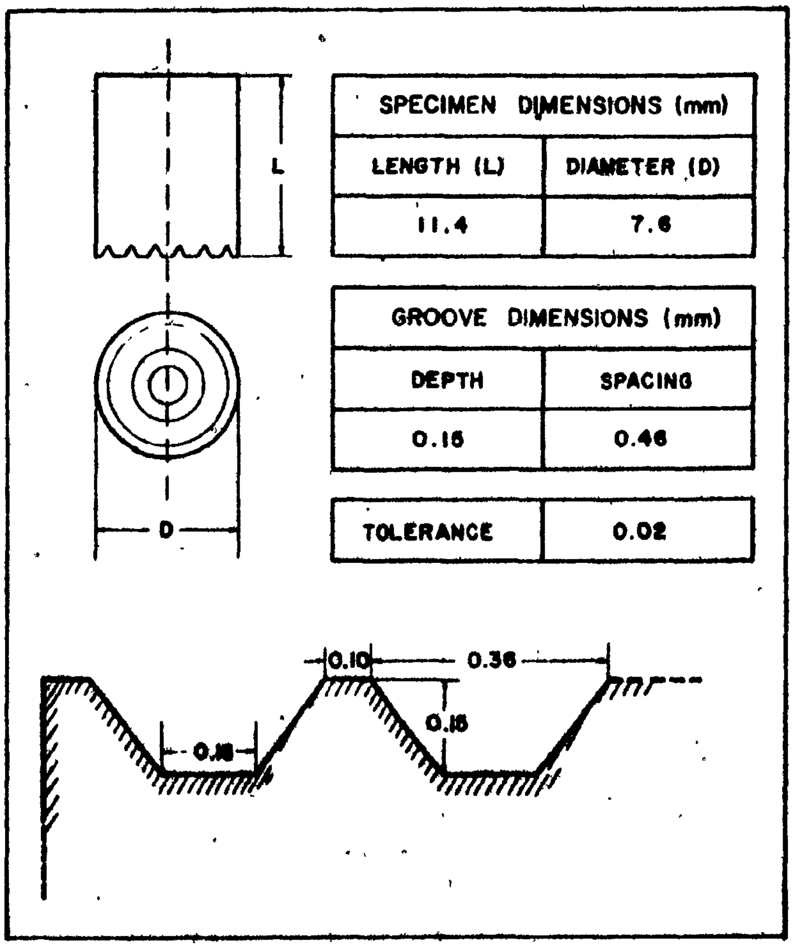

SPECIMEN DIMENSIONS (mm)	
LENGTH (L)	DIAMETER (D)
11.4	7.6

GROOVE DIMENSIONS (mm)	
DEPTH	SPACING
0.16	0.46

TOLERANCE	0.02

Figure 2.2 Specimen dimensions and groove geometry

annealing envelopes (10 specimens per pack) and the envelopes were introduced into a fused quartz furnace tube heated by a Marshall three-zone split furnace. The annealing envelopes were placed together in a zone where the temperature variation was less than ± 1°C from the set point value. The quartz tube was sealed and connected to an argon supply system. The chamber was evacuated and purged with argon five times before argon was allowed to flow through the chamber at 0.6 l/min, a positive pressure of 30 kN/m^2 being maintained throughout. The annealing temperature was monitored by a chromel-alumel thermocouple placed next to the sample packs. At the end of 16 hours, the envelopes containing the specimens were removed from the furnace and quenched in water. The samples treated in this way were bright with no trace of surface oxide.

2.3 EXPERIMENTAL EQUIPMENT

The compression test assembly was designed for the 10,000 kg (20,000 lb) Instron testing frame shown in Figure 2.3. The Instron frame was a model TT-D and was equipped with an extra decade speed reducer, which produced a crosshead speed range of 50 cm/min (20 in/min) to 0.05 cm/min (0.002 in/min).

The basic design of the compression assembly used in these experiments has been described in detail elsewhere(39,134,136,140). The important features of the compression train are the loading members, consisting of the upper and lower anvils and supports illustrated in Figure 2.4. One of the features of the apparatus is the facility by which the test samples can be quenched after each test. This was achieved by using a hollow lower anvil support.

Before starting experimentation, the present author modified the basic design described above to make it more suitable for interrupted tests. In addition, a completely new design of loading train was prepared for tests at temperatures in excess of 1000°C. Details of the modifications to the original equipment as well as the new loading train will now be described.

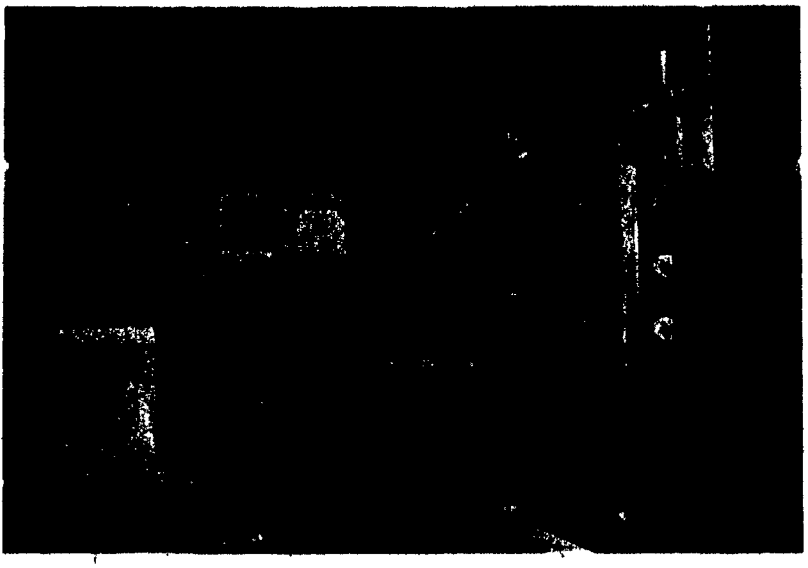

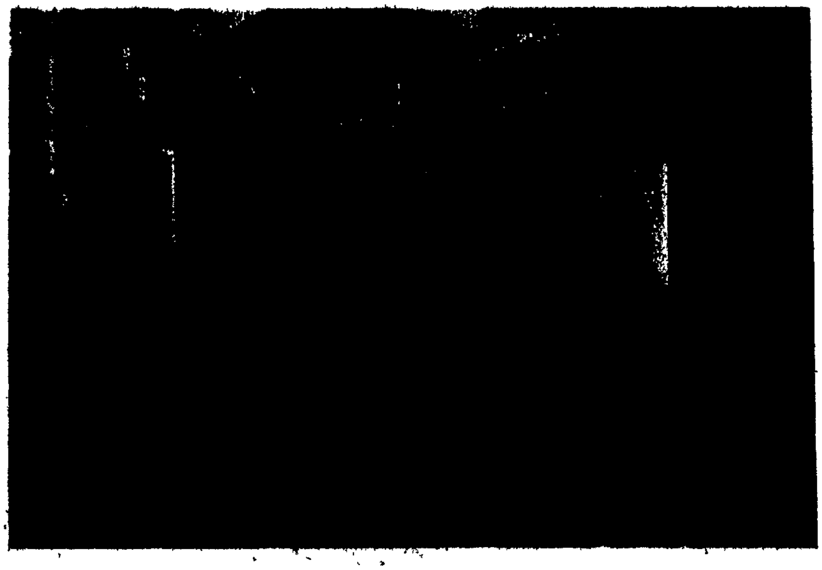

Figure 2.3 General layout of the equipment

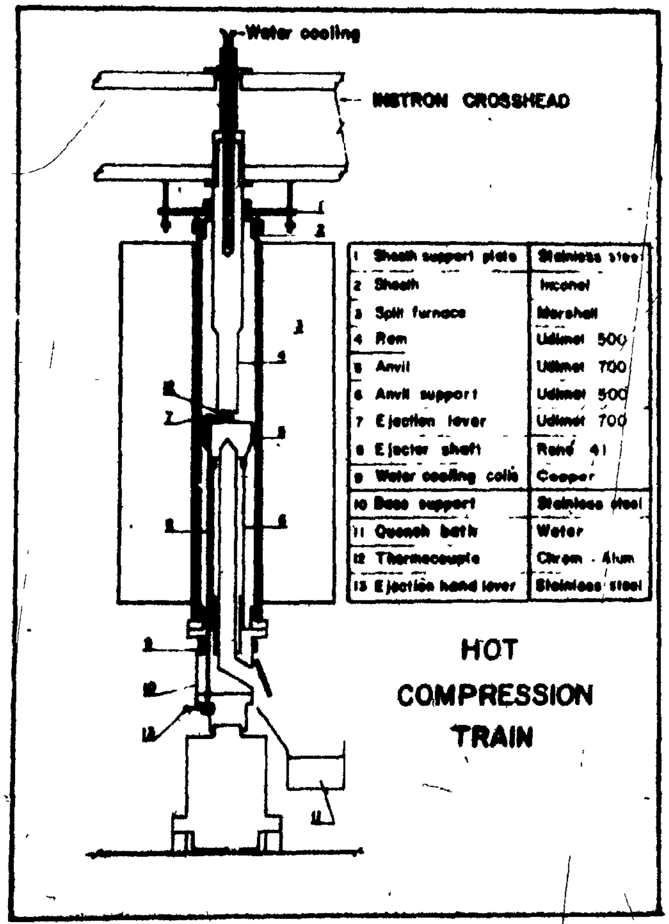

1	Sheath support plate	Stainless steel
2	Sheath	Inconel
3	Split furnace	Marshall
4	Ram	Udimet 500
5	Anvil	Udimet 700
6	Anvil support	Udimet 500
7	Ejection lever	Udimet 700
8	Ejector shaft	René 41
9	Water cooling coils	Copper
10	Base support	Stainless steel
11	Quench bath	Water
12	Thermocouple	Chrom - Alum
13	Ejection hand lever	Stainless steel

Figure 2.4 Cross-section of the hot compression train

2.3.1 Compression Tools for High Temperature Service

The essential features of a compression train are the upper and lower anvils and their supports. The design of these components depends critically on the service temperature and therefore on the materials chosen for their fabrication. In the present work, the tests carried out on copper were in the temperature range 400 - 600°C. In this range of temperatures, the conventional equipment utilizing nickel-base superalloy tooling was considered adequate. However, experience with earlier tests(39,70) indicated that there is a tendency for the superalloy anvil faces to become indented after three or four test cycles. The loss of smoothness of the anvil faces leads to imperfect flow of material at the anvil/sample interface, in spite of the use of suitable lubricants.

To overcome this difficulty, it was decided to use high purity alumina inserts in the anvil surfaces. Such ceramic inserts have to be retained positively by the superalloy anvils because a substantial tensile force is generated during unloading of the samples. This force is required to break the adhesive glass film between the sample and the anvils which is present by virtue of the glass lubricant. The solution to this problem involved the preparation of flat discs of alumina with conical edges, as shown in Figure 2.5. The semi-apex angle of the conical surface was chosen so as to minimize looseness of the inserts when the difference in thermal expansion coefficient between the two materials is taken into account.

The insert was attached to the upper anvil using a conical nut, as shown in Figure 2.5. The same technique could not be used on the lower anvil because of the presence of services such as the argon supply tube, the quench lever and thermocouples. Here, a tapered circular recess was machined into the center of the lower anvil. The maximum diameter of the recess was designed to be 120 μm less than maximum diameter of the insert. To attach the insert to the lower anvil, the anvil was first heated to ∿800°C and the unheated ceramic facing was then inserted into position. On cooling, the ceramic insert was held rigidly in place by the contraction of the superalloy. At high temperatures, the insert was still positively retained, as the difference in the amounts of thermal

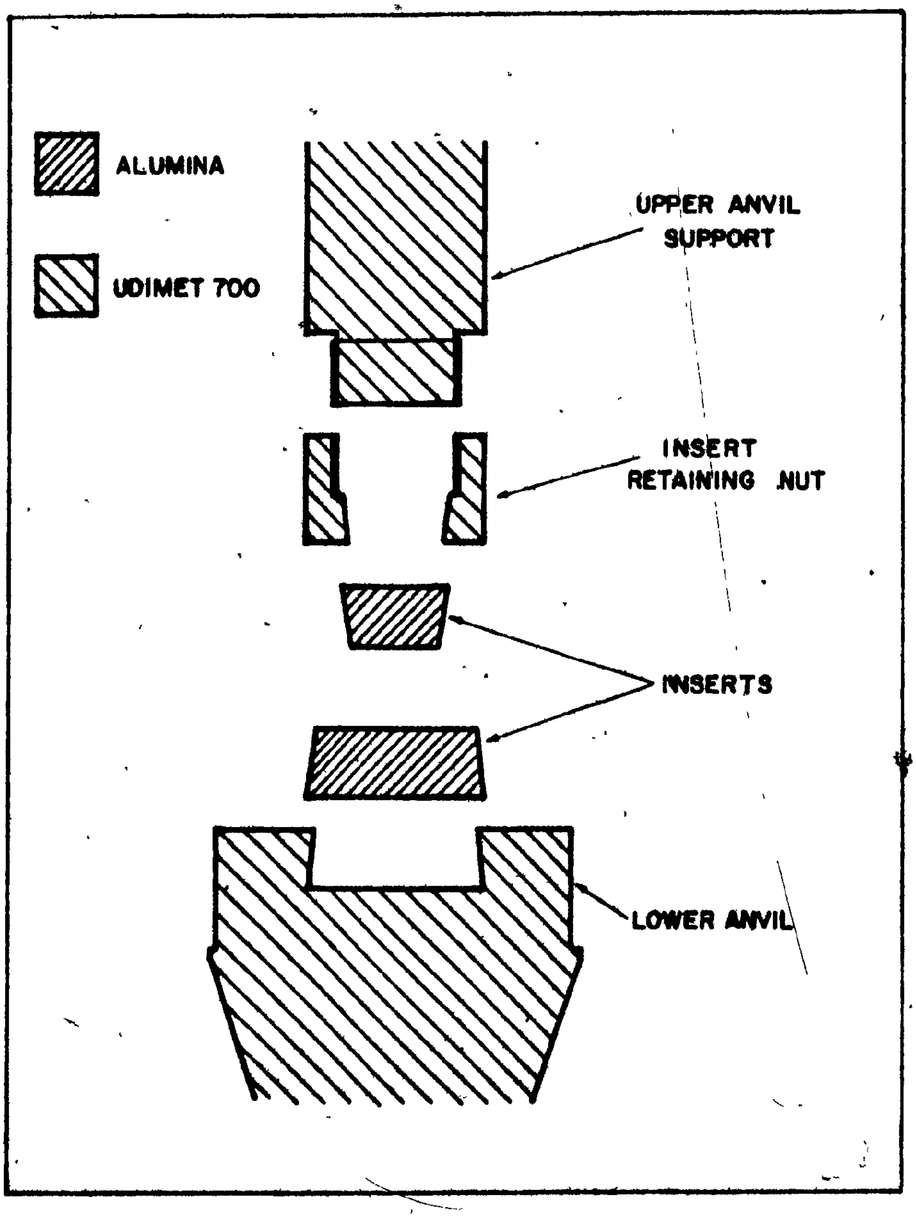

Figure 2.5 Schematic representation of the geometry of ceramic inserts in the upper and lower anvils

expansion in the two materials was insufficient to loosen it. Before placing the anvils in service, the surfaces of the ceramic inserts were ground flat.

2.3.1.1 Molybdenum Based Alloy Tools

The recommended maximum operating temperature for nickel-base superalloys is 950°C. For temperatures in excess of 1000°C, the precipitation hardening agents tend to redissolve, which leads to a considerable drop in the strength of the components. For the experiments on the Nb-bearing HSLA steels, however, the austenitizing treatment called for heating the compression tools to 1200°C. In view of this, it was decided to experiment with alternative tooling materials. To begin with, a set of tools identical in design to the nickel base superalloy ones was made from TZM[†]. This material retains its high strength characteristics up to 1300°C. However, as it is a molybdenum-based alloy, it is very susceptible to oxidation at elevated temperatures. To overcome this difficulty, the tools were plasma spray coated with magnesium-zirconate. The coated tooling was found to behave well at elevated temperatures up to 1200°C. Unfortunately, the rapid temperature cycling inherent in the test procedure ultimately led to spalling of the protective coating, with consequent oxidation of the tools. Furthermore, the thermal cycling caused rapid grain growth in the TZM alloy, which resulted in embrittlement of the material, and ultimately led to cracking of the components during re-machining and maintenance. Because of all these difficulties, it was decided to abandon the use of TZM alloys.

2.3.1.2 Ceramic Tools

In consequence, the compression train was completely redesigned to accomodate the use of solid bars of high purity alumina for the upper and lower anvils. The alumina bar stock was especially prepared and supplied by McDanel Refractories Inc. in the form of 3.8 cm (1¼") diameter slip cast round bars.

[†] Trade mark of the Climax Molybdenum Company.
Composition: minimum 0.5% Ti, 0.1% Zr, 0.01% C, balance Mo.

In high temperature compression testing, precise definition of the initial yield stress requires that the anvil faces are parallel and perpendicular to the axis of loading. In the case of all the tooling systems described above, the end faces were ground perpendicular to the loading axis prior to the assembly of the equipment. This procedure typically resulted in the anvil faces being parallel to within 12 minutes of arc. This corresponds to a strain difference of less than 0.002 across the present samples.

The lower anvil was mounted in a nickel-base superalloy component which was press fitted into a water cooled stainless steel base rigidly fixed to the Instron load cell. The upper tool was mounted in a nickel-base superalloy fitting water cooled internally along half its length. Adequate water cooling of the extreme ends of the tools was necessary to prevent damage to the "O" ring seals and the the load cell. The entire loading assembly was contained within a tubular, fuzed quartz chamber, which itself was water cooled at its extreme ends. The compression chamber assembly was enclosed in a split furnace, which could be raised or lowered on the crosshead.

The lifting of the furnace with the crosshead was part of the new design and was necessary for two reasons. It was required primarily to reduce the severe thermal gradient set up in the unmodified tooling during the insertion of a specimen at the start of each experiment. (In the original design, this was done by opening the split furnace and then raising the crosshead). It also served to avoid a large drop in temperature (∼200°C)(39,134,136) during the same operation. In this way, by raising the furnace and crosshead in unison, the sample could be placed on the lower anvil and the drop in the chamber temperature could still be maintained in the vicinity of 30°C. Once the system was closed again, the temperature returned to its previous level within 2-5 minutes.

The primary difficulty associated with the use of the ceramic tools, even with these precautions, was their suseptibility to thermal shock. There appears to be little information available to enable the experimentor to minimize failure due to this effect. The first set of tooling was subjected to rapid heating and cooling rates in an attempt to define the operating limits and finalize the design. It was found that, as long as the heating and cooling rates did not exceed 7°C/min, up to 40 tests could be carried out with a single set of tools before replacement became necessary. For the full set of Nb steel tests, 8 sets of ceramic tools were used and the main features of this assembly are illustrated in Figure 2.6.

2.3.1.3 Furnace Support Mechanism

In the design of the furnace lift mechanism, two functions were of primary concern. To begin with, it was required that the furnace could be removed from around the test chamber, so that maintenance could be carried out on the test chamber components. Secondly, it was necessary to ensure that the furnace could ride up and down with the crosshead at all times, except when the anvils were within 3cm of being in contact. In this way, the furnace and the hot zone would remain stationary relative to the tools during a test.

These two requirements were satisfied by attaching the furnace to a case hardened bearing shaft mounted at the rear of the Instron crosshead. This shaft was rigidly fixed to the moving crosshead and was supported by a linear ball bearing mounted on the lower part of the Instron frame. The two halves of the furnace were connected together by means of the standard Satec hinge mechanism. The extreme ends of the hinge shaft were fixed to another linear ball bearing assembly placed on the lift bearing shaft above the first linear bearing assembly. The furnace could thereby be removed from around the test chamber by using the double hinge mechanism. Furthermore, the furnace could be raised along with the crosshead by placing a fixed collar on the shaft immediately below the furnace bearing. The collar was located on the shaft so that once the anvils were within 3 cm of contact, the furnace was supported via the lower crosshead by the furnace table only. On the other hand, when the crosshead was raised, the furnace was lifted along with the crosshead by the collar.

2.3.2 Strain Rate Control

During uniaxial compression at a constant deformation rate, the true strain rate continuously increases; for example, in a true strain interval of one, the strain rate increases by a factor of 2.3(141). To

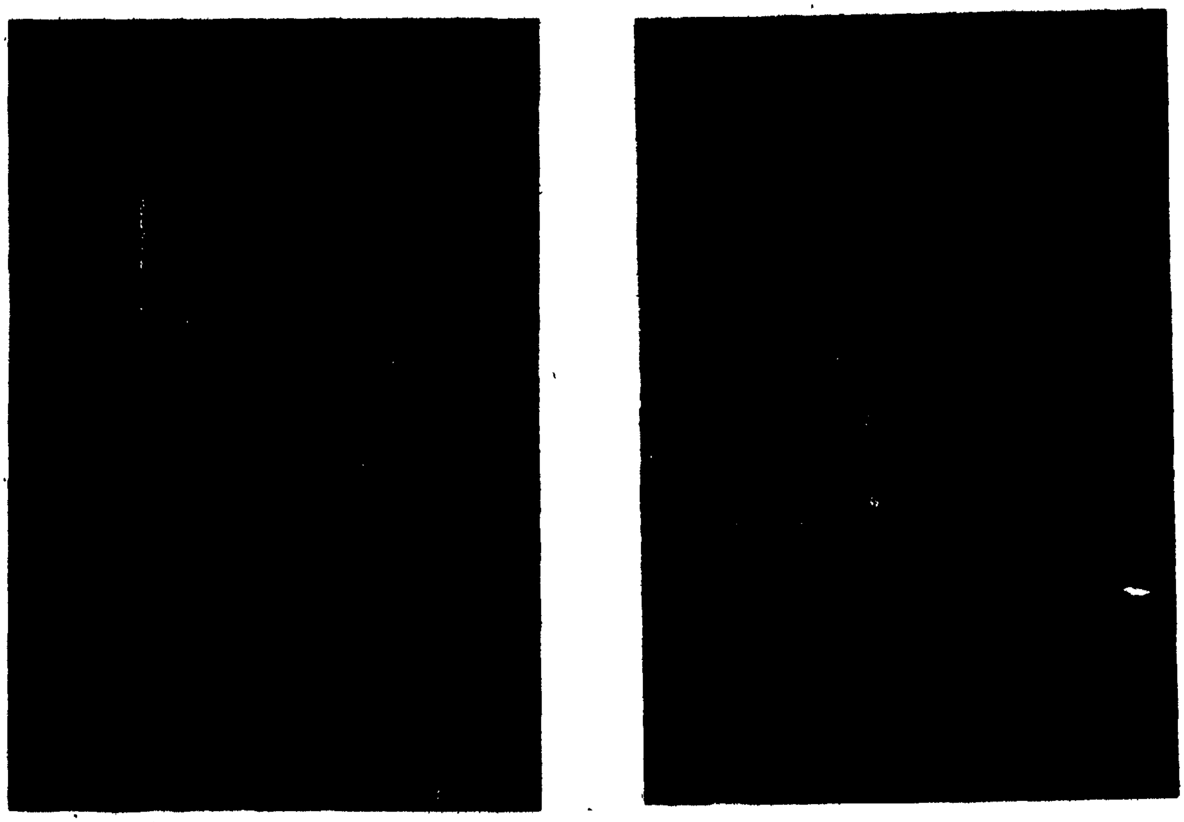

Figure 2.6 General view of the high temperature alumina assembly

obtain a constant true strain rate, the crosshead velocity had to be made to vary in proportion to the instantaneous height of the specimen. The relation between instantaneous height and crosshead velocity can be obtained as follows.

The true strain in compression is given by:

$$\varepsilon = -\ln\frac{h_o}{h} \qquad (2.1)$$

where h_0 is the initial height of the cylinder and h is the instantaneous height. Differentiation with respect to time leads to:

$$\dot{\varepsilon} = \frac{1}{h}\frac{dh}{dt} \qquad (2.2)$$

Under constant strain rate conditions,

$$\dot{\varepsilon} = \dot{\varepsilon}_c = \text{const}$$

so that the crosshead velocity v, is given by:

$$v = dh/dt = \dot{\varepsilon}_c h \qquad (2.3)$$

Equation 2.3 shows that v must decrease linearly with h if $\dot{\varepsilon}$ is to be maintained constant. To achieve this condition, a closed loop control system was built. The basic idea of the device was to take the crosshead position during compression as representative of the instantaneous specimen height.

When the Instron is equipped with the variable speed accessory, the crosshead velocity is linearly dependent on the angular position of the 10-turn speed regulating potentiometer (b) in Figure 2.7. This potentiometer can be replaced by another speed regulating potentiometer (a) whose slidewire can be arranged to follow the crosshead position. In this way, the motion of the crosshead will cause its speed to vary so that, with the appropriate mechanical link between crosshead and potentiometer, the strain is maintained constant during testing. A description of this apparatus has already been given in detail elsewhere (39,134,136,140).

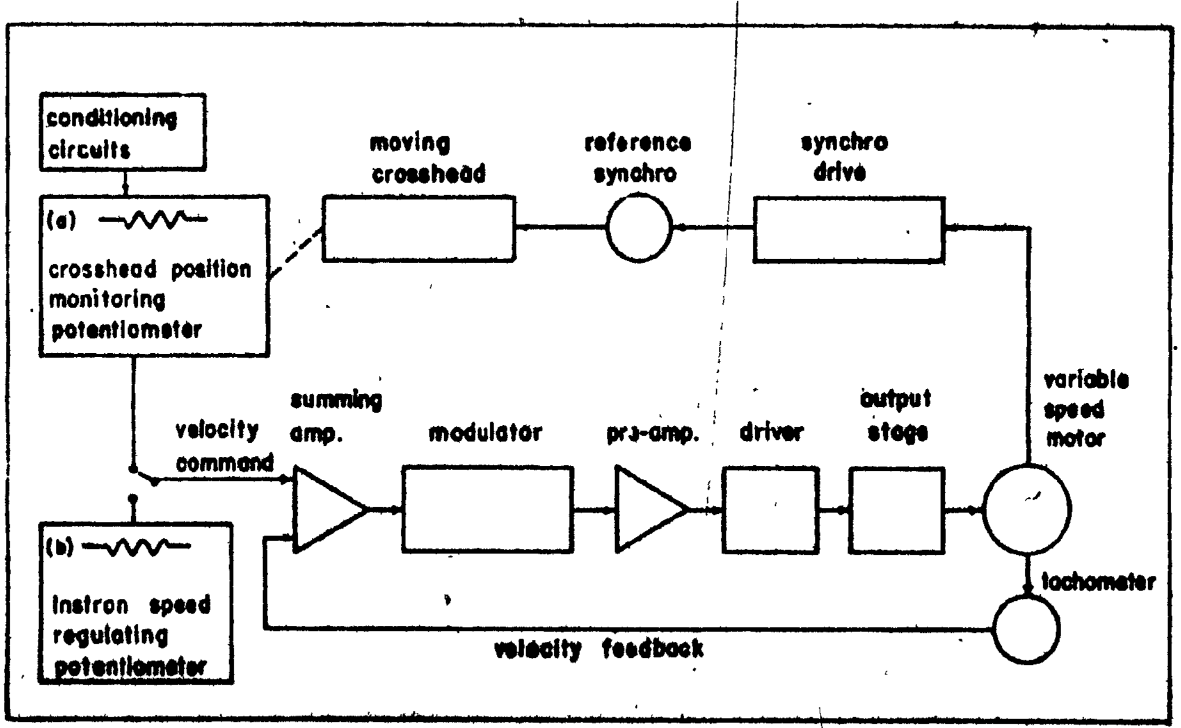

Figure 2.7 Block diagram of the crosshead speed control system

In the use of the apparatus, there are three main sources of error$^{(140)}$. The first arises from drift in the gain of the variable speed servo amplifier and is really inherent to the Instron. The drift is small and leads to deviations from the base speed of less than 1%. The second source of error, which is actually very small (±0.2%), comes from non-linearities in the position monitoring potentiometer.

A third and more serious source of error arises from the elasticity of the compression train and the effect this has on the specimen strain rate. Under most testing conditions, this leads to a specimen strain rate which is lower than the nominal one, that is than the strain rate based on the crosshead velocity. It may be shown$^{(140)}$ that the difference between the nominal strain rate and the specimen strain rate $\Delta\dot{\varepsilon}$ is given by

$$\Delta\dot{\varepsilon} = m/l(dL/dt) \qquad (2.4)$$

where m is the machine stiffness, l is the sample length and dL/dt the rate of increase of the developed load.

The load-time curves recorded in the present experiments indicated that the rate of increase in developed load was a function of both strain rate and temperature, larger values of dL/dt occurring at the higher strain rates and lower temperatures, so that the greatest error in strain rate occurs under these conditions. However, under the experimental conditions used in the present experiments, the strain rate error never exceeded 5%.

2.3.3 Temperature Control

The constant temperatures used in the present investigation were produced by means of a Satec three-zone platinum wound split furnace. Temperature control was provided through a current proportioning Leeds and Northrup Electromax II controller, which in turn drove 3 Magnetics Inc. SCR controllers in a master/slave configuration. The temperatures next to the furnace heating elements were monitored by three Pt/Pt-13% Rh thermocouples (one for each zone). Any one of the three zones could be used as the master. In this work, only the central zone was controlled. The current to each zone could be adjusted independently, using 3 potentiometers mounted on the front panel of the temperature control console. During the initial setting up of the apparatus, these potentiometers were adjusted to give a uniform (±2°C) temperature zone between the anvil ends.

Temperature measurement <u>within</u> the test chamber was by means of two Pt/Pt - 13% Rh thermocouples placed beside the sample. One output was recorded continuously on a Leeds and Northrup Speedomax H recorder and could be read directly on a Thermo-Electric digital temperature display. The second output was a reference thermocouple connected to a manual Leeds and Northrup millivolt potentiometer. The latter was used to calibrate or check the temperature readings on the other instruments.

2.3.4 <u>Atmosphere Control</u>

All the compression tests in the present investigation were carried out under a flowing argon atmosphere to prevent oxidation of the samples and tooling at high temperatures. Since the test procedure (Section 2.5) involved placing the samples in the furnace with the latter at high temperature, it was necessary to establish a pure argon atmosphere in the shortest possible time. To this end, the gas supply system shown in Figure 2.8 was built; it was designed so that the test chamber could be evacuated rapidly and purged with argon after insertion of the test pieces. The chamber was evacuated by means of a Precision Scientific Co. 75 l/min two-stage rotary pump. A vacuum of 5×10^{-2} torr was usually reached within approximately 40 seconds of pumping. Having evacuated the furnace chamber, argon was admitted to the chamber once more. When a positive pressure was attained, as indicated on the pressure gauge, the argon was allowed to escape to atmosphere through an oil-filled bubbler. The argon used was high purity grade 47* supplied by the Canadian Liquid Air Co., which was further purified by being passed through an Engelhard Deoxo unit to catalytically remove traces of H_2, O_2 and CO_2. The gas was finally dried in two towers containing Drierite compound ($CaSO_4$).

---

* Maximum impurities: O_2 = 0.1 ppm; N_2 = 23.0 ppm; H_2 = 2.0 ppm; CO_2 = 0.5 ppm; H_2O = 5.0 ppm; total hydrocarbon = 0.5 ppm.

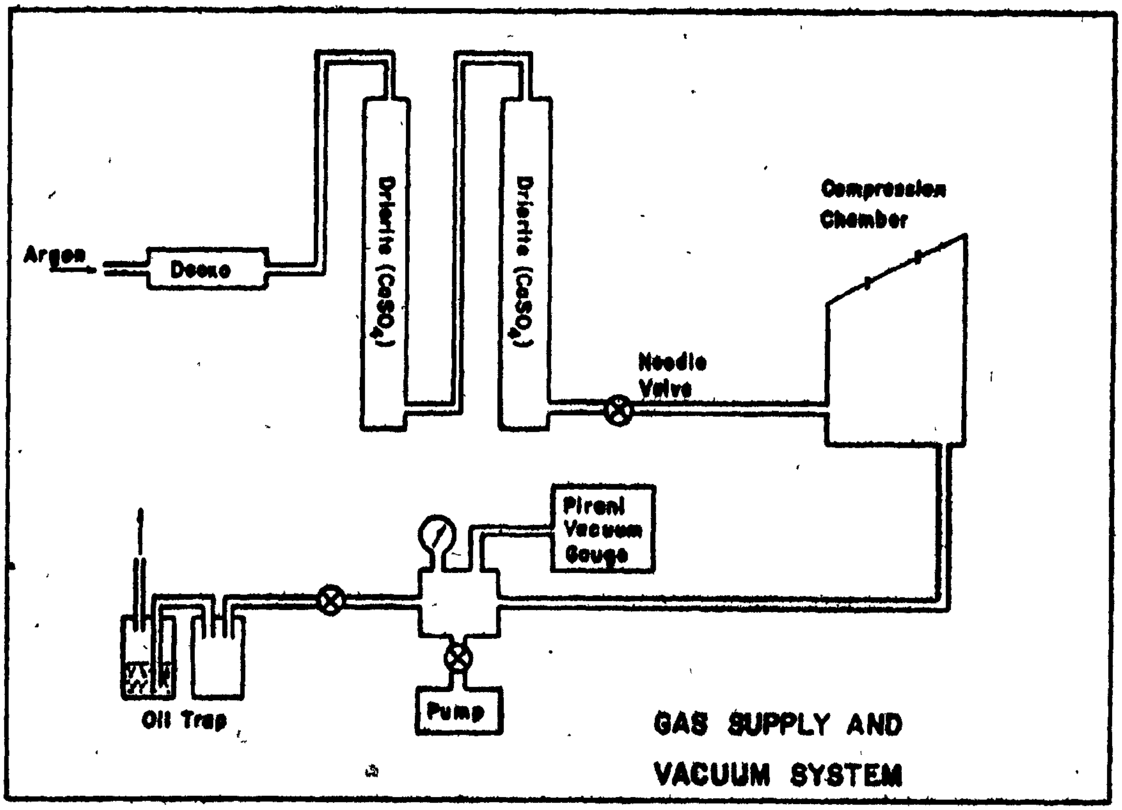

Figure 2.8 Schematic diagram of the gas supply and vacuum system

2.3.5 High Temperature Lubrication

One of the greatest experimental difficulties in hot compression is to minimize friction between the sample and the anvils. Low friction is required to minimize barreling and thus to maintain the condition of homogeneous deformation throughout the test. Interface friction can be greatly reduced by using suitable lubricants(142,143), such as teflon(144) and liquid glass(39,134-138,145-149). Furthermore, if appreciable strains are to be imposed, it is advisable to cut circular grooves into the end faces of the samples(142,147-152). These act as lubricant reservoirs, and by collapsing during testing, feed further lubricant onto the expanding specimen/tool interface. Tool friction is also decreased by use of hard, polished platens, which should be protected from oxidation by testing in a controlled atmosphere.

Glasses have been used for some time as lubricants at elevated temperatures. It has been suggested(145) that glasses with a viscosity of 10^4 poise at the testing temperature are required to give adequate lubrication. Nevertheless, it has also been reported(134) that there does not seem to be a close correlation between viscosity and the coefficient of friction at the sample-anvil interface, so that the 10^4 poise value does not seem to be a critical one.

For tough pitch copper in the temperature range from 450-600°C, the glass powder used in the present experiments had the composition recommended by Uvira(3) for this temperature range. The components† were finely ground to -200 mesh, mixed thoroughly, and melted at about 1000°C in a ceramic crucible. The melt was then poured into water and the glass granules were crushed and reground to a -200 mesh powder.

The high silica glass lubricants used successfully with our superalloy tooling(39,134-137) were found to react with the alumina tooling. The reaction produced a network of fine cracks on the anvil faces.

Alternative glass compositions were suggested by Dr. N. Leopold (153) of the University of Kentucky, and supplied by the Corning Glass Works. For the temperature range between 900-1200°C, the best lubrication was achieved with Corning Glass Number 7050. The lubricant was applied as a suspension in acetone and was deposited on the end faces of the

---

† B_2O_3 = 15 wt%, PbO = 75 wt%, window glass 10 wt%

specimens, as well as along the sides of the specimens, to prevent excessive oxidation during the initial placement of the sample in the hot furnace.

2.4 AUTOMATIC TEST CONTROL AND DATA ACQUISITION

As mentioned above, the primary aim in the present work was to study the softening of materials between intervals of hot working. To this end it was necessary to make precise measurements of the initial flow stress (i.e. the 0.2% yield stress) during the first and second loading cycles (see Figure 2.1). Furthermore, close control was required over the strain at which the interruption was to take place and over the delay time prior to reloading. Some difficulties had been experienced in earlier tests(39) where all the operations of the Instron machine had been controlled by the operator. In these tests the unloading and reloading functions had been achieved by manually operating the Instron control buttons. In addition, stress/strain curves were produced by the laborious picking of load and displacement pairs from a chart record and calculating the true stress and true strain. These procedures had necessarily led to a certain lack of reproducibility with regard to the interruption strain and delay times of below two seconds duration. Furthermore, the initial flow stress during the first and second loading tended to be rather poorly defined because of the relatively few data points used to define the flow curve, and because of systematic errors incurred during manual digitization of the chart records. In view of the repetitious nature of the tests, coupled with the large number of tests required to define the softening behaviour, it was decided to automate the test procedure.

2.4.1 Instron/Computer Interfacing

A large scale CGE 4020 process control computer was available for use by our laboratory on a time sharing basis. The interface between the Instron machine and the computer consists of two parts. The first, the control interface, was designed and built by Luton to allow the Instron test machine to be operated under software control. The interfacing hardware was made up of six 36 Vdc relays arranged in a logic sequence so that the switching of two reed relays in the computer digital output module could duplicate the primary control functions of the Instron machine. The coded functions were down, stop, return and neutral. The last function has the effect of resetting the test machine for manual operation. This function was of particular importance, as it allowed the operator to carry out the initial setting-up of the test manually, in the normal way described below.

In addition to the control interface, a two-channel analogue interface was also built. In early tests using computer control, load signals from a 10,000 kg Instron load cell, and the output from an LVDT mounted on the moving crosshead were amplified by means of the preamplifiers contained in a Hewlett-Packard 7701A recorder (i.e. an HP8803A low level preamplifier and an HP8805A carrier preamplifier, respectively). The high level signals (range ±3 Vdc) from these devices were transmitted to the computer by 2 channels of an 18 channel cable of about 150 m. length. Here the signals were digitized under program control, by means of a Vidar Model 521 analogue/digital converter. Although this arrangement proved adequate for tests of short duration and high load level, it was not suitable for use with long term tests and low load levels. The extremely stiff Instron load cell produced output signals at the μV level, and was consequently prone to pick-up of electrical noise from other apparatus in the laboratory. Furthermore, the LVDT-carrier preamplifier combination was prone to drift over longer periods of time. Such variations in the load and displacement signals severely limited the development of optimum process control programs.

To overcome these difficulties, an analogue interface was built that utilized a Lebow Model 3116 load cell of 2000 kg capacity and a Hewlett-Packard Model 7DCDT-500 displacement transducer with a range of ±1 cm as primary elements. These devices were excited by two Hewlett-Packard Series 62000 dc power supplies. The output of the DCDT is 2.7 V/cm and is transmitted directly to the computer. The output of the load cell is 15 mV/1000 kg. This signal is amplified by means of an Analog Devices 605 integrated amplifier with a gain factor of 100. The high level output signal of the primary devices, coupled with the use of high stability power sources, minimizes line noise problems as well as imparting long term stability to the measuring system.

As mentioned above, the analogue digital conversion was carried out by means of a Vidar 521 A/D converter. This is a multi-range instrument with a maximum scan rate of 50/s at a conversion rate of 1.66 ms.

2.4.2 Test Control Programs

Control of the compression test and data acquisition are achieved with the aid of two main program segments. The task of the first segment is to allow the operator to enter test and machine parameters and to calibrate the load and displacement transducers. The second program segment is used to control the testing machine and acquire load and displacement data. Some more important aspects of the operation of these programs will now be discussed in turn.

The first function of the calibration program is to check whether sufficient storage space is available to store the data of the current test in the file area of the 4020 disk mass storage unit. The total file area available for the test data is 12,288 words. A typical test requires about 1024 locations to completely characterize the test; consequently the data of about 12 complete tests can be stored before the file is full. Once full, the test data in the scratch file area is transferred to magnetic tape as a permanent record.

If the scratch file area is not full, the calibration program permits the operator to enter the test identification code and the test parameters in conversational mode. The data required to define the test set-up are the sample height and diameter, the initial crosshead speed and return speed, the interruption and total strain, the delay time and the load range. Once these data have been entered, the program carries out calibration procedures on the load and displacement channels. Here, the excitation voltage of the two transducers is measured and recorded for later use in the determination of loads and displacements. The current reading of the DCDT is compared with that obtained during the initial set-up of the apparatus when the anvils are in contact (see below) and the distance between the top of the specimen and the upper anvil printed out on the teletype. This procedure is important since, as will be shown below, the strain to interruption is determined by lapsed time from the beginning of the test. Therefore the precision with which the start position of the anvil is known will determine the accuracy of the unloading strain. With this information in mind, the operator adjusts the crosshead position so that the upper anvil is 0.40 ±0.02 mm above the top of the specimen. The test program assumes this operation is complete when the time marks of the test are calculated. The final operation of this program is to compute the appropriate conversion ranges from the load and displacement signals based on the maximum load and maximum strain data entered previously.

When these preliminary procedures are completed, the test control program is turned on, and the test may be started by means of a system program interrupt accomplished by pressing the "break" button on the teletype.

The first task of this program is to ensure that no other functional program can run during the test. This is achieved by modification of the system program which has the effect of suspending the time sharing operations. With this accomplished, the computer operates as if it were dedicated to the control of the Instron alone. This function was required because of the close control of time required to bring about reproducible interruption strains.

The program then sets the Instron crosshead in motion and digitizes the load and displacement signals. The rate of data acquisition is determined by the strain rate of the test so that about 200 load-displacement pairs are obtained for each loading cycle. Furthermore, during the earlier part of each loading cycle, the rate of scanning is adjusted so that one pair is obtained for each strain increment of 0.001. This high rate of scanning is continued up to a true strain of 0.1. At higher strains, the scanning rate is reduced to give one data pair for every 0.005 strain interval. Once the lapsed time from the beginning of the test is equal to the time required to reach the strain of interruption, the program switches the Instron to the return mode to unload the sample. During the unloading sequence, the load is monitored at a rate of 50/s until zero load is detected; at this point the crosshead motion is stopped. The program then delays for the required holding time and then restarts the crosshead. With the second loading cycle, the data acquisition proceeds in the manner already described above. The lapsed time to the true strain to interruption and the delay at zero load are both timed to the nearest 8.3 ms.

At the completion of the test, the crosshead is reversed in the return mode to unload the sample and permit it to be ejected from the compression chamber into a quench tank. The data acquired during the test is stored in the disk file area for later use.

2.4.3 Automatic Data Handling

The data accumulated during the test consist of the voltage output from the load and displacement transducers. The true stress-true strain curves were obtained from the data by the use of yet another computer program. At any instant, the uniaxial force F_i and the measured crosshead displacement d_i were obtained from these data and the calibration factors present as constants in the computer program. To obtain the true specimen strain from the crosshead displacement, a correction had to be made for the elastic compression of the compression tooling and the elastic extension of the drive screw members of the Instron testing frame. The distortion of the loading members was measured as a function of load by recording the load and displacement while the crosshead was driven at constant speed with the anvils in contact. These tests were carried out over a range of crosshead speeds and different temperatures. The results of all these tests are shown in Figure 2.9. It can be seen that, within experimental error, the machine distortion d_m is independent of temperature and crosshead speed. This result is not unexpected as most of the components that contribute to the elastic contraction and extension lie outside the high temperature zone. The data in Figure 2.9 were fitted by an expression of the form:

$$d_m = a(F_i + b)^d - c \qquad (2.5)$$

where a, b, c and d are constants.

The true instantaneous specimen height h_i is then given by

$$h_i = h_o - d_i + a(F_i + b)^d - c \qquad (2.6)$$

where h_o is the initial sample height.

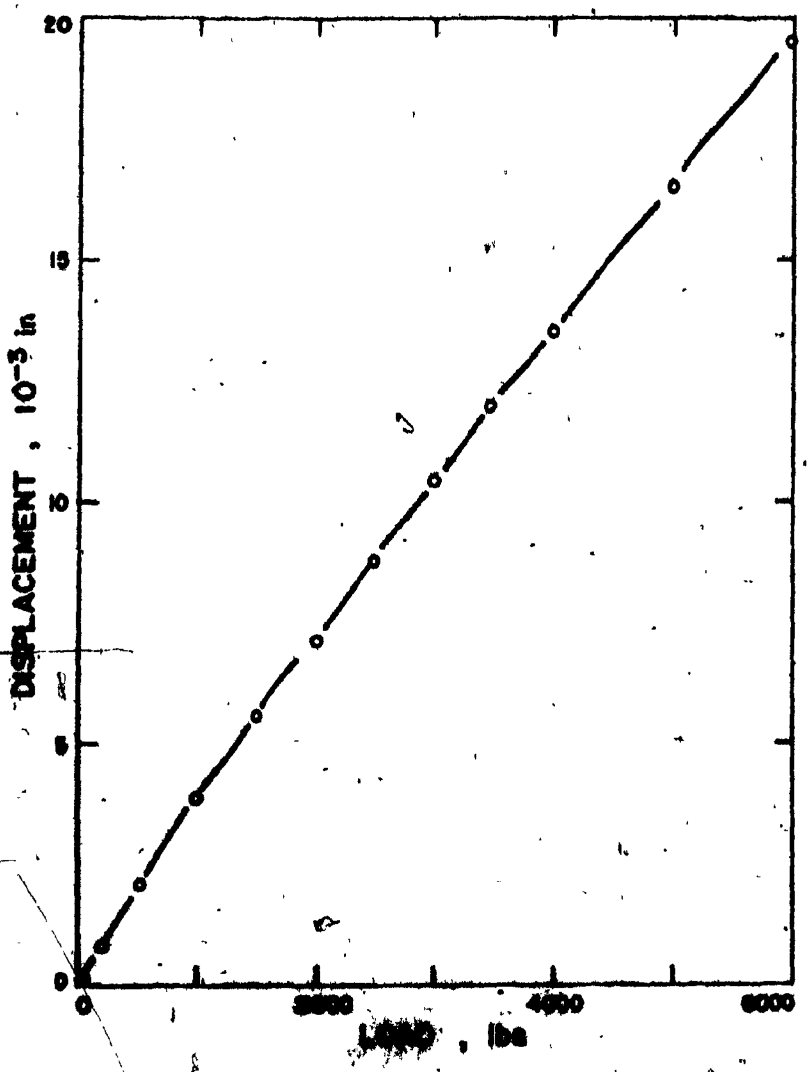

Figure 2.9 Elastic distortion of the Instron frame and hot compression train in the absence of a specimen

Once these corrections have been made, the true strain is calculated from the familiar relation

$$\epsilon_i = -\ln h_i/h_0 \tag{2.7}$$

where the minus sign is used to avoid the necessity of calling compressive strain negative. The true stress σ_i is obtained from the expression

$$\sigma_i = F_i h_i/A_0 h_0 \tag{2.8}$$

where A_0 is the original area of cross-section of the sample.

The true stress and true strain values for each of the data pairs obtained during the test run were computed in the curve plotting program in the manner described above. The true stress-true strain curves were plotted by the use of an on-line California Computers, Calcomp digital curve plotter. The program defined the curves by simply plotting the discrete points rather than by fitting a smooth curve. Three curves were drawn for each test, as shown in Figure 2.10. The first is a complete stress-strain curve, Figure 2.10a, including both loading cycles. The other two, Figure 2.10b and 2.10c, represent the first 0.1 strain of each loading cycle. In these latter plots, the strain scale is expanded by a factor of 10 to facilitate the determination of the yield stress or proof stress. The yield stress values were defined by the use of an offset method(154), as illustrated schematically in Figure 2.11. On the stress-strain diagram, the interval OM is the specified value of offset (0.002). The line MN is drawn parallel to the loading line in the microstrain region (OA). The value of the flow stress at the intersection (R) is taken as the yield stress.

2.5 TEST PROCEDURE

Prior to starting a series of tests, the furnace and Instron controls were adjusted for the desired experimental conditions and temperature. Once the test chamber had come to temperature, the anvils were brought together so that they were just in contact and the various crosshead position safety switches were adjusted to prevent self-compression of the testing train. With the anvils in contact, calibration

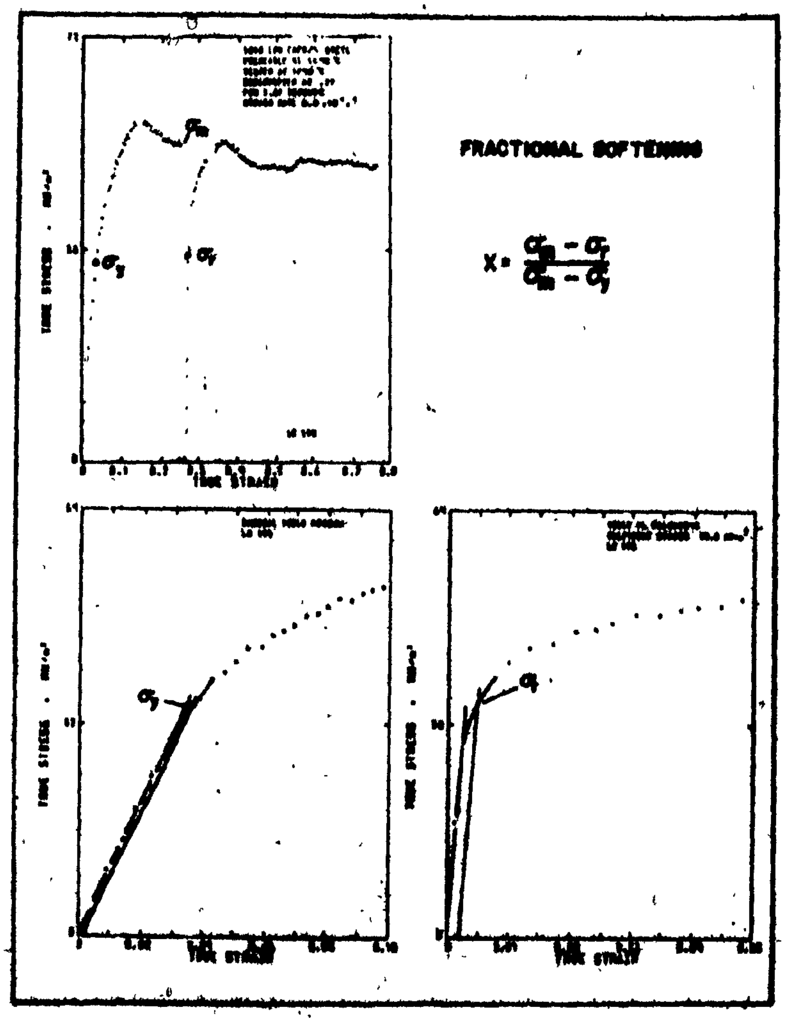

Figure 2.10 Typical set of computer plotted curves obtained for one of the experimental conditions

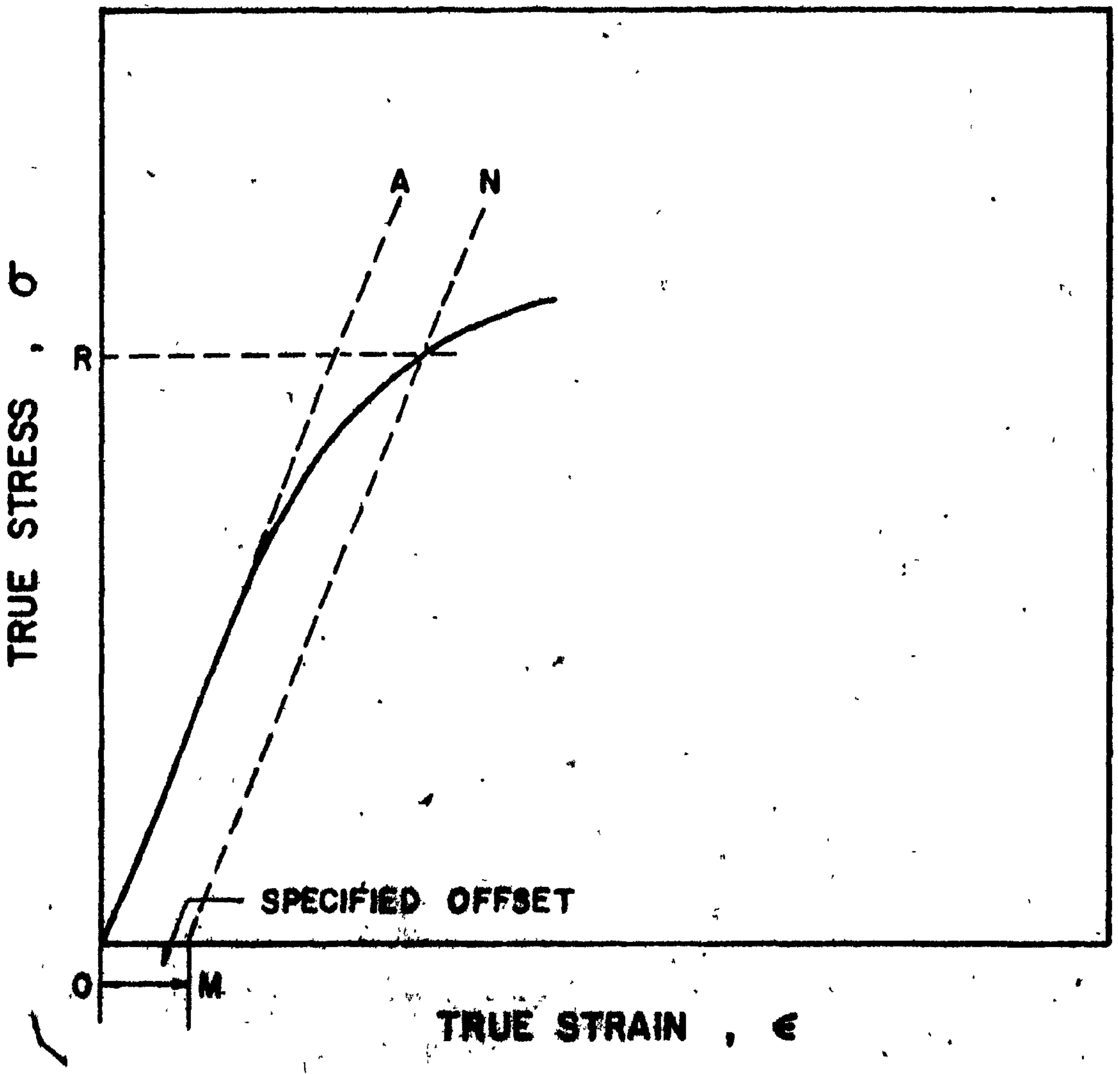

Figure 2.11 True stress-true strain diagram for determination of the yield stress by the offset method

of the constant strain rate device was performed with the micrometer screw being used to simulate crosshead motion. The constant true strain rate device circuits were found to be very stable so that a complete series of tests could be carried out at the given temperature without recalibration. Only when the temperature was changed was a new calibration of the constant strain rate apparatus necessary. While the anvils were in contact, a small program was initiated on the GE4020 computer which measured the excitation and output voltages of the DCDT transducer. The zero reading made in this way was stored in a table for subsequent use in the calibration program described above. The gauge length and the return dials on the Instron frame were then adjusted so that the specimen would not be compressed beyond a strain of 0.9, even if computer control of the test failed.

To start a test, the furnace was raised on the crosshead, and a glass coated sample placed between the compression platens. The chamber was lowered and closed while argon was introduced into the system. The chamber was evacuated and purged with argon four times before a constant flow of argon at 0.6 l/min was maintained. A relatively pure argon atmosphere was fully established after three to four minutes. In the case of the Nb-bearing steel, the specimens were preheated at the temperature of austenitization for 30 minutes and then cooled to the testing temperature at a cooling rate depending on the testing temperature. Samples were held at the testing temperature for 5 minutes, to allow the temperature to stabilize prior to compression. The tough pitch copper specimens, on the other hand, were brought directly to the testing temperature and held for a period of 30 minutes prior to compression. During this holding period, the calibration program described above was initiated and the machine and test parameters entered in conversational mode. Once the prior treatment of the test specimens was complete, the test was begun as described previously.

On completion of a test cycle, the sample was removed from between the anvils and, in the case of the tough pitch copper samples, quenched to room temperature.

Once a new sample was introduced into the test chamber and the preheating procedure begun, the plotting program was started so that the stress-strain data of the current test would be available before the commencement of the next one. In this way the softening behaviour observed under one set of testing conditions could be used to decide on the testing conditions for the next test. For example, if no softening had been observed after a 10s delay in the previous test, the delay time for the current test would be chosen to be longer than 10s.

Once the softening behaviour of tough pitch copper was established for a given prior hot working treatment, samples were prepared for metallography. For these samples, only one deformation cycle was used. The samples were strained to the given strain and unloaded automatically; a stop watch was started as the sample was unloaded. When the desired delay period was complete, the quench mechanism was activated and the watch stopped when the sample entered the water. These samples were sectioned, mounted and prepared for metallographic examination.

The data obtained in the present study represent the results of about 1000 compression tests. The complete stress-strain curves obtained for the different testing temperatures, strain rates and interruption strains are presented in Appendix 2.1.

The yield stress measurements made on the expanded stress-strain diagrams of the initial portion of each strain cycle were used to characterize the softening behaviour of the material. These data will be presented along with the metallographic results in the chapter that follows.

CHAPTER 3

EXPERIMENTAL RESULTS

The purpose of the present research has already been stated in the previous chapter, along with a description of the development of the experimental technique to its current level of sophistication. As already described in Section 2.2, special attention was given to the choice of experimental materials, since one of the main aims of the current study was to verify the hypothesis proposed earlier by the present author(39,69,70). In this work, it was of interest to determine whether the hypothesis was restricted to the behaviour of carbon steels, or whether it applies generally to FCC materials at high temperatures. For ease of presentation, the experimental results are divided into the following two groups:

1. effect of hot working on the progress of static softening processes; and
2. effect of grain size on the high temperature mechanical properties;

but before they are introduced, the experimental conditions that were used will be presented.

3.1 EXPERIMENTAL CONDITIONS

The tests were carried out on three main materials: tough pitch copper, a 0.06% C low carbon steel and a Nb(Cb)-treated 0.07% C steel. The tests were conducted at constant true strain rates from 8×10^{-3} to $8 \times 10^{-2} s^{-1}$ and in the temperature range from 450 to 1040°C.

The experiments performed on tough pitch copper were of three types:

a) The first series of experiments was carried out at three temperatures: 450, 500 and 540°C and at three different strain rates. The latter were chosen so that similar flow curves were obtained for the three temperatures (i.e. a peak stress of 103 MN/m^2 and a steady state stress of 84 MN/m^2). Various interruption strains (see Table 3.1) were then imposed so as to establish the effect of prior working on the softening behaviour.

b) The second series of experiments was carried out at the single temperature of 500^{0}C at a fixed strain rate (1.8 x $10^{-2}s^{-1}$) and employed various interruption strains, Table 3.1. After different delay times, the specimens were quenched and used to determine the recrystallization behaviour, as well as the mean grain size and the grain size distribution.

c) The third series of experiments was designed to establish the influence of grain size on the high temperature yield stress. The experimental procedure for producing different grain sizes was rather involved and will be discussed in more detail in Section 3.3. It consisted essentially of prestraining the strain-annealed samples to a strain of 0.40 at 540^{0} or 600^{0}C and at strain rates of 8 x 10^{-2}, 1.8 x 10^{-2}, 3.7 x 10^{-3} and 7.5 x $10^{-4}s^{-1}$. After holding for sufficient times to allow complete recrystallization to take place, the samples treated at 540^{0}C were quenched to room temperature to permit grain size measurements. The second temperature of 600^{0}C was selected so that larger grain sizes than were obtained at 540^{0}C could be produced. These samples were cooled to 540^{0}C and held to allow complete recrystallization before quenching to room temperature. In this way, it was possible to produce different stable grain sizes in the range 0.056 to 0.81 mm. Another series of samples was given an identical prestraining and recrystallization treatment but instead of being quenched to room temperature, was reloaded at 540^{0}C to determine the yield stress as a function of grain size at the various strain rates. The mechanical testing conditions for this series of experiments are shown in Appendix 3.1.

All the low carbon steel experiments were carried out in the austenite region at constant strain rates of 8 x 10^{-2} and 8 x $10^{-3}s^{-1}$. The temperatures selected were 815, 930 and 1040^{0}C. A homogenization time of 20 minutes at each temperature was employed. The mechanical testing conditions for this material are shown in Table 3.2.

The experiments performed on the low carbon steel modified with Nb were carried out at three temperatures in the austenite region at constant strain rates of 8 x 10^{-2} and 8 x $10^{-3}s^{-1}$. The specimens were preheated at 1150^{0}C for 30 minutes to allow dissolution of the Nb(CN) precipitates and then cooled at 10^{0}C/min to one of the test temperatures of 815, 930

TABLE 3.1

Mechanical Testing Conditions for Tough Pitch Copper

Test Group	Test Temperature °C	Strain Rate s^{-1}	Interruption Strain
1	450	1.8×10^{-3}	0.05, 0.10, 0.15, 0.40
	500	1.8×10^{-2}	0.05, 0.10, 0.15, 0.18, 0.30, 0.40, 0.52
	540	8×10^{-2}	0.05, 0.10, 0.15, 0.40
2	500	1.8×10^{-2}	0.05, 0.10, 0.15, 0.18, 0.28, 0.40, 0.52, 0.64

TABLE 3.2

Mechanical Testing Conditions for the 0.06% C Steel

Test Temperature	Strain Rate s^{-1}	Interruption Strain
815	8×10^{-2}	0.25
930	8×10^{-2} 8×10^{-3}	0.25
1040	8×10^{-2} 8×10^{-3}	0.25

TABLE 3.3

Mechanical Testing Conditions for the 0.07% C Nb-modified Steel

Test Temperature	Strain Rate s^{-1}	Interruption Strain
815	8×10^{-2}	0.30
930	8×10^{-2} 8×10^{-3}	0.25 0.10, 0.25
1040	8×10^{-2} 8×10^{-3}	0.10, 0.25 0.10, 0.25

or 1040°C. Table 3.3 shows the mechanical testing data for the Nb-modified low carbon steel.

3.2 EFFECT OF HOT WORKING ON THE PROGRESS OF STATIC SOFTENING

3.2.1 True Stress-True Strain Curves

The true stress-true strain curves of Figure 3.1 show the strain rate dependence of the flow curves in the model material, tough pitch copper, at 450°C. The effect of temperature on the flow curves for the plain carbon and Nb-modified steels is shown in Figures 3.2 and 3.3 for a strain rate of 8 x $10^{-2}s^{-1}$.

It is clear that the curves for all three materials exhibit similar features. They are typical for the materials that recrystallize dynamically(40) when deformed at temperatures above half their melting points. It can be seen that an increase in temperature or a decrease in strain rate leads to a lowering of the flow stress. As the temperature is decreased or the strain rate increased, the strain to reach the peak stress increases; also the peak in flow stress becomes much broader. Although the strain to the peak and the strain to steady state flow normally increase with decrease in temperature in plain carbon austenite, Figure 3.2, the broadening in the Nb-treated carbon steel appears to be much greater than can be attributed to the temperature dependence of the recrystallization process alone. This strong broadening suggests that Nb(CN) precipitation is initiated during deformation at 930°C, thereby retarding the dynamic recrystallization process. This retardation, in turn, has the effect of broadening the flow stress peak.

At the lowest temperature, 815°C, Figure 3.3, no drop in flow stress is observed. This may be attributed to the considerable volume fraction of ferrite present at 815°C, which does not exhibit the phenomenon of dynamic recrystallization. It is also possible that the precipitation of Nb(CN) is sufficiently advanced at 815°C for dynamic recrystallization to be retarded to such an extent that it is not initiated even after a true strain of 0.8.

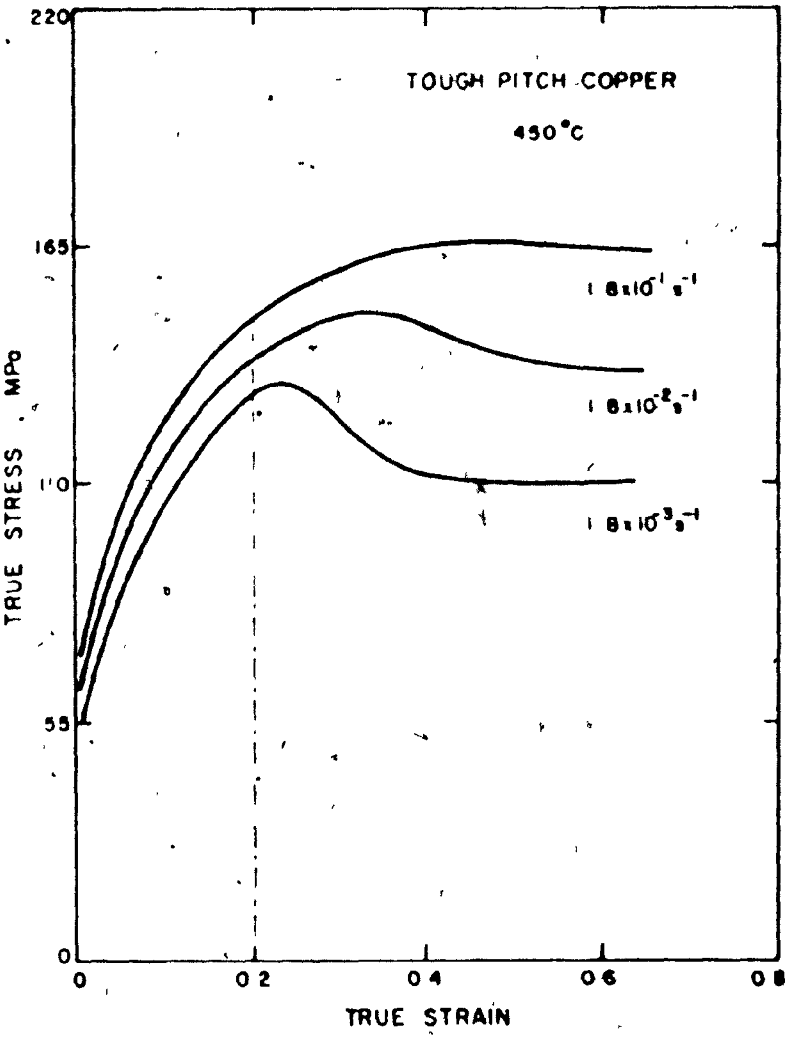

Figure 3.1 Strain rate dependence of the flow curve in tough pitch copper at 450°C

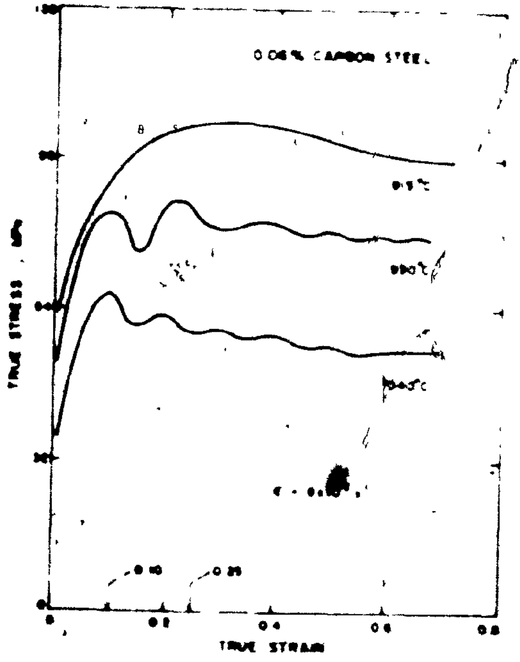

Figure 3.2 Temperature dependence of the flow curve in the 0.06% C steel at $8 \times 10^{-2} s^{-1}$

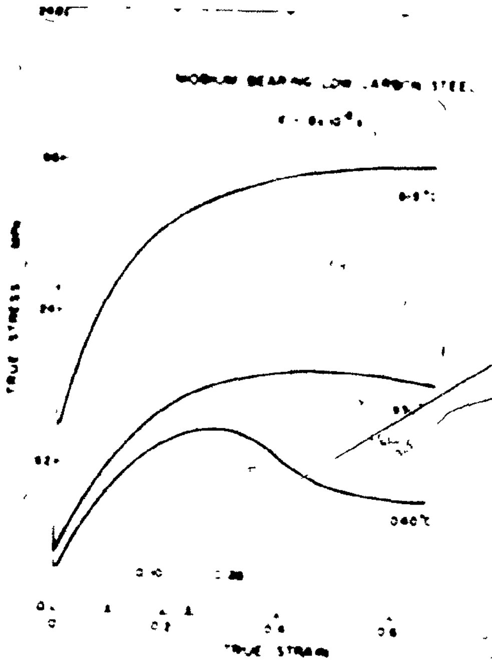

Figure 3.3 Temperature dependence of the flow curve in the Nb-treated steel at $8 \times 10^{-2} s^{-1}$

3.2.2 Selection of Interruption Strain

The tough pitch copper was deformed at temperatures of 450, 500 and 540°C. Two sets of interruption strains were chosen, in the first set, the material was undergoing dynamic recovery only, whereas in the second set, dynamic recrystallization was taking place as well. The strains selected were 0.05, 0.10, 0.15, 0.1[illegible] for the dynamic recovery region and 0.30, 0.40 and 0.52 for the dynamic recrystallization region. This procedure could be followed at all three experimental temperatures as the strain rates were adjusted so as to maintain the congruence of the flow curves over the temperature range.

The true strain to unloading of 0.25 employed in the 0.06% C steel at [illegible] $\times 10^{-2}$ is indicated in Figure 3.2. At the higher temperatures, 930 and 1040°C, the unloading strain of 0.25 is well within the steady state regime and therefore within the dynamic recrystallization regime. At the lower temperature, 815°C, initiation of dynamic recrystallization is shifted to higher strains, above the unloading strain of 0.25, so that interruption took place within the dynamic recovery region.

The true strains to unloading of 0.1 and 0.25 employed in the experiments on the Nb-treated low carbon steel are indicated in Figure 3.3. At 1040°C, the unloading strain of 0.25 is close to the maximum in flow stress and is certainly in excess of the strain required to initiate dynamic recrystallization. At 930 and at 815°C, the strain to the maximum is shifted to higher strain values, so that the unloading strains are below the critical strain for dynamic recrystallization.

3.2.3 Results of Interrupted Compression Testing

In order to determine the softening behaviour in the present materials, a series of interrupted stress-strain tests was performed, with increasing delay times before the resumption of deformation. The effect of different holding times on the subsequent stress-strain behaviour was illustrated in Figure 2.1 and is reproduced here for convenience.

After a short holding time, t_1, the flow stress on reloading rises rapidly to a stress level comparable with the unloading stress, σ_m. On the other hand, after a long delay, t_6, the flow stress on reloading, σ_r, approaches that observed during the initial loading, σ_y,

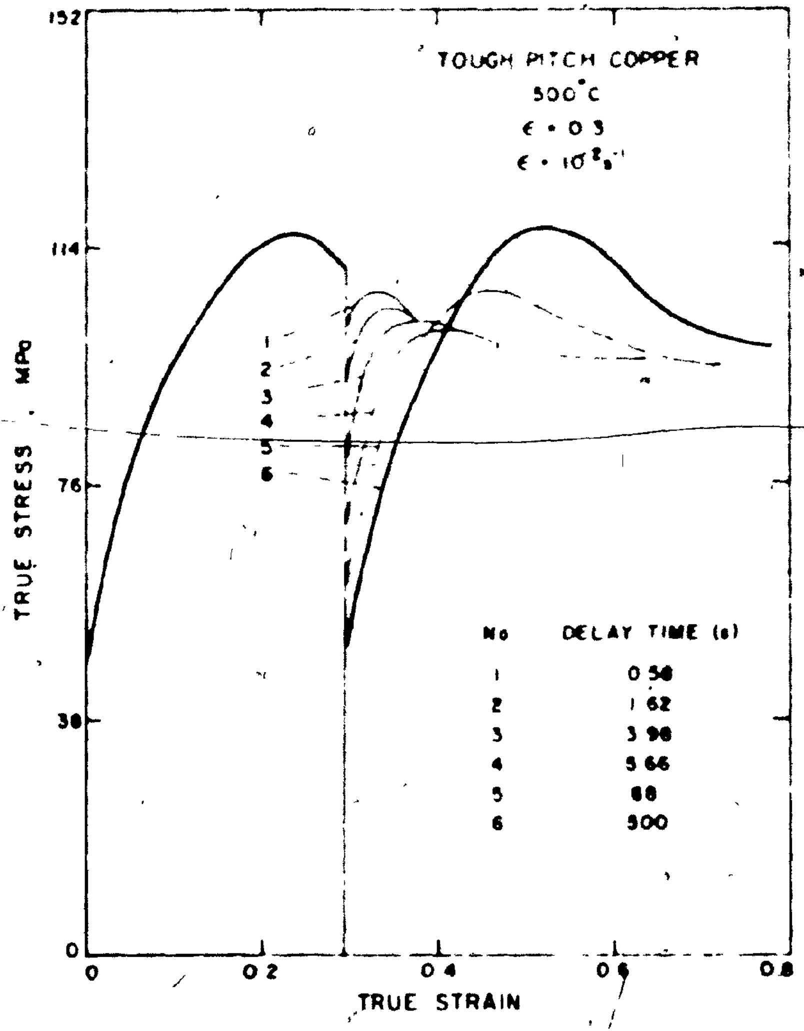

Figure 3.4 Effect of increasing delay time on the interrupted flow curve

of annealed material. The latter indicates that the work hardening introduced during initial straining is completely removed during the delay. The reader is referred to Appendix 2.[illegible] for the remainder of the data. The degree of softening is then calculated from the equation

[illegible] x 100 %   (3.1)

The amounts of softening associated with the various experimental conditions are presented in Appendix [illegible]. The progress of softening with time in tough pitch copper, low carbon steel, and Nb-treated steel will be now described in turn, with special emphasis on the effect of strain, temperature, strain rate and the concentration of alloying elements on the softening behaviour of these materials.

a) Effect of Strain

The results of a large number of interrupted tests indicate that after hot working static softening in FCC materials proceeds by the sequential operation of up to three distinct processes(39). The relative importance of each of these processes depends critically on the prior hot working strain. This effect is illustrated in Figure 3.5, where the softening curves obtained on the present tough pitch copper are displayed. These tests were carried out at 500°C at a strain rate of 1.8 x $10^{-2}s^{-1}$ and the samples were held at the testing temperature after seven different amounts of prestrain. The location of the interruption strains was chosen to be before the peak flow stress for conditions a, b, c and d and after the peak flow stress for conditions e, f and g.

For small amounts of prior strain (curves a and b), that is at a strain considerably less than that required to reach the maximum in flow stress, only one stage of softening is observed. This first cycle of softening has been attributed to static recovery(39,66,67,89,90), and is completed in about 1000s (curve a) or 500s (curve b). By this time, 40 or 50% of the work hardening introduced during prestraining is removed. The recovered structure is clearly very stable since no further softening occurs even after 15 hours. This implies that a strain of 0.10 is less than the critical strain for static recrystallization.

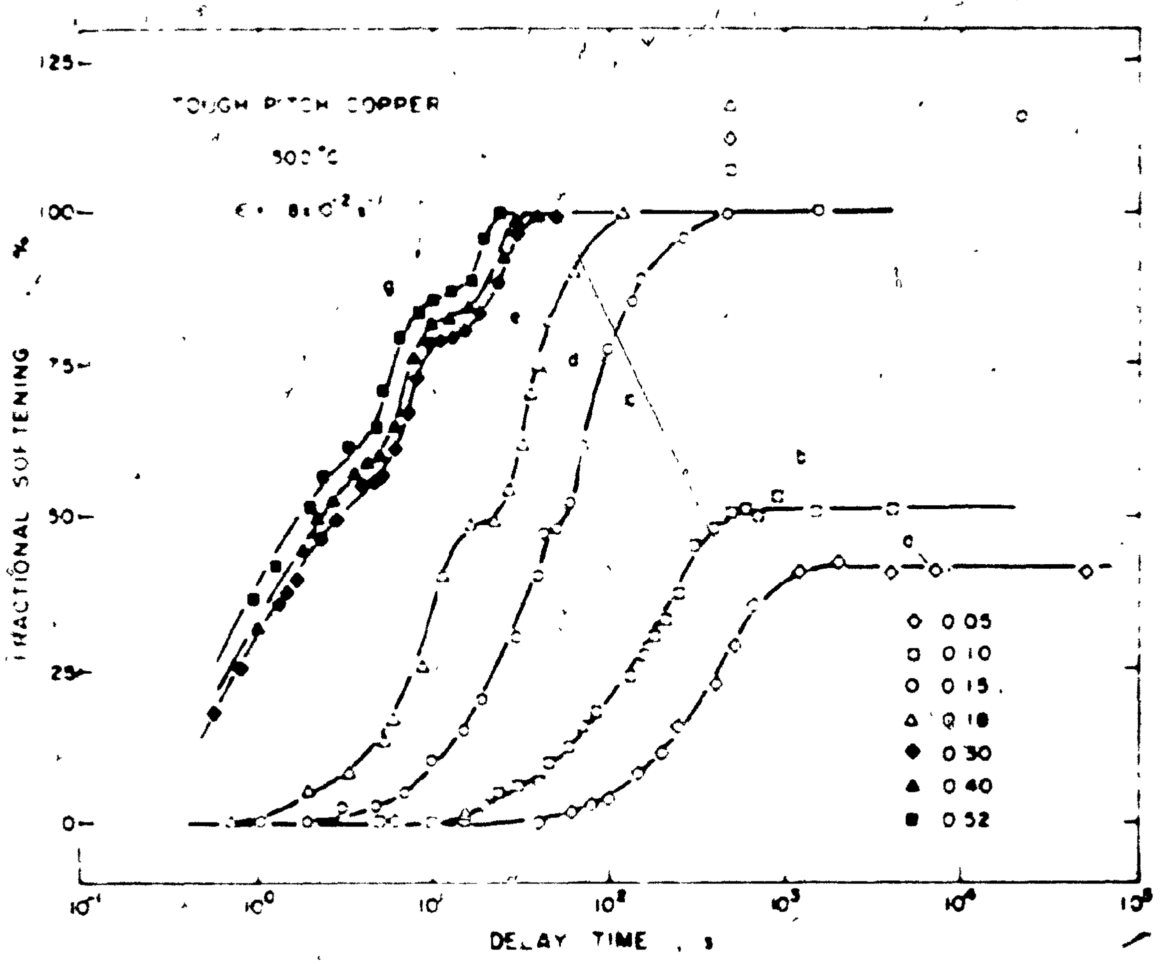

Figure 3.5 Effect of strain on static softening in tough pitch copper

when the amount of prestrain is increased to 0.15 (curve c) or [illegible] (curve d), the first cycle of softening is complete after 50s and 20s, respectively. These results suggest that the rate of recovery was increased because of the higher driving forces associated with the greater dislocation densities present at interruption at these increased strains. Following the earlier work, the second stage of softening can be associated with static recrystallization. This conclusion will be justified in more detail later. Since all four strains were below that required to reach the peak of the uninterrupted stress-strain curve, it is further assumed that dynamic recrystallization did not take place during prestraining. According to this view, static softening was initiated in a dynamically recovered structure.

The next three strains were selected to be, curve e, between the peak and steady state strains, and, curve f and g, well into the steady state regime. Curve e represents the softening response of material in which dynamic recrystallization has just begun and is not yet fully developed. Curve g, on the other hand, is representative of the progress of softening in material in which dynamic recrystallization is fully developed. It should be noted that in curves e, f and g, the amount of softening produced by static recovery is very difficult to identify because metadynamic recrystallization is taking place concurrently(39). The latter occurs by the continued growth of dynamic recrystallization nuclei after the deformation is stopped, and does not, therefore, require an incubation period.

The additional softening arrest in the upper half of the last three curves (e, f and g) can be attributed to classical recrystallization. According to this view, the incubation period required for the initiation of classical recrystallization takes place during the continued operation of metadynamic recrystallization.

The association of the various microstructural processes outlined above with particular features of the softening curves follows the pattern introduced in our earlier work and is consistent with the results of the mechanical tests. It should, however, be considered as tentative until the results of the metallographic investigation, which will be presented in Section 3.2.5 below, are introduced and evaluated.

It should be noted that, once the critical strain for static recrystallization has been exceeded, i.e. as the strain is increased from 0.15 (curve c) to 0.52 (curve g), the time for 50% softening decreases by two orders of magnitude. This marked effect of strain has been noted by other workers(36,104,109) and can be attributed to the displacement of classical recrystallization, which requires an incubation time, by metadynamic recrystallization, which does not.

b) Effect of Temperature

Experiments dealing with the effect of temperature on the rate of softening were carried out on copper samples having equivalent structures and internal stresses. This type of experiment can be done by selecting combinations of temperature and strain rate such that the resulting flow stresses at interruption are approximately equal(16). The softening curves obtained in this manner are shown in Figures 3.6a and b for 450 and 540°C, respectively. In the study on low carbon steel, the testing strain rate was, for simplicity, held constant instead, leading to the results shown in Figure 3.7.

The softening curves obtained with the tough pitch copper displayed a generally sigmoidal form, but with intermediate inflection plateaus. It can be seen that the rate of recrystallization is temperature dependent, as is the length of the softening arrest or plateau. At interruption strains of 0.05 and 0.10 at 450°C, or 0.05 at 540°C, softening did not go to completion, but levelled out at about 42, 50 or 42%, respectively. Even after delay times of 100,000s, no further softening was observed, evidently because the critical strain for static recrystallization had not been reached. At an interruption strain of 0.15, at both temperatures, the softening curves go to completion (100%), but with an intermediate inflection plateau. It is of interest to note that the length of the inflection plateau decreases with an increase in temperature, presumably because of the higher activation energy associated with recrystallization than with recovery.

The softening curves obtained after 0.40 strain relate to material which was recrystallizing dynamically prior to interruption. Because of the rapid progress of softening at 540°C under these conditions,

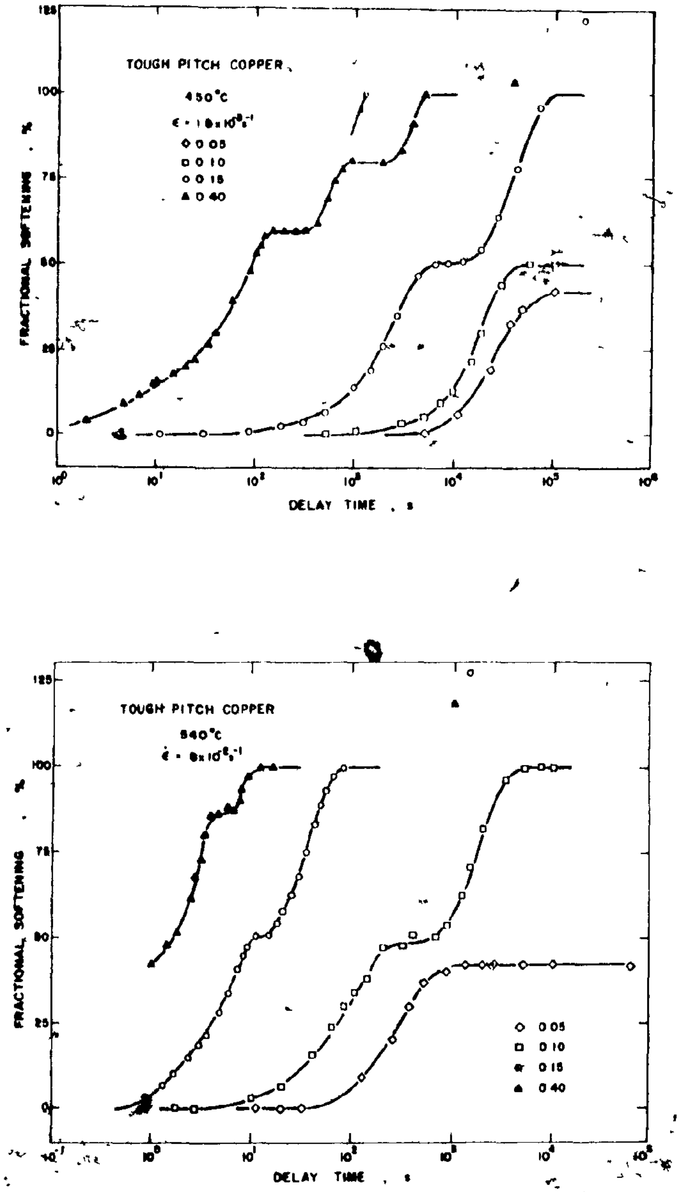

Figure 3.6 Effect of temperature on the softening rate in tough pitch copper

the earlier part of the softening curve could not be determined. Nevertheless, in both of the ε = 0.40 curves, two inflection plateaus are evident.

The effect of temperature on the rate of softening in the 0.06% C steel is shown in Figure 3.7, and can be seen to be qualitatively similar to that already described for the tough pitch copper. In interpreting the three softening curves, it should be noted that interruption did not occur at equivalent points along the stress-strain curves in the three sets of tests (see Figure 3.2). For example, a strain of 0.25 at 815°C lies before the peak of the flow curve, which is why the incubation plateau is so clearly evident. The same strain at 930° and 1040°C, on the other hand, corresponds to points after the peak, i.e. after dynamic recrystallization has begun, so that only the arrest following metadynamic recrystallization can be seen. It follows from this discussion that when interruption strains below the steady state strain are used, part of the increase in softening rate apparently associated with an increase in temperature can be attributed instead to the influence of strain which has been discussed above.

c) Effect of Strain Rate

The data shown in Figures 3.8a and b were obtained on the 0.06% C steel at temperatures of 930 and 1040°C, respectively, and at strain rates of 8×10^{-2} and $8 \times 10^{-3} s^{-1}$. The results reported by Weiss et al (107) for a steel containing 0.04% Nb and <0.005% Ti under similar conditions of temperature and strain rate are also included for purposes of comparison in Figure 3.8a. It is evident that when the strain rate in the plain carbon steel is increased by one order of magnitude, the rate of softening also increases by about an order of magnitude. In the Nb-modified steel, a two order of magnitude change in strain rate produces less than a hundredfold change in the rate of softening. In both materials, the increase in the rates of both recovery and recrystallization can be attributed to the increase in retained dislocation density, and therefore in the driving force for softening, that accompanies the increase in strain rate.

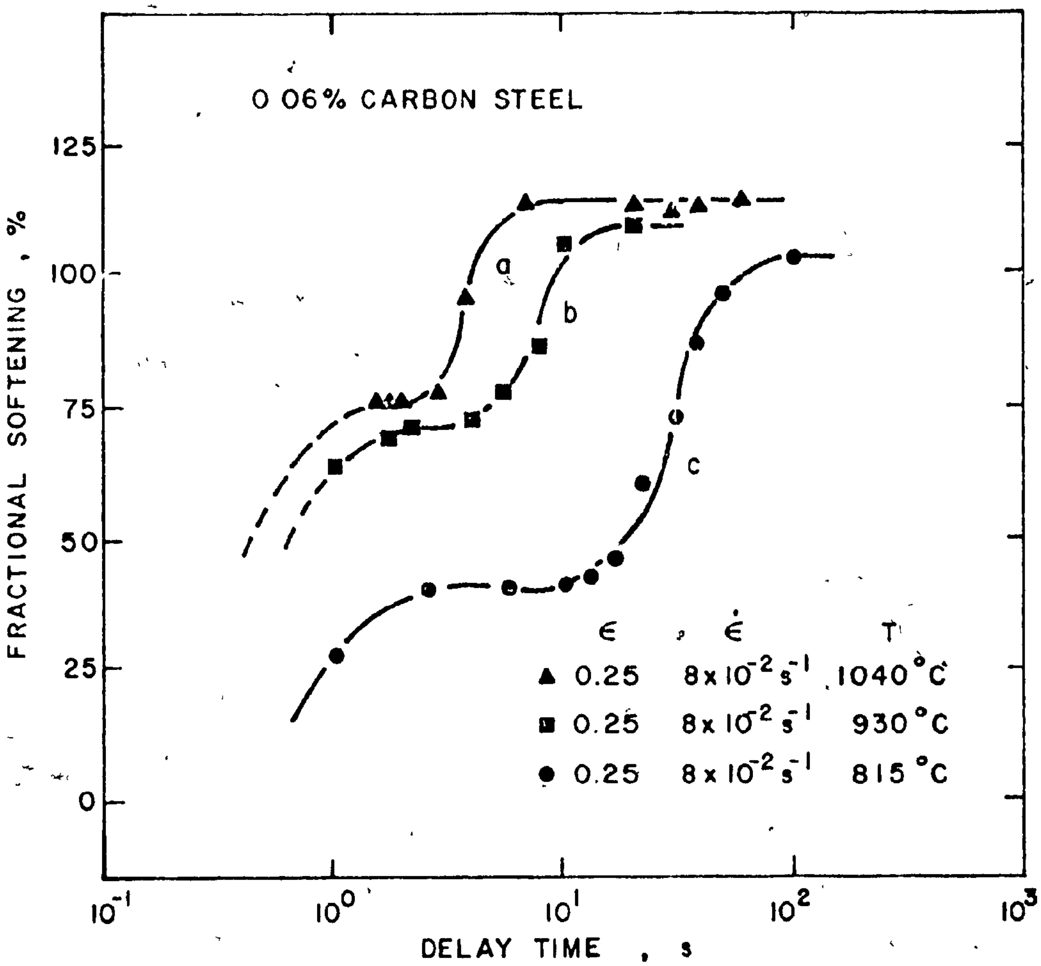

Figure 3.7 Effect of temperature on the softening rate in the 0.06% C steel

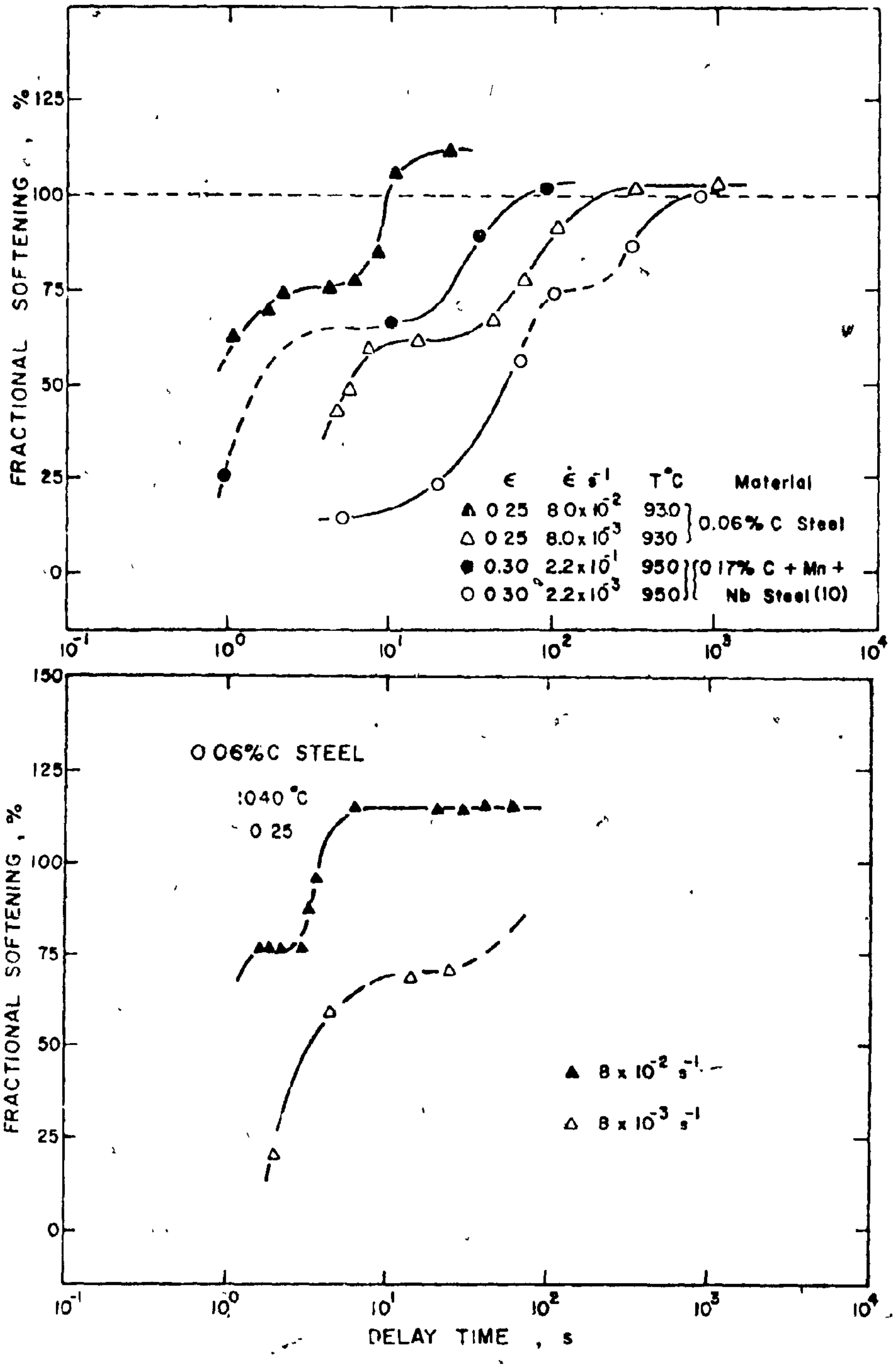

Figure 3.8 Effect of strain rate on the softening behaviour of two low carbon steels at

a) 930^{0}C and 0.25 strain

b) 1040^{0}C and 0.25 strain

d) Effect of Alloying Elements

The effect of adding minor amounts of Nb and other elements on the softening rate of plain carbon steel is displayed in Figure 3.9. This plot also includes the softening curve determined at the lower strain rate ($2.2 \times 10^{-3}s^{-1}$) by Weiss et al(107), which was incorporated in Figure 3.8, as well as the softening curves obtained by the present author in her earlier work(39,69,70). Comparison of the two softening curves for the low carbon steel shows that the addition of about 0.07% Nb decreases the softening rate by just over an order of magnitude. A somewhat larger difference in rate is observed when the 0.42% C steel is compared with the Nb-modified C-Mn steel, although in this case the effect of Nb addition is somewhat obscured by the differences in the prior strain, strain rate and temperature which must also be taken into account. It is of interest in this context that the softening curve for the 0.68% C steel is somewhat to the right of the 0.42% C steel curve, although these were determined under nearly identical conditions.

3.2.4 Effect of Strain, Temperature and Strain Rate on the Isothermal Softening of the 0.07% C Nb-modified Steel

It is clear from the results obtained in the current investigation that the softening behaviour of Nb-bearing steel is far more complex than that of plain carbon steel. This added complexity is thought to arise not only from the influence of NbC precipitation on the recovery and recrystallization kinetics, but also from the effect of Nb and C depletion on the basic strength of the matrix. The nature of the interaction between precipitation on the one hand, and the processes of recovery and recrystallization on the other, makes the complete description of the structural changes occurring during and after hot working very difficult. In view of this added complexity, the softening behaviour of the Nb-bearing steel will be presented, in this and subsequent chapters, in separate sections.

The effect of strain, temperature and strain rate on the isothermal softening of this material is shown in Figures 3.10a to c. The general shape of the curves presented is broadly similar to that obtained with plain carbon austenite and with copper and copper alloys. It is

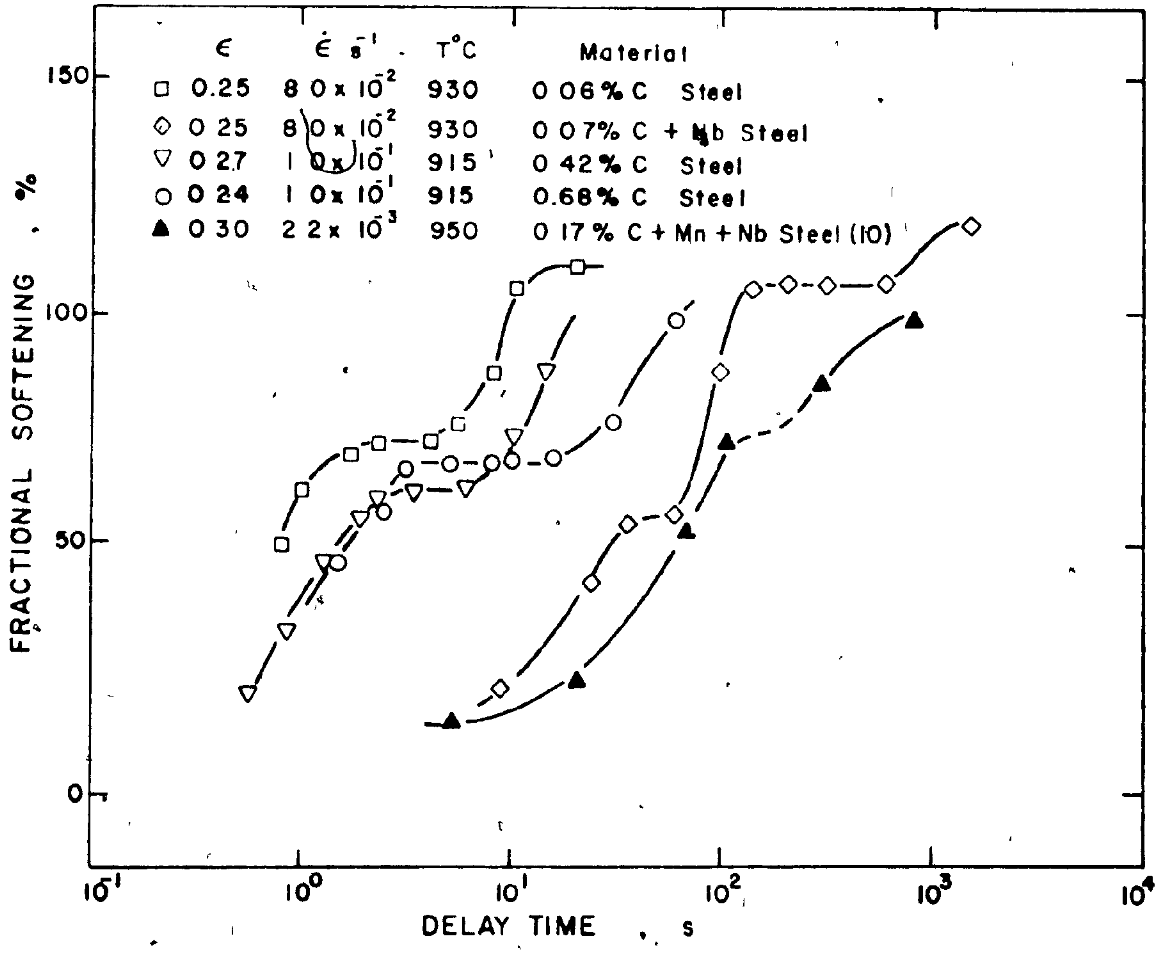

Figure 3.9 Effect of niobium and other alloying elements on the softening behaviour of plain carbon steel

clear that at a given temperature, the rate of softening is most strongly affected by the strain to unloading. At 1040°C and $\dot{\epsilon}$ $8 \times 10^{-2}s^{-1}$ (Figure 3.10a), the time for 50% softening decreases from 250s to 5s as the interruption strain is increased from 10 to 25%.

The shape of the softening curve also changes with strain. The softening curves obtained after 0.10 prestrain exhibit an inflection plateau at about 50% softening. This arrest in the softening process probably arises from a changeover from recovery to classical recrystallization as the dominant softening mechanism. By contrast, the inflection plateau obtained after 0.25 prestrain, which appears at 90% softening, can probably be associated with the exhaustion of the metadynamic recrystallization process, which occurs only after dynamic recrystallization has been initiated. After a further delay, softening continues, presumably through the operation of classical recrystallization.

The effect of a one order of magnitude increase in strain rate can also be deduced from Figure 3.10. At 1040°C and $\epsilon = 0.25$, the time for 50% softening decreases from 13s to 5s when the strain rate is increased from $8 \times 10^{-3}s^{-1}$ to $8 \times 10^{-2}s^{-1}$. At 930°C, a one order of magnitude increase in strain rate also speeds up restoration, but less markedly (Figure 3.10b). A further feature of interest in Figure 3.10b is that after 0.25 prestrain, the shapes of the isothermal softening curves differ for the two experimental strain rates. At $8 \times 10^{-2}s^{-1}$, dynamic recrystallization did not occur during prestrain (see Figure 3.3) and consequently the inflection plateau may arise from the recovery/classical recrystallization changeover. However, at the lower strain rate, all three processes are likely to operate concurrently, but are probably exhausted after different times, which results in the multiple arrests observed. Given that, as observed above, the softening processes are somewhat more complex in Nb-bearing steels than in plain carbon steels, it is apparent that a more detailed interpretation of the plateaus evident in Figure 3.10 will require further data and supporting evidence.

The softening behaviour after 0.10 prestrain was not examined at 930°C because only 14% softening was obtained after a 10-hour delay. It was considered that longer delay times were of no practical value and consequently beyond the scope of this investigation. At the lowest

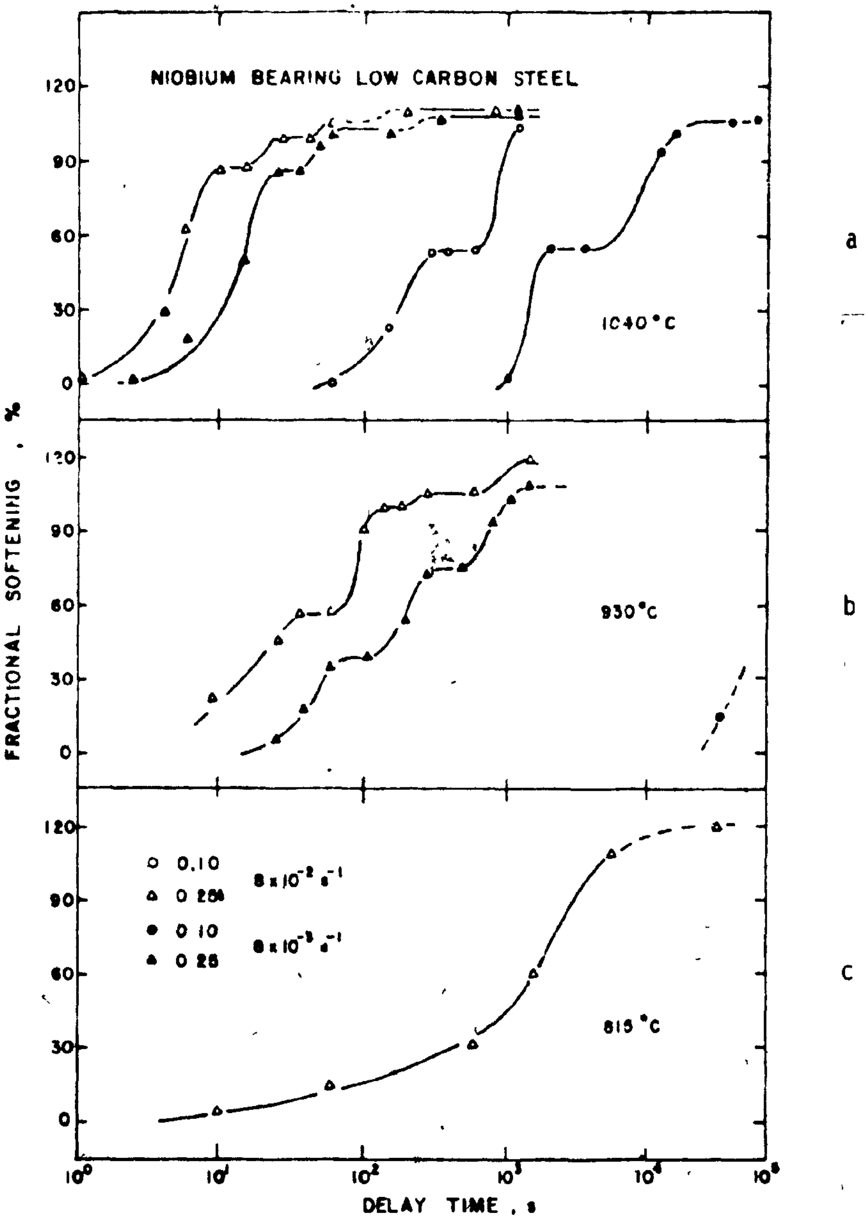

Figure 3.10 Effect of strain, temperature and strain rate on the softening behaviour of the 0.07% C Nb-modified steel

temperature, 815°C (Figure 3.10c), only one test condition was examined, $\dot{\epsilon}$ $8 \times 10^{-2} s^{-1}$ to ϵ 0.30. Since few points were obtained, because of the excessively long delays involved, no plateau was detected. However, the possibility of the presence of such an arrest should not be disregarded. It should also be noted that at 815°C, the overall amount of softening reaches a value of 120% after 8.5 hours, a point to which we will return below.

3.2.5 Results of the Metallographic Investigation

3.2.5.1 Introduction

In order to test the hypothesis proposed as an explanation of the softening curves observed above, a second series of tests was carried out. In this series, the progress of the structural changes that occur following an interval of hot work was studied metallographically. In the tests, samples of tough pitch copper were subjected to the same initial thermal-mechanical cycle as those used in the softening experiments. In the present case, however, all the samples were water quenched to room temperature after the appropriate delay times; i.e., the deformation was not resumed for the determination of the post-delay yield strengths. The specimens produced in this way were sectioned and prepared for metallographic examination. The sample preparation procedure is given along with the compositions of the electropolishing solutions in Appendix 3.3.

Initially it was decided that the progress of static recrystallization would be followed by means of point counting, the unrecrystallized grains being identified by the presence of dislocation etch pits. This technique, however, proved to be inadequate because of the rather uneven pitting attack obtained in the polycrystalline samples. In view of this, it was decided, instead, that the progress of recrystallization would be followed by analyzing the changes in the distribution of the grain sizes determined on planar sections of the sample. It was found that this technique, although very tedious, was a highly sensitive measure of the extent of recrystallization. The results of these experiments will now be described in detail.

3.2.5.2 Grain Size Distributions and their Modification with Time

The present method of grain size analysis was carried out on tough pitch copper samples prestrained 0.05, 0.10, 0.15 and 0.40 at 500°C and a strain rate of $1.8 \times 10^{-2} s^{-1}$. All the samples were sufficiently etched to provide a clear delineation of the grain boundaries. In excess of 400 linear intercept measurements were made on each sample on two sections cut transversely to the compression axis. One section was taken close to the midheight of the sample and the other near one of the ends. This sectioning procedure was used to minimize the influence of any localization of deformation on measurements of the grain structure. The individual intercept lengths were equally subdivided into 25 discrete size groups in the size range 0.2 to 2 mm. This size range was selected as it included 99% of the intercepts measured in undeformed samples. For those samples which contained a significant fraction of intercept lengths of less than 0.2 mm, the size range between 0 and 0.2 mm was divided into a further 25 subgroups. The relative frequency of intercepts within each size class was defined as

$$f_i = \frac{n_i}{N} \qquad (3.2)$$

where n_i is the number of intercepts within the size class and N is the total number of intercepts. The discontinuous distribution curves obtained in this way are shown in Figures 3.11 (a to d).

Figure 3.11a represents the data obtained from samples quenched after delays between 65.5 and 50,000s following prestraining to 0.05. The softening curve obtained by interrupted mechanical testing after the same prestrain (curve a, Figure 3.5), is shown in the top left corner. The points indicated on the softening curve represent the experimental conditions for which the corresponding intercept distribution was obtained. It is evident from this figure that the intercept class corresponding to the mode as well as the width of the distribution is unchanged by increasing the delay time. The mean linear intercept grain size obtained from the individual measurements is constant to within ±6 %. Furthermore, the mean linear intercept grain size of these samples is equal to that of the undeformed sample, i.e. prior to prestraining.

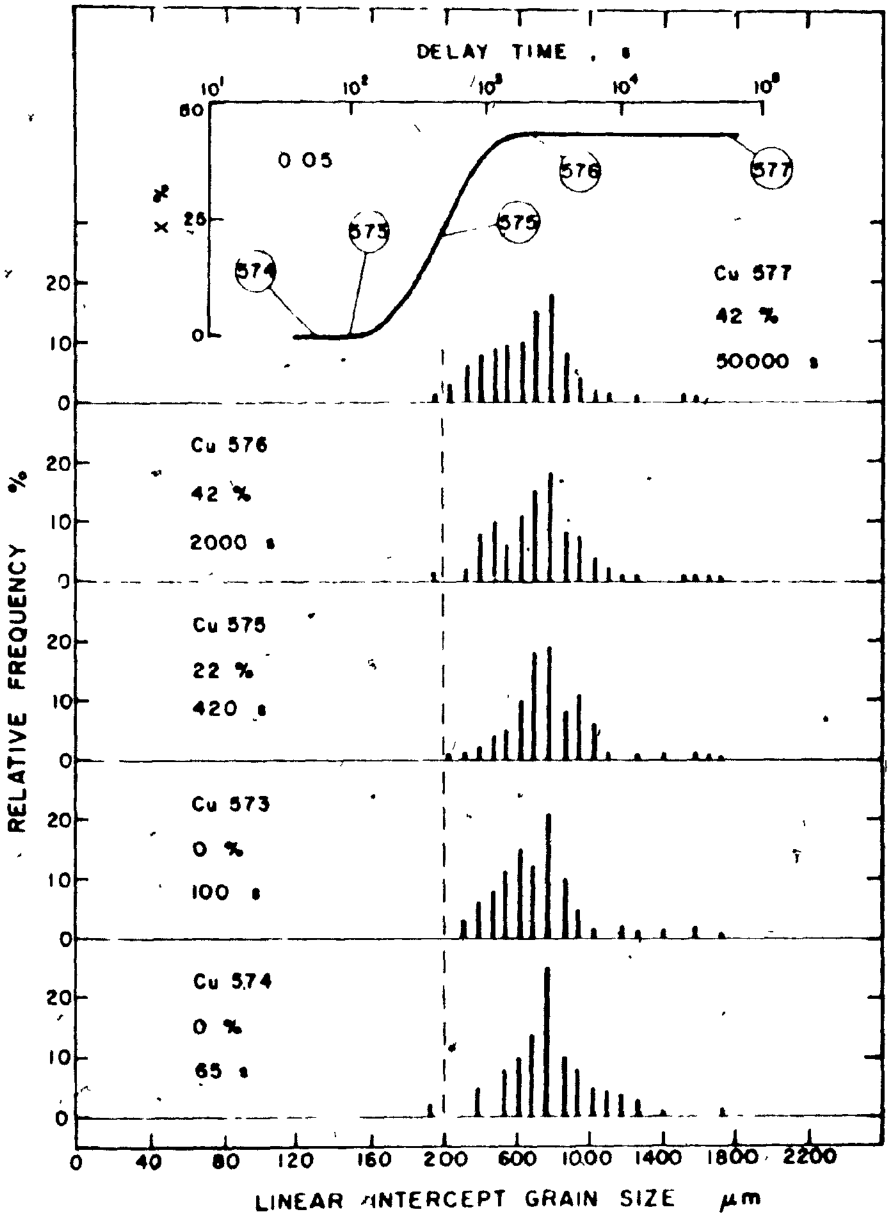

Figure 3.11a)Discontinuous frequency distribution of grain size in tough pitch copper held at 500°C after ε = 0.05 prestrain

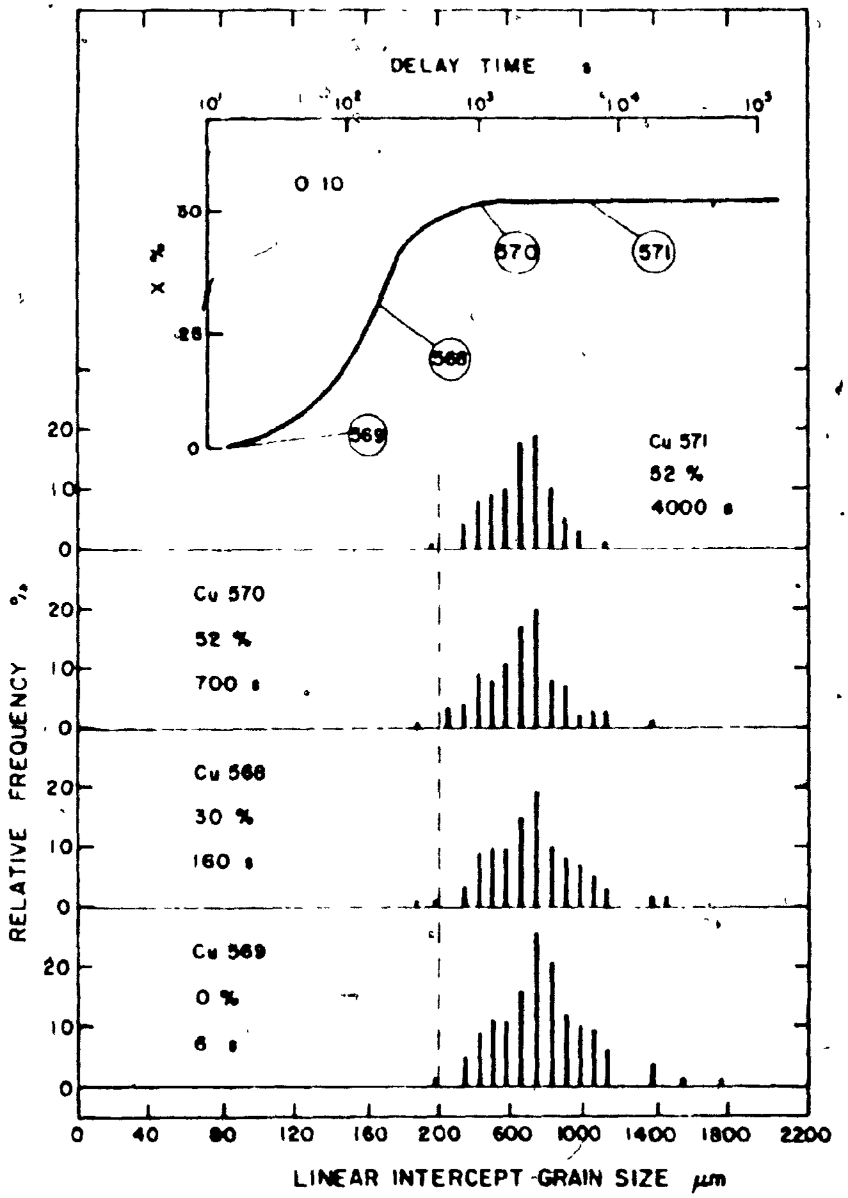

Figure 3.11 b) Discontinuous frequency distribution of grain size in tough pitch copper held at $500^{\circ}C$ after $\varepsilon = 0.10$ prestrain

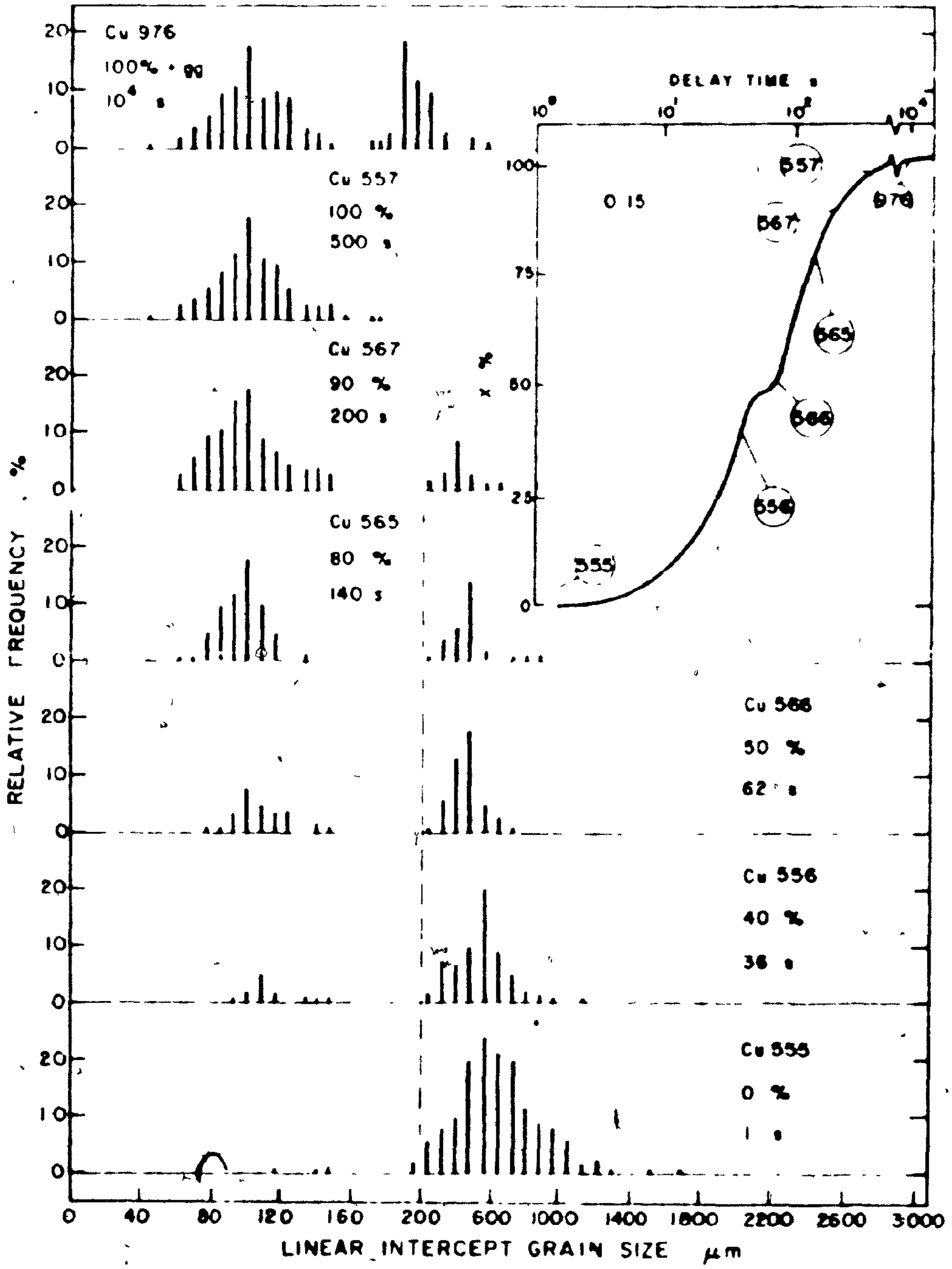

Figure 3.11 c) Discontinuous frequency distribution of grain size in tough pitch copper held at 500°C after $\varepsilon = 0.15$ prestrain

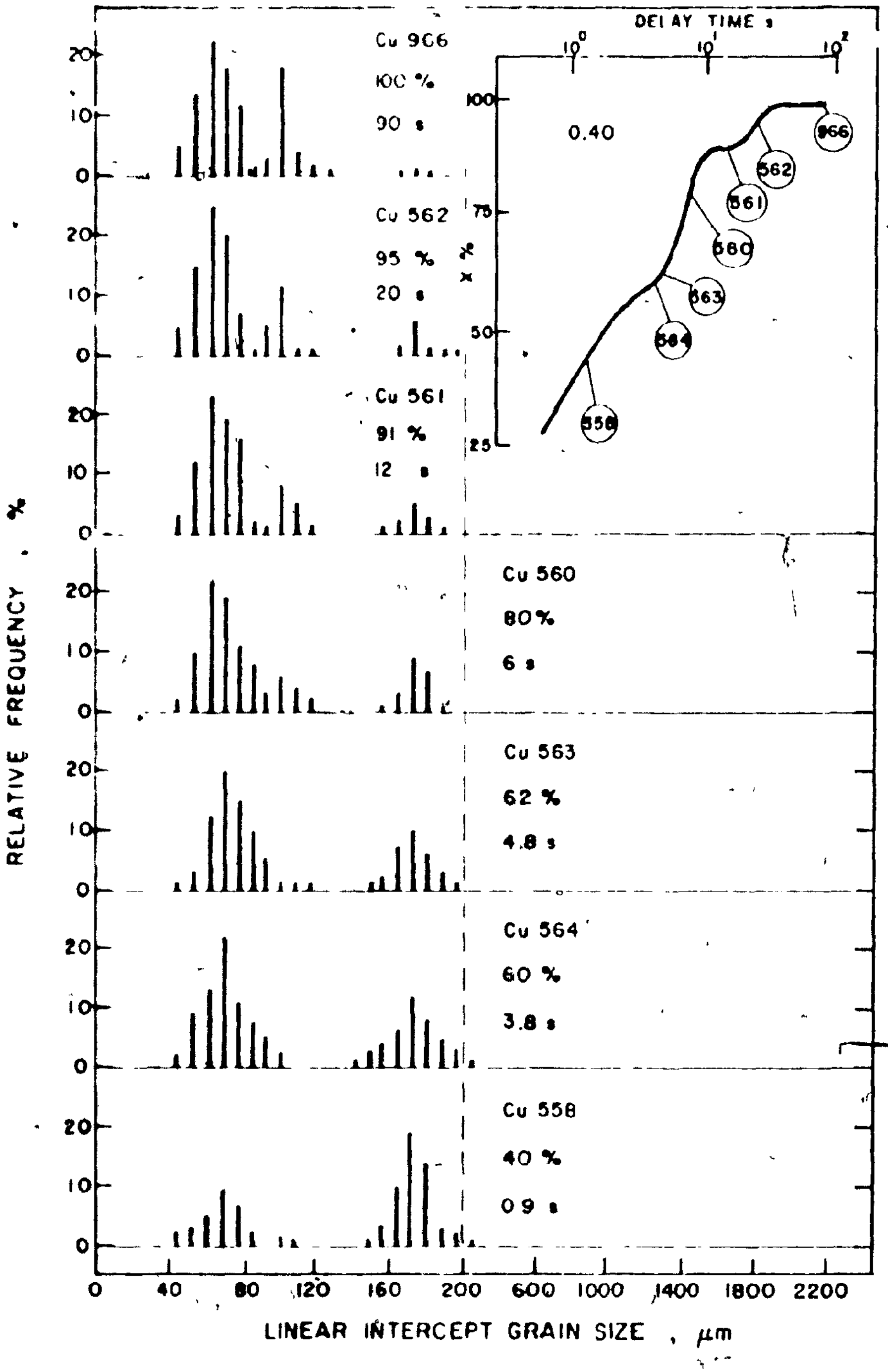

Figure 3.11 d) Discontinuous frequency distribution of grain size in tough pitch copper held at 500°C after $\epsilon = 0.40$ prestrain

Similar conclusions can be drawn from the linear intercept distributions obtained after a prestrain of 0.10, shown in Figure 3.11b. Here the prestraining conditions and the delay times correspond to those used to develop curve b in Figure 3.5. These findings are in agreement with the hypothesis that a hot working prestrain in excess of 0.10 is required at 500^{o}C and 1.8 x 10^{-2}s^{-1} to initiate static recrystallization. The grain size and intercept distribution is then unchanged with delay time, since softening occurs only by static recovery.

By contrast, Figure 3.11c represents the grain size distributions obtained for samples after a prestrain of 0.15. The static softening curve obtained for this condition (curve c of Figure 3.5) indicates that two softening processes occur; these were tentatively identified as static recovery and static recrystallization. It is evident from the lowest grain intercept distribution that no significant change took place within the first second of holding in either the modal class or the distribution width; i.e. the distribution was similar to that of the undeformed material. However, after 40s, a new intercept size class has started to appear, centred on a mean size of 0.09 mm. After longer delay times, this new distribution grows at the expense of those grouped about the original grain size. Finally, after 120 to 600 s the entire population of intercept lengths is grouped about the new mean grain size of 0.09 mm. On delaying for a further 3 hours, an additional 0.19 mm grouping begins to develop. This latter effect is taken as evidence for grain growth, and the associated further softening can then be attributed, not to a reduction in dislocation density within the grains, but rather to the increase in grain size itself (see Section 3.2 below).

Turning now to the data described by the distribution curves shown in Figure 3.11d, these were obtained on samples which were strained beyond the peak in the flow curve and had therefore undergone dynamic recrystallization. The first intercept distribution was obtained on a sample which had been unloaded after a prestrain of 0.40 and quenched after a delay of 1s. Here two groupings of intercept lengths are evident. The longer lengths are grouped about a mean size of 0.17 mm; this is smaller than the original grain size of 0.56 mm. It is evident from the distributions obtained after longer delay times that the number of these larger grains decreases with increasing time. This grouping of intercept lengths is therefore associated with the dynamically recrystallized grains formed during prior straining. The number of grains within the second intercept group, formed about a mean size of 0.04 mm, increases as the delay time increases. These latter grains are consequently associated with the static recrystallization processes. Since 30% of all the intercepts lie within this group after only 1s of delay, it can be concluded that these grains are formed by metadynamic recrystallization. As the delay time increases, the dynamically recrystallized grains are gradually replaced by the metadynamically formed ones.

In the sample held for 6s prior to quenching, the short intercept distribution starts to be skewed towards longer lengths, and after 9 and 11s, a third discrete distribution starts to appear, grouped about a mean size of 0.08 mm. Once this grouping of grains begins to appear, the number of intercepts associated with the metadynamically recrystallized grains does not increase with further holding. Instead, the decrease in the number of dynamically formed grain intercepts is compensated by the increase in the number of intercepts associated with the third size grouping. In terms of the present analysis, the grains with a mean size of 0.08 mm are considered to be formed by classical static recrystallization. The number of intercepts within this grouping continues to increase at the expense of the dynamically recrystallized ones, until the latter are almost completely consumed after a delay time of 90s, which corresponds to full softening.

3.2.5.3 Static Recovery

The grain size distributions introduced in the previous section indicate fairly clearly that no change in grain size occurred during holding at a temperature of 500°C after a prestrain of less than 0.15 at $1.8 \times 10^{-2} s^{-1}$. It was concluded, therefore, that the softening observed under these conditions (curves a and b in Figure 3.5) was produced by static recovery of the hot worked substructure. In an attempt to confirm this contention, a study was carried out of the changes in the dislocation substructure by means of etch pit techniques. In this work, the dislocation etch pits were produced using the solution suggested by Gupta and Strutt(155) which is described in Appendix 3.3. The etching conditions were carefully controlled in an attempt to ensure that the etch pit density would be comparable for all the samples. However, as pointed out earlier, pitting attack was not uniform across the section of the polycrystalline samples; in some grains no pits were observed, whereas in others, numerous pits were clearly evident. This effect was judged to arise from the orientation dependence of etch pitting.

In view of this difficulty, as well as the problem of the under estimation of dislocation density inherent in the method(156), the results described below are taken as only a qualitative indication of the substructural changes associated with static recovery.

The change in etch pit density that accompanies recovery is indicated in Figure 3.12, obtained from samples prestrained 0.05 at 500°C and $1.8 \times 10^{-2}s^{-1}$. It can be seen that in a sample quenched within 10s of the removal of the stress, a high concentration of dislocations is present. The area density is $4 \times 10^6/cm^2$, but is unreliable in this micrograph, because many overlapping pits were observed, and not all dislocations led to pit formation. After holding for about 100s, the average pit density appears to decrease to some extent. This decrease is accompanied by a tendency towards a more orderly arrangement of the pits, and a coarsening of the dislocation substructure. It is evident that this trend is continued as the holding time is increased to about 1000s and beyond. Furthermore, continued holding does not appear to significantly change the dislocation density. These observations are in qualitative agreement with the progress of softening observed after prestraining 0.05 at $1.8 \times 10^{-2}s^{-1}$ at 500°C, and support the notion that softening by recovery saturates at a certain value well below that associated with full restoration.

3.2.5.4 Static Recrystallization

The grain size distributions described in Section 3.2.5.2 above lend themselves to the determination of the volume fraction recrystallized. To begin with, it is assumed that the size distribution of the unrecrystallized grains is unchanged during prestraining up to the critical strain required to initiate dynamic recrystallization. This size distribution

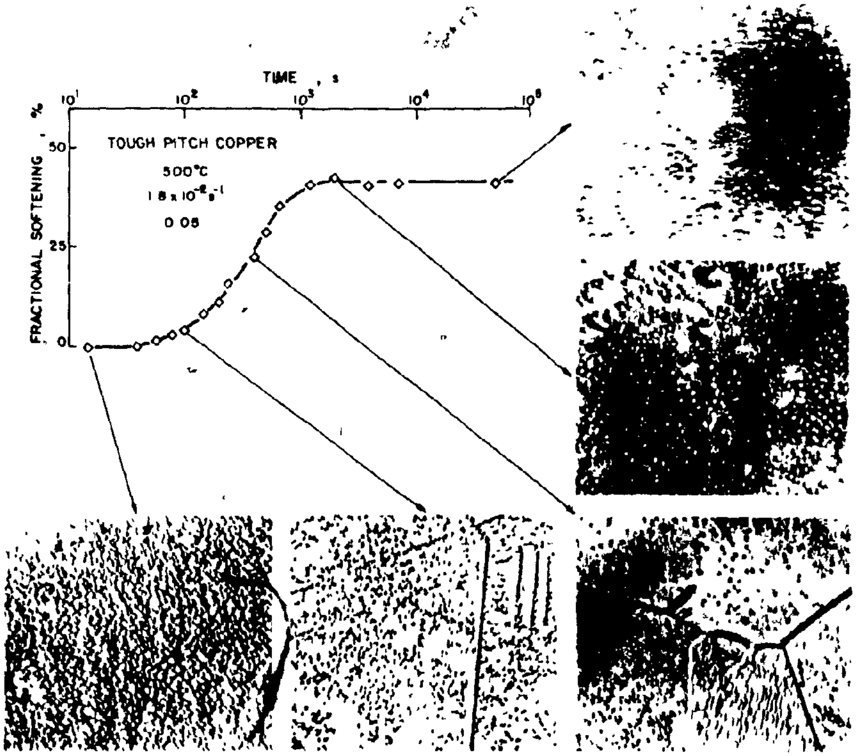

Figure 3.12 Dislocation structure revealed by etch-pitting after 0.05 prestrain in tough pitch copper. X900

a & b) regions with high dislocation density
c & d) cellular structure

is the same as that of the undeformed material, as is evident in Figure 3.11(a) and (b), as well as in the lowest distribution in Figure 3.11(c). It can then be assumed that the intercept lengths which fall into size classes greater than 0.2 mm are obtained from the population of unrecrystallized grains only. With this assumption, the linear fraction L_L recrystallized can be obtained from the individual intercept measurements. The volume fraction V_V recrystallized is then known, since it may be shown that(157)

$$V_V = L_L \tag{3.3}$$

This relationship was originally proposed by the French geologist Delesse(158) and forms the basis of most metallographic methods of volume fraction determination.

The volume fraction of material recrystallized as a function of delay time obtained in this way for samples prestrained to 0.05, 0.15 and 0.4 at 500°C is tabulated in Appendix 3.4. These data are presented as the solid curves in Figure 3.13. For comparison purposes, the corresponding softening curves taken from Figure 3.5 are plotted on the same axes. The softening curve (a) obtained after 0.05 prestrain shows a maximum softening of 40% after a delay time of about 1000s. Under such conditions, however, no change in grain distribution was observed and consequently the volume fraction recrystallized remains zero at all delay times. After 0.15 prestrain, recrystallization begins after about 40s delay, by which time the fraction recrystallized is 5%. At this same period, the corresponding mechanical softening curve shows 40% softening (broken curve c). This observation is in agreement with our hypothesis that, after relatively low prestrains, the primary component of softening is recovery based, and is of course not detectable by quantitative metallography.

The measurements of volume fraction recrystallized also indicate that recrystallization has already begun before the softening attributable to recovery is complete. The inflection plateau in the softening curve can then be seen to arise from the gradual diminution of softening by recovery as this process becomes saturated. Finally the

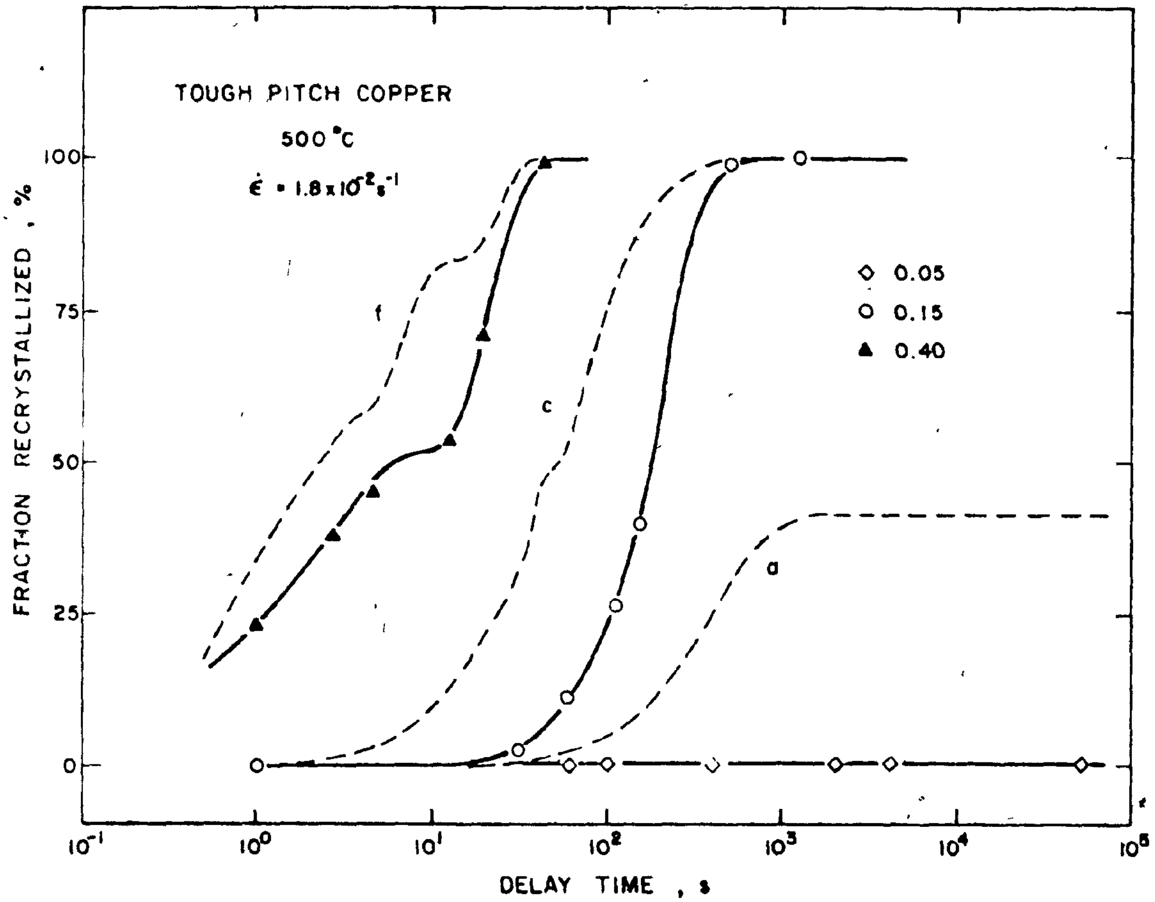

Figure 3.13 Progress of recrystallization in tough pitch copper at 500°C after prestraining at $1.8 \times 10^{-2}s^{-1}$

softening curve approaches that obtained by quantitative metallography as recrystallization goes to completion.

In the case of recrystallization data obtained on samples which were prestrained to 0.40, two intercept distributions were already evident, even after a delay as short as 1s. The distribution associated with the larger intercepts, grouped about a mean size of 0.17, was attributed above to the dynamically recrystallized grains. The shorter distribution, on the other hand, was considered to have been produced by the metadynamic recrystallization which occurs in the interval between unloading and quenching. It is evident from Figure 3.11(d) that the dynamically recrystallized grains are gradually consumed as more metadynamic grains are formed. Reference to Figure 3.13, however, shows that more softening occurs than is indicated by the recrystallization data. This difference is once more attributable to static recovery, which appears to go to saturation in about 10s (i.e. at the <u>second</u> mechanical arrest).* Here the recovery takes place in dynamically recrystallized grains which have not yet undergone metadynamic recrystallization.

In contrast to the data obtained after 0.15 prestrain, the 0.4 prestrain recrystallization data show an inflection plateau and the interrupted mechanical testing data show two arrests. The second arrest has already been attributed to the saturation of static recovery. After the first mechanical arrest (i.e. the metallographic arrest), a third distinct intercept size grouping starts to appear in Figure 3.11d. This group can be associated with the formation of <u>classically</u> recrystallized grains within the dynamically recrystallized matrix (i.e. with grains which required a nucleation or incubation time). Figure 3.11d also indicates that the process of metadynamic recrystallization (i.e. the "no-delay" process producing the finest new grains) goes to saturation in the vicinity of the first arrest, and that continued recrystallization after the arrest occurs primarily by the growth in the volume fraction of the grains within the third, intermediate, group. Finally, the softening and recrystallization curves approach one another as recrystallization goes to completion.

---

*The evidence for associating the saturation of the recovery process with the <u>second</u> mechanical arrest will be considered in detail in Section 4.3.3.2 below.

3.3 EFFECT OF GRAIN SIZE ON THE HIGH TEMPERATURE MECHANICAL PROPERTIES OF COPPER

After the work described above was completed, a further study was carried out on the effect of grain size on the high temperature mechanical properties of copper. Attention was especially given to the effect of grain size on the high temperature yield strength, since only limited data are presently available on this subject(159-163).

At high temperatures, the strength-grain size relationship is in considerable doubt for a number of reasons. These are associated with the nature of grain boundaries; for example, with the manner in which they can lead to strengthening by acting as obstacles to mobile dislocations. The presence of boundaries, on the other hand, also makes grain boundary sliding possible, which becomes an additional mode of deformation, and can thus lead to softening. Because of these opposing tendencies, most materials exhibit an "equicohesive temperature", i.e. a temperature above which fine-grained material is weaker than coarse-grained material (164), rather than the reverse, which is normally observed at more moderate temperatures.

One of the difficulties involved in an investigation of the Hall-Petch relation at high temperatures is the difficulty of maintaining a stable grain size during the course of the experiments. In the present study, this problem was overcome by the choice of the material (tough pitch copper)(165) and by the use of a prior heat treatment which produced both coherent and incoherent precipitates of β particles on the grain boundaries, making them somewhat more stable(166,167).

3.3.1 Comparison of the Flow Curves of Three Cuprous Materials

As was mentioned earlier, the presence of small amounts of impurities in tough pitch copper does exert a considerable influence on the rate of softening. The effect on flow behaviour in three copper alloys is presented in Figure 3.14. The stress-strain curve obtained for high purity copper is typical of a material undergoing dynamic recrystallization. The flow stress rises rapidly to a peak value, which occurs at a strain of about 0.1, and thereafter drops to a steady stress level, in the neighbourhood of which regular oscillations in flow stress

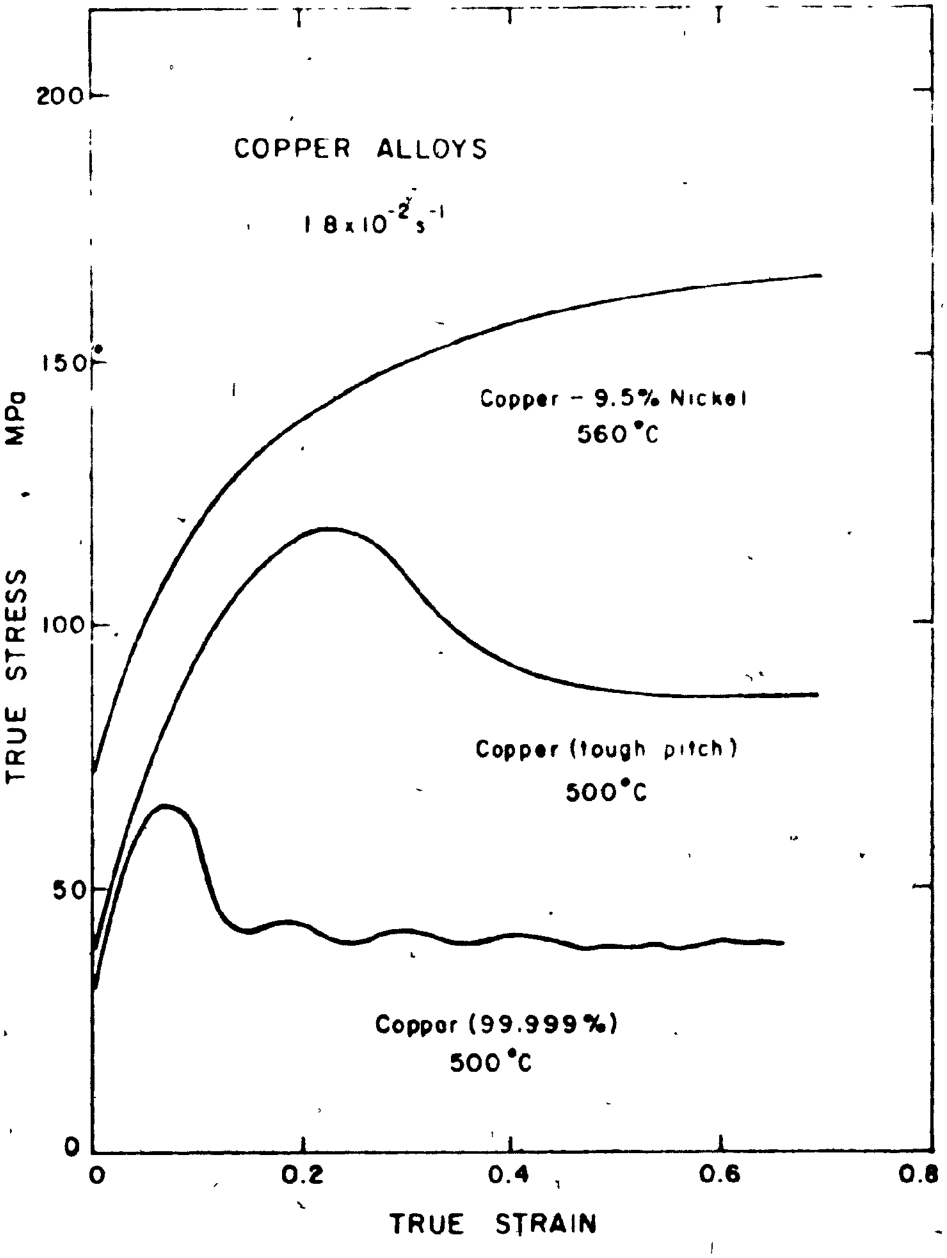

Figure 3.14 Comparison of the flow curves of three cuprous materials

are observed. When tough pitch copper is deformed under the same experimental conditions, work hardening dominates to much larger strains, until the initiation of dynamic recrystallization finally produces a single peak in the flow curve. The rate of dynamic recrystallization, in this case, is slower than in the high purity copper, leading to a broadening of the peak, and to a slower descent to the steady state level. The retardation of dynamic recrystallization in tough pitch copper is probably due to the presence of cuprous oxide particles, which can be expected to hinder both the nucleation and the growth of new grains. The flow curve for Cu-9.5% Ni is typical of a material which softens during deformation only by dynamic recovery.

3.3.2 Effect of Pre-Treatment on the High Temperature Yield Stress of Copper

One of the features of interest in the investigation was the effect of various prior heat treatments on the initial yield strength of the copper specimens. These were subsequently deformed at 540°C and a strain rate of $8 \times 10^{-2}s^{-1}$ and the different flow curves obtained are displayed in Figure 3.15, with a legend indicating the pre-treatment employed.

To begin with, all the specimens were annealed for 16h at 900°C and then either slowly cooled or quenched to room temperature The specimens were reheated to the testing temperature, 540°C, and held for different holding times before deformation.

When a combination of a slow cool to room temperature and 0.3h of holding at the testing temperature was employed, a yield strength of 68 MN/m^2 was obtained, curve 1, Figure 3.15. A longer holding time of 10h before testing (condition 2), markedly reduced the yield stress to about two-thirds of the above value. In cases 3 and 4, the specimens were quenched to room temperature instead. The holding times at test temperature of 0.3 and 10h, respectively did not affect the yield value appreciably (45 MN/m^2).

Although no transmission electron microscopy has yet been carried out on the present materials, the results can be given a tentative interpretation in terms of the Cu-O equilibrium diagram shown in Appendix 3.5.

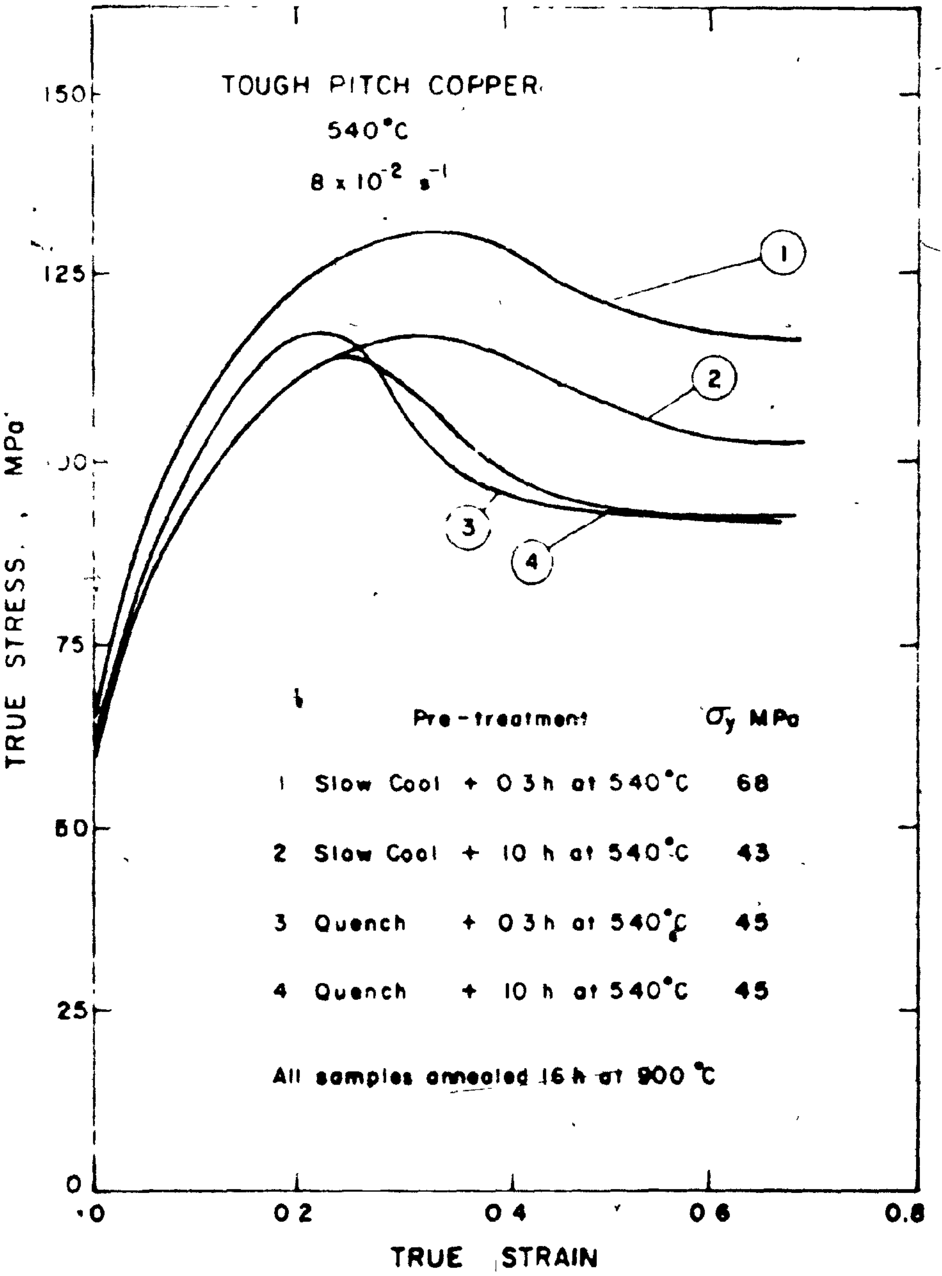

Figure 3.15 Effect of pre-treatment on the high temperature yield stress of copper

At 900°C (the annealing temperature), the structure consists of an α_0 matrix and particles, where is Cu_2O and is in relatively coarse form(167). During furnace cooling (condition 1), the oxygen solubility is decreased, is no longer stable, and fine particles of are precipitated out, probably on dislocations, where is CuO. Since the γ phase is formed at lower temperatures than the phase, and is more finely distributed, the material with the precipitates should exhibit a higher yield strength, as indeed shown in Figure 3.15. As far as condition 2 is concerned, the long pre-heating time at the testing temperature may lead to particle decohesion and coarsening, as well as to the reverse -to- transformation. The lower yield values, 43 MN/m^2 for this condition may thus be associated with a coarser particle distribution. With regard to conditions 3 and 4, rapid quenching can be considered to arrest the -to- transformation, resulting in a structure of coarse - and -Cu. This structure of course remains stable on reheating, even for very long holding times, and does not lead to appreciable particle strengthening.

3.3.3 Dependence of the Recyrstallized Grain Size on the Experimental Parameters

The present study was based on the assumption that the flow stress of a partially recrystallized material depends principally on the degree of recrystallization, and secondarily on the amount of recovery that has occurred in the unrecrystallized material. However, the possibility that the flow stress can also be influenced by the recrystallized grain size has not been ignored. A separate project was therefore carried out to determine the dependence of the recrystallized grain size on the prior hot working conditions. The various grain sizes produced were then used to establish the effect of grain size on the reloading flow stress. Before considering the influence of grain size on the high temperature flow stress, the effect of the hot working conditions on the grain sizes produced will be considered briefly.

3.3.3.1 Grain Size and Strain

Experiments dealing with the effect of strain on the grain size were carried out at 500°C and $1.8 \times 10^{-2}s^{-1}$, leading to the results shown in Figure 3.16. The grain size was determined after prestrains of 0.05, 0.10, 0.15, 0.18, 0.28, 0.40, 0.52 and 0.64, as indicated on the flow curve.

The grain sizes of the samples subjected to strains of 0.05 and 0.10, which are below the critical strain for static recrystallization, were the same as the initial grain size, but contained subgrains as revealed by etch-pitting. These data are not shown on Figure 3.16. When the prestrain exceeded the critical strain for static recrystallization the grain size decreased with increasing strain. At large strains, however, a steady state was reached where the grain size remained constant with further strain.

3.3.3.2 Grain Size, Strain Rate and Temperature

The data shown in Figure 3.17 were obtained at two temperatures, 540° and 600°C, and over a range of strain rates covering about two order of magnitude ($\sim 10^{-1}$ to $\sim 10^{-3}s^{-1}$). It is evident that when the strain rate is increased, the grain size decreases. This effect is more pronounced at the higher temperature (600°C), which can be expected, when it is recalled that both the dislocation density and the mechanical properties in general are more rate sensitive at higher temperatures.

The effect of temperature is also displayed in Figure 3.17 The results indicate that the grain size increases with temperature and that the grain size difference is larger at lower strain rates, i e $\Delta d \approx 0.31$ mm at $7.5 \times 10^{-4}s^{-1}$, and decreases to $\Delta d \approx 0.12$ mm at $8 \times 10^{-2}s^{-1}$

3.3.3.3 Effect of Grain Size on the High Temperature Yield Stress

The experiments dealing with the effect of grain size on the high temperature yield stress were carried out at various combinations of strain rate and temperature selected so as to produce the largest possible variation in recrystallized grain size. The results shown in Figure 3.18 represent four of the combinations of strain rate and temperature at which prestraining was performed, resulting in recrystallized

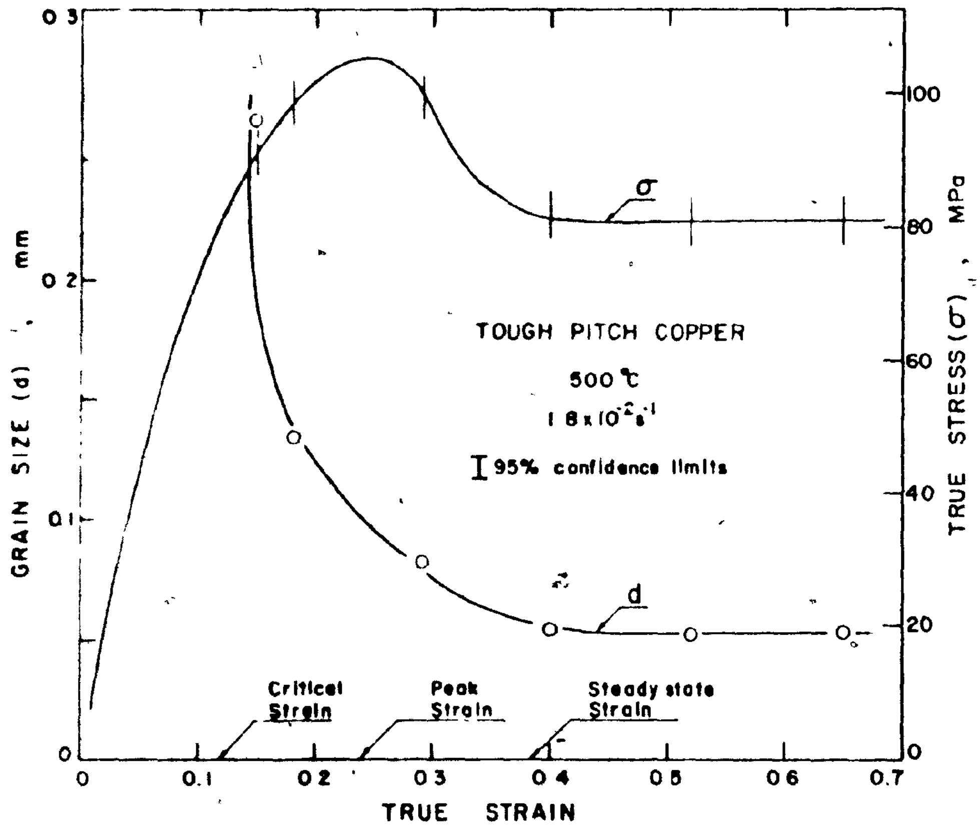

Figure 3.16 The effect of strain on the grain size of copper

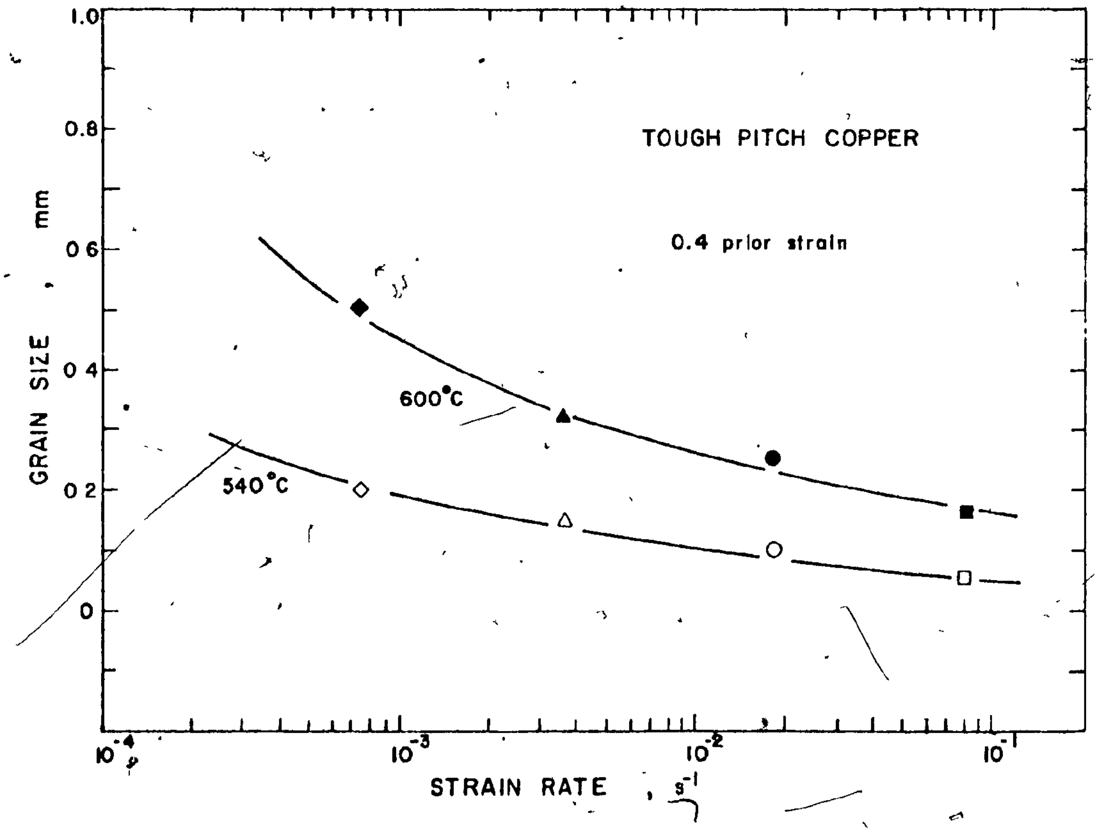

Figure 3.17 Effect of strain rate and temperature on the grain size

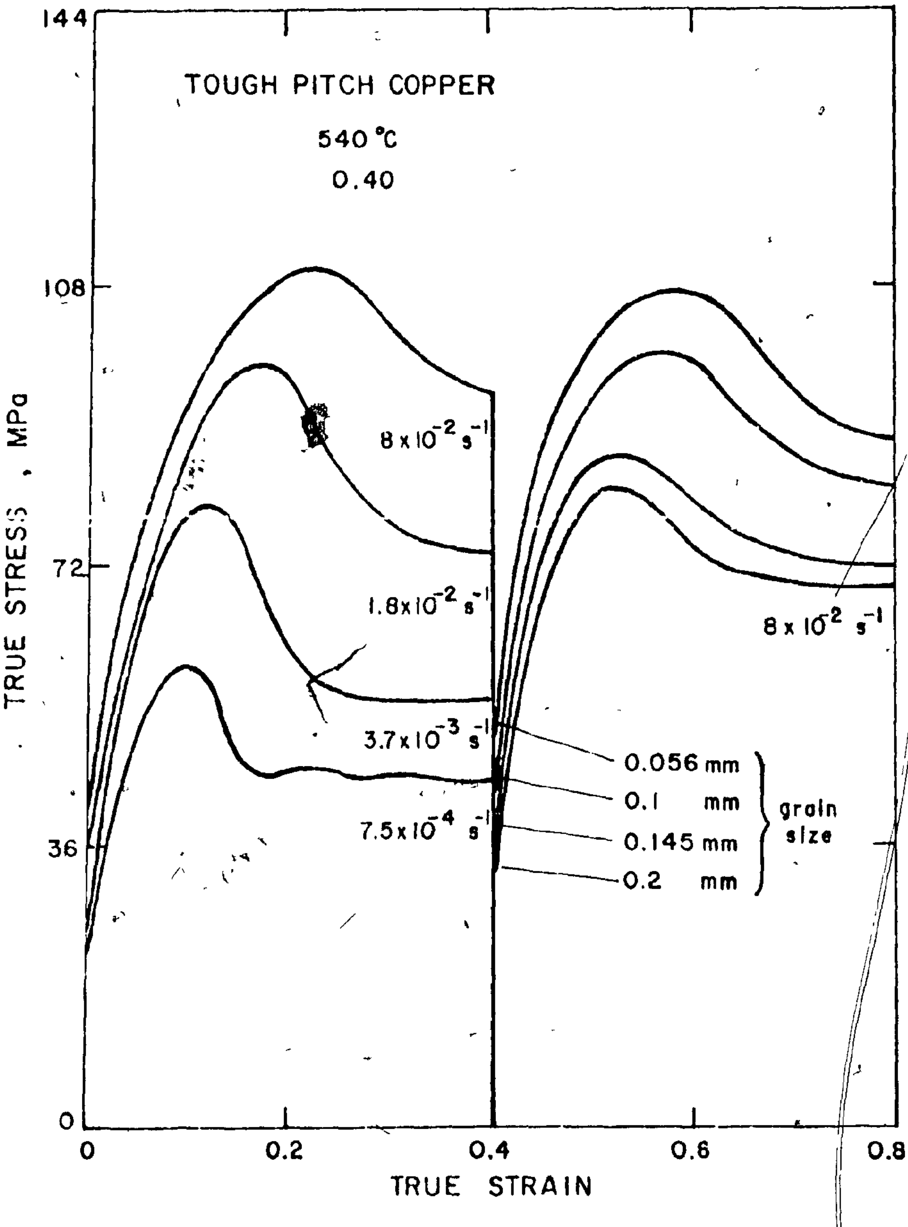

Figure 3.18 An example of the flow curves obtained by interrupted compression at four different $\dot{\varepsilon}$-s where, following a delay, reloading was carried out at a new strain rate. The grain sizes produced are indicated under the appropriate flow curve. On retesting at a single strain rate of 8 x $10^{-2}s^{-1}$ the yield stress was observed to be grain size dependent as was the shape of the flow curve

grain sizes of 0.2, 0.145, 0.10 and 0.056 mm, respectively. The reloading strain rate for this set of experiments was the same, $8 \times 10^{-2}s^{-1}$. The resulting yield stresses on reloading varied with the prestraining strain rate and therefore with the recrystallized grain size. The stress-strain diagrams for other combinations of strain rates and temperatures are given in Appendix 3.6.

From this type of data, the dependence of the yield stress on grain size was plotted in a Hall-Petch manner, as shown in Figure 3.19. It is evident that under the present experimental conditions, the high temperature yield stress increases linearly with the inverse square root of the grain size. (Note that the data of Figure 3.18 are represented by open symbols on curve a of Figure 3.19.)

The strain rate dependence of the grain boundary strengthening coefficient k is shown in Figure 3.20. It is of interest that the value of k gradually decreases with decreasing rates of deformation. It is therefore possible that in the creep range of strain rates ($<10^{-4}s^{-1}$), the value of k may become rather small (i.e. <0.8 MN/m^2 mm$^{\frac{1}{2}}$), which would explain the deductions concerning the invalidity of the Hall-Petch relation that are often made in high temperature creep studies[168]. Similarly, an increase in temperature may also lead to a decrease in k, because its effect on thermal activation is analogous to that of a decrease in strain rate.

According to Figure 3.20, the Hall-Petch relation can be written in the form:

$$\sigma_y = \sigma_0(T,\dot{\varepsilon}) + 0.8\, d^{-\frac{1}{2}} + g(T,\dot{\varepsilon})d^{-\frac{1}{2}} \tag{3.4}$$

Here the first component on the right hand side of the equation represents the yield stress of a single crystal, and the second and third terms arise from the contributions of grain size to the athermal and thermal flow stress components of the developed stress, respectively. The presence of both athermal and thermal components of grain boundary strengthening is worthy of note in that it suggests that the boundaries can serve as both local and long range obstacles at elevated temperatures.

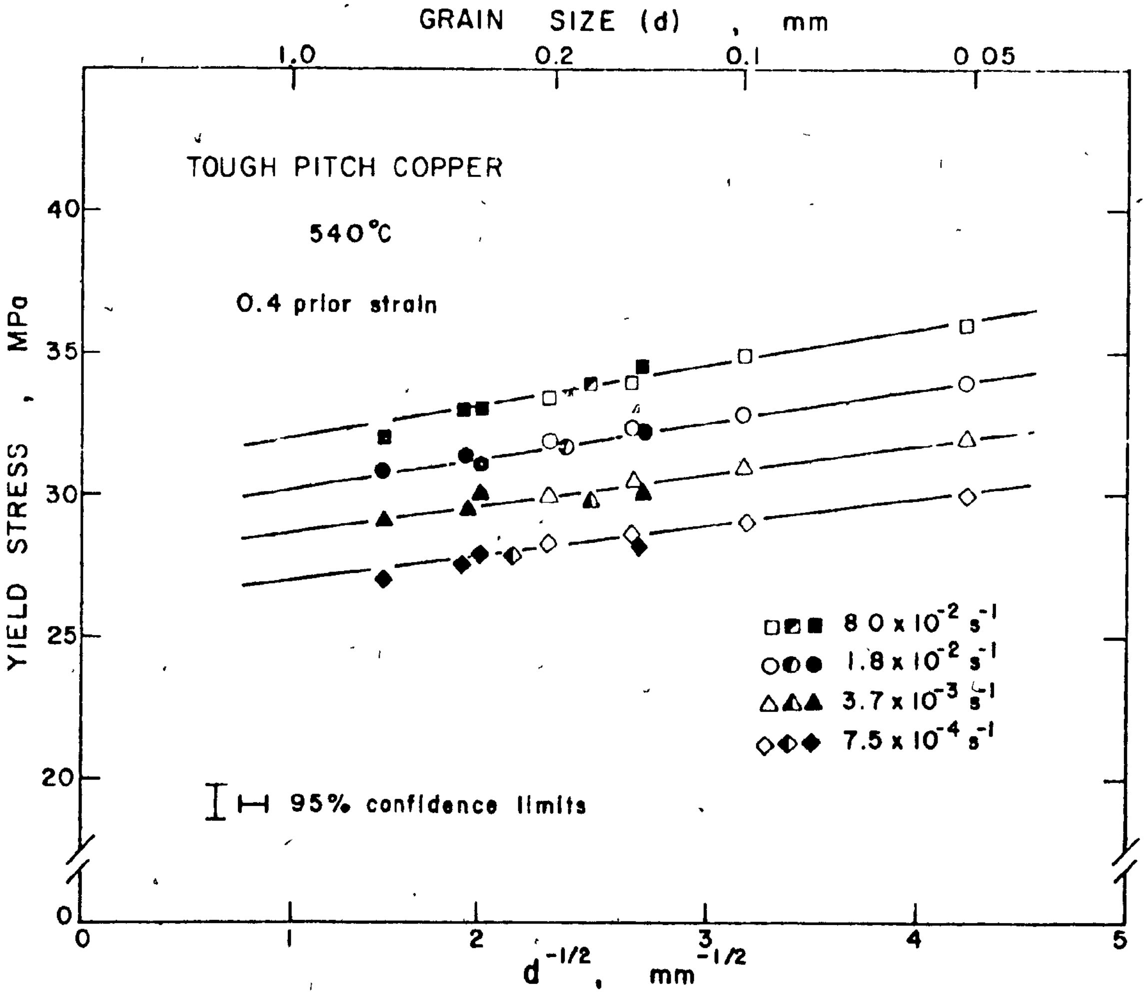

Figure 3.19 The effect of grain size on the high temperature yield stress of copper

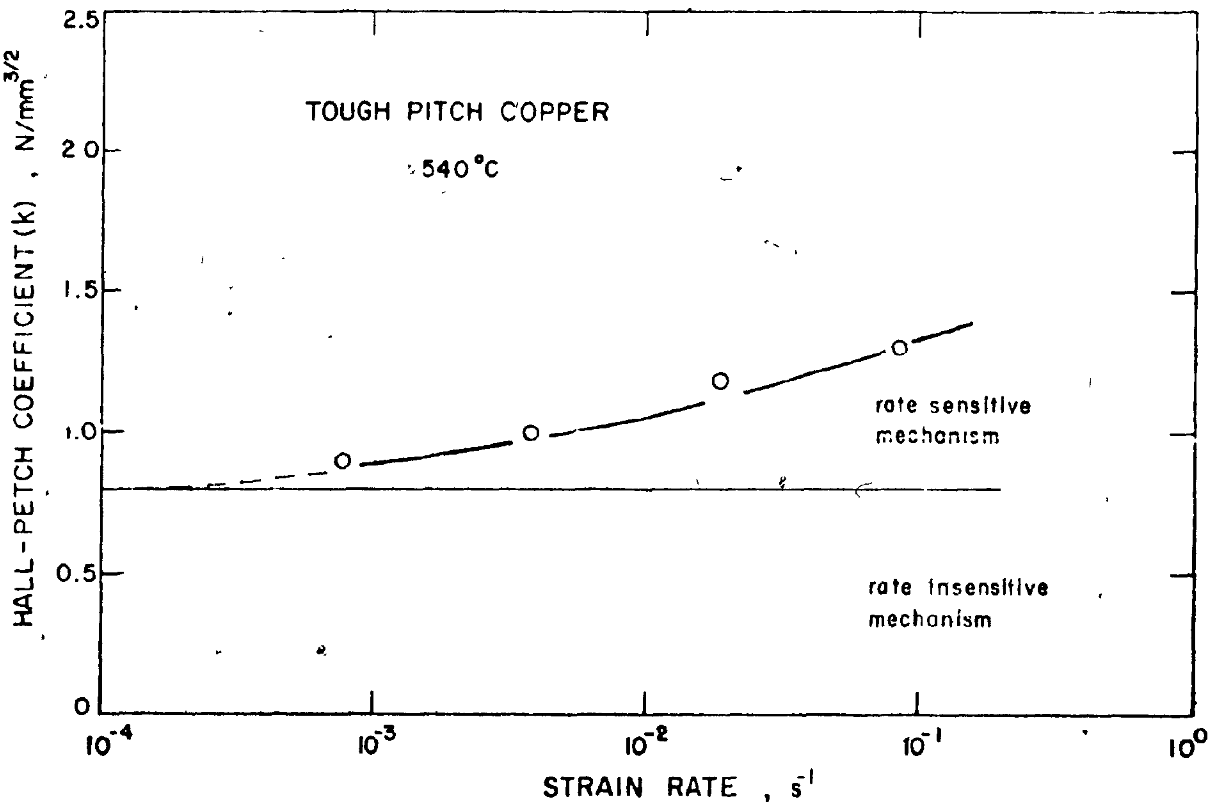

Figure 3.20 Strain rate dependence of the grain boundary strengthening coefficient k

CHAPTER 4

DISCUSSION

4.1 INTRODUCTION

In the previous chapter, two important sets of results were introduced. The first set concerned the effect of hot working on the softening behaviour of the three selected experimental materials; the second, the effect of grain size on the high temperature mechanical properties. Since the main aim of our study was to throw more light on the softening mechanisms taking place after high temperature deformation, it is the purpose of the present chapter to further analyze these two sets of results. The more detailed analysis of the softening behaviour will allow us to arrive at a better understanding of the mechanisms of both dynamic and static restoration in FCC metals at elevated temperatures.

As pointed out earlier, the present results are in good qualitative agreement with our model for static softening following high temperature deformation. We will, therefore, first review this model briefly and then describe qualitatively the expected dependence of the three main softening mechanisms on the experimental parameters. This will be followed by a discussion of the kinetics of the individual processes. Finally, we will discuss the results obtained on plain carbon and microalloyed austenite in the light of the analysis of the copper data.

4.2 HYPOTHESIS FOR THE STATIC RESTORATION PROCESSES

The results presented above have shown that the overall softening rate is affected by prior strain, strain rate and temperature, as well as by the addition of certain alloying elements. We have also seen that up to four static restoration mechanisms are involved in producing full softening, and that softening arrests can appear when individual softening processes go to completion. It was this feature of the softening behaviour that was largely responsible for the elaboration of the inter-relationships between the softening mechanisms that was described above.

In terms of the model, the data suggest that the following combinations of static softening process can operate after high temperature deformation:

1. static recovery only,
2. static recovery and classical recrystallization,
3. static recovery, classical recrystallization and grain growth,
4. static recovery, classical recrystallization and metadynamic recrystallization, and
5. static recovery, classical recrystallization, metadynamic recrystallization and grain growth.

It should be mentioned that a further softening component was observed in the microalloyed austenite which may be attributable to precipitation; however, for the sake of clarity, this effect will be discussed separately in a later section of this chapter.

The inter-relation between the static restoration mechanisms is considered in more detail in Figure 4.1, in which the proportions of softening attributable to each process are shown schematically. The steepest line on the left hand side of the diagram (Figure 4.1a) indicates the occurrence of work hardening in the absence of any of the dynamic softening mechanisms (taken here as linear with a slope of E/300). In the high stacking fault energy metals, the concurrent operation of dynamic recovery reduces the flow stress so that the flow curve is of the form represented in Figure 4.1b. In metals of moderate or low stacking fault energy, such as the present experimental materials, dynamic recrystallization produces additional softening during deformation after a critical strain has been exceeded, leading to the flow curve represented by the heavy line in Figure 4.1c.

If straining is interrupted in dynamically recovered materials, softening takes place by static recovery and by static classical recrystallization, as shown in Figure 4.1d. Below the critical strain for static recrystallization, softening takes place by static recovery only, whereas at higher strains, both mechanisms contribute to the softening. The softening following hot work in materials which recrystallize dynamically is quite complex, as shown in Figure 4.1d. This figure is reproduced in Figure 4.2 for ease of interpretation.

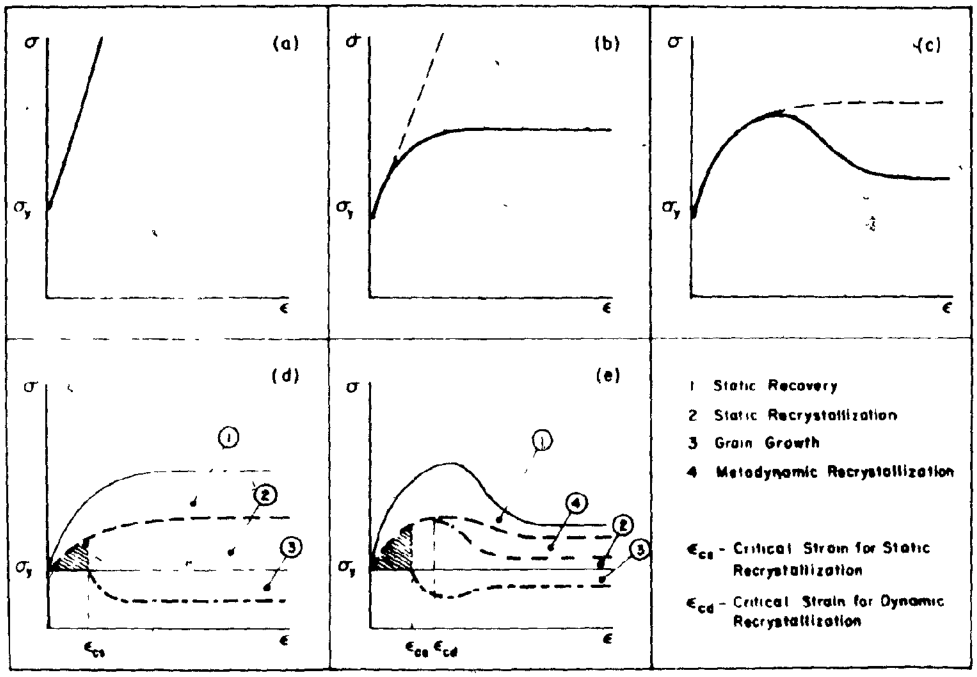

Figure 4.1 The interrelation between the static restoration mechanisms

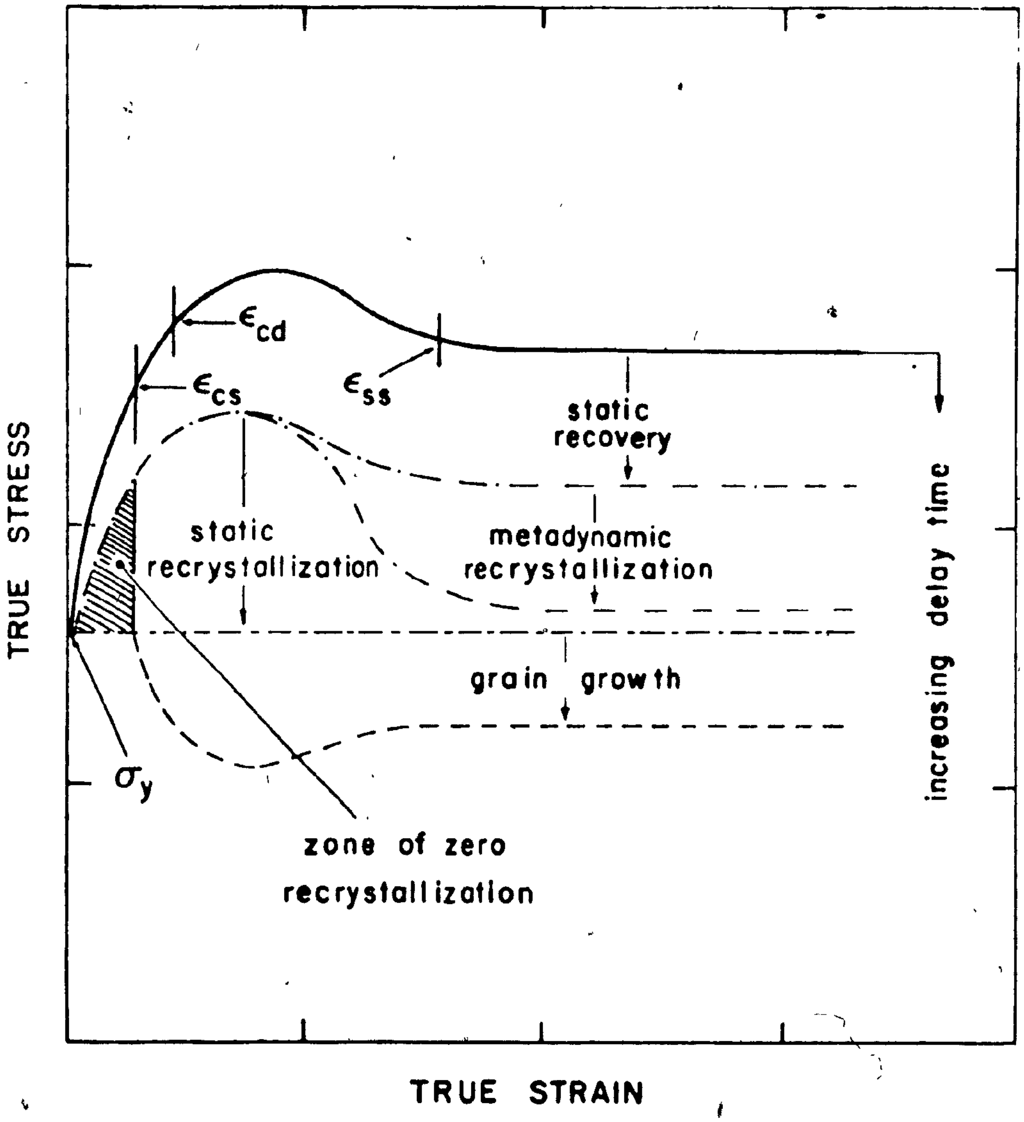

Figure 4.2 Schematic presentation of static softening following hot working in dynamically recrystallized materials

If the deformation is interrupted at a small strain, e.g., below the critical strain for static recrystallization ϵ_{cs}, then softening can only take place by static recovery, and the latter cannot, as indicated by the diagram, completely reduce the flow stress to the level of the undeformed material

If the interruption strain exceeds ϵ_{cs} but is less than the critical strain required to initiate dynamic recrystallization ϵ_{cd}, then the cycle of softening by recovery is followed, after a delay attributable to the formation of recrystallization nuclei, by one of classical recrystallization and full softening can be achieved. Such a sequence of mechanisms can lead to a single softening arrest. It is important to point out that the formation of recrystallization nuclei requires prior recovery to take place$^{(169)}$.

If the interruption strain exceeds ϵ_{cd} but is less than the strain required to reach steady state flow ϵ_{ss}, then static recovery and metadynamic recrystallization occur concurrently, followed eventually by classical recrystallization. Immediately on interruption, metadynamic recrystallization takes place by the continued growth of the dynamically formed recrystallization nuclei. At the same time, the material which has not yet been critically strained for dynamic recrystallization, or which has recrystallized dynamically and which has not been sufficiently strained for the initiation of a new cycle of dynamic recrystallization, softens by static recovery. It is in this latter material that the subsequent classical recrystallization takes place once sufficient time has elapsed for the formation of nuclei. In this interval, the proportion of softening attributable to metadynamic recrystallization increases with strain, as indicated in the diagram, apparently because the density of dynamic recrystallization nuclei also increases with strain. Under these circumstances, two arrests or inflections are possible in the softening curve, one associated with the saturation of the recovery process and the other with the exhaustion of metadynamic recrystallization. Finally, at interruption strains within the steady state region, the proportion of softening attributable to classical recrystallization becomes very small and all the processes occur with great rapidity. As a result, the softening arrests or inflections can be entirely absent.

If the material is held long enough after straining and at a high enough temperature, grain growth can occur, causing an additional softening component. The softening due to grain growth is probably attributable to the decrease in grain boundary density, as has been discussed above.

Before the strain and temperature dependences of the individual processes are discussed, the kinetics of these processes will be considered in turn.

4 3 EMPIRICAL SOFTENING KINETICS

The kinetics of the softening taking place after deformation at high temperatures are difficult to evaluate. The sequential operation of up to four distinct processes precludes the direct application of equations of the form proposed by Avrami(74,75) which are restricted to a single rate process. This observation is supported by the detailed metallographic study of the recrystallization of copper due to Schweizer and Form(68) as well as by the work described above.

In the present study, an attempt was therefore made to fit empirical relationships which are applicable to the individual softening processes. These relationships are used to evaluate the temperature and strain dependence of the processes. It is the interrelationship between the kinetics of the individual processes that finally leads to the complex form of the softening curves illustrated in Figures 3.5 and 3.6.

4.3.1 Basic Considerations

Before the individual softening processes can be separated and their strain and temperature dependences evaluated, it is necessary to define an empirical rate equation for each sector of the softening curves. A rate equation expresses the functional dependence of the rate of a process on the fraction of the process, x, that has been completed at given time t, that is;

$$dx/dt = k\, f(x) \qquad (4.1)$$

where f(x) is any function of x and k is the rate constant. By separating the variables and integrating Equation 4.1 we obtain;

$$g(x) = kt \tag{4.2}$$

where g(x) is another function of x. The analysis of experimental data then involves the problem of finding a g(x) which adequately fits the data and which also has a physically reasonable functional form.

The progress of softening, whether it occurs by recovery or by recrystallization, must be considered as a heterogeneous process. Both processes involve the formation of recovered or recrystallized domains within a work hardened matrix. The rate of such processes does not depend only on the growth of such domains. In the case of recrystallization, the rate is influenced by the rate of nucleation and the effect of the impingement of newly recrystallized grains. As recovery proceeds, on the other hand, the process is expected to become exhausted as a stable dislocation substructure is formed and the dislocation density within the subgrains is reduced to a stable level.

Many solid state reactions, including the formation of new phases(71), precipitation reactions(76), the formation of solute atmosphere about dislocations(170), and recrystallization(74,75), are adequately described when the function g(x) in Equation 4.2 above is of the form

$$g(x) = \{\ln(1/1-x)\}^m \tag{4.3}$$

Here m is a constant, so that Equation 4.2 becomes

$$\ln\{1/(1-x)\} = (kt)^n \tag{4.4}$$

where n = 1/m. Rearranging Equation 4.4 we obtain

$$x = 1-e^{-(kt)^n} \tag{4.5a}$$

or, more usually,

$$x = 1-e^{-k't^n} \tag{4.5b}$$

This expression is simply the general form of the Johnson-Mehl equation (1.24), which was originally determined for the case of the formation of pearlite from austenite. Differentiation of 4.5 with respect to time gives a rate equation of the form

$$dx/dt = k'' t^{n-1} (1-x) \qquad (4.6)$$

where $k'' = nk^n = nk'$. This type of rate equation yields a sigmoidal (semi-logarithmic) transformation curve which adequately describes recrystallization(74,75). It is also of the form of the recovery curves of Figures 3.5 and 3.6 and represents first order kinetics when n in Equation 4.4 is set to 1.0.

We now turn to the problem of the separation of the components of softening observed following the hot working of tough pitch copper. The empirical kinetics appropriate to each softening process will be described in turn.

4.3.2 Recovery Kinetics

The fractional softening, as we recall, is defined by the equation

$$X = (\sigma_m - \sigma_r)/(\sigma_m - \sigma_y) \qquad (4.7)$$

where σ_m is the maximum stress on unloading, σ_y the initial yield stress, and σ_r is the yield stress on reloading. If it is assumed that the increase in flow stress from the initial yield to the unloading stress arises from an increase in internal stress only, then the denominator in Equation 4.7 is equal to the internal stress at the beginning of the holding period. This assumption presupposes that no significant change in the thermal component of the flow stress occurs on straining. After interruption, the internal stress is decreased by recovery and by recrystallization. If we consider the recovery stage only, then the internal stress (or residual workhardening) after any holding interval is given by

$$\sigma_i = \sigma_r - \sigma_y \qquad (4.8)$$

Data for copper deformed at 500°C and $1.8 \times 10^{-2} s^{-1}$ and interrupted at strains of 0.05 and 0.10 are used to illustrate the progress of recovery in Figure 4.3. Here the net work hardening part of the flow curve is included for reference. It is evident from Figure 4.3 that for a given interruption strain, the internal stress decreases to an asymptotic level which depends on the prior strain or on the value of internal stress at the beginning of the delay period. To describe the recovery process, it is necessary to set up an expression for the fractional recovery. If the asymptotic value of the internal stress produced by full recovery is σ_∞, the fractional softening at the completion of recovery X_∞^r is given by the equation

$$X_\infty^r = \frac{\sigma_m - \sigma_\infty}{\sigma_m - \sigma_y} \qquad (4.8)$$

The superscript r is used here to denote the softening fraction attributable to recovery only. The <u>degree</u> of recovery x_r is given by,

$$x_r = \frac{X^r}{X_\infty^r} = \frac{\sigma_m - \sigma_r}{\sigma_m - \sigma_\infty} \qquad (4.9)$$

Given the form of the recovery curves obtained in the present experiments, we can substitute for x_r in Equation 4.4 to obtain the integrated rate equation in terms of the softening fraction X^r, viz.,

$$\ln\{X_\infty^r / X_\infty^r - X^r\} = k^r t^n \qquad (4.10)$$

The superscript r on the rate constant is used here only to denote recovery.

Alternatively we may write Equation 4.10 in the more familiar form

$$X^r = X_\infty^r \, (1 - e^{-k^r t^n}) \qquad (4.11)$$

The value of the exponent n in Equation 4.10 above can be obtained by plotting log $\ln\{X_\infty^r/(X_\infty^r - X)\}$ against log t.

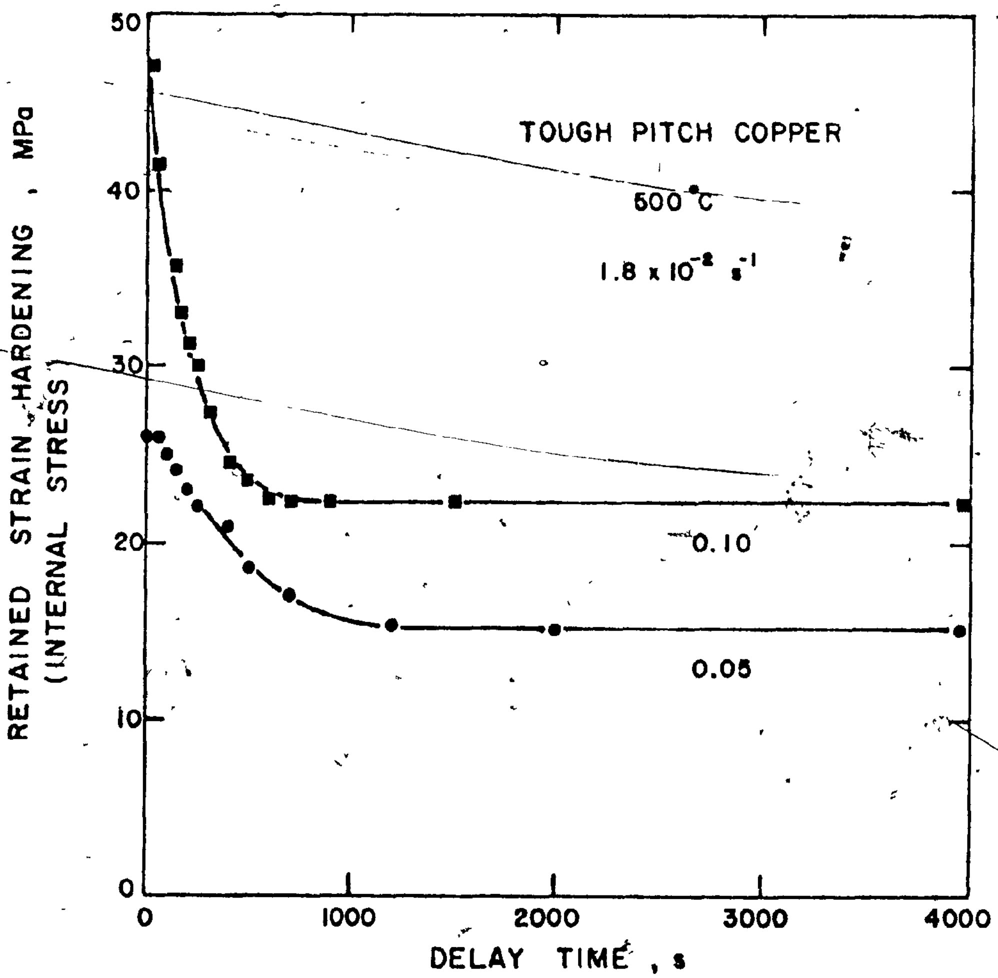

Figure 4.3 The progress of static recovery in copper after straining at 500°C and $\dot{\varepsilon} = 1.8 \times 10^{-2} s^{-1}$ to prestrains of 0.05 and 0.10

The data obtained for tough pitch copper at 450, 500 and 540°C under conditions where only static recovery was taking place are represented in this way in Figure 4.4.

It should be noted that the slopes of the curves appear to be independent of strain and temperature and exhibit a constant value of 1.33. Thus it is evident that the present recovery data do not follow the first order reaction kinetics observed in experiments on the recovery of cold worked metals$^{(62)}$. The rate constant k^r for each of the prior deformation conditions that exhibited recovery only was obtained from plots of $\ln\{X^r_\infty/X^r_\infty - X^r\}$ versus $t^{1.33}$, as shown in Figure 4.5. It is evident that k^r increases rapidly with both strain and temperature and thereby reflects the displacement of the recovery curves in Figures 3.5 and 3.6 and Figure 4.6 below to shorter times as the temperature and strain are increased. It is also of importance to note that the value of X^r_∞ obtained from those experiments in which recovery was the only static softening mechanism increases with strain, but is apparently independent of temperature. The quality of the fit to the experimental data, obtained by the use of Equation 4.10, is demonstrated in Figure 4.6, where the softening curves generated by means of the equation using the constants determined above, are plotted along with the data points.

The physical significance of the temperature and strain dependence of the empirical constants will be discussed later, along with the dependences obtained from the composite curves presented in Section 4.3.4 below.

4.3.3 Kinetics of Recovery and Recrystallization

It has been shown in the previous section that an integrated rate equation of the form of Equation 4.5(b) adequately fits the recovery curves obtained under conditions where recovery is the only static softening process. However, as pointed out earlier, Equation 4.5 is also the general form of the Johnson-Mehl equation which is used to describe the kinetics of recrystallization. In most earlier studies of recrystallization following either cold or hot working, the progress of recrystallization was followed by means of metallography and therefore it was unnecessary to consider the influence of concurrent recovery. In the present

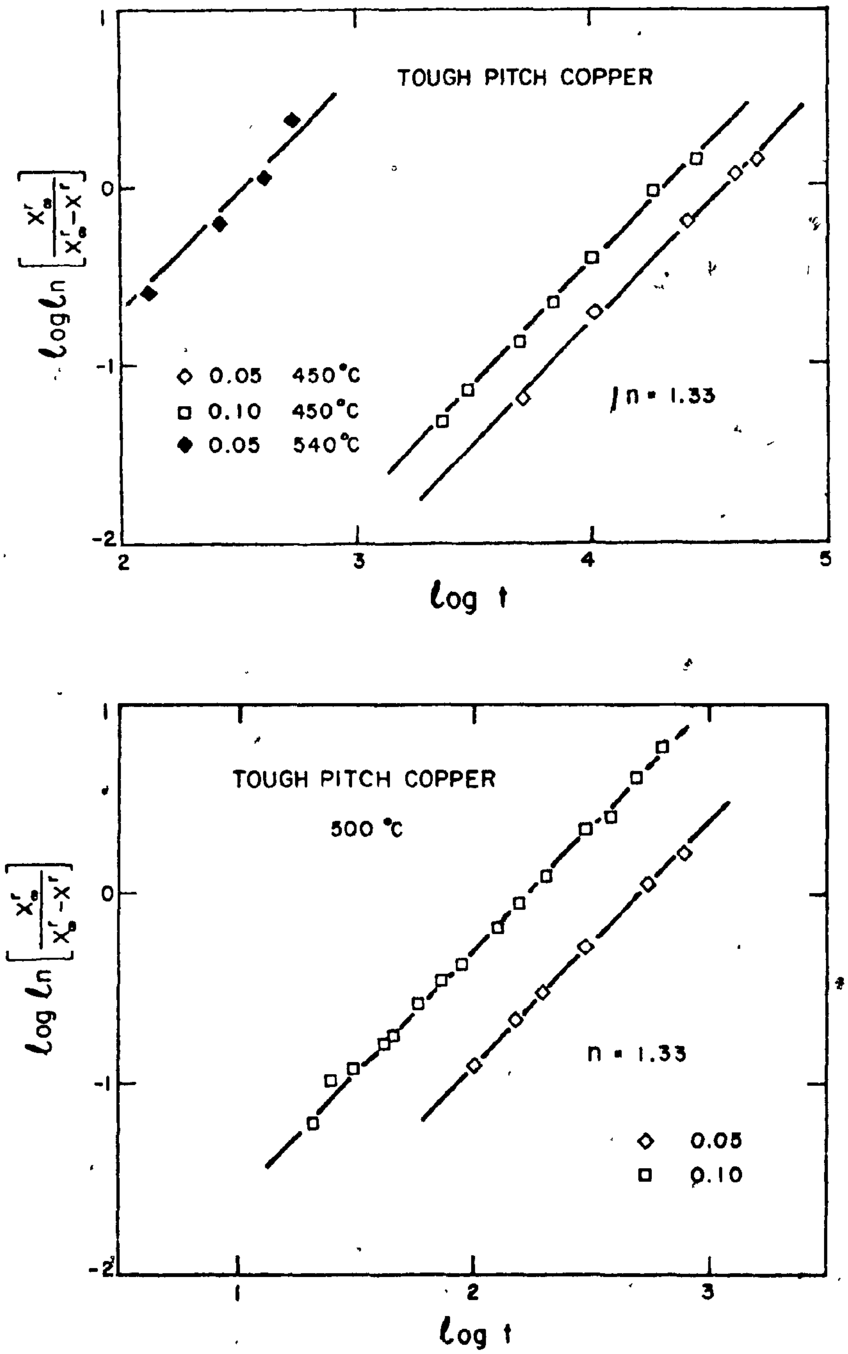

Figure 4.4 Graphical presentation of Equation 4.10 in tough pitch copper

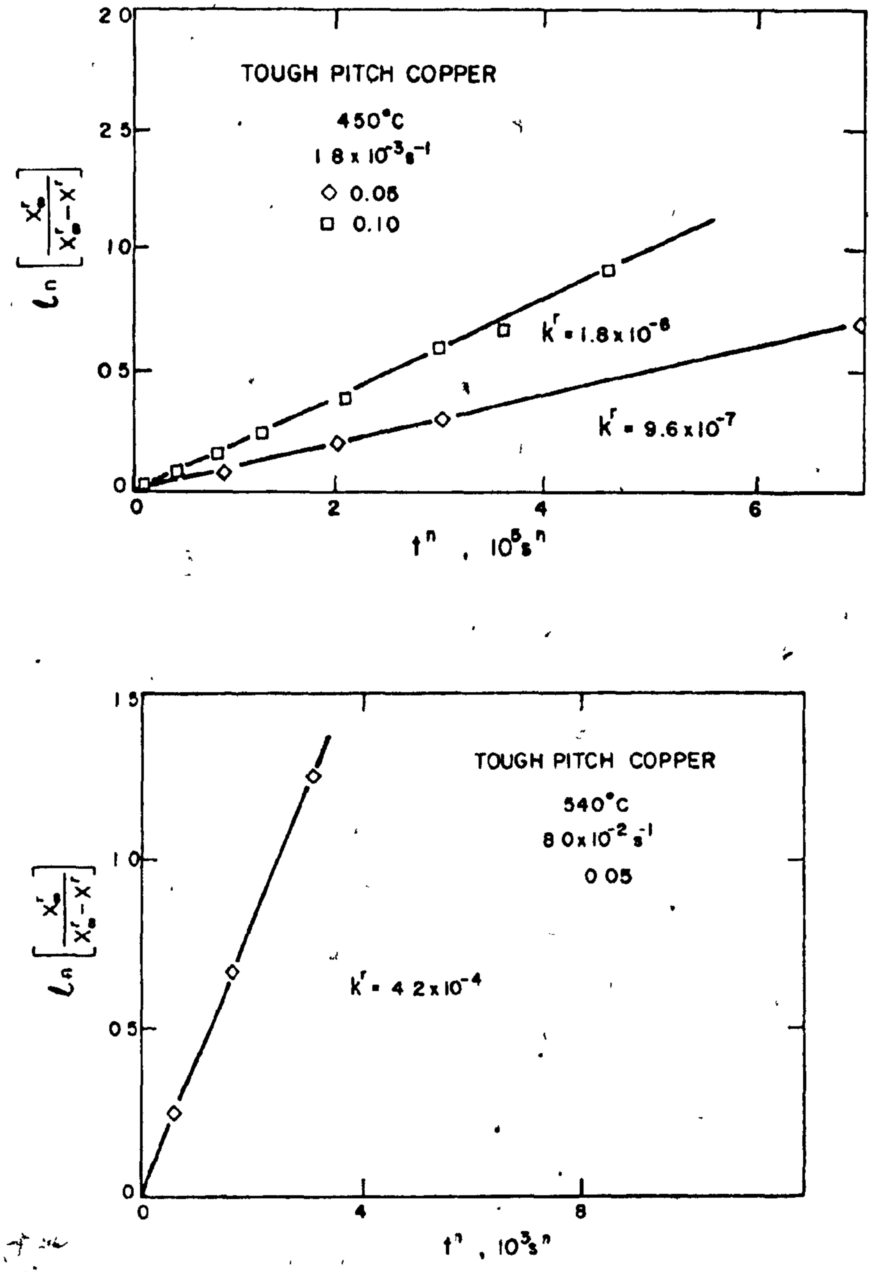

Figure 4.5 Graphical determination of the rate constant k^r.

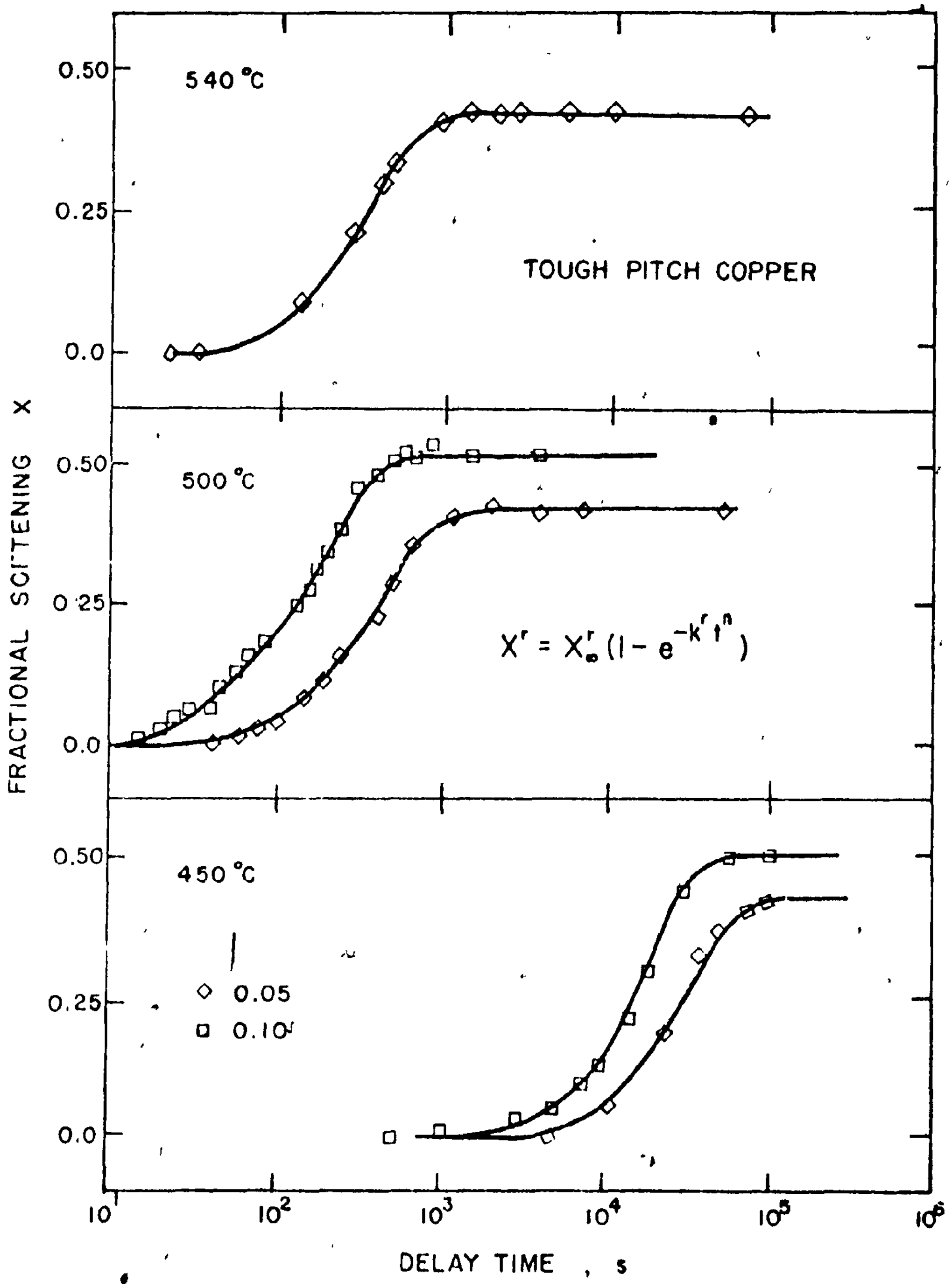

Figure 4.6 Fit of Equation 4.10 to experimental data points for static recovery

study, where the structural changes were followed by mechanical means, the recovery component of softening must be included in the rate equation. Furthermore, when dynamic recrystallization occurs during prior hot working, the softening component due to metadynamic recrystallization must be included as well. Since the detailed mechanisms of these processes differ, the empirical constants in the relevant rate equations are expected to differ also.

The overall softening produced when the three softening processes occur together will in general be given by the sum of the individual softening components, i.e.

$$X = X^r + X^R + X^M \tag{4.12}$$

where the superscripts R and M refer to classical recrystallization and metadynamic recrystallization respectively. When the overall softening has gone to completion, all the processes saturate, so that

$$X_\infty = X_\infty^r + X_\infty^R + X_\infty^M = 1 \tag{4.13}$$

Having established that static recovery after hot working is described by an equation of the form of Equation 4.5 and assuming that the recrystallization processes are described by equations of similar form, we may define the components of softening as follows

$$X^r = X_\infty^r(1-e^{-k^r t^n}) \tag{4.11}$$

$$X^R = X_\infty^R(1-e^{-k^R t^p}) \tag{4.14}$$

and $$X^M = X_\infty^M(1-e^{-k^M t^q}) \tag{4.15}$$

Before these equations can be used, however, the values of X_∞^r, X_∞^R and the X_∞^M must be estimated from the experimental data.

4.3.3.1 Recovery and Classical Recrystallization

We first turn our attention to the softening curves obtained under the conditions where recovery and classical recrystallization operate together. The model and the metallographic results suggest that after prestraining 0.15 and 0.18, only these two processes will operate. Under such circumstances, Equation 4.12 above becomes

$$X = X^r + X^R \qquad (4.16)$$

and Equation 4.13 is reduced to

$$X^r_\infty + X^R_\infty = 1 \qquad (4.17)$$

It is evident from the grain size distributions for a prestrain of 0.15 at 500°C that recrystallization begins only after a delay time of 30s. Reference to the appropriate softening curve in Figure 3.5 shows that one inflection plateau is apparent in the curve at these strains. This observation suggests that the maximum softening due to recovery alone does not increase beyond 50% once the critical strain for static recrystallization is exceeded. It then follows from Equation 4.17 that under these conditions

$$X^r_\infty \simeq X^R_\infty = 0.5 \qquad (4.18)$$

Furthermore, since the processes act sequentially, and the recovery process is complete or almost complete prior to the commencement of recrystallization, in the interval up to 50% softening, we can set $X^r = X$. The kinetics of recovery can thus be again evaluated in the manner described in Section 4.3.2 above. The curves representing the recovery kinetics for prestrains of 0.10 at 540°C, 0.15 at 450, 500 and 540°C and 0.18 at 500°C are shown in Figure 4.7(a). It is evident that these data are well represented by a straight line with a slope n of 1.33, as found for the lower prestrains for which recovery was the only operative softening process.

Having established the constants k^r and n in Equation 4.11 above, the value of x^r can be determined for all values of delay time so that X^R can be evaluated with the aid of Equation 4.16. The data obtained by this means for the same experimental conditions are plotted in the manner of Equation 4.10 in Figure 4.7(b). Here the slopes of the curves p have a value of 2.2 which is apparently independent of strain and temperature. The rate constant for the recrystallization, on the other hand, is strongly dependent on strain and temperature. The values of the rate constants are tabulated together with those relevant to the other processes in Table 4.1.

The quality of the fit of the two-component softening curves based on Equations 4.11, 4.14 and 4.16 to the experimental data is demonstrated in Figure 4.8, where the data points were determined for prestrains of 0.15 and 0.18 at 500°C.

4.3.3.2 Recovery, Static and Metadynamic Recrystallization

We turn our attention now to the problem of separating the components of softening in the case where all three processes, i.e. recovery, classical and metadynamic recrystallization, operate together. The principal problem in this case is the estimation of the maximum fractional softening, i.e. X_∞^r, X_∞^R and X_∞^M that can be produced by each of the processes. The evaluation of these parameters was only possible for the softening curve obtained after a prestrain of 0.40 at 500°C. This was the only condition where all three processes were operative and for which metallographic as well as softening data were available.

Examination of the grain size distributions for this condition (Figure 3.10(d)) shows that after 3.8s (which corresponds to the end of the first cycle of softening), 36% of the volume has recrystallized. This is attributable solely to metadynamic recrystallization, so that X_∞^M may be taken as 0.36. After a delay time of 3.8s, 64% of the material was still unrecrystallized statically, although it had recrystallized dynamically, as shown by the decrease in the grain size from that of the undeformed material.

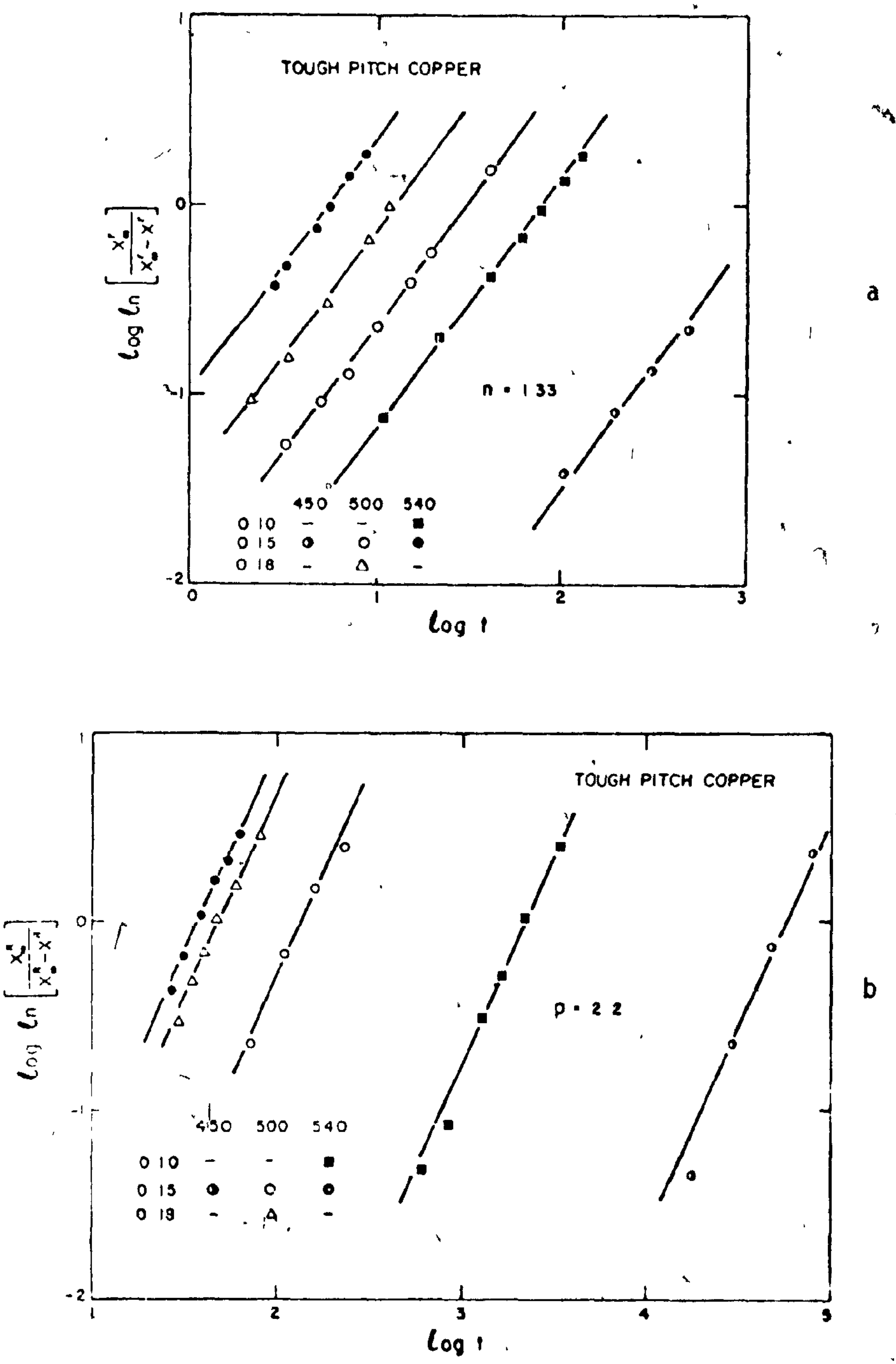

Figure 4.7 Log-log plots of Equations 4.11 and 4.10 for the recovery and static recrystallization components, respectively.

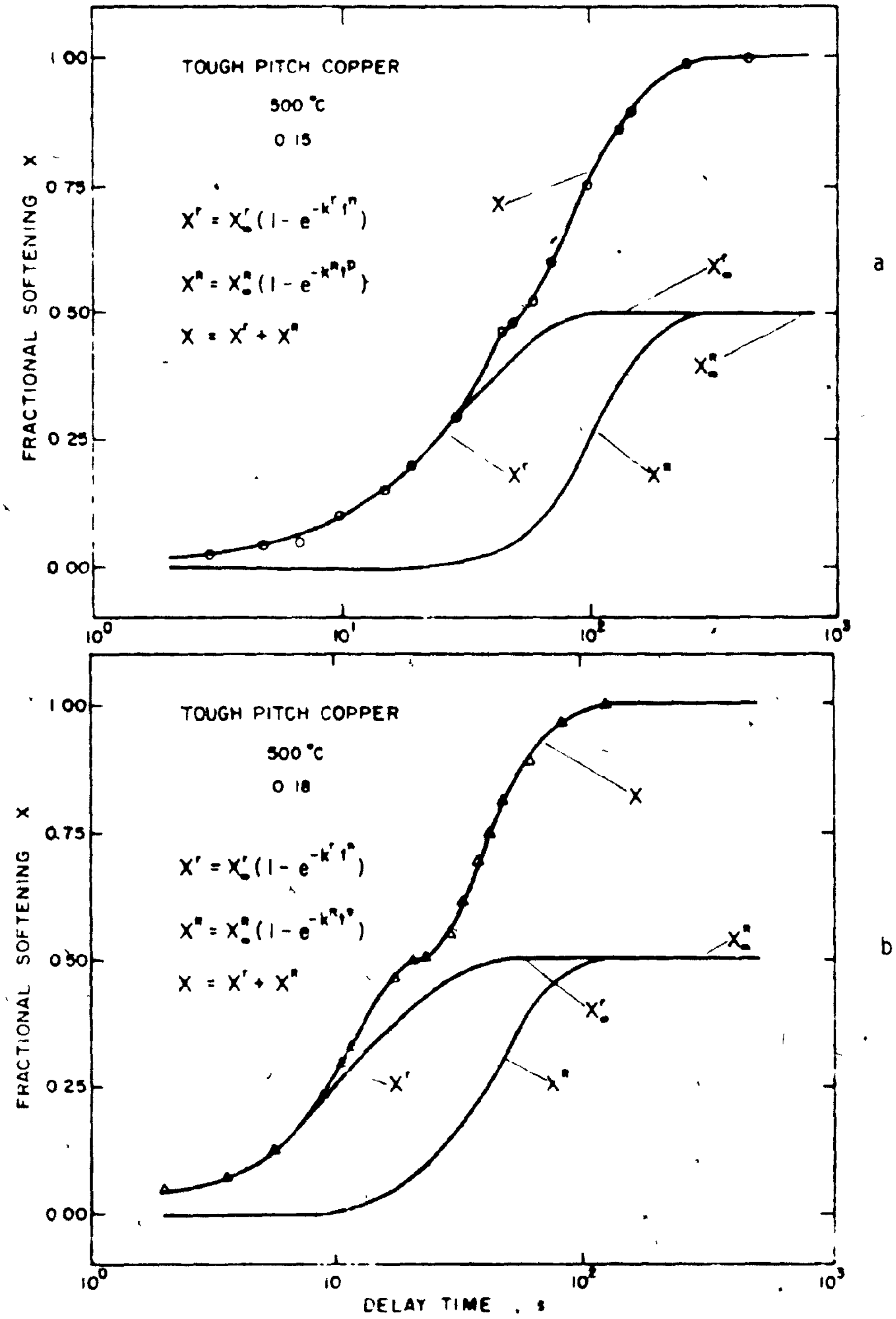

Figure 4.8 Comparison between the two-component softening curves based on Equations 4.11, 4.14 and 4.16 and the experimental data obtained at 500°C

It was shown above that the relative amount of softening by recovery increases with strain to a value of 50% at a strain of 0.18. Although the saturation level for recovery cannot be measured for strains beyond the peak, because of the intervention of metadynamic recrystallization, it can be estimated by several means. On the assumption that the saturation level can continue to increase with strain, estimates of 60% or 70%, for example, can be obtained (173). In the present work, the saturation level for recovery was determined by an iterative process, using various estimated saturation levels for the three processes. Four such iterations are shown in Appendix 4.1, of which the fourth is reproduced below as Figure 4.12.

It is of interest that the saturation levels that gave the best fit to the experimental data were the following:

X_∞^M	0.36
X_∞^r	0.40
X_∞^R	0.24

The latter two values correspond to the case where 63% of the softening in the material which recrystallizes classically is produced by static recovery.

The various fits shown in Appendix 4.1 were only attempted after values had been chosen for the rate constants k^r and k^R, which depend strongly on strain and temperature. The time exponents for the three processes, on the other hand, were assumed to remain constant, as discussed above. In the present work, it was found that the strain dependence of the rate constants could be represented by the equations:

$$k^r = Ae^{B\varepsilon} \tag{4.19}$$

and

$$k^R = Ce^{D\varepsilon} \tag{4.20}$$

as shown in Figure 4.9. In a material that undergoes dynamic recrystallization, the stored energy reaches a maximum at or near the peak of the flow curve. It is, therefore, reasonable to assume that the rate constant will reach a maximum value at this critical value of strain. In view of this, the horizontal curves in Figure 4.9 were fitted to intersect the inclined line at various strains in the vicinity of the peak strain. The values of k^r and k^R obtained in this way were used, along with the values of X_∞^r, X_∞^R, n and p determined above, to calculate alternative curves for X^r and X^R. The best fit to the experimental data after the saturation of metadynamic recrystallization was obtained with k^r and K^R evaluated at 0.9 ε_p (i.e. 0.225).

The curves representing the data obtained in this way are plotted in the manner of Figure 4.4 in Figure 4.10. Once the values of k^r and k^R were established and X^r and X^R calculated as a function of delay time, the function X^M (i.e. the progress of metadynamic recrystallization) was calculated by difference with the aid of the equation,

$$X^M = X - (X^r + X^R) \tag{4.21}$$

The data thus obtained are plotted in the usual manner in Figure 4.11. The slope q of the curve was found to be approximately equal to 1 and the rate constant k^M took a value of 1.5. The individual softening curves are plotted in Figure 4.12 along with their sum which is seen to represent the overall softening data very faithfully. The good fit depends, of course, on the numerous assumptions already outlined above, and so the values of the rate and other constants which correspond to the fit and which are tabulated in Table 4.1, can only be regarded as qualitative. They do, however, establish that the three-component softening process is a consistent one.

We will now consider the physical significance of the rate constants and time exponents determined in the foregoing section.

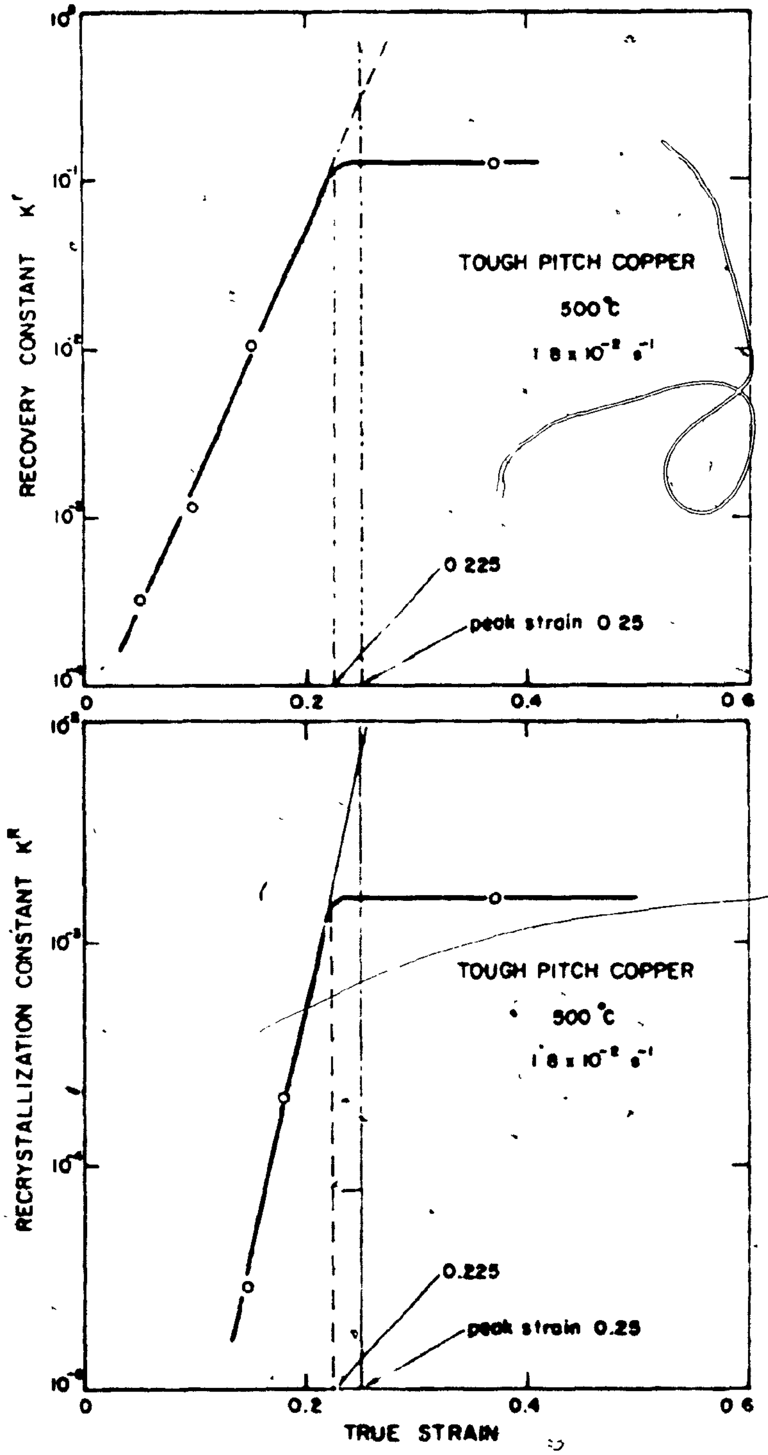

Figure 4.9. The strain dependence of the rate constants for recovery and static recrystallization

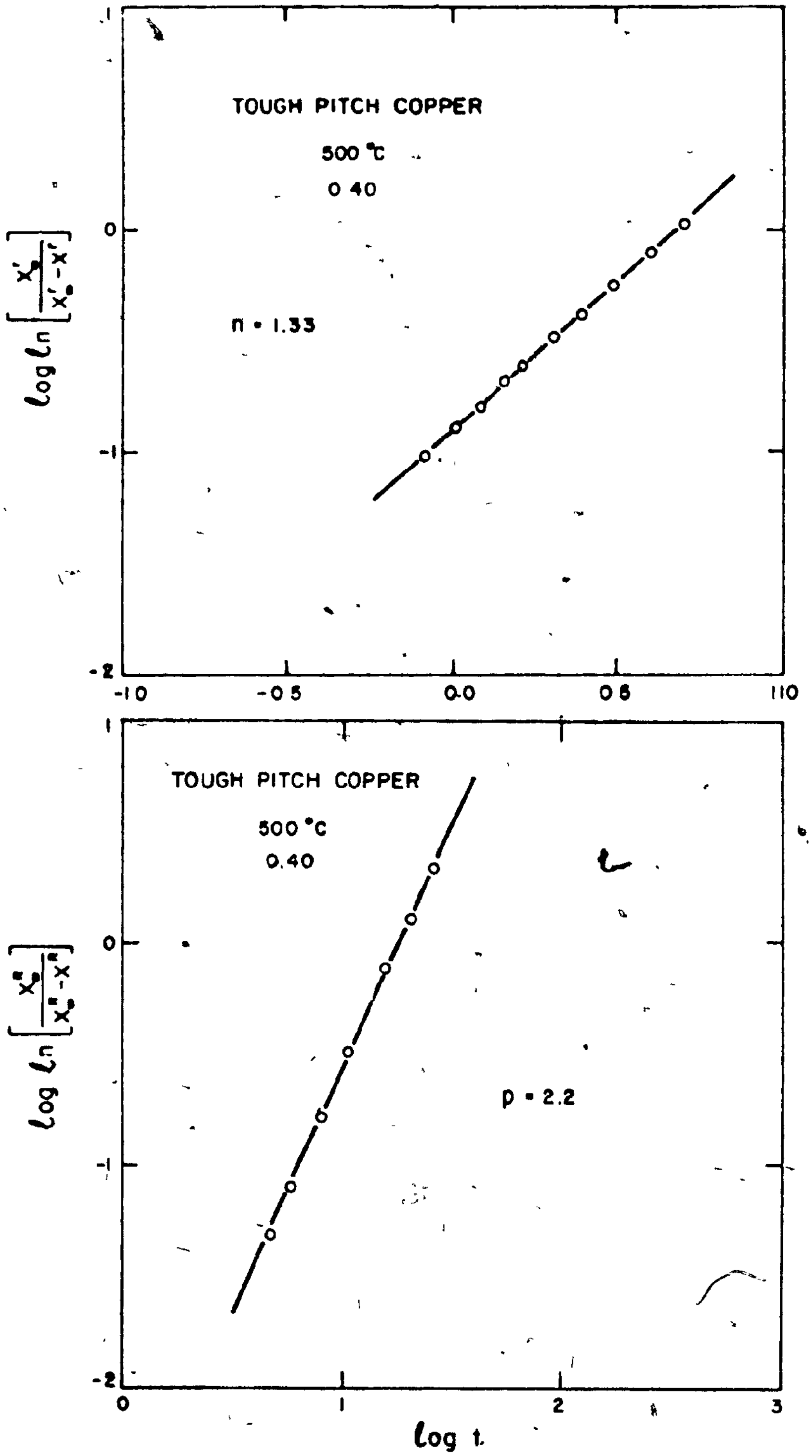

Figure 4.10 Log-log plots of Equations 4.11 and 4.10 for recovery and static recrystallization, respectively

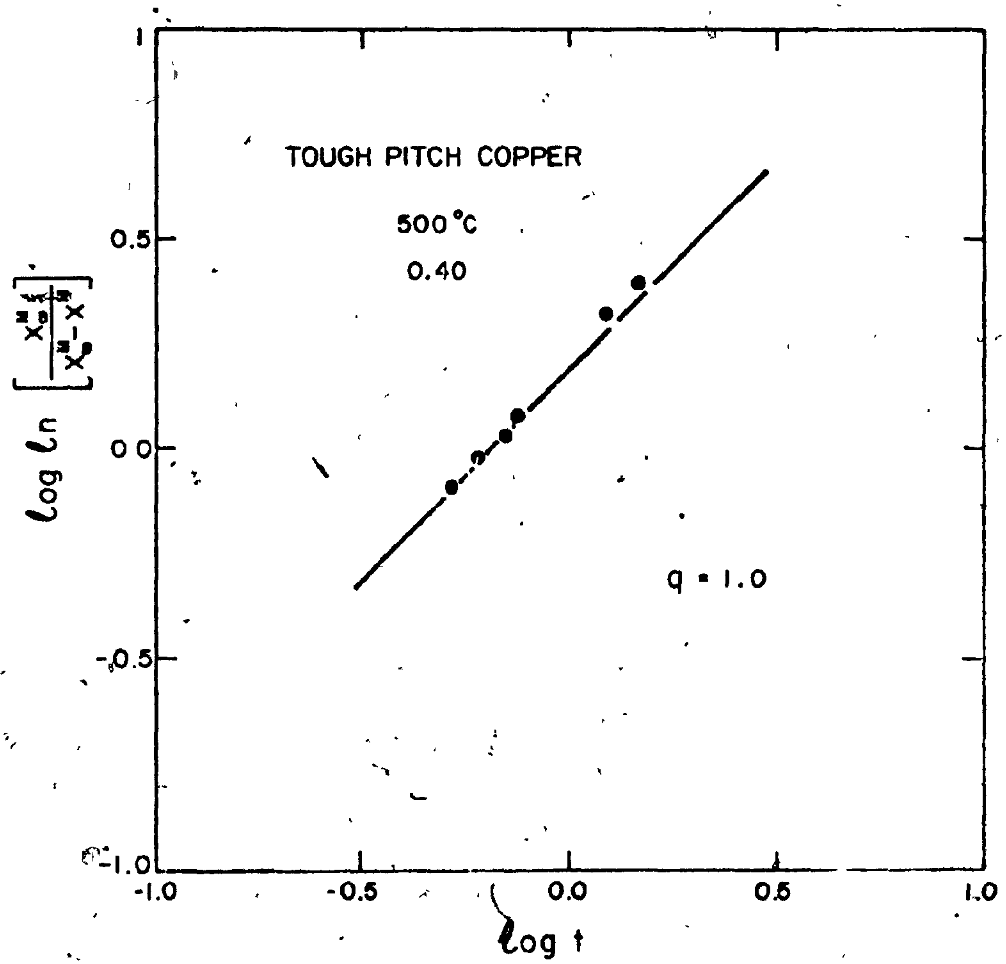

Figure 4.11 Graphical determination of the time exponent q in metadynamic recrystallization

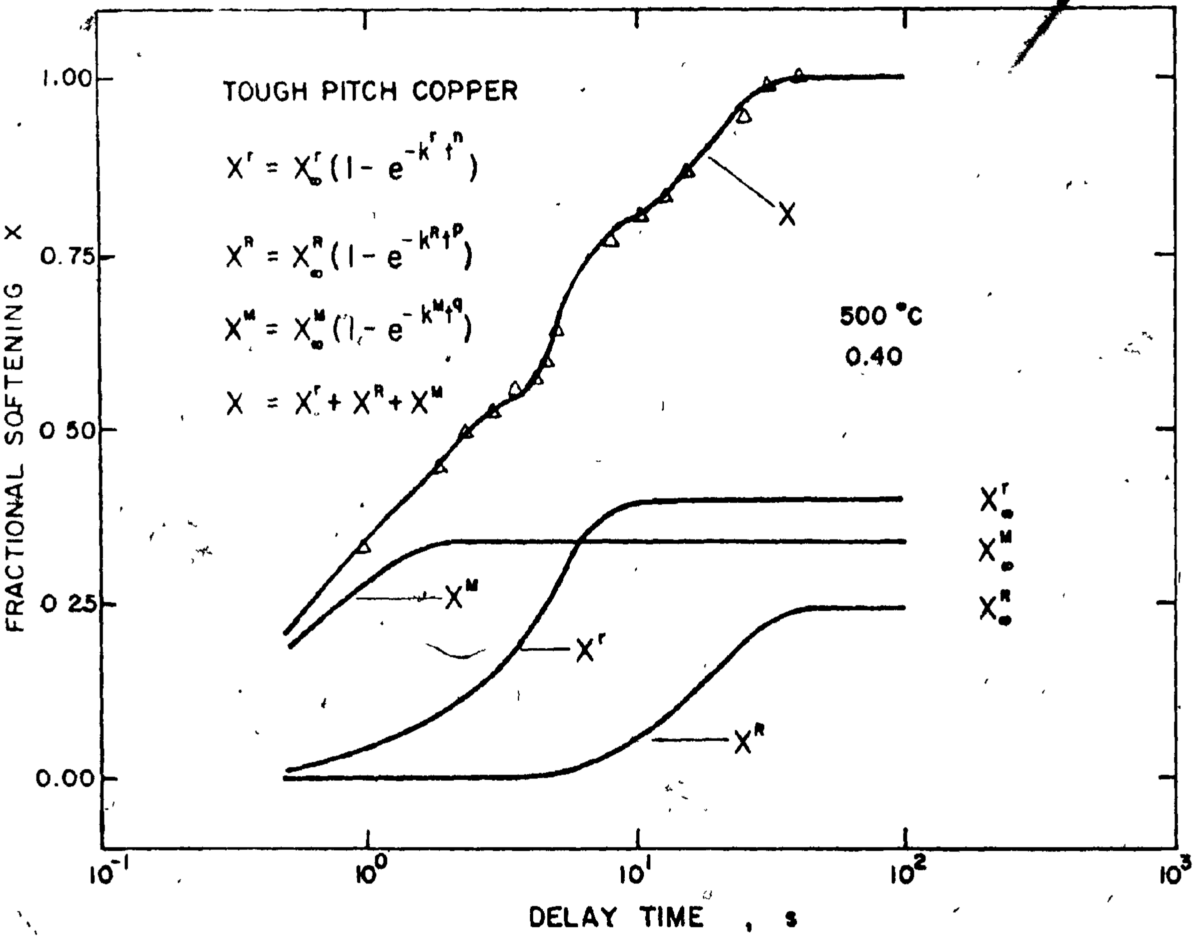

Figure 4.12 The experimental data as fitted by the three softening curves based on Equations 4.11, 4.14 and 4.12

TABLE 4.1

Empirical Constants for Equation 4.12 obtained from the Softening Data

Temp {^{0}C}	Strain Rate {s^{-1}}	Pre-Strain	Recovery			Classical Recrystallization			Metadynamic Recrystallization		
			k^r	n	X_∞^r	k^R	p	X_∞^R	k^M	q	X_∞^M
1	2	3	4	5	6	7	8	9	10	11	12
450	1.8×10^{-3}	0.05	9.6×10^{-7}	1.3	0.42	-	-	-	-	-	-
		0.10	1.8×10^{-6}	1.3	0.50	-	-	-	-	-	-
		0.15	3.1×10^{-5}	1.3	0.50	5.4×10^{-11}	2.2	0.50	-	-	-
500	1.8×10^{-2}	0.05	3.2×10^{-4}	1.3	0.42	-	-	-	-	-	-
		0.10	1.1×10^{-3}	1.3	0.50	-	-	-	-	-	-
		0.15	1.1×10^{-2}	1.3	0.50	2.7×10^{-5}	2.2	0.50	-	-	-
		0.18	3.0×10^{-2}	1.3	0.50	2.0×10^{-4}	2.2	0.50	-	-	-
		0.40	1.2×10^{-1}	1.3	0.40	1.6×10^{-3}	2.2	0.24	1.50	1.0	0.36
540	8×10^{-2}	0.05	1.2×10^{-4}	1.3	0.42	-	-	-	-	-	-
		0.10	2.4×10^{-3}	1.3	0.50	5.4×10^{-8}	2.2	0.50	-	-	-
		0.15	1.2×10^{-1}	1.3	0.50	3.0×10^{-4}	2.2	0.50	-	-	-

4.3.4 Physical Significance of the Empirical Recovery Equation

We now turn to consider the physical significance of a relationship of the form of Equation 4.11. In the classical experiments on recovery after cold work, the process has been shown to follow simple first order kinetics. First order kinetics imply that the recovery process begins immediately at time equals zero. In the present case, however, it is evident that recovery does not start at the full rate immediately after the cessation of deformation. Instead, it achieves its maximum rate only after about 5% recovery. For a process of the present type to be described by simple linear kinetics, it is necessary to invoke an 'incubation time' τ, during which no change occurs. The integrated first order rate equation in terms of degree of recovery then becomes

$$x_r = 1-e^{-k(t-\tau)} \tag{4.22}$$

where k is a constant. Such a relation is shown fitted to the data in Figure 4.13, which also includes a curve representing Equation 4.11.

It can be seen from Figure 4.13 that during the initial period of holding, processes take place which do not markedly change the level of the retained work hardening or internal stress: such processes could be the migration of interior dislocations to the cell walls. The major process of softening, which takes place after the 'incubation' interval, could then be due to the annihilation of redundant dislocations within the cell boundaries.

Although a relation of the form of Equation 4.22 can be used to describe the present data in the mid-range of the process, softening actually takes place more rapidly at the end of this stage of recovery. On the other hand, Equation 4.11 fits the data better but is less amenable to physical interpretation.

We have already noted above that the recovery part of the softening process saturates well below full softening. Thus Equation 4.22 is in the normalized form in which x_r varies from zero initially to one at saturation. It is convenient for direct comparison with standard treat-

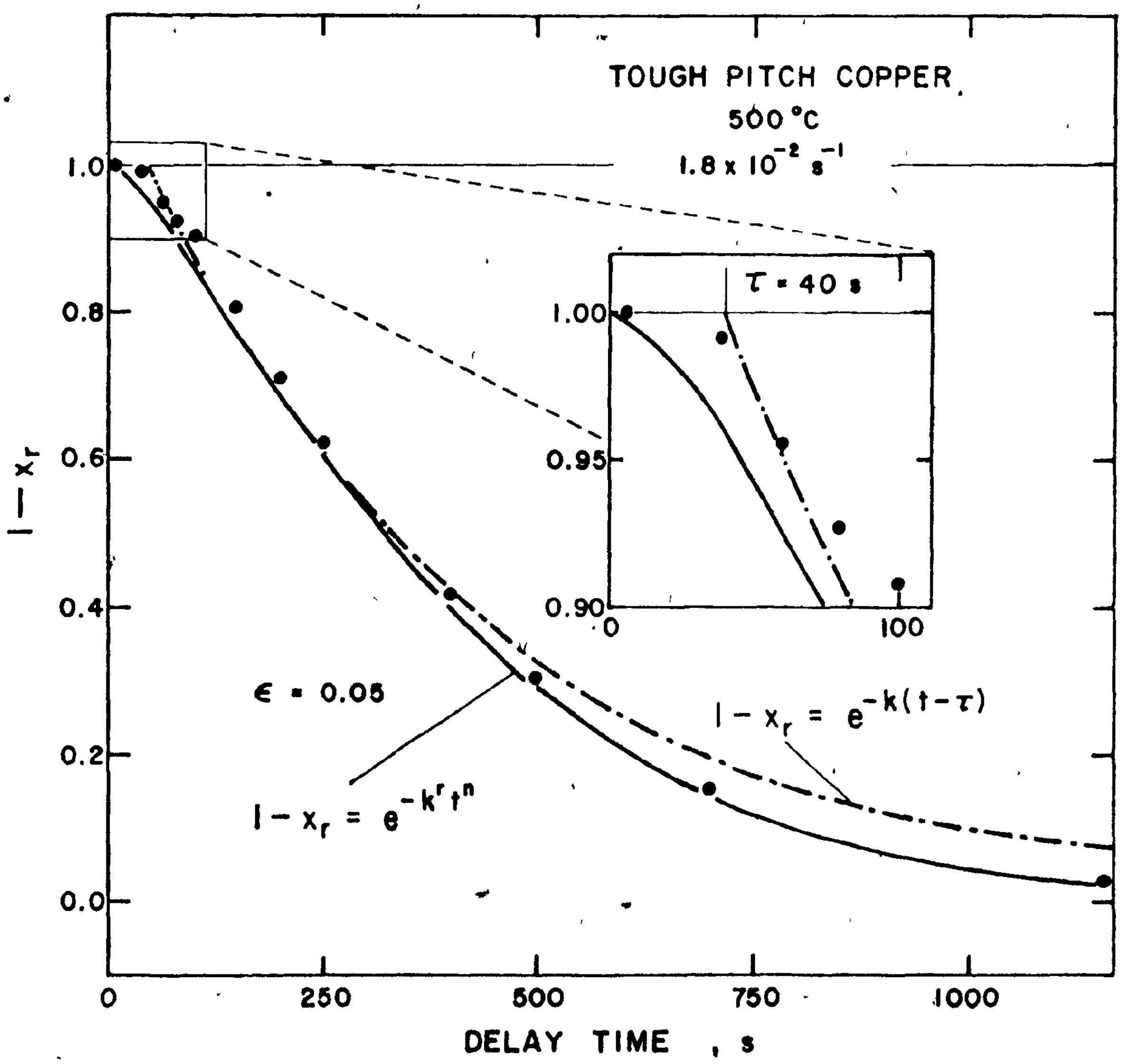

Figure 4.13 A graphical comparison of the empirical recovery relation (Equation 4.11) and the linear kinetics equation (Equation 4.22) with the data for recovery of tough pitch copper

ments of recovery to express the process in terms of flow stress components such as σ_i, the internal stress. The differential form of Equation 4.22 is given by

$$\frac{d(1-x_r)}{dt} = -k(1-x_r) \qquad (4.23)$$

By noting further that

$$1-x_r = \frac{\sigma_i-\sigma_i^{\infty}}{\sigma_i^{0}-\sigma_i^{\infty}} \qquad (4.24)$$

where σ_i^{0} is the initial value and σ_i^{∞} the saturation value of the internal stress, it may be shown that

$$\frac{d\sigma_i}{dt} = -k(\sigma_i-\sigma_i^{\infty}) \qquad (4.25)$$

where $(\sigma_i-\sigma_i^{\infty})$ is the excess internal stress (i.e. the excess over the saturation level). It is of particular interest that the kinetics of this type of softening are only approximately first order if expressed in terms of the excess internal stress. Furthermore, the internal stress may be taken as being proportional to the square root of the dislocation density. In the light of the foregoing arguments, it may therefore be concluded that the rate of change of dislocation density during recovery follows first order kinetics.

It is evident from the experimental results that the rate of recovery is not only dependent on the level of the excess stress, but is also temperature sensitive. The temperature dependence of the recovery process is shown in Figure 4.14, where the time for 50% recovery is plotted against inverse temperature for different amounts of prestrain. Since the prestraining in the present experiments was carried out at the same temperature corrected strain rate, the starting structure and internal stress are expected to be nominally the same for a given prestrain at the three temperatures. It is evident from Figure 4.14 that in tough pitch copper the activation energy for recovery increases as the temperature decreases. This unusual behaviour suggests that at the lower temperatures some process is operative (for example oxide precipitation) which inhibits static recovery.

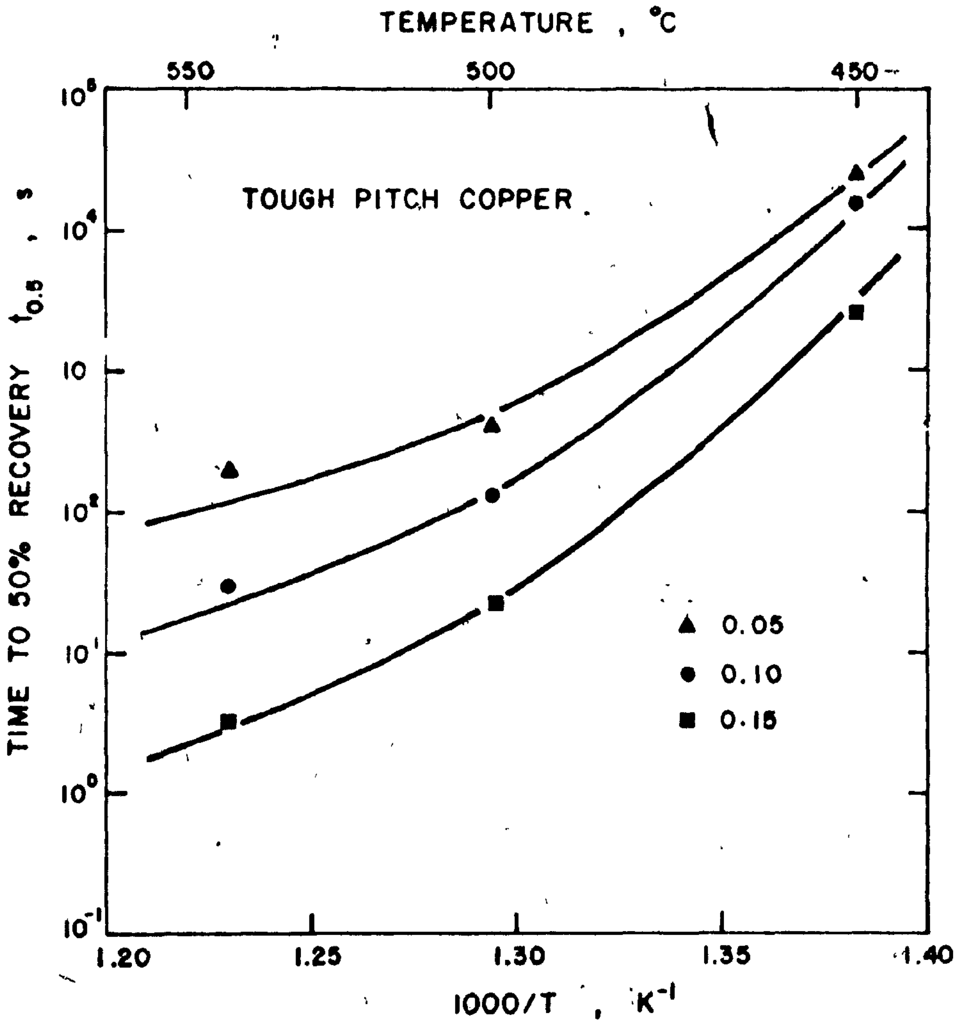

Figure 4.14 Arrhenius plot of $t_{0.5}$ versus 1/T

4.3.5 The Critical Strain for Recrystallization

It is evident from the description of the present research that the role of the critical strain for static recrystallization ε_{cr} is an important one. It is the purpose of this section to summarize and discuss our observations regarding this variable.

If the critical strain for static recrystallization is exceeded, softening by static recovery can only take place during the incubation period prior to recrystallization. Furthermore, if the critical strain for recrystallization is not reached, the recovery processes do not lead to full softening, but saturate at a softening level well below 100%; i.e., full softening cannot be produced by recovery processes alone. The softening curves of Figure 3.5 and 3.6 reveal that the maximum relative softening that can be produced by static recovery alone before the peak is about 50%. This compares with softening levels of about 40% produced by recovery alone in aluminum(111).

At 500°C, Figure 3.5, a pre-strain of 0.10 (curve b), was followed by a recovery cycle lasting some 10,000 seconds. As softening did not go to completion, it can be concluded that the critical strain exceeded 0.10. From curve c, it can be seen that, after an interruption strain of 0.15, softening by recovery was complete after about 50 seconds, and then recrystallization proceeded to completion. The critical strain for this material, at 500°C, is thus between 0.10 and 0.15 strain. The above value is in reasonable agreement with those quoted in the literature, which are of the order of 0.10 strain(50).

The critical strain for dynamic recrystallization is of special importance for the present discussion since softening by metadynamic recrystallization can only take place in a dynamically recrystallized structure. It is strain rate and temperature dependent(40) and is generally assumed to be less than the peak strain. According to Rossard(41) the critical strain for dynamic recrystallization is of the order of 0.[illegible] ε_p. In the present study the critical strain in copper was estimated to be about 0.9 ε_p at 500°C.

4.3.6 Metadynamic Recrystallization

It is well established by the present results that a softening process called metadynamic recrystallization indeed takes place after large prestrains in a dynamically recrystallized structure. It was confirmed that the process does not require an incubation period after the termination of deformation, that it proceeds very rapidly and that it goes to completion when all the nuclei formed during deformation are exhausted. A new characteristic of this process was also observed, which is that metadynamically recrystallized grains are smaller (at least under the present conditions) than either dynamically or statically recrystallized grains. This observation, if general, is a very valuable one if we consider the importance of grain size refinement in the processing of steel and other materials.

The question that naturally comes to mind is the following one. How can the nuclei formed during deformation lead to smaller grain sizes when recrystallization follows straining than do the same nuclei when the deformation is not interrupted? Let us therefore consider this in more detail. To begin with, we will assume, following Sandstrom and Lagneborg(35), that a moving grain boundary leaves behind it a region which is relatively free of dislocations. With concurrent deformation, the dislocation density begins to increase again once the boundary has passed. This development is represented in Figure 4.15a by a plot of dislocation density versus distance in the direction of grain boundary motion. Here the grain boundary is moving to the right into unrecrystallized material. The rate of increase in dislocation density behind the moving boundary (and therefore the distance x_{cr}) is determined by the net rate of work hardening, which is in turn strain, strain rate and temperature dependent, and is expected to vary locally within the material.

If an embryo, once formed, is to grow into a critical nucleus (i.e. the smallest nucleus which is stable), then the strain difference across the embryo boundary must be greater than the value required for grain boundary migration. Such embryos are continuously being formed, but whether or not they achieve criticality depends, not only on the energy difference, but also on the width of the essentially dislocation-free zone behind the moving boundary x_{cr}. If x_{cr} is greater than $d_{cr}/2$, where d_{cr} is the critical nucleus diameter, then embryo growth can proceed. If, on the other hand, x_{cr} is smaller than $d_{cr}/2$, the embryonic nucleus will cease to develop; it is destroyed by the concurrent straining. Potential nucleation sites of this type, that never reach the critical nucleus stage <u>during</u> deformation, can nevertheless grow easily <u>after</u> the

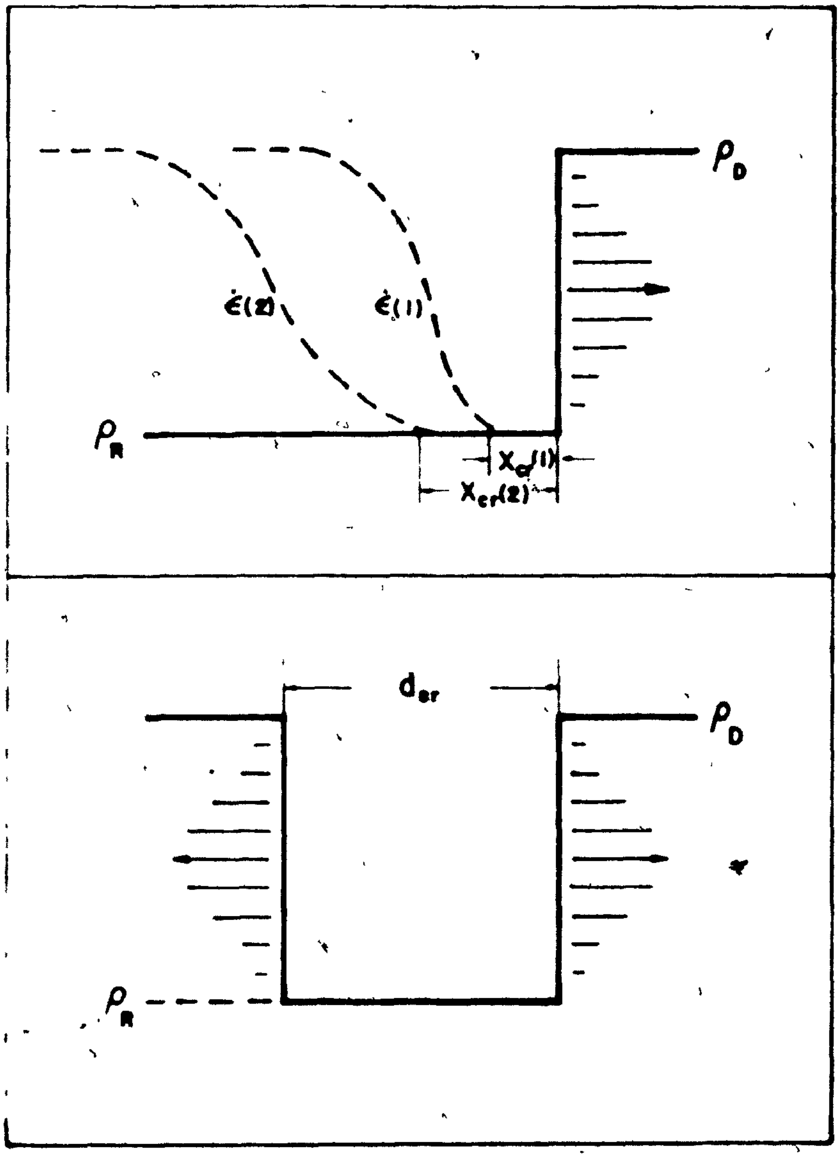

Figure 4.15 Schematic illustration of the inhibition of nucleus formation during concurrent deformation

interruption of deformation, as illustrated in Figure 4.15b. Once more, the nucleus grows by bulging of the grain boundaries brought about by the strain energy difference $\tau(\rho_d - \rho_R)$ The bulging leads again to the formation of new grains, but these are smaller in size than those formed dynamically. This arises because of the larger number of nuclei that are free to grow once concurrent deformation is interrupted.

4.4 STATIC RESTORATION IN THE HIGH STRENGTH LOW ALLOY Nb STEEL

It is clear from the results obtained on the three experimental materials that the proposed softening model leads to a realistic interpretation of the softening processes that take place after an interval of hot work. An attempt will now be made to discuss the results on the Nb-bearing steel in the light of the restoration model. However, concurrent precipitation in this steel adds a new dimension to the problem, because of the interaction between the kinetics of precipitation on the one hand and those of recovery and recrystallization on the other.

Nevertheless, it is possible to speculate about the interaction between precipitation and softening by assuming that the results of Le Bon et al(57) on a HSLA steel containing 0.035wt.% Nb apply to the present material. This work compares the rate of NbC precipitation after hot working with that without prior working. Although their steel contained half the Nb and twice the C contained in the present material, and the strain rate used for the study was one and a half orders of magnitude higher than ours, the results will be considered to give an approximate indication of the degree of precipitation that may prevail in the present study. The times for 5, 50 and 100% and maximum softening on holding after 25% prior hot working are shown for the present material in Figure 4.16 The crosshatched regions on the diagram indicate the range over which NbC precipitation occurred in the work of Le Bon et al. It is evident that at 1040°C, softening is likely to be complete before significant precipitation has occurred. The occurrence of further softening beyond 100% observed for delay times greater than 100s may then be attributed to softening of the γ matrix due to Nb and C depletion. Although this increment of softening could in principle be produced by a grain

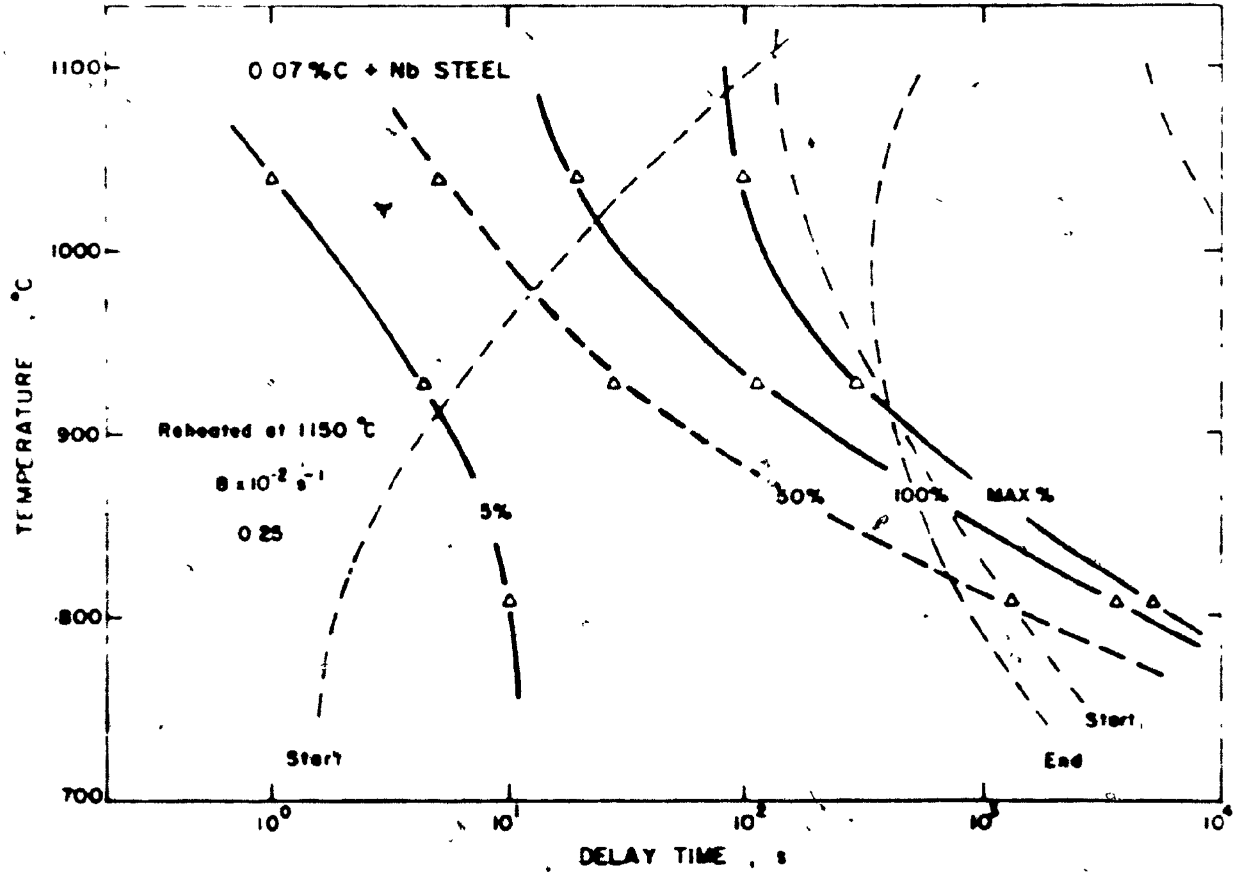

Figure 4.16 Correlation of the softening rates observed in the present 0.07% C + Nb steel, (taken from Figure 3.10), with the precipitation rates determined in the work of Le Bon et al.(57)

—·— precipitation with 0.25 prior strain

—··— precipitation without prior strain

size effect, it is more likely that the grain size is decreased during recrystallization, and it would therefore be expected to produce a flow stress increase (i.e. hardening and not softening).

After only 10% prestrain at 1040°C, the time to initiate softening is in excess of 100s, so that the softening processes are likely to operate concurrently with precipitation. This may cause some retardation of the recrystallization process, however, at this high temperature, even after complete precipitation, only half the available Nb and C are precipitated as carbide (see Figure 4.17)(172). In view of this, the volume fraction of NbC precipitated is expected to be small compared with that present at the lower temperatures, so that the retardation effect is probably somewhat smaller than in the other tests.

At the intermediate temperature of 930°C, the time for the start of precipitation is of the order of 10s and precipitation could therefore, occur concurrently with the prior deformation itself. This could lead to the retardation of dynamic recrystallization by pinning of the sub-boundaries and grain boundaries. Such retardation should not only lead to a broadening of the flow stress peak, but is also likely to affect all the static softening processes.

At the lowest testing temperature, the data of Le Bon et al suggest that the precipitation of NbC is well advanced before significant softening occurs. At this temperature, the effect of concurrent NbC precipitation appears to have its maximum retardation effect. This may arise, on the one hand, from the high volume fraction of precipitate present at complete precipitation (97% of the Nb and C are present as precipitates, see Figure 4.17), and on the other, from the fine dispersion of precipitate expected at the lower temperature. It should be pointed out that at 815°C with Nb and C in solution, the material would be expected to consist of a mixture of austenite and ferrite. However, as NbC is precipitated, both C and Nb are withdrawn from solution, which would tend to increase the volume fraction of ferrite present. The large reduction in the flow stress (see Figure 4.18) which occurs after holding times greater than 5000s may be attributed in part to this phase change effect. Note that the data of Le Bon et al. suggest that NbC precipitation is complete after about 1000s.

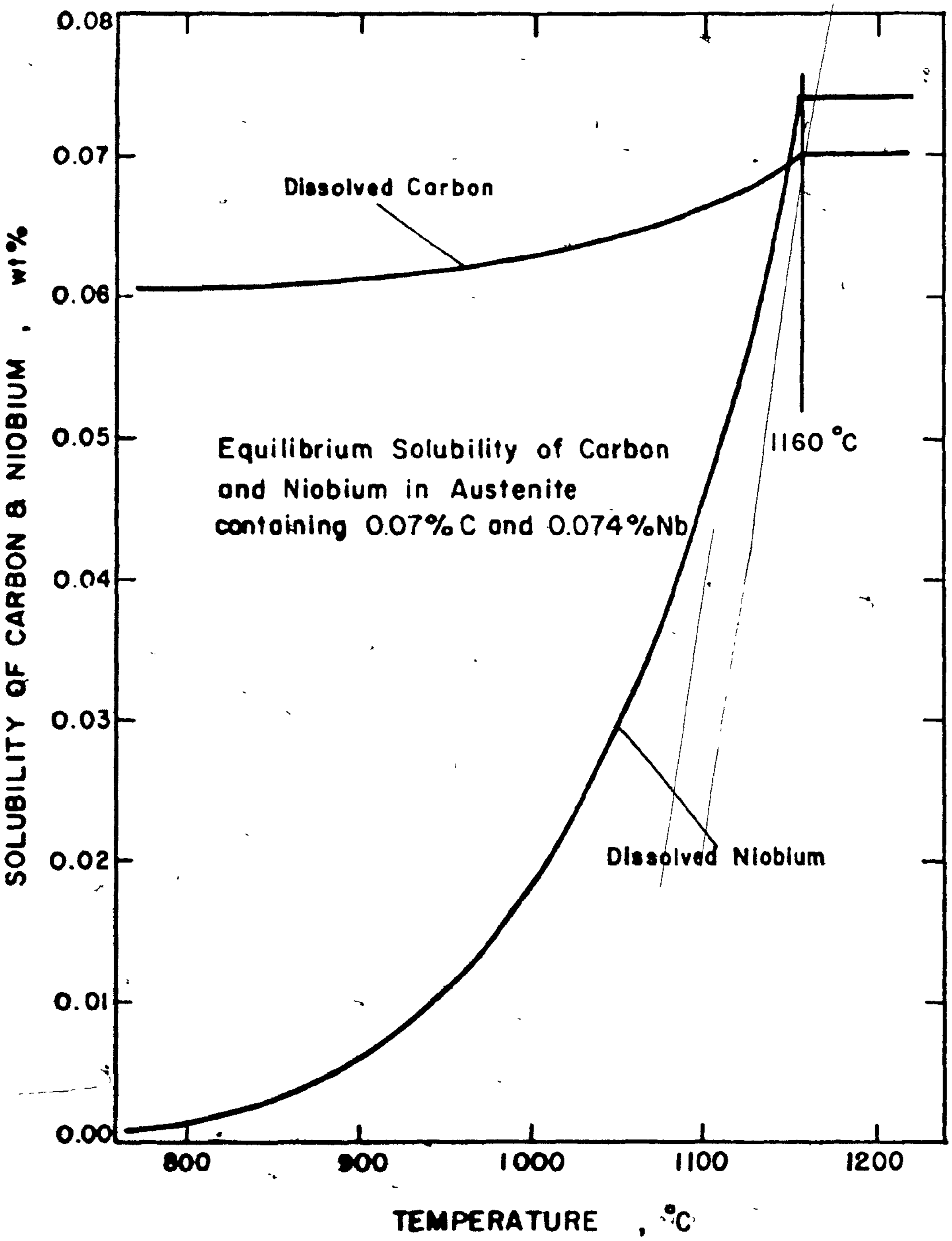

Figure 4.17 Solubility of Nb and C in austenite for the Nb-bearing steel

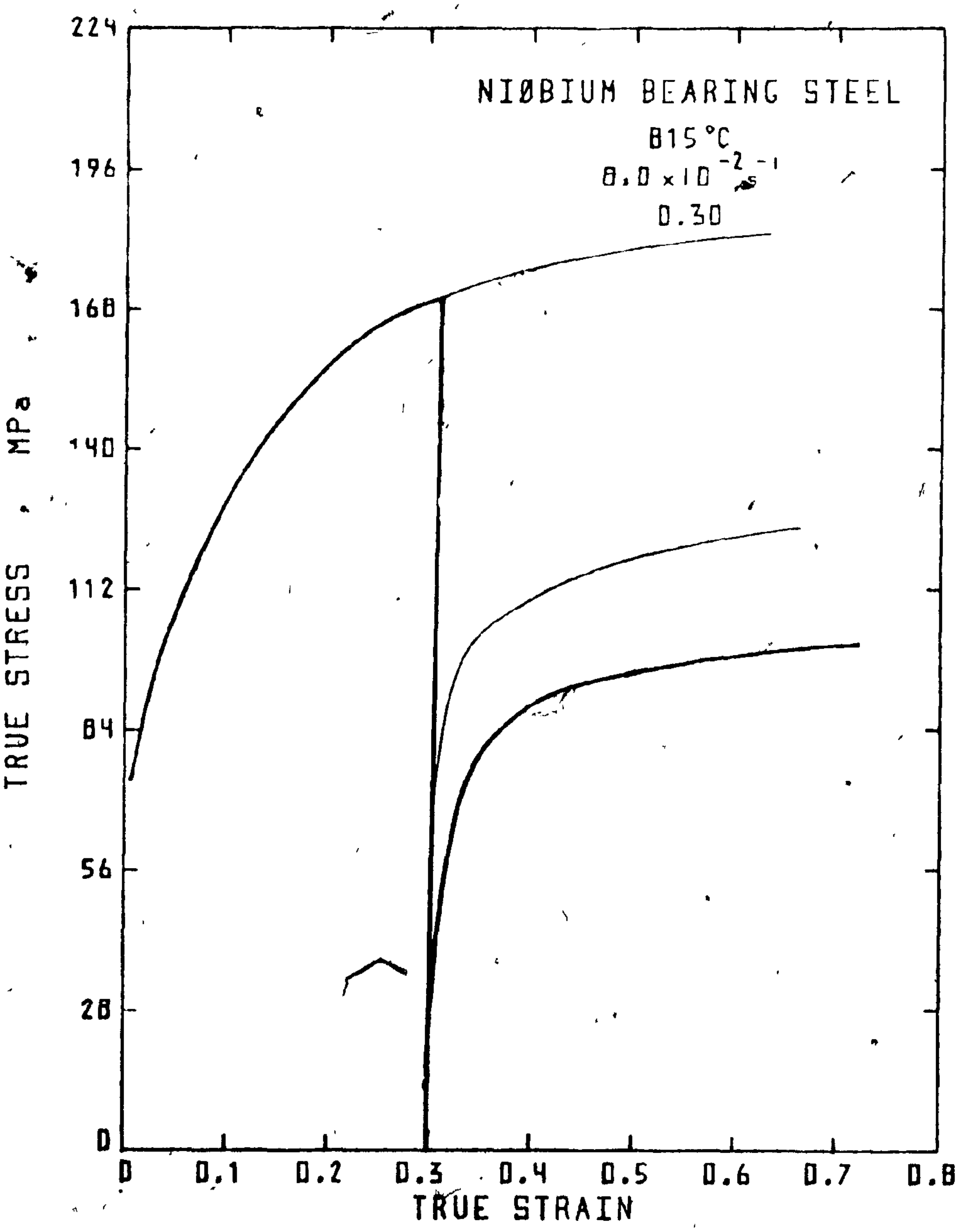

Figure 4.18 Interrupted stress-strain curves obtained in the 0.07% C +Nb steel at 815ºC, showing the large reduction in flow stress after intermediate holding times of 5500 or 33,000 seconds

4.4.1 The Effect of Precipitation on the Activation Enthalpy

An Arrhenius plot of the times for 50% softening after 0.25 prestrain is shown in Figure 4.19. It can be seen that the slope of this plot is a function of holding temperature. The curvature shown is equivalent to an increase in the activation enthalpy for softening with increases in the likelihood of concurrent precipitation.

4.4.2 Recrystallization Rates in the Industrial Hot Rolling Range

The present experiments were conducted in the temperature range 815 to 1040°C. The range limitation was an experimental one, arising from a) the necessity for using expensive and short-lived ceramic tooling for temperatures above 1000°C, and b) the minimum unloading and reloading time of about a half second, during which a large fraction of softening takes place, again at temperatures above about 1000°C. Nevertheless, it is of interest to consider the extent to which softening rates in the breakdown range of temperatures can be predicted from test results of the nature described above.

An example of the type of extrapolation that can be made is given in Figure 4.20. This construction is based on the Arrhenius relationship and on the assumption that the overall "activation energy" associated with softening does not change appreciably over the experimental range. The construction indicates that in the breakdown temperature range of 1100 to 1200°C, 50% softening occurs in less than a second after a prior strain of 0.25 in both the low carbon and Nb-modified steels. Thus, in these materials, recrystallization is essentially complete between mill stands. By contrast, in the finishing temperature range, full recrystallization may take from 10 to 100 seconds, and this can be increased to over 1000 seconds by the addition of niobium and other elements.

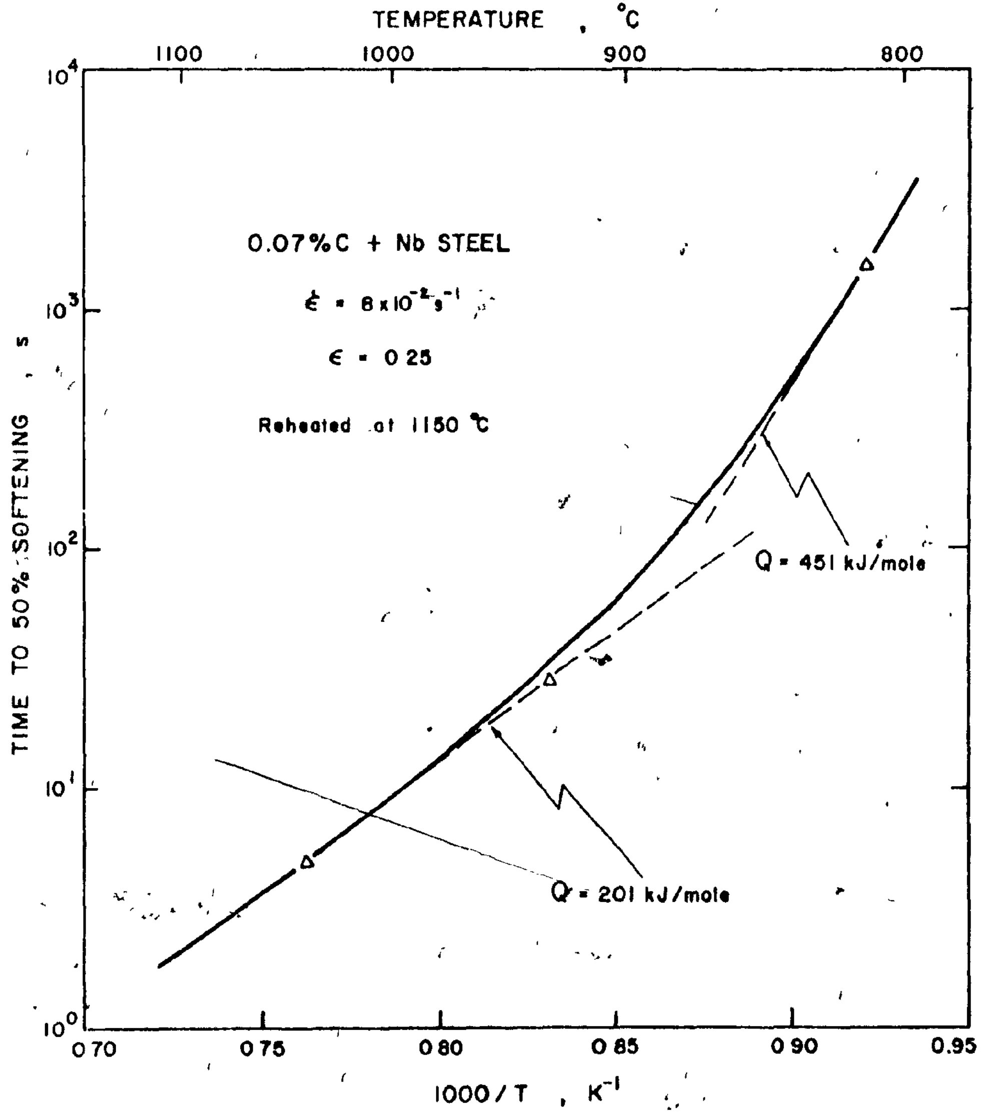

Figure 4.19 Activation enthalpy for static softening in the 0.07% C +Nb steel

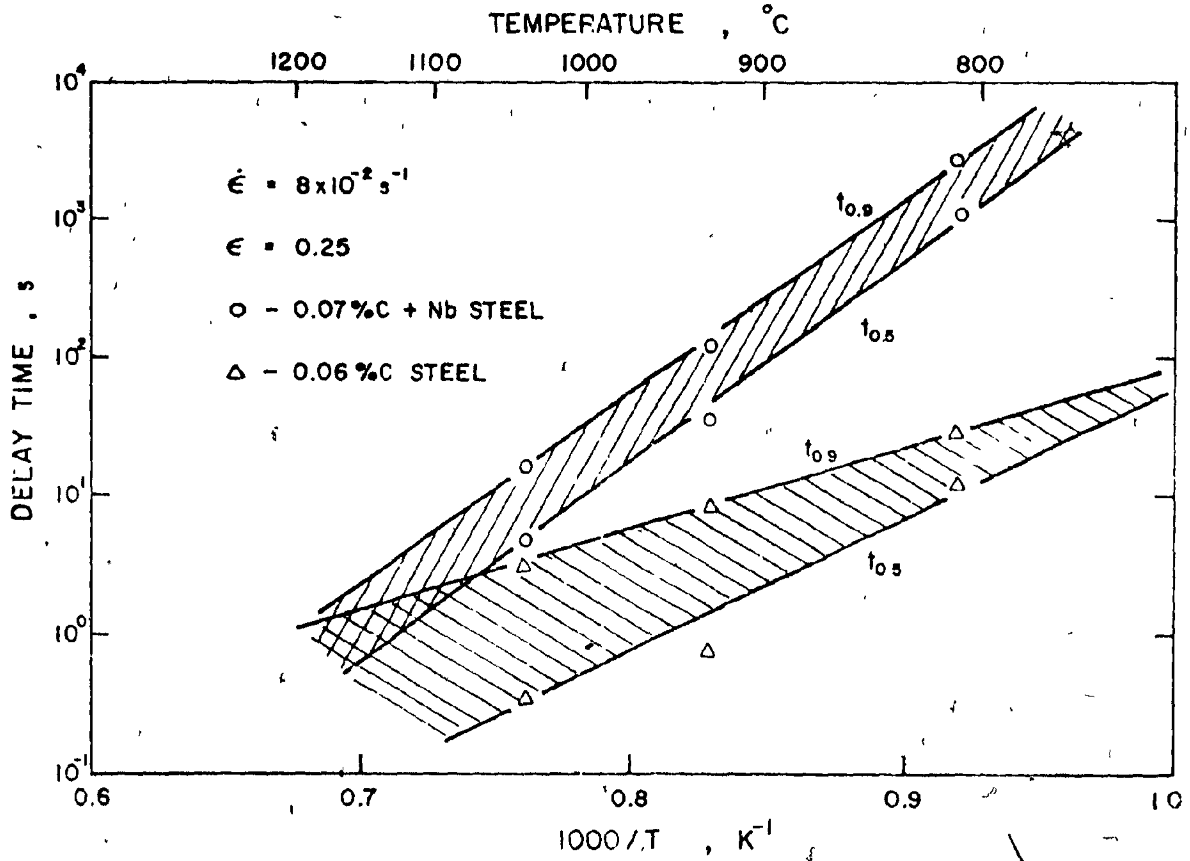

Figure 4.20 Expected softening times in the breakdown temperature range based on the present experimental results.

CONCLUSIONS

The present investigation involved the softening behaviour of a 0.06%C plain carbon steel, a 0.07%C Nb-bearing steel and tough pitch copper. It was carried out by means of interrupted compression testing in the temperature range from 450 to 1040°C and at strain rates between 8×10^{-3} and $8 \times 10^{-2} s^{-1}$. A second series of experiments was carried out at the single temperature of 500°C at a fixed strain rate ($1.8 \times 10^{-2} s^{-1}$) and employed various interruption strains. After increasing delay times, specimens were quenched to room temperature. These samples were polished and etched and examined metallographically. The distribution of grain sizes within each sample was used to determine the degree of recrystallization at a given delay time. The technique was sufficiently sensitive to distinguish between the two recrystallization processes that occur after prestraining.

The results were interpreted in terms of a three-mechanism softening model and the kinetics of each process were examined. As a result of the study, the following general conclusions were reached:

1. The flow stress in all three materials is strongly strain rate and temperature dependent, increasing with increasing strain rate and decreasing temperature. A decrease in temperature or an increase in strain rate also leads to an increase in the peak strain and the peak in flow stress becomes much broader under these conditions. The broadness of the flow curves in the Nb-treated carbon steel appears to be much greater than can be attributed to the temperature dependence of the recrystallization process alone. This broadening suggests that Nb(CN) precipitation is initiated before or during deformation, thereby retarding the dynamic recrystallization process, which in turn has the effect of broadening the flow stress peak.
2. The results of a large number of interrupted tests indicate that, after hot working, static softening in FCC materials proceeds by the sequential operation of up to three distinct

processes. The three processes are static recovery, classical recrystallization and a distinct mechanism identified as metadynamic recrystallization. The relative importance of each of these processes depends critically on the prior hot working strain. A critical strain of about 10% is required to initiate classical recrystallization, whereas strains of 25% or more are generally required to produce metadynamic recrystallization.

3. The three softening mechanisms can interact to produce a smooth softening curve, or a curve with either one or two inflection plateaus. The following individual cases can be distinguished, in order of increasing interruption strain.
    a) For small amounts of prior strain, that is at a strain considerably less than that required to reach the maximum in flow stress, only one stage of softening is observed. This first cycle of softening has been attributed to static recovery alone.
    b) When the amount of prestrain is increased beyond the critical strain for static recrystallization, softening occurs by means of both static recovery and classical recrystallization and a single plateau is observed.
    c) When the flow curve is interrupted between the peak stress and the steady-state stress, dynamic recrystallization is followed by all three softening processes, and two inflection plateaus can be seen.
    d) When the flow curve is interrupted in the steady-state region, the subsequent softening is attributable to static recovery, metadynamic and static recrystallization, but under certain conditions, all three processes operate concurrently and a single sigmoidal curve is produced.

4. The rate of static recovery increases with temperature as well as with the strain rate and interruption strain. The latter effect can be attributed to the increase in retained dislocation density that accompanies increases in strain rate or prior strain. The rate of recovery decreases somewhat with the addition of certain solutes and when fine precipitates are present. The relative amount of softening that can be produced by static recovery increases with strain to about 50% of the work hardening that is introduced. When the maximum degree of softening brought about by recovery has been attained, a softening arrest is generally seen.
5. The process of classical recrystallization after high temperature deformation, like that of recrystallization after low temperature deformation, involves an incubation time during which recrystallization nuclei are formed. In the present experiments, this time ranged from 1 to 8000 seconds. The experimental activation energies associated with classical recrystallization are substantially higher than those associated with static recovery, thus the length of the incubation plateau or softening arrest depends on temperature, and is shorter at higher temperatures.
6. Metadynamic or post-dynamic recrystallization can only occur if dynamic recrystallization is initiated during prior straining. It takes place only when the interruption strain exceeds the strain required to attain the peak in the flow curve. According to this mechanism, the recrystallization nuclei formed during straining, and which grow during deformation, continue to grow when straining is interrupted. Thus no incubation time is involved, and the overall softening rate can be up to two orders of magnitude faster than when final softening takes place by classical recrystallization.

7. When straining is interrupted at equivalent regions along a flow curve, the rate of recrystallization, by either mechanism, is observed to be highly temperature dependent. When interruptions are performed at constant temperature and interruption strain, the rate of softening increases with strain rate as a result of the higher dislocation densities accumulated at higher deformation rates. The marked effect of strain on the rate of softening involves the changeover from recrystallization by a classical mechanism involving an incubation time to post-dynamic recrystallization, which utilizes nuclei formed during deformation.
8. The addition of niobium (and of other alloying elements) decreases the overall softening rate by one to two orders of magnitude. The alloying elements reduce to some extent the rates of dynamic recovery, static recovery, and both classical and metadynamic recrystallization. However, the major effect of Nb addition seems to be to prevent the formation of dynamic recrystallization nuclei until much larger strains are attained, and therefore, to prevent the occurrence of post-dynamic (i.e., rapid) static recrystallization at normal levels of prior strain.
9. Experiments dealing with the effect of hot working conditions on the recrystallized grain size lead to the conclusion that the latter is strain, temperature and strain rate dependent. The dependencies observed are described below.
   a) The grain size of samples subjected to strains of 0.05 and 0.10, which are below the critical strain for static recrystallization, were the same as the initial grain size, but contained subgrains as revealed by etch pitting. A qualitative study of the changes in dislocation substructure carried out on these specimens indicated that softening by recovery saturates at a certain value well below that associated with full restoration.

b) When the prestrain exceeded the critical strain for static recrystallization, the grain size decreased with increasing strain. At large strains, a steady state was reached where the grain size remained constant with further strain.

c) The recrystallized grain size decreased with an increase in strain rate. This effect was more pronounced at the highest temperature (600°C), which is reasonable when it is recalled that both the retained dislocation density and the mechanical properties in general are more rate sensitive at higher temperatures. The effect of temperature was also marked and the results indicate that the recrystallized grain size of tough pitch copper increases with working temperature.

10. A plot of the high temperature yield stress vs. grain size drawn up in the Hall-Petch manner shows that in tough pitch copper the former increases linearly with the inverse square root of the grain size. The value of k gradually decreases with decreasing rates of deformation and can be written as: $k = 0.8 + g(T,\dot{\varepsilon})\{N/mm^{3/2}\}$. Similarly, an increase in temperature also leads to a decrease in k, probably because its effect on thermal activation is analogous to that of a decrease in strain rate. This leads to a Hall-Petch relation of the form:

$$\sigma_y = \sigma_0(T,\dot{\varepsilon}) + 0.8d^{-\frac{1}{2}} + g(T,\dot{\varepsilon})d^{-\frac{1}{2}}$$

Here the first component on the right-hand side of the equation represents the yield stress of a single crystal, and the second and third terms arise from the contributions of grain size to the athermal and thermal flow stress components of the developed stress, respectively.

11. The time dependence of the individual softening processes can be specified by means of experimental relationships which can also be used to describe the temperature and

strain dependence of these processes. The data fitted the following relationships.

a) when recovery is the only operating process.

$$X \quad X^r \quad X_\infty^r(1-e^{-k^r t^n})$$

b) when two softening processes (i.e., static recovery and static recrystallization) operate together, the overall degree of softening is given by:

$$X = X^r + X^R$$

where

$$X^R = X_\infty^R(1-e^{-k^R t^P})$$

c) when the three softening processes operate together, the overall softening produced is given by:

$$X = X^r + X^R + X^M$$

where

$$X^M = X_\infty^M(1-e^{-k^M t^q})$$

The fractional softening at the completion of recovery (X_∞^r) approaches 50% asymptotically and appears to saturate under most conditions. In tough pitch copper, the time exponents n, p and q are strain and temperature independent and exhibit constant values of 1.33, 2.2 and ~1, respectively. The rate constants k^r (for recovery), k^R (for recrystallization) and k^M (for metadynamic recrystallization are strongly dependent on temperature and strain. With an increase in temperature or strain, the rates of the individual processes increase.

12. Grain size measurements suggest that grain refinement is strongly dependent on the operating softening mechanism. On the interruption of deformation at strains inferior to that required to initiate dynamic recrystallization, the original grains are replaced by new grains formed by classical recrystallization. The mean size of grains formed in this way decreases as the prestrain increases

and is 0.09 mm, (for example), at a prestrain of 0.15. The dynamically recrystallized grains formed <u>during</u> deformation, on the other hand, have a mean size of 0.17 mm; i.e., they are somewhat larger at the strain rates used than the classically recrystallized grains. These grains are partially replaced by still smaller grains (e.g. 0.04 mm) by metadynamic recrystallization when straining is interrupted. The classical recrystallization which takes over from metadynamic recrystallization at longer delay times produces grains with a mean size similar to those produced by the same mechanism at lower strains, i.e. 0.08 mm. Prestraining into the steady state regime of flow therefore produces mixed grain structures on complete recrystallization. On continued holding after complete recrystallization, grain growth was observed in tough pitch copper at 500^{0}C and 15% prestrain, leading to an approximately twofold increase in grain size. This process also gave rise to a component of softening. This latter component was attributed to a decrease in grain boundary density rather than to a decrease in dislocation density.

STATEMENT OF ORIGINALITY AND CONTRIBUTION TO KNOWLEDGE

The present work includes the following original contributions

1. A quantitative method was developed for the investigation of the softening behaviour of metals based on mechanical measurements at the deformation temperature. The test method is founded on the principle that the yield stress at high temperatures is a sensitive measure of the structural state of the material. Samples are loaded at a constant true strain rate to some prescribed strain and then unloaded and held at zero load for increasing time intervals. The samples are subsequently reloaded at the same strain rate as before. The magnitude of the yield stress on reloading is governed by the degree of structural change that has occurred during the holding interval and can therefore be taken as a measure of the progress of the static softening process. Such measurements, based on the yield stress in compression, have not been previously made to the author's knowledge.
2. For the experiments on the Nb-bearing HSLA steels, the experimental treatment called for heating the compression tools to 1200°C. In view of this, new tooling materials were introduced. Solid bars of high purity alumina were used for the upper and lower anvils. The entire loading assembly was contained within a tubular, fused quartz chamber, which itself was water-cooled at its extreme ends. The compression chamber assembly was enclosed in a platinum split furnace, which could be raised or lowered on the crosshead. This is probably the first time that highly instrumented, isothermal, constant true strain rate compression experiments were carried out at such high temperatures.
3. The mechanical testing results have indicated, and the metallographic results have confirmed, that an additional recrystallization process takes place after deformation

at high temperatures This very rapid recrystallization, christened metadynamic (or post-dynamic) recrystallization, is a type of static softening process that can occur only after previous dynamic recrystallization (i.e. recrystallization concurrent with deformation). According to this view, the recrystallization centres nucleated during deformation will, on interruption, continue to grow into the surrounding deformed material. This process is only completed when all the nuclei formed during deformation are exhausted. As this type of recrystallization does not require a nucleation interval, it proceeds very rapidly upon the termination of deformation. Although unusual and rapid forms of recrystallization have been reported by a number of workers, the special features of metadynamic recrystallization were first distinguished and identified in the present study.

4. As a result of the clarification of the role of metadynamic recrystallization in static restoration, a new and detailed model of the inter-relationships between the four softening mechanisms following high temperature deformation has been proposed. The model suggests that the following combinations of static softening process can operate:
    1. static recovery only,
    2. static recovery and static recrystallization,
    3. static recovery, static recrystallization and grain growth,
    4. static recovery, static and metadynamic recrystallization, and
    5. static recovery, static and metadynamic recrystallization and grain growth.

It should be added that some evidence for a fifth softening mechanism was observed which may involve matrix depletion and precipitation.

5. The sequential operation of up to four distinct softening processes precludes the meaningful application of a single integrated rate equation to the softening data. Instead, the present results were fitted by means of an equation made up of three components of the form proposed by Avrami for classical recrystallization alone. These relationships can be used to evaluate the temperature and strain dependence of the individual processes.
6. A qualitative study carried out of the changes in the dislocation substructure by means of an etch pit technique, as well as the progress of softening observed by means of mechanical testing, support the observation that softening by recovery saturates at a certain value well below that associated with full restoration.
7. It is evident from the grain size distribution curves obtained in tough pitch copper, that more than two groupings of intercept lengths are present. The observations indicate that, under the present deformation conditions, the finest grain size is produced by metadynamic rather than by dynamic or static recrystallization. This observation, if general, is relevant to the steel processing industry, where the production of fine grained materials is of considerable economic importance.
8. The presence of both athermal and thermal components of grain boundary strengthening was observed, suggesting that grain boundaries can serve as both local and long range obstacles at elevated temperatures. It is thus a conclusion of the present work that a Hall-Petch relation of the following form applies at high temperatures:

$$\sigma_y = \sigma_0(T,\dot{\varepsilon}) + 0.8d^{-\frac{1}{2}} + g(T,\dot{\varepsilon})d^{-\frac{1}{2}}.$$

Here σ_y and σ_0 have units of MPa and the grain size is in mm.

REFERENCES

1. C.M. Sellars and W.J. McG. Tegart, Mém. Sci. Rev. Met., 63, 731-746 (1966).
2. H.J. McQueen, W.A. Wong and J.J. Jonas, Can. J. Phys., 45, 1225-1233 (1967).
3. J.L. Uvira and J.J. Jonas, Trans. TMS-AIME, 242, 1619-1626 (1968).
4. W.A. Wong and J.J. Jonas, Trans. TMS-AIME, 242, 2271-2280 (1968).
5. A.H. Cottrell in An Introduction to Metallurgy, William Clowes and Sons, London, p.405 (1967).
6. D. Hardwick and W.J. McG. Tegart, J. Inst. Metals, 90, 17-21 (1961-62).
7. H. Ormerod and W.J. McG. Tegart, J. Inst. Metals, 92, 297-299 (1963-64).
8. C. Rossard, Met. Cor-Ind., 35, No.415, 102-115; No.416, 140-153; No.417, 190-205 (1960).
9. H.J. McQueen, W.A. Wong and J.J. Jonas, Acta Met., 15, 586-588 (1967).
10. H.P. Stuwe, "Deformation Under Hot Working Conditions" (Special Rep. No.108) London (Iron and Steel Inst.) 1-6 (1968).
11. C.M. Sellars and W.J. McG. Tegart, Acta Met., 14, 1136-1138 (1967).
12. O.D. Sherby and P.M. Burke, Progr. Mater. Sci., 13, 325-390 (1968).
13. D.J. Abson and J.J. Jonas, private communication.
14. A.K. Mukherjee, J.E. Bird and J.E. Dorn, Trans. ASM, 62, 155-179 (1969).
15. F. Garofalo in Fundamentals of Creep and Creep Rupture in Metals, MacMillan Series in Materials Science, MacMillan, New York, p.258 (1966).
16. J.J. Jonas, C.M. Sellars and W.J. McG. Tegart, Met. Reviews, 14, 1-24 (1969).

17. J.-P.A. Immarigeon and J.J. Jonas, Acta Met., 22, 1235-1247 (1974).

18. A.H. Clauer, B.A. Wilcox and J.P. Hirth, Acta. Met., 18, 381-397 (1970).

19. A. Orlova and J. Cadek, Phil. Mag., 21, 495-508 (1970).

20. P.W. Davies, G. Nelmes, K.R. Williams and B. Wilshire, Met. Sci. J., 7, 87-92 (1973).

21. D. McLean in "The Physics of High Temperature Creep in Metals", Reports on Progress in Physics, 29, 1-33 (1966).

22. D. McLean, J. Inst. Metals, 80, 507-519 (1951-52).

23. H.J.G. Carvalhinhos, Ph.D. Thesis, University of Sheffield (1966).

24. H.P. Stuwe, Acta Met., 13, 1337-1342 (1965).

25. H.J. McQueen, Trans. Japan Inst. Met., 9, Suppl. 170-177 (1968).

26. H.J. McQueen, J. Metals, 20, 31-38 (1968).

27. H.J. McQueen, Materials Technology - An Inter-American Approach, ASME (New York), 379-388 (1968).

28. T. Hasegawa, H. Sato and S. Karashima, Trans. J.I.M., 11, 231-238 (1970).

29. C. Rossard and P. Blain, Mém. Scient. Revue Métall. 56, 285-300 (1959).

30. C.M. Sellars and A.G. Quarrell, J. Inst. Metals, 90, 329-335 (1961-62).

31. D. Hardwick, C.M. Sellars and W.J. McG. Tegart, J. Inst. Metals, 90, 21-22 (1961-62).

32. H.J. McQueen, Proc. Internat. Conf. on Strength of/Metals and Alloys, Tokyo (1967).

33. H.J. McQueen and S. Bergerson, Metal. Sci. J., 6, 25-29 (1972).

34. J.P. Sah, G.J. Richardson and C.M. Sellars, Metal Science, 8, No.10, 325-331 (1974).

35. R. Sandstrom and R. Lagneborg, Scripta Met., 9, 59-65 (1975); Acta Met., 23, 387-398 (1975).

36. G. Glover and C.M. Sellars, Met. Trans., 4, 765-775 (1973).

37. R.A. Petkovic, M.J. Luton and J.J. Jonas, Can. Metall., Quart., in press.

38. G.J. Richardson, C.M. Sellars and W.J. McG. Tegart, Scripta Met., 1, 97-101 (1967).

39. R.A. Petkovic (previously Djaic), M. Eng. Thesis, McGill University, Montreal (1971).

40. M.J. Luton and C.M. Sellars, Acta Met., 17, 1033-1043 (1969).

41. C. Rossard, "3rd Int. Conf. on Strength of Metals and Alloys, Inst. of Metals" and Iron Steel Inst., London, Vol.II, 175-203 (1973).

42. R.C. Gifkins, J. Inst. Metals, 87, 255-261 (1958-59).

43. G.J. Richardson, C.M. Sellars and W.J. McG. Tegart, Acta Met., 14, 1225-1236 (1966).

44. J.E. Bailey and P.B. Hirsch, Proc. Roy. Soc., 267, 11-30 (1962).

45. H.J. McQueen and J.E. Hockett, Met. Trans., 1, 2997-3004 (1970).

46. W.J. McG. Tegart in "Ductility", Am. Soc. Metals, Metals Park, Ohio, 133-177 (1968).

47. D.M. Keane, C.M. Sellars and W.J. McG. Tegart, Conf. on Deformation Under Hot Working Conditions, Iron and Steel Institute (Special Report No.108), 21-28 (1968).

48. G.A. Redfern and C.M. Sellars, Ibid., 29-37 (1968).

49. J.R. Cotner and W.J. McG. Tegart, J. Inst. Metals, 97, 73-79 (1969).

50. H.J. McQueen and J.J. Jonas, Recovery and Recrystallization During High Temperature Deformation in "Plastic Deformation of Materials", ed. R.J. Arsenault, Academic Press, N.Y., 393-493 (1975).

51. K. Fink, W. Lueg and G. Burger, Arch., Eisenhuttenwessen, 26, 665-688 (1955).

52. P.J. Wray, private communication (1974).

53. B.J. Sunter and N.M. Burman, J. Australian Inst. Metals, No.2, 17, 91-100 (1972).

54. F.N. Rhines and P.J. Wray, ASM. Trans. Q., 54, 117-128 (1961).

55. S. Fulop and H.J. McQueen in "Superalloy Processing", Metals and Ceramics Information Center, Columbus, Ohio, H1-H21 (1972).

56. R. Bromley and C.M. Sellars, "Third Int. Conf. on Strength of Metals and Alloys, Inst. of Metals and Iron and Steel Inst., London, Vol.1, 380-385 (1973).

57. A. LeBon, J. Rofes-Vernis and C. Rossard, Mém. Sci. Rev. Mét., 70, 577-588 (1973).

58. J.M. Oblak and W.A. Owczarski, Met. Trans., 3, 617-626 (1972).

59. R. Drouard, J. Washburn and E.G. Parker, Trans. AIME., 197, 1226-1230 (1953).

60. D. Kuhlmann-Wilfsdorf, Zeit. fur Physik , 124, 468-481 (1948).

61. J.T. Michalak and H.W. Paxton, Trans. AIME, 221, 850-857 (1961).

62. J.G. Byrne in Recovery, Recrystallization and Grain Growth, MacMillan, New York, 90 (1965).

63. R. Leguet, D. Whitwham and J. Herenguel, Mém. Sci., Revue. Métall., 59, 649-653 (1962).

64. J. Pluhar and P. Zuna, J.I.S.I., 207, 58-62 (1969).

65. J. Pluhar et al., Mém. Sci. Rev. Mét., 66, 117-123 (1969).

66. G, Glover and C.M. Sellars, Met. Trans., 3, 2271-2280 (1972).

67. T.L. Capeletti, L.A. Jackman and W.J. Childs, Met. Trans., 3, 789-796 (1972).

68. M. Schweizer and W. Form, J. of the Institute of Metals, 101, 24-32 (1973).

69. R. Petkovic (previously Djaic) and J.J. Jonas, Met. Trans. 4, 621-624 (1973).

70. R. Petkovic (previously Djaic) and J.J. Jonas, J. Iron Steel Inst., 210, 256-261 (1972).

71. W.A. Johnson and R.F. Mehl, Trans. AIME, 135, 416-428 (1939).

72. W.A. Anderson and R.F. Mehl, Trans. AIME, 161, 140-166 (1945).

73. J.K. Stanley and R.F. Mehl, Trans. AIME, 150, 260-274 (1942).

74. Melvin Avrami, J. Chem. Phys., 7, 1103-1112 (1939).

75. Melvin Avrami, J. Chem. Phys., 8, 212-224 (1940).

76. J.E. Bailey in "Electron Microscopy and the Strength of Crystals, ed. by G. Thomas and J. Washburn, John Wiley, New York and London, 535-574 (1963).

77. F.E. Burke and D. Turnbull, Progr. Met. Phys., London, Pergamon Press, 3, 220-291 (1952).

78. R.W. Cahn, Proc. Phys. Soc., London, 63, 323-336 (1950).

79. R.W. Cahn in "Physical Metallurgy", R.W. Cahn, ed., Wiley, New York, 925-987 (1965).

80. A.H. Cottrell, Progr. in Metal Phys. 4, p.255 (1953).

81. W.C. Leslie, J.T. Michalak and F.W. Aul in "Iron and Its Dilute Solid Solutions", C.W. Spencer and F.E. Werner, eds., Interscience, New York, 119-216 (1963).

82. R.A. Vandermeer and P. Gordon in Recovery and Recrystallization of Metals, L. Himmel ed., Interscience, New York, 211-240 (1963).

83. H. Hu in Electron Microscopy and the Strength of Crystals, Interscience, New York, p.564 (1963).

84. S. Weissmann, T. Imura and N. Hosokawa, in Recovery and Recrystallization of Metals, L. Himmel, ed., Interscience, New York, 241-267 (1963).

85. H. Hu, Trans AIME, 224, 75-83 (1962).

86. J.C.M. Li, J. Appl. Phys., 33, 2958-2965 (1962).

87. F. Bourelier and J. Montuelle, Mém. Sci. Rev. Métal, 65, 65-76 (1968).

88. S. Gorczyca, Mém. Sci. Rev. Met., 57, 153-161 (1960).

89. G.A. Wilber, J.R. Bell, J.H. Bucher and W.J. Childs, Trans. TMS-AIME, 242, 2305-2308 (1968).

90. J.N. Cordea and R.E. Hook, Trans. AIME, 1, 111-118 (1970).

91. R.A. Grange in Fundamentals of Deformation Processing, University Press, Syracuse, p.299 (1964).

92. J.T. Michalak and W.R. Hibbard, Trans. AIME, 209, 101-106 (1957).

93. P. Gordon, Trans. AIME, 227, 699-705 (1963).

94. B.F. Decker and D. Harker, Trans AIME, 188, 887-890 (1950).

95. G.A. Hayes and J.C. Shyne, Metal. Sci. J., 5, 19-25 (1971).

96. F.J. Humphrey and J.W. Martin, Acta Met., 14, 775-781 (1966).

97. Isao Kozasu and Hiroyuki Kubota, TMS-AIME, Fall meeting, Detroit (1968).

98. G.R. Ogram, The Strengthening of Steels by Alloy Additions, Iron and Steel, 356, July (1965), 398, August (1965), 484, September (1965).

99. W.H. Herrnstein, J.A. Straatmann and R.A. Bosch, Strengthening in Low Carbon-Titanium Steels, AIME-TMS, Spring meeting, Pittsburgh, PA., (1969).

100. J.D. Jones and A.B. Rothwell, Deformation Under Hot Working Conditions, ISI Pub., 108, 78-82 (1968).

101. K. Lucke and K. Detert, Acta Met., 5, 628-637 (1957).

102. J.W. Cahn, Acta Met., 10, 789-798 (1962).

103. K. Lucke and H. Stuwe, Recovery and Recrystallization of Metals, Interscience, New York, p.131 (1963).

104. A.T. English and W.A. Backofen, Trans. TMS-AIME, 230, 396-407 (1964).

105. H. Buhler, D. Bobbert and A. Rose, Stahl und Eisen, 90, 21-28 (1970).

106. R. Wusatowski, J. Iron and Steel Inst., 204, 727-736 (1966).

107. H. Weiss, A. Gittins, G.G. Brown and W.J. McG. Tegart, MRL 41/1, April (1972).

108. A. Gueussier and R. Castro, Rev. Met., 55, 1023-1040 (1958).

109. W.B. Morrison, J. Iron Steel Inst., 210, 618-623 (1972).

110. G.R. Dunstan and R.W. Evans, Metallurgia, 79, 96-99 (1969).

111. R.W. Evans and G.R. Dunstan, J. Inst. Metals, 99, 4-14 (1971).

112. C.M. Sellars, private communication.

113. R. Tamhankar, J. Plateau and C. Crussard, Rev. Met., 55, 383-387 (1958).

114. C. Crussard and R. Tamhankar, Trans. AIME, 212, 718-730 (1958).

115. P.A. Portevin, Rev. Met., 59, 915-931 (1962).

116. C. Rossard and P. Blain, Rev. Met., 55, 573-594 (1958).

117. C. Rossard, Rev. Met., 65, 181-195 (1968).

118. C. Rossard and P. Blain, ibid., 61, 949-962 (1964).

119. C. Rossard and P. Blain, ibid., 59, 223-235 (1962).

120. C. Rossard and P. Blain, Mem. Sci. Rev. Met., 57, 173-175 (1960).

121. C. Rossard, A. LeBon, D. Thivellier, and J. Manenc, Mem. Sci. Rev. Met., 66, 263-270 (1969).

122. J.L. Robbins, H. Wagenaar, O.C. Shepard and O.D. Sherby, J. Met., 2, 271-286 (1967).

123. R. Akeret and A. Kunzli; Z. Metallk., 57, 789-796 (1966).

124. F.E. White, Rev. Met., 63, 991-997 (1966).

125. G.E. Dieter, J.V. Mullin and E. Shapiro, Deformation Under Hot Working Conditions, Iron and Steel Inst., London 7 (1968).

126. E. Shapiro and G.E. Dieter, Met. Trans., 1, 1711-1719 (1970).

127. C. Rossard and B. Fazan, Cahiers du CESSID, Ed. Berger-Levrault, Paris (1966).

128. H.P. Stüwe and H. Turck, Z. Metallk., 55, 699-705 (1964).

129. M.J. Luton and W.J. McG. Tegart, Met. Sci. J., 3, 142-146 (1969).

130. G.P. Lewis and W.J. McG. Tegart, J. Inst. Metals, 92, 249-251 (1963-64).

131. R.A. Reynolds and W.J. McG. Tegart, J. Iron Steel Inst., 200, 1044-1059 (1962).

132. J.L. Robbins, O.C. Shepard and O.D. Sherby, Ibid., 199, 175-180 (1961).

133. J.L. Robbins, O.C. Shepard and O.D. Sherby, Trans. ASM, 60, 205-216 (1967).

134. M.J. Luton, Ph.D.Thesis, McGill University, Montreal (1971).

135. J-P.A. Immarigeon, M.Eng. Thesis, McGill University, Montreal (1970).

136. J-P.A. Immarigeon, Ph.D. Thesis, McGill University, Montreal (1974).

137. B. Heritier, M.Eng. Thesis, McGill University, Montreal (1972).

138. J.L. Uvira, Ph.D. Thesis, McGill University, Montreal (1967).

139. E. Shapiro, private communication, Olin Corporation, Conn.

140. M.J. Luton, J-P.A. Immarigeon and J.J. Jonas, Constant True Strain Rate Apparatus for use with Instron Testing Machines, J. Physics E, Sci. Inst., 7, 862-864 (1974).

141. H.J. McQueen and J.J. Jonas, in Metal Forming, Interrelation Between Theory and Practice, ed. A.L. Hoffmanner, Plenum Publ. Corp., New York, 393-428 (1970).

142. N. Loizou and R.B. Sims, J. Mech. Phys. Solids, 1, 234-243 (1953).

143. J.A. Bailey and A.R.E. Singer, J. Inst. Metals, 92, 288-289, 378, 404-408 (1963-64).

144. H. Buhler and H.W. Wagener, Z. Metallk., 55, 668-673 (1964).

145. J.F. Alder and V.A. Phillips, J. Inst. Metals, 83, 80-86 (1954-55).

146. P.M. Cook, Proc. Conf. Properties of Mat. at High Rates of Strain, Inst. Mech. Engin., London, 86-97 (1957).

147. J.E. Hockett, Proc. ASTM, 59, 1309-1319 (1959).

148. O. Kienzle and H. Buhler, Z. Metallk., 55, 668-673 (1964).

149. M.J. Luton and J.J. Jonas, Proc. 2nd Int. Conf. Strength of Metals and Alloys (Asilomar, 1970), ASM, Metals Park, 1100-1105.

150. J.E. Hockett, High Speed Testing, Vol.VI, The Rheology of Solids, Interscience, N.Y., 205-226 (1967).

151. J.E. Hockett, Trans. TMS-AIME, 239, 969-976 (1967).

152. D.V. Wilson and G.W. Rowe, J. Inst. Metals, 95, 25-26 (1967).

153. N. Leopold, private communication, University of Kentucky, Lexington.

154. Standard Methods of Compression Testing of Metallic Materials at Room Temperature, ASTM Standard, E9-67.

155. V.P. Gupta and P.R. Strutt, Canad. Journal of Physics, Vol. 45, 1213-1220 (1967).

156. J.E. Bird, A.K. Mukherjee and J.E. Dorn in Quantitative Relation between Properties and Microstructure, D.G. Brandon and A. Rosen, Israel Univ. Press, Jerusalem, p.255 (1969).

157. E.E. Underwood in Quantitative Stereology, Ed., Addison-Wesley Publishing Co., p.274 (1970).

158. A. Delesse, "Pour détermine la composition des roches," Ann. des Mines, 13, 379-388 (1848).

159. R.P. Carreker and W.R. Hibbard, Acta Met., Vol.1, 654-663 (1953).

160. R.P. Carreker, Trans. AIME, 209, 113-115 (1957).

161. P. Feltham and J.D. Meakin, Phil. Mag. 2, 105-112 (1957).

162. J.W. Aldrich and R.W. Armstrong, Met. Trans., 1, 1947-1951 (1970).

163. H. Fujita and T. Tabata, Acta Met., Vol. 21, 355-365 (1973).

164. W.A. Backofen, I.R. Turner and D.H. Avery, ASM Trans. Quart., 57, 980-991 (1964).

165. S. [illegible] and C.J. Ball, J. Inst. Metals, Vol.100, 226-232 (1972).

166. P.K. Sengupta, B. Chaterjee and J. Rezek, Can. Met. Quarterly, 11, 601-603 (1972).

167. J. Rezek, Can. Met. Quarterly, 13, 545-553 (1974).

168. P. Shahinian and J.R. Lane, Trans. ASM, 45, 177-199 (1953).

169. J. Friedel in *Dislocations*, Pergamon Press, Addison-Wesley Pub. Co., Reading, Mass., p.276 (1964).

170. A.H. Cottrell and B.A. Bilby, Proc. Phis. Soc. A62, 49 (1949).

171. T. Surek, M.J. Luton and J.J. Jonas, Phys. Stat. Sol, 57 647-659 (1973).

172. H. Nrrdberg and B. Aronsson, J. Iron and Steel Inst., 1263-1266 (1968).

173. R.A. Petkovic, unpublished work.

APPENDIX 2.1

The Complete Flow Curves Obtained in Tough Pitch Copper, 0.07%C + Nb Bearing Steel and 0.06%C Low Carbon Steel for the Various Testing Conditions

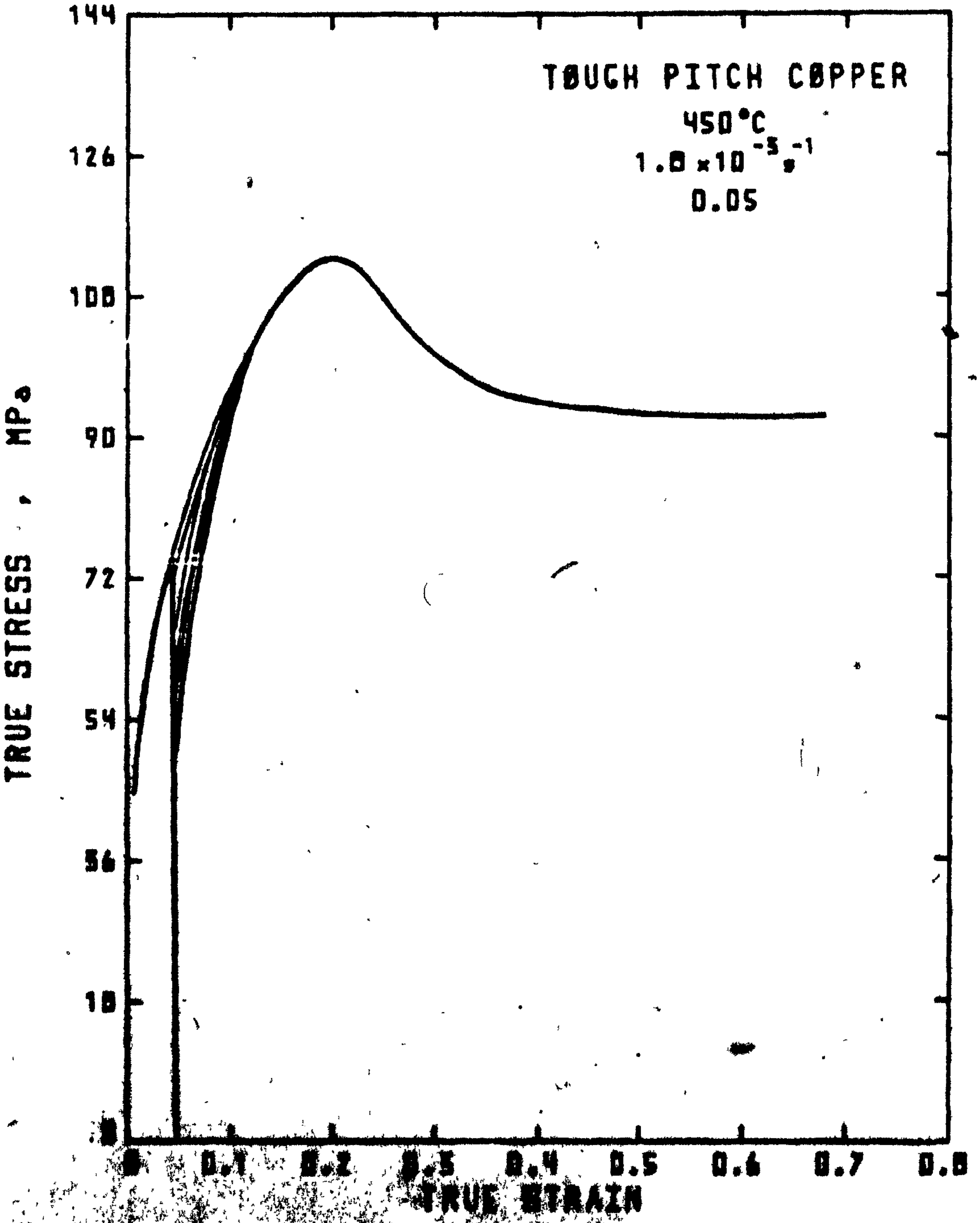
TOUGH PITCH COPPER
450°C
1.0 ×10^{-5}s^{-1}
0.05
TRUE STRESS , MPa
144
126
108
90
72
54
36
18
0
TRUE STRAIN
0
0.1
0.2
0.3
0.4
0.5
0.6
0.7
0.8

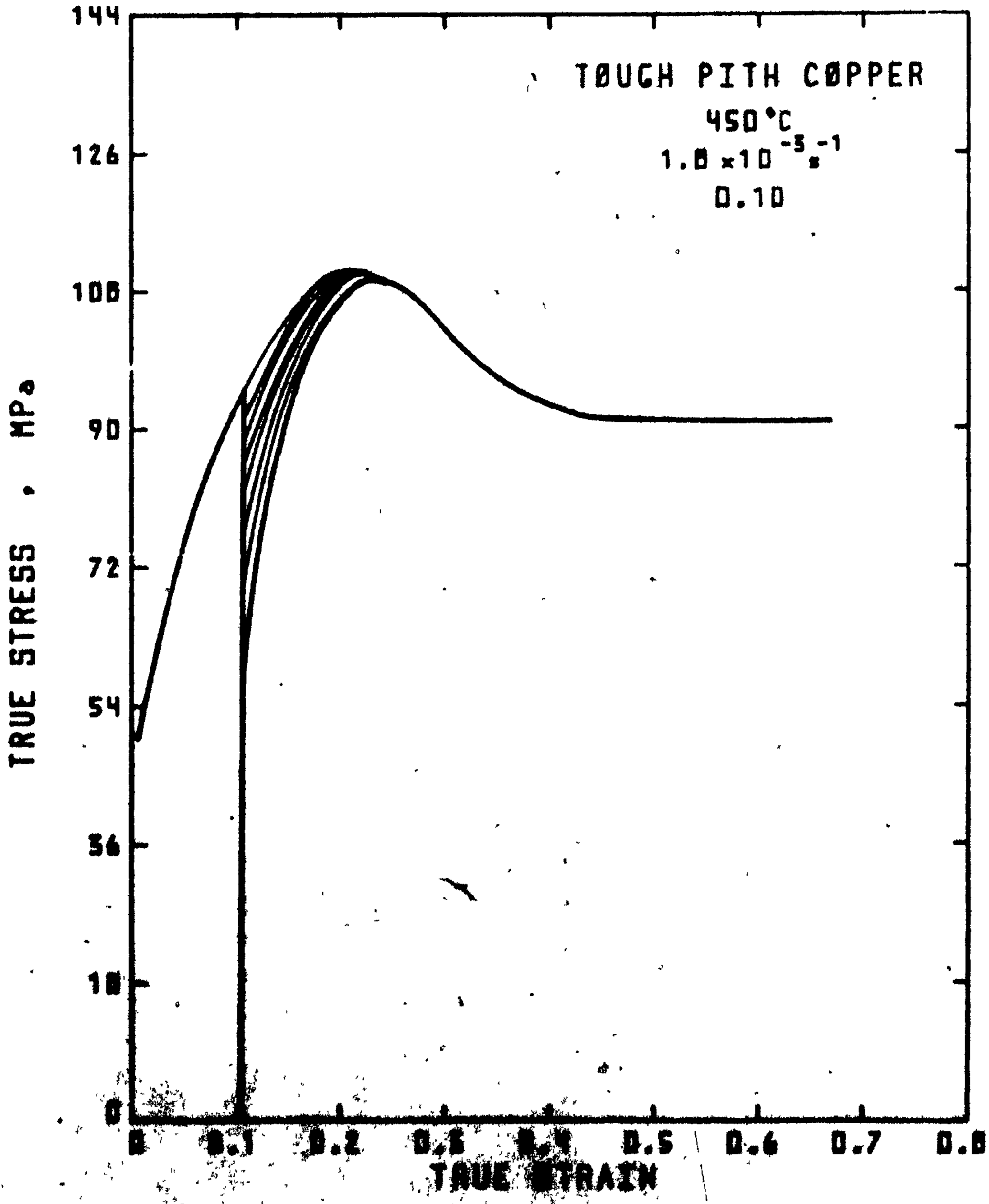
TOUGH PITH COPPER
450°C
1.8 x 10^-3 s^-1
0.10
TRUE STRESS , MPa
144
126
108
90
72
54
36
18
0
0
0.1
0.2
0.3
0.4
0.5
0.6
0.7
0.8
TRUE STRAIN

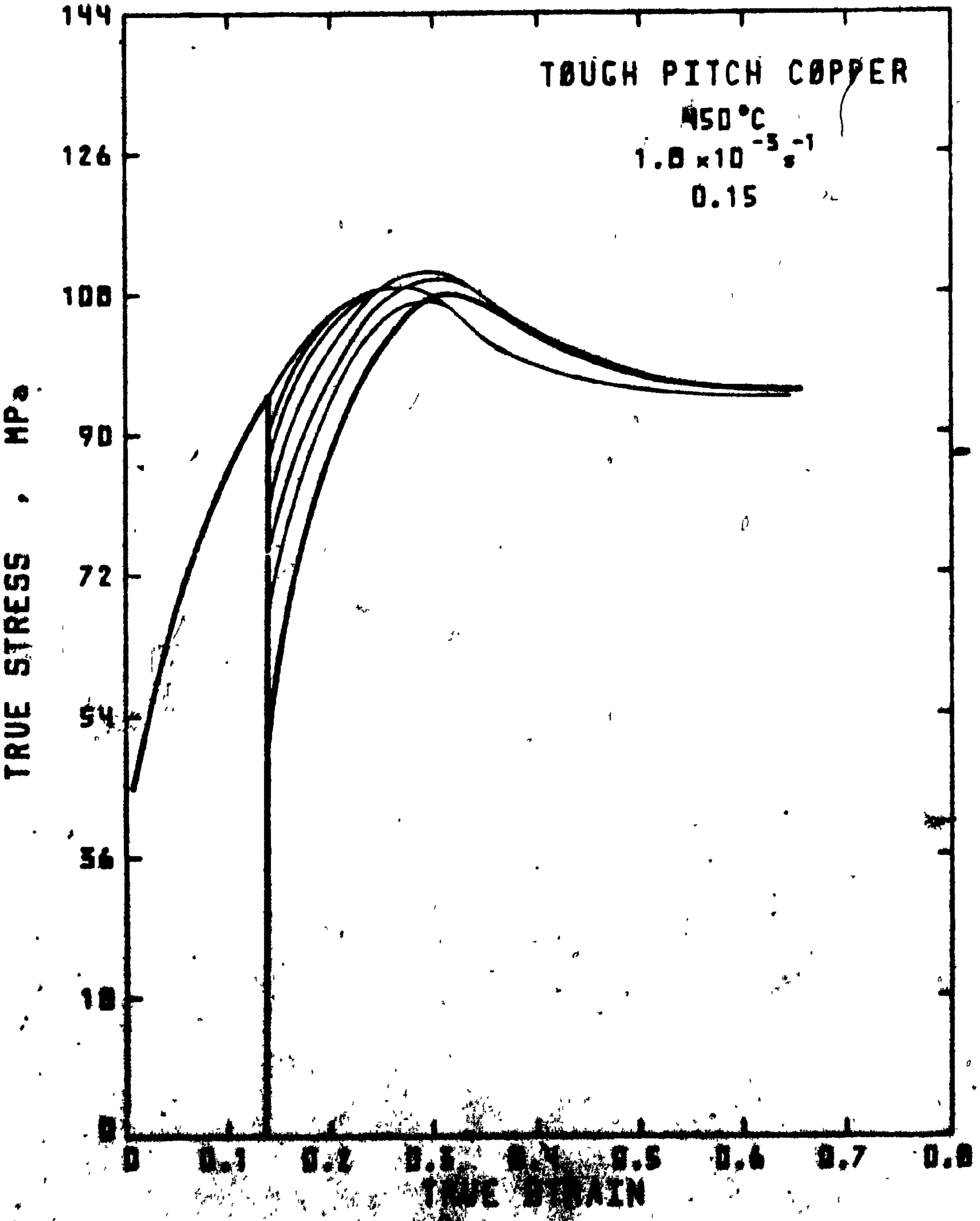
TØUGH PITCH CØPPER
450°C
1.0×10⁻³s⁻¹
0.15
144
126
108
90
72
54
36
18
0
TRUE STRESS , MPa
0
0.1
0.2
0.3
0.4
0.5
0.6
0.7
0.8
TRUE STRAIN

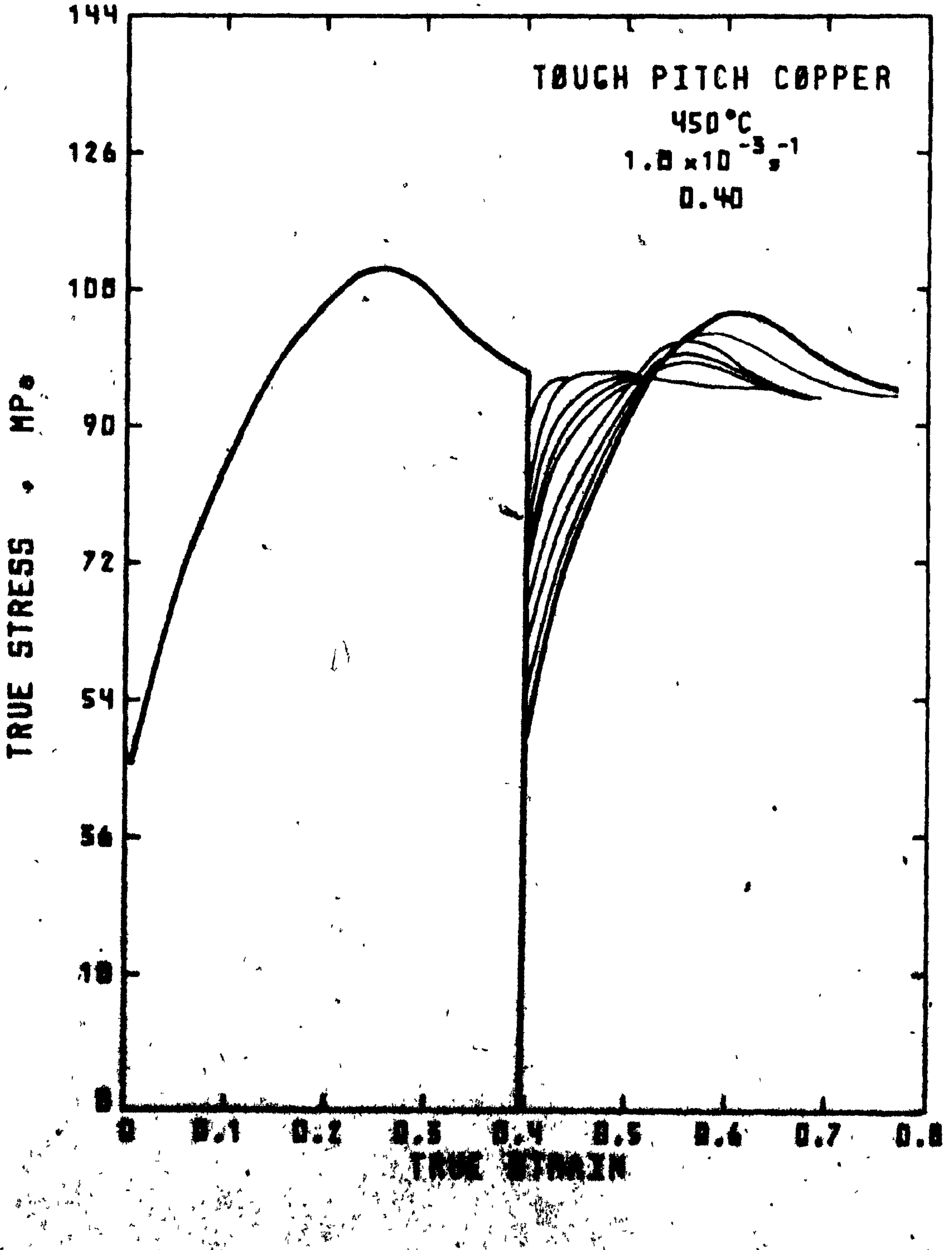
TOUGH PITCH COPPER
450°C
$1.0 \times 10^{-3} s^{-1}$
0.40
TRUE STRESS , MPa
144
126
108
90
72
54
36
18
0
TRUE STRAIN
0
0.1
0.2
0.3
0.4
0.5
0.6
0.7
0.8

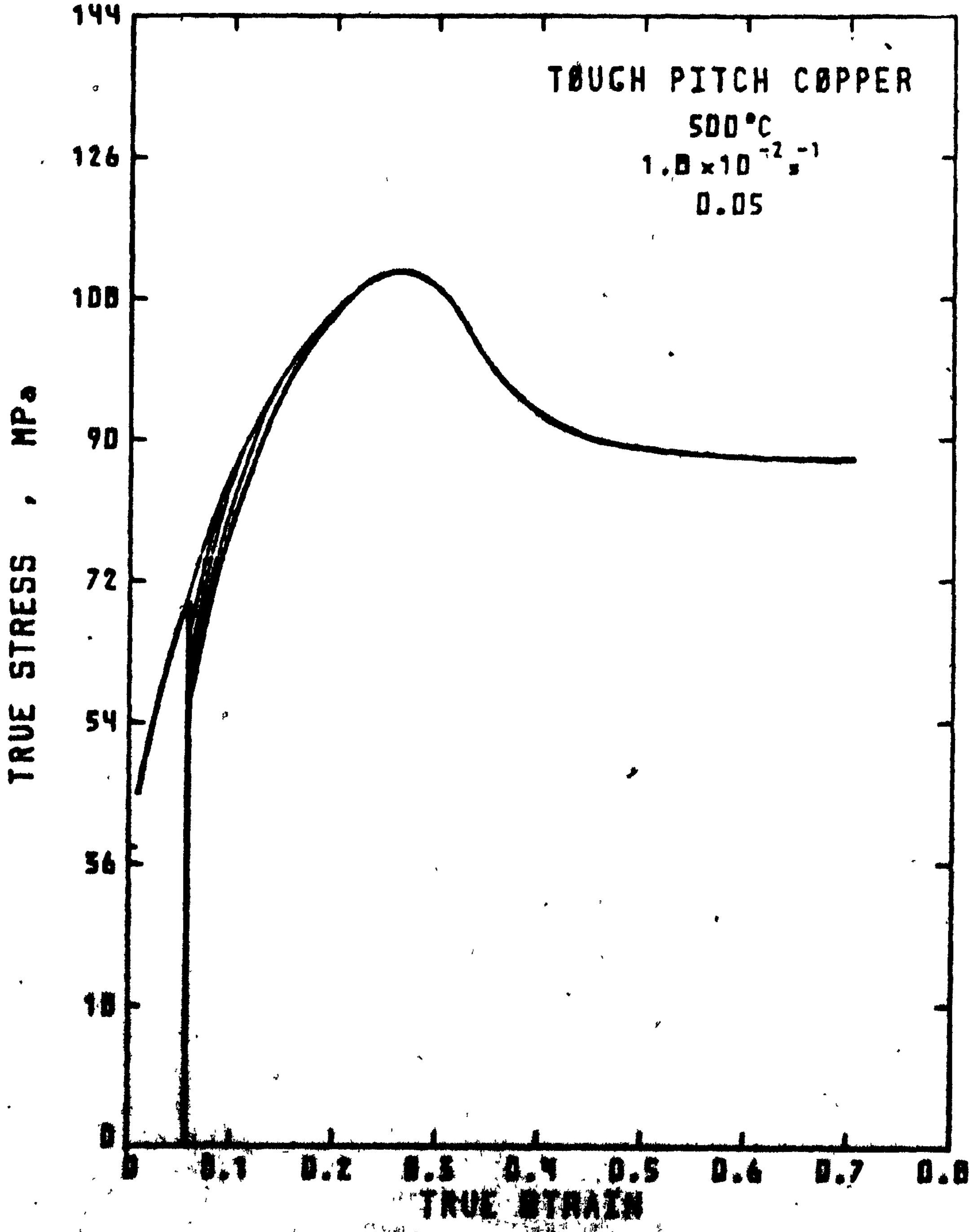
TØUGH PITCH CØPPER
500°C
$1.8 \times 10^{-2} s^{-1}$
0.05
144
126
108
90
72
54
36
18
0
TRUE STRESS , MPa
0
0.1
0.2
0.3
0.4
0.5
0.6
0.7
0.8
TRUE STRAIN

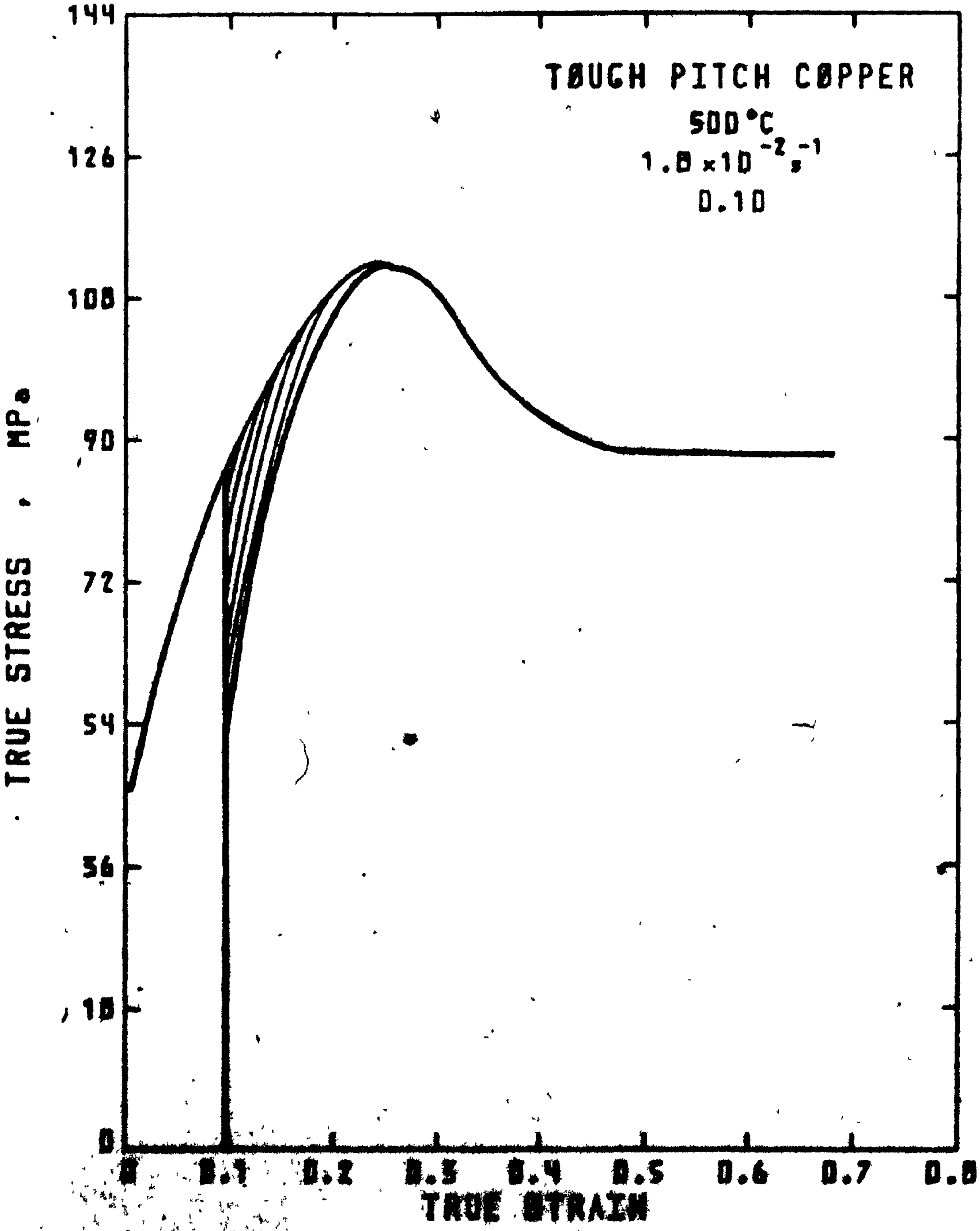
TØUGH PITCH CØPPER
500°C
1.0×10^-2 s^-1
0.10
TRUE STRESS , MPa
TRUE STRAIN
144
126
108
90
72
54
36
18
0
0
0.1
0.2
0.3
0.4
0.5
0.6
0.7
0.8

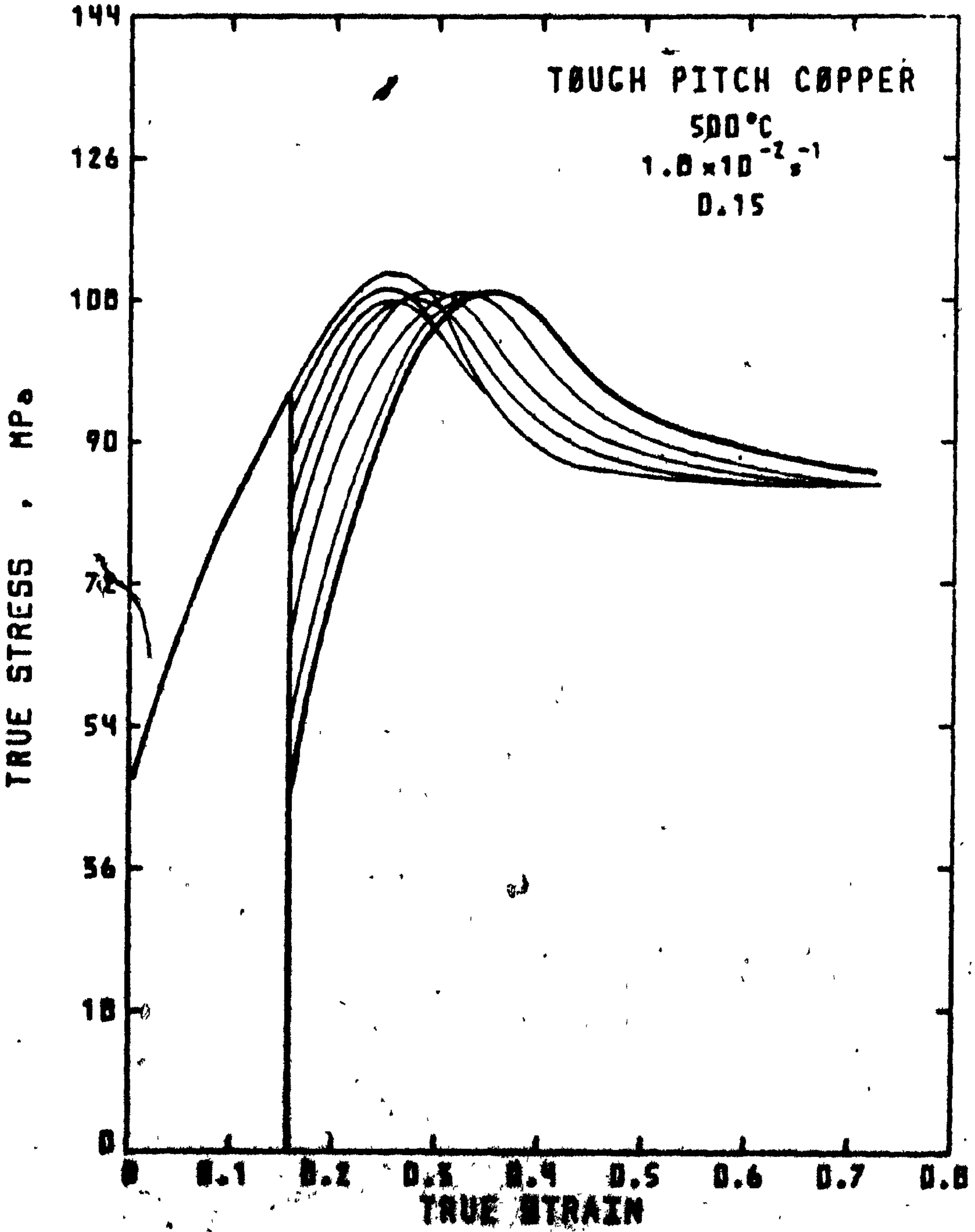
TOUGH PITCH COPPER
500 °C
$1.0 \times 10^{-2} s^{-1}$
0.15
TRUE STRESS , MPa
144
126
108
90
72
54
36
18
0
0
0.1
0.2
0.3
0.4
0.5
0.6
0.7
0.8
TRUE STRAIN

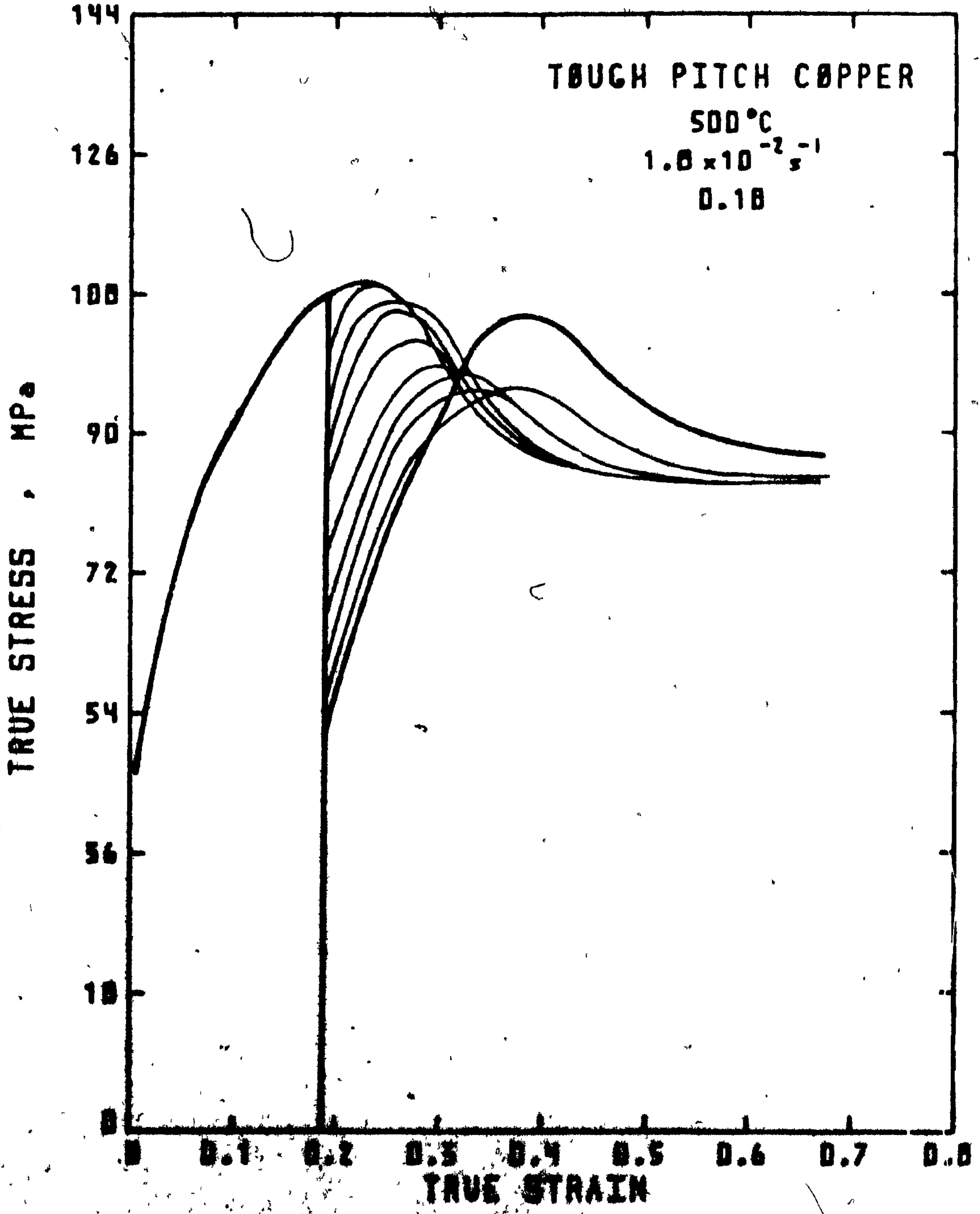
TOUGH PITCH COPPER
500°C
1.0×10⁻² s⁻¹
0.18
TRUE STRESS , MPa
144
126
108
90
72
54
36
18
0
TRUE STRAIN
0
0.1
0.2
0.3
0.4
0.5
0.6
0.7
0.8

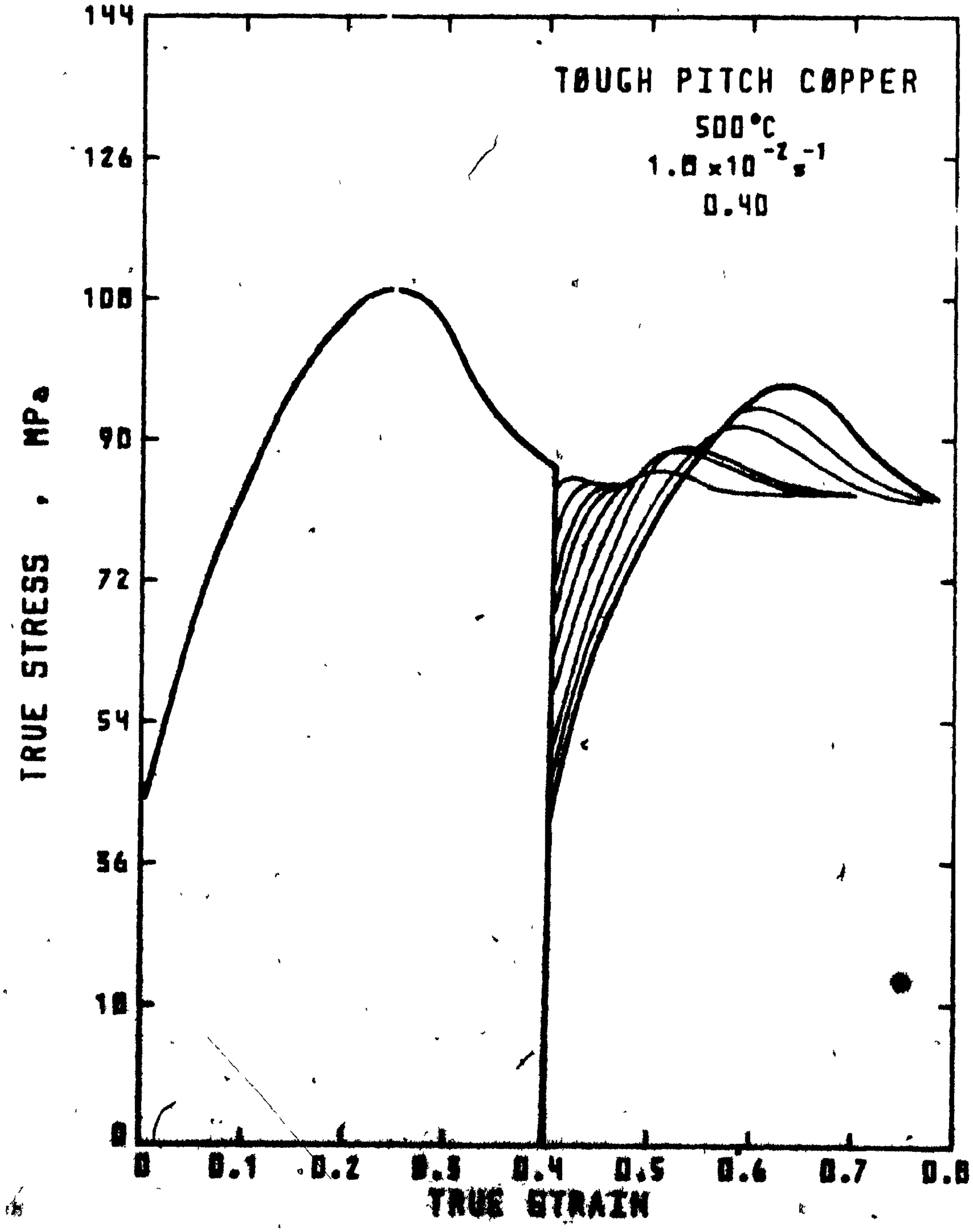
TØUGH PITCH CØPPER
500°C
$1.0 \times 10^{-2} s^{-1}$
0.40
TRUE STRESS , MPa
144
126
108
90
72
54
36
18
0
TRUE STRAIN
0
0.1
0.2
0.3
0.4
0.5
0.6
0.7
0.8

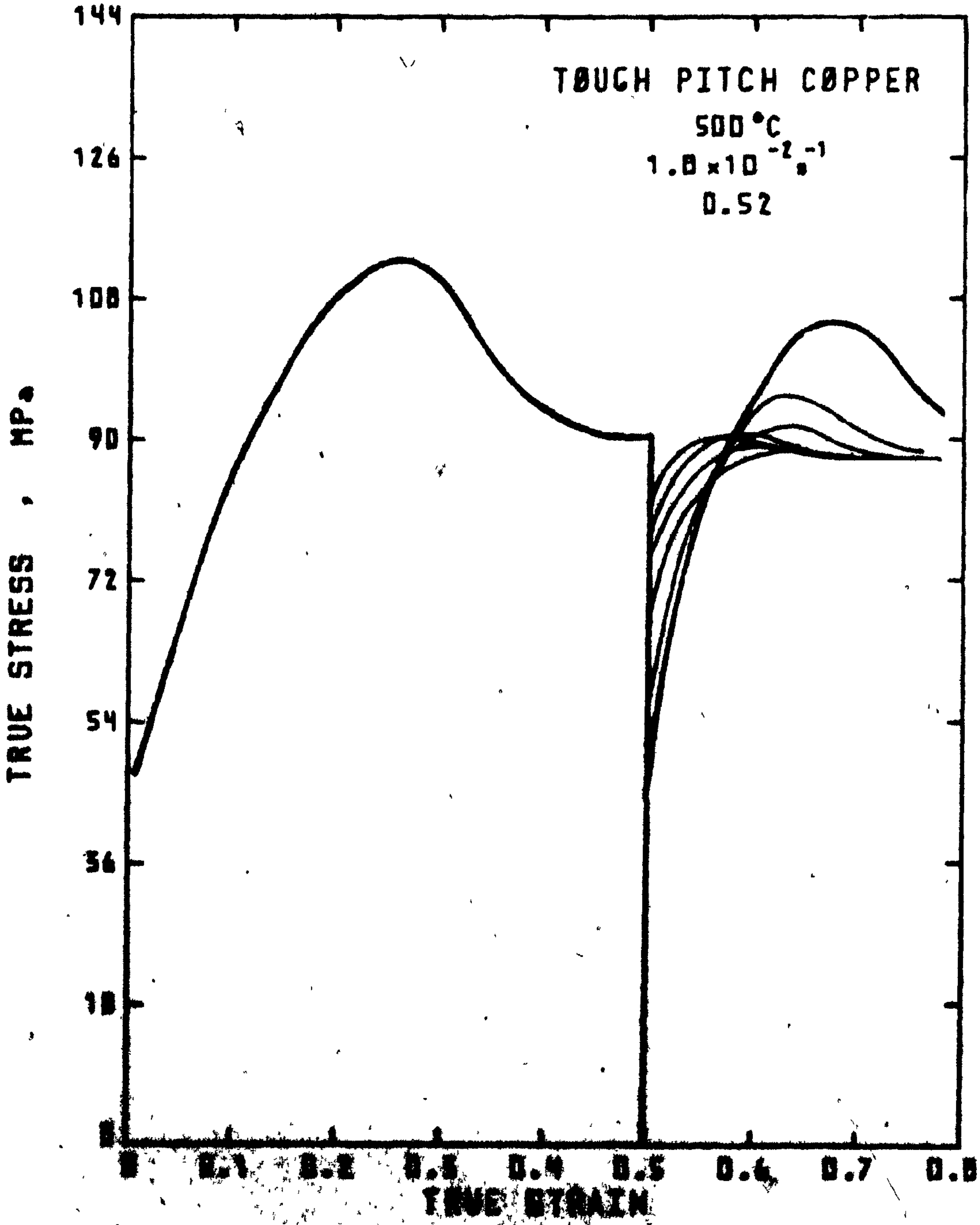
TØUGH PITCH CØPPER
500 °C
1.0 x 10^-2 s^-1
0.52
TRUE STRESS , MPa
144
126
108
90
72
54
36
18
0
TRUE STRAIN
0
0.1
0.2
0.3
0.4
0.5
0.6
0.7
0.8

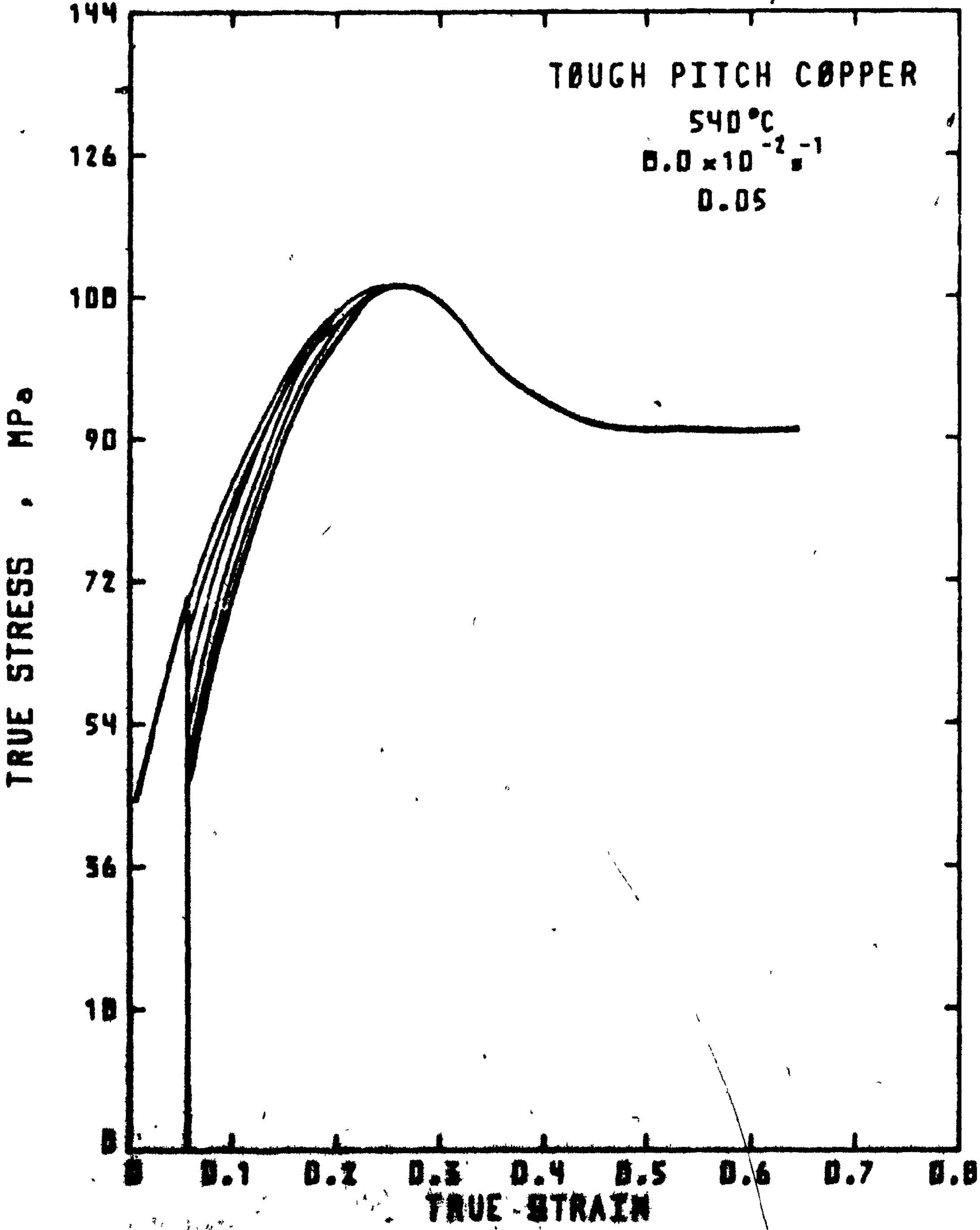
TOUGH PITCH COPPER
540°C
8.0 x 10^-2 s^-1
0.05
TRUE STRESS , MPa
144
126
108
90
72
54
36
18
0
TRUE STRAIN
0
0.1
0.2
0.3
0.4
0.5
0.6
0.7
0.8

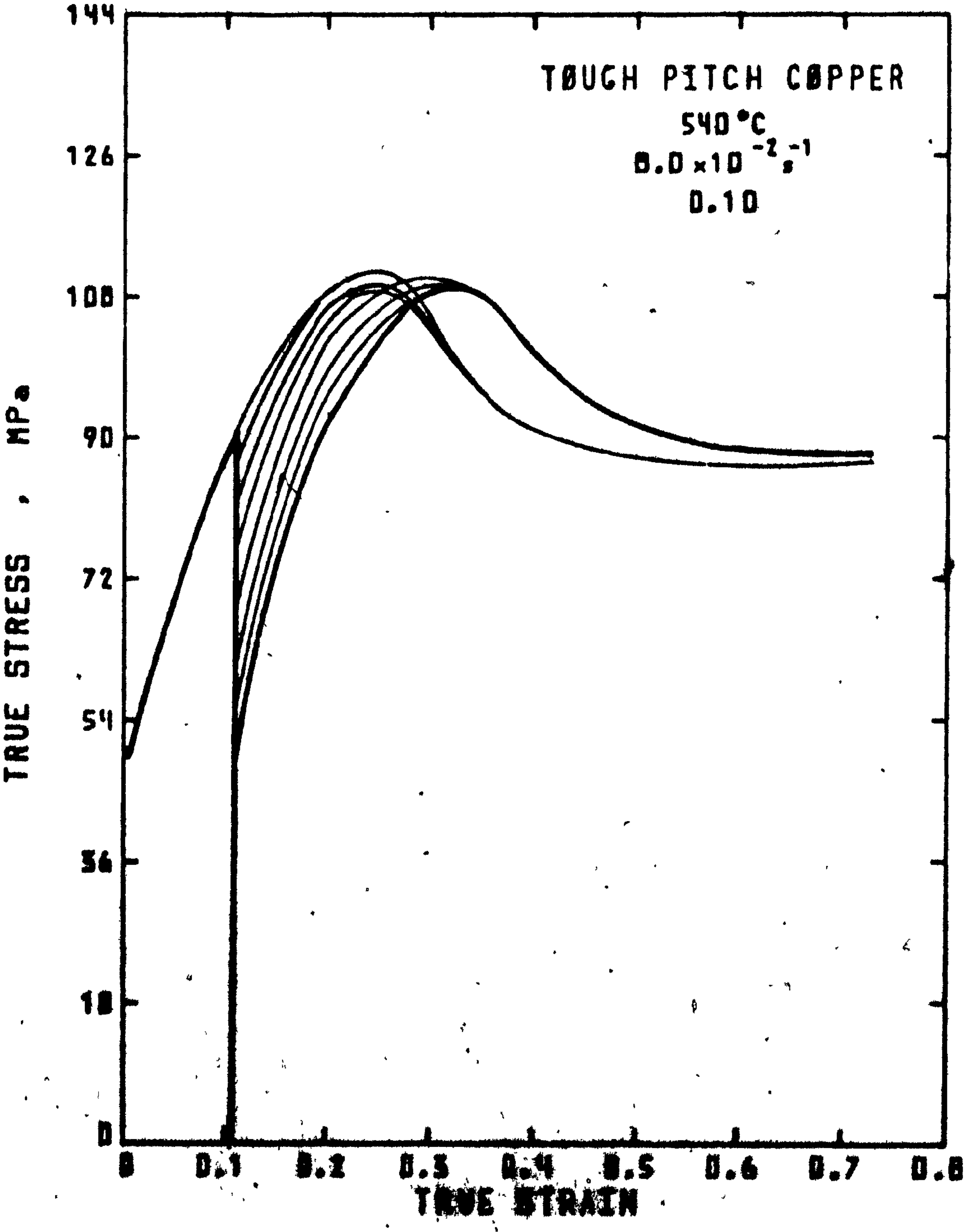
TOUGH PITCH COPPER
540 °C
8.0×10^{-2}s^{-1}
0.10
TRUE STRESS , MPa
144
126
108
90
72
54
36
18
0
0
0.1
0.2
0.3
0.4
0.5
0.6
0.7
0.8
TRUE STRAIN

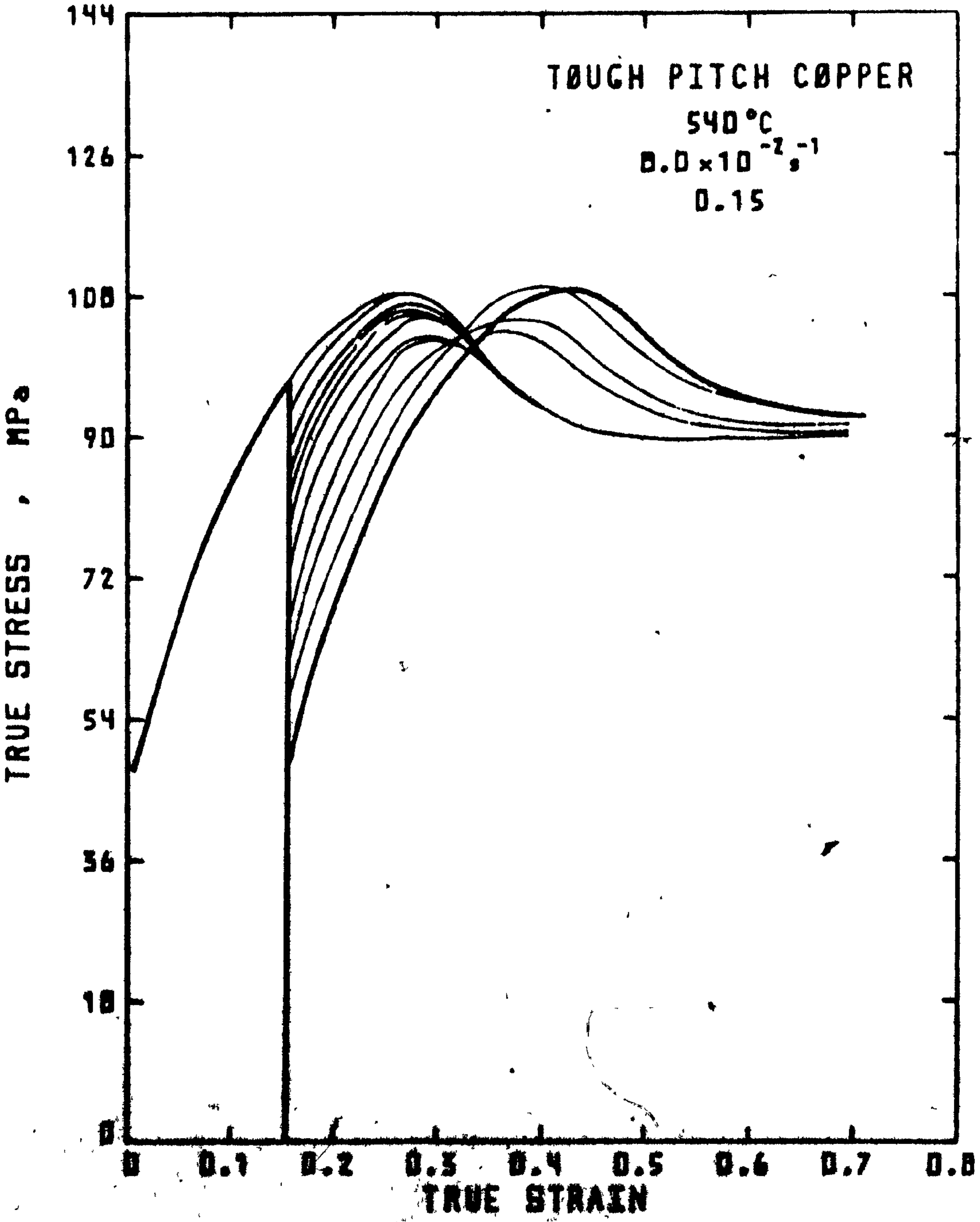
TOUGH PITCH COPPER
540°C
$8.0\times10^{-2}\,s^{-1}$
0.15
TRUE STRESS , MPa
144
126
108
90
72
54
36
18
0
TRUE STRAIN
0
0.1
0.2
0.3
0.4
0.5
0.6
0.7
0.8

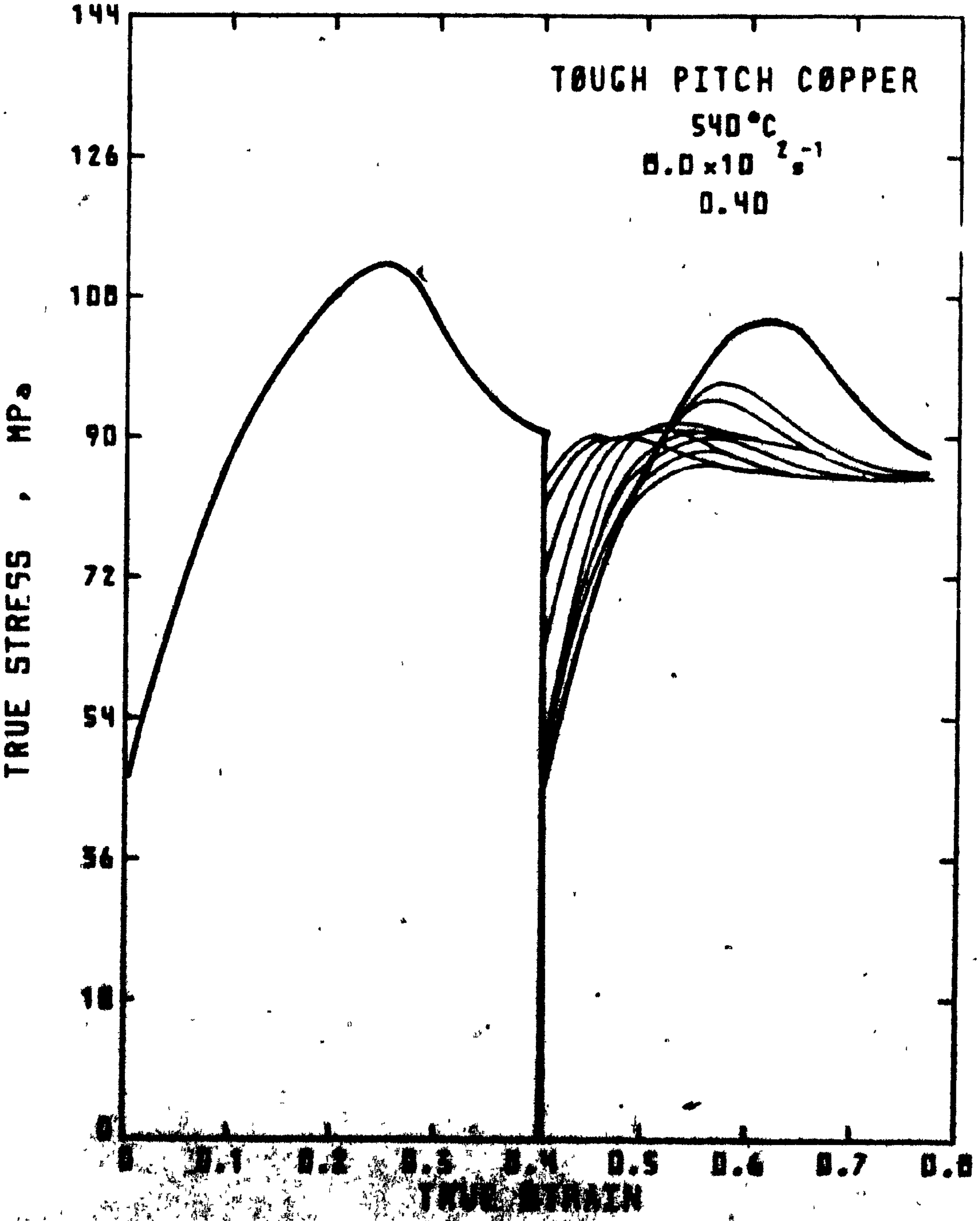
TOUGH PITCH COPPER
540°C
$8.0\times10^{2}s^{-1}$
0.40
144
126
108
90
72
54
36
18
0
TRUE STRESS , MPa
0
0.1
0.2
0.3
0.4
0.5
0.6
0.7
0.8
TRUE STRAIN

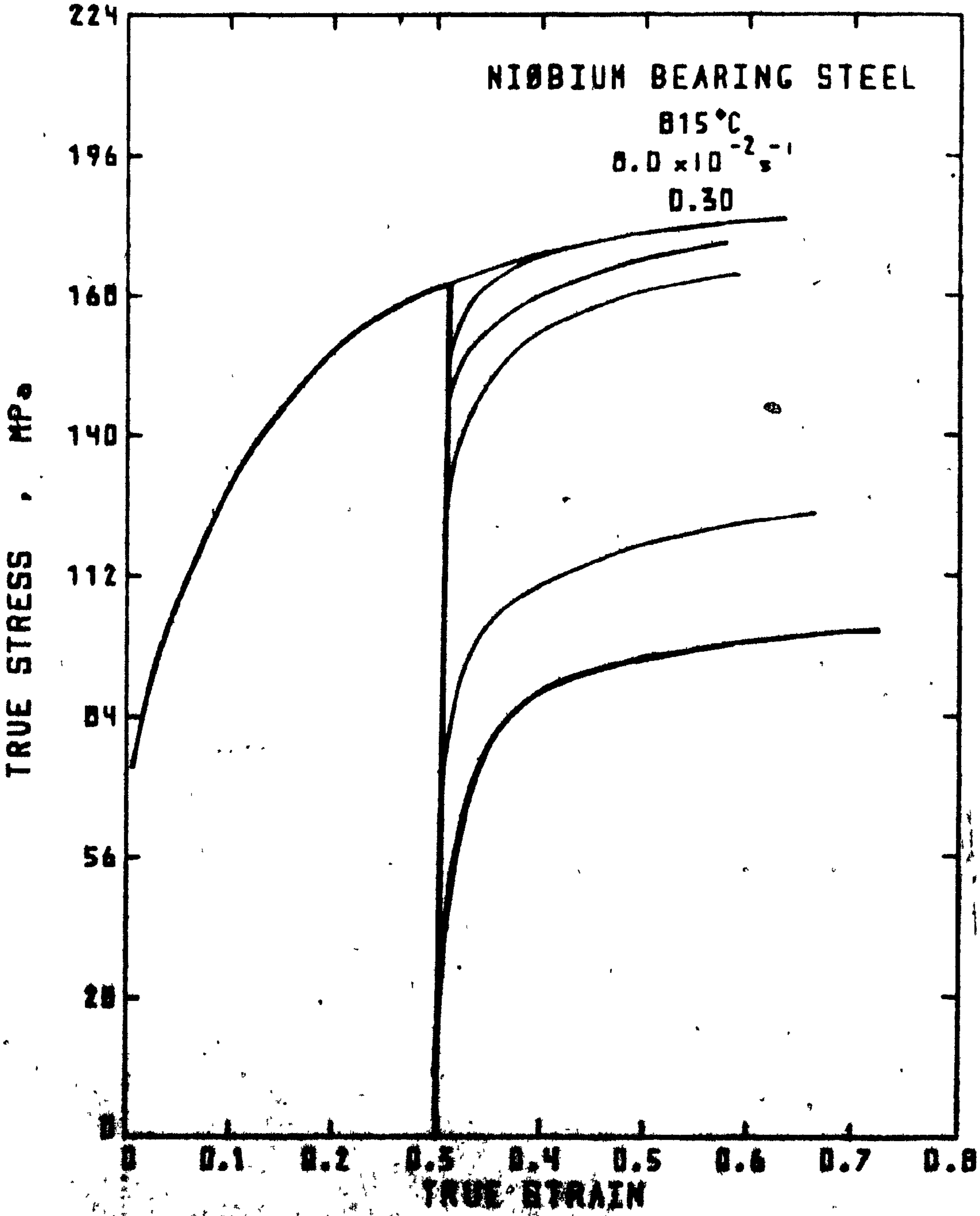
NIØBIUM BEARING STEEL
815°C
8.0 ×10⁻² s⁻¹
0.30
TRUE STRESS , MPa
224
196
168
140
112
84
56
28
0
TRUE STRAIN
0
0.1
0.2
0.3
0.4
0.5
0.6
0.7
0.8

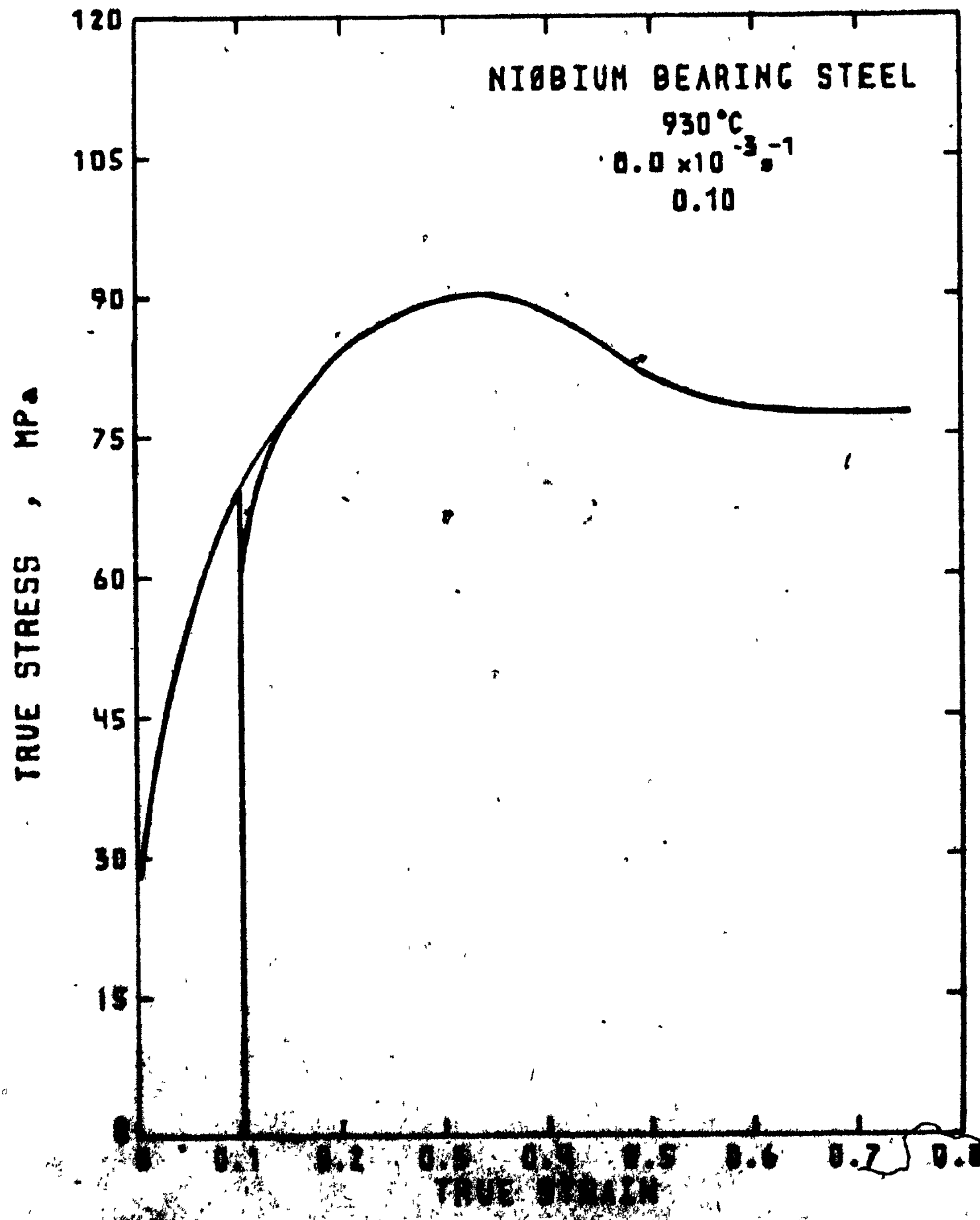
NIØBIUM BEARING STEEL
930°C
$6.0 \times 10^{-3} s^{-1}$
0.10
TRUE STRESS , MPa
120
105
90
75
60
45
30
15
0
0
0.1
0.2
0.3
0.4
0.5
0.6
0.7
0.8
TRUE STRAIN

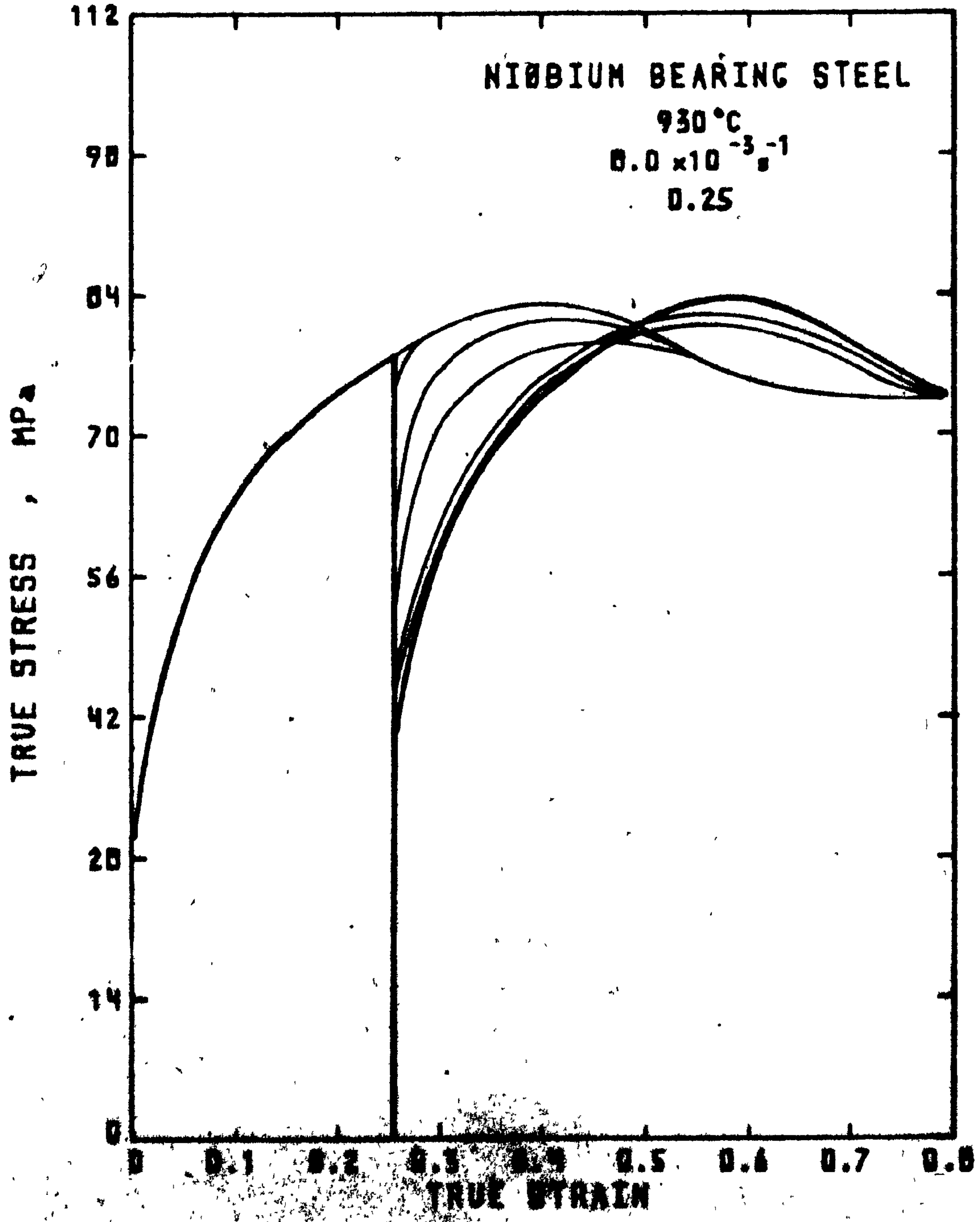
NIOBIUM BEARING STEEL
930°C
8.0 ×10-3 s-1
0.25
TRUE STRESS , MPa
112
98
84
70
56
42
28
14
0
TRUE STRAIN
0
0.1
0.2
0.3
0.4
0.5
0.6
0.7
0.8

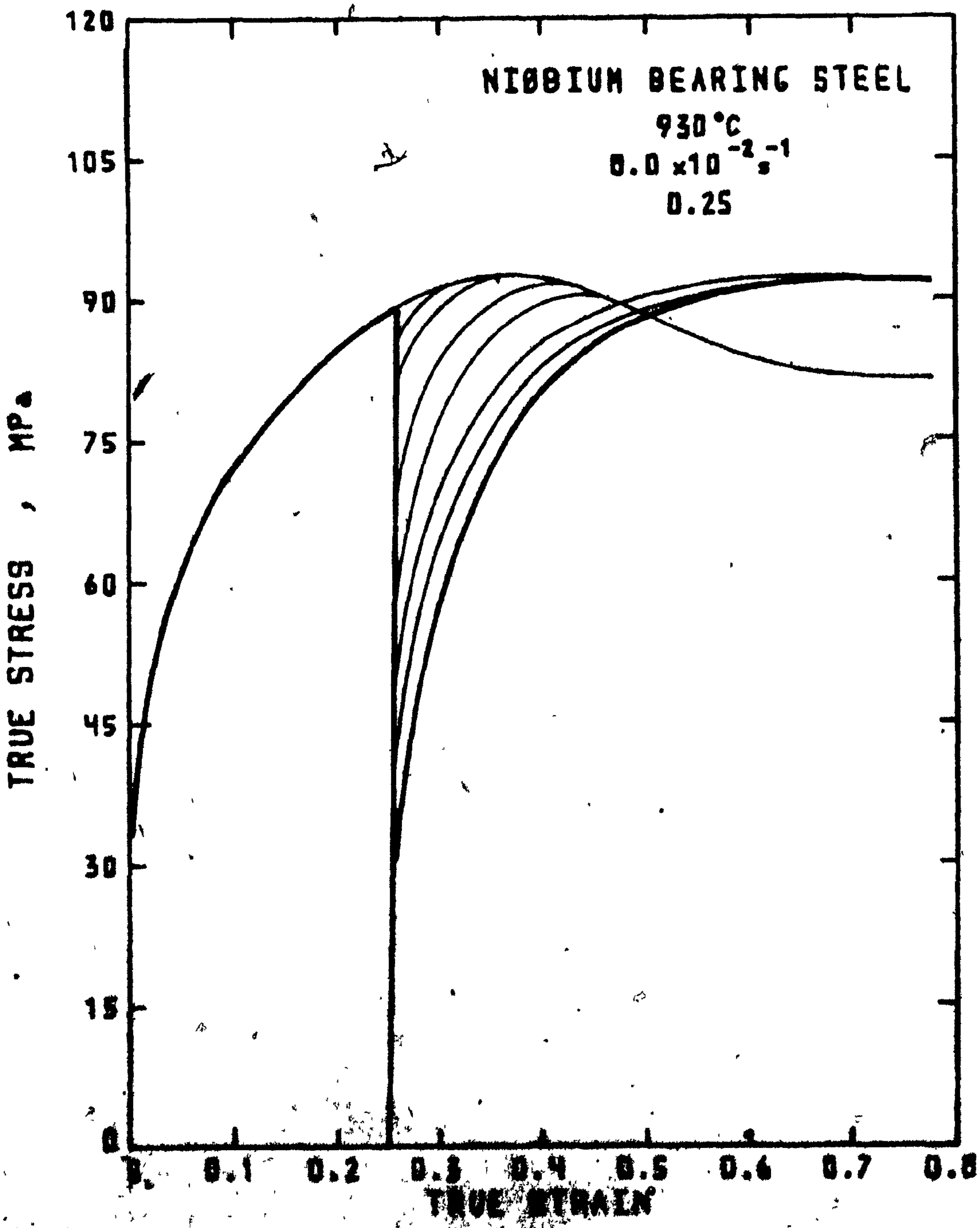
NIØBIUM BEARING STEEL
930 °C
8.0 x10^{-2} s^{-1}
0.25
TRUE STRESS , MPa
120
105
90
75
60
45
30
15
0
TRUE STRAIN
0.
0.1
0.2
0.3
0.4
0.5
0.6
0.7
0.8

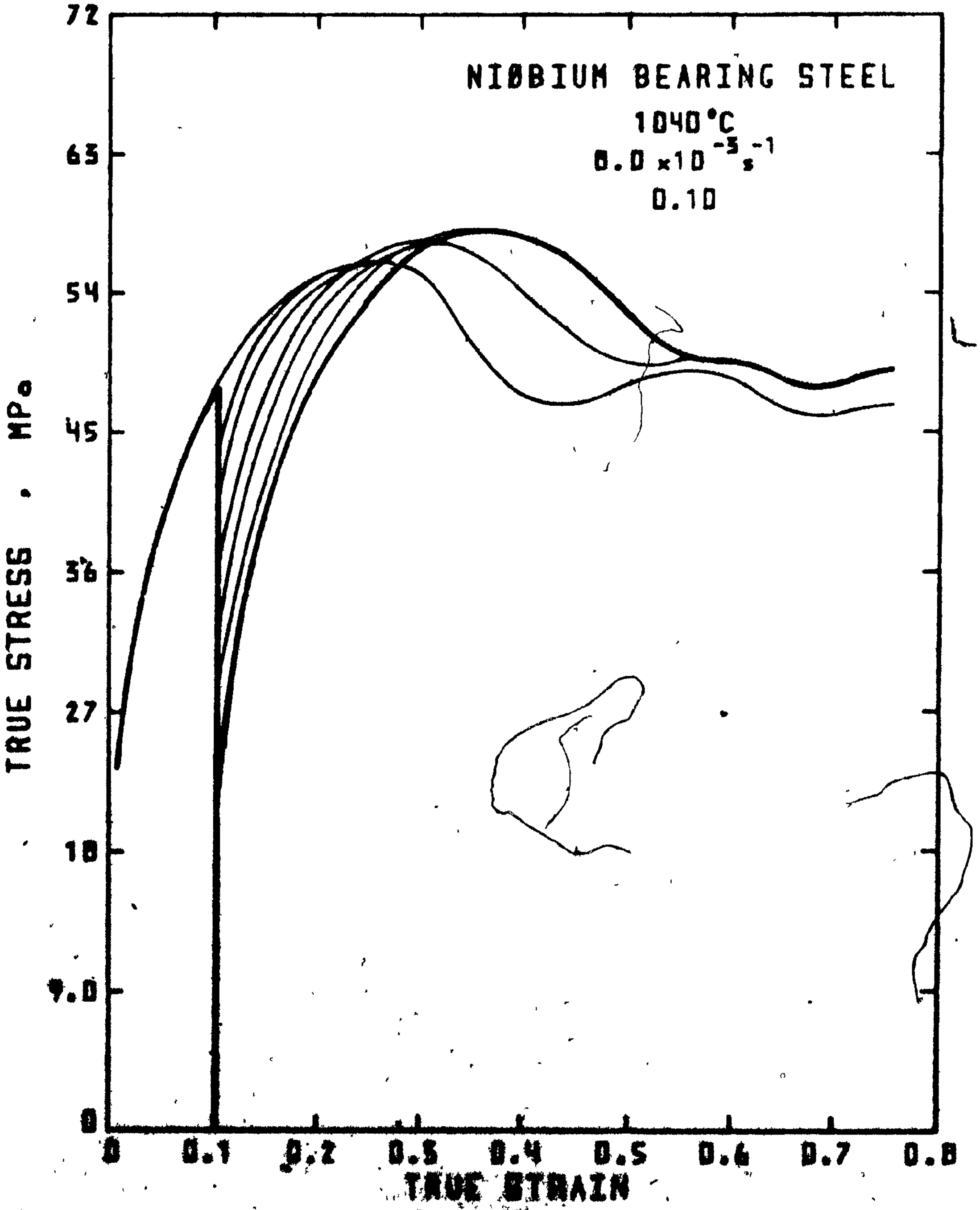
NIØBIUM BEARING STEEL
1040°C
8.0 ×10^{-3} s^{-1}
0.10
TRUE STRESS , MPa
72
63
54
45
36
27
18
9.0
0
TRUE STRAIN
0
0.1
0.2
0.3
0.4
0.5
0.6
0.7
0.8

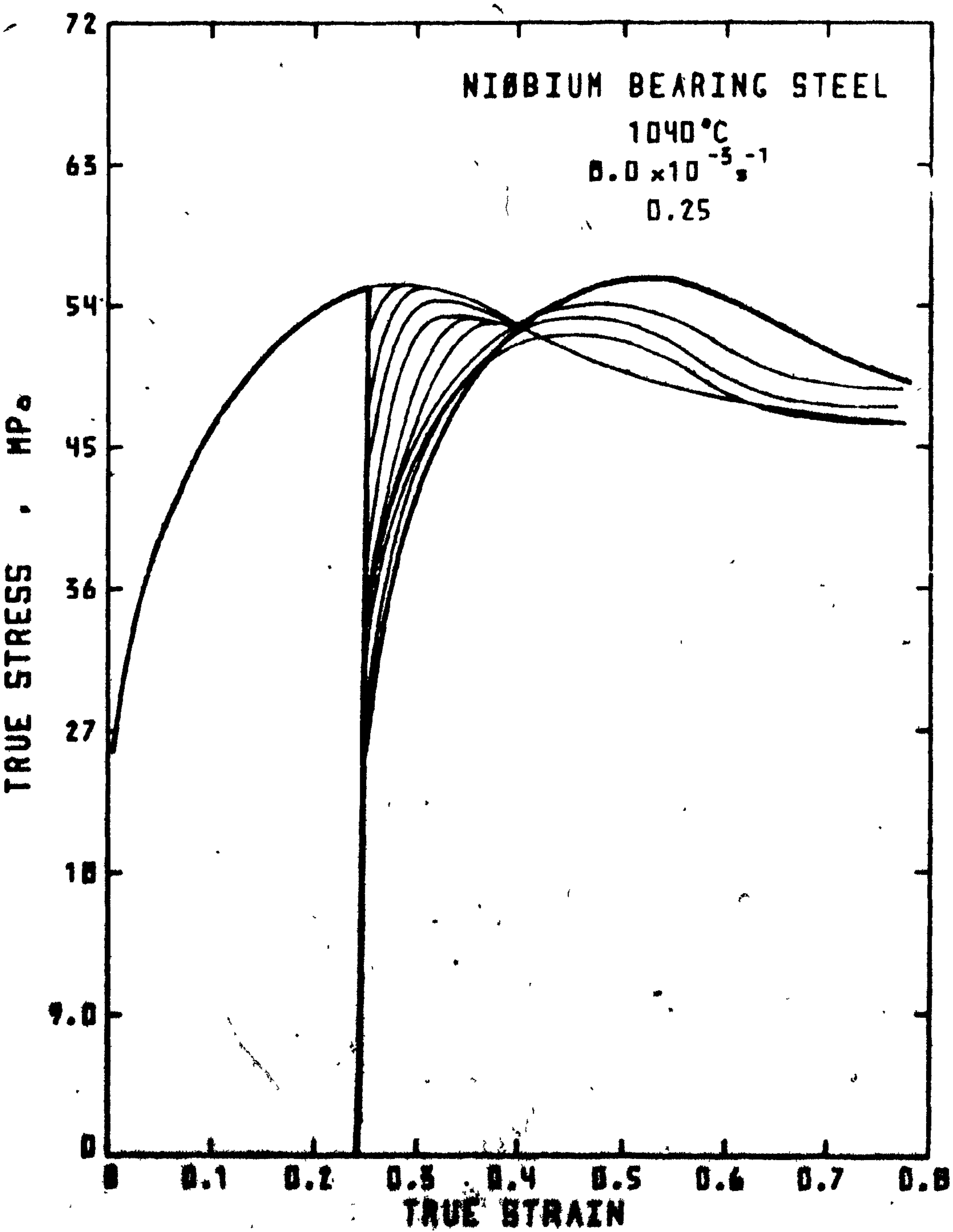
NIØBIUM BEARING STEEL
1040°C
8.0 x10^{-3}s^{-1}
0.25
TRUE STRESS , MPa
72
63
54
45
36
27
18
9.0
0
TRUE STRAIN
0
0.1
0.2
0.3
0.4
0.5
0.6
0.7
0.8

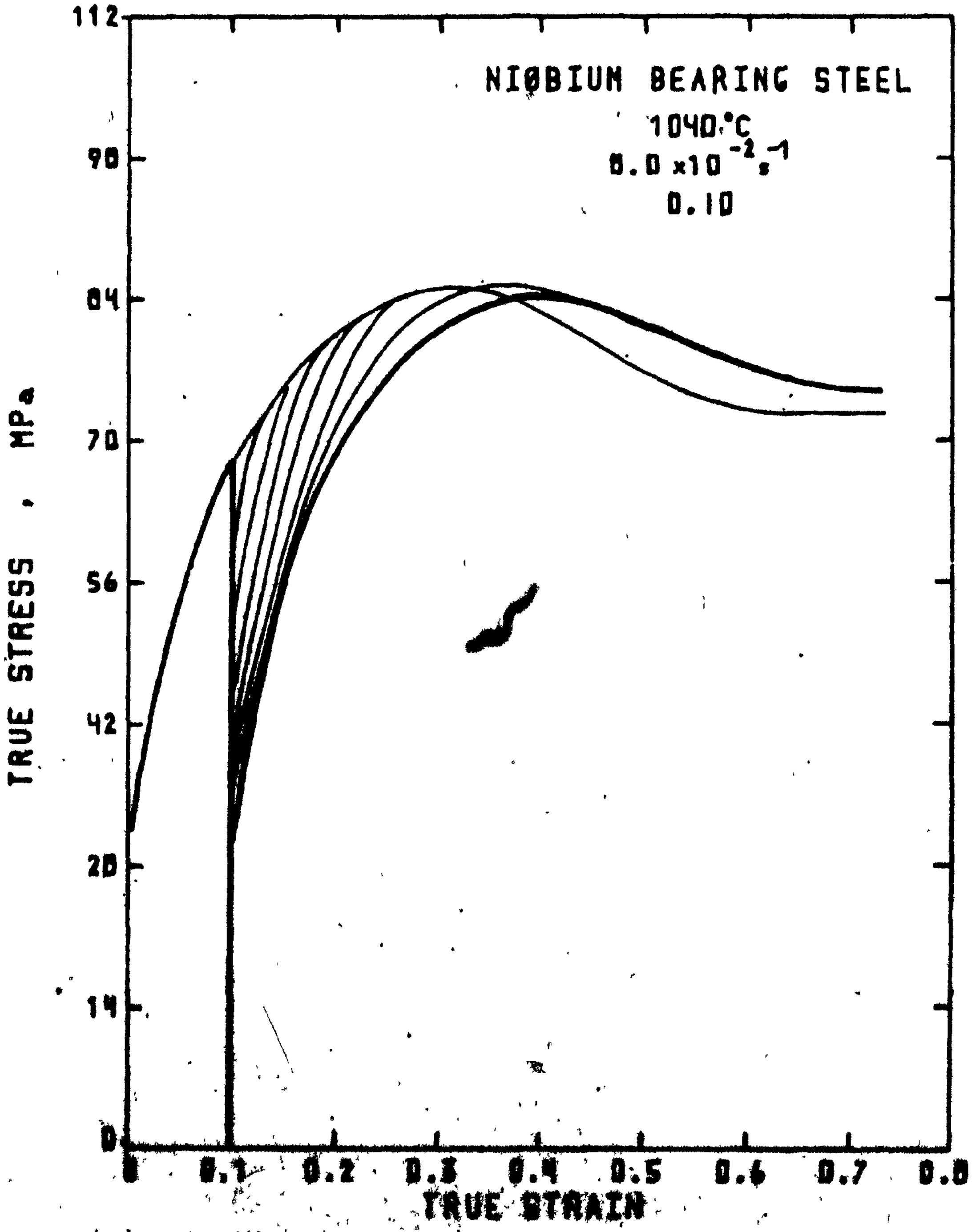
NIØBIUM BEARING STEEL
1040°C
$8.0 \times 10^{-2} s^{-1}$
0.10
TRUE STRESS , MPa
112
98
84
70
56
42
28
14
0
TRUE STRAIN
0
0.1
0.2
0.3
0.4
0.5
0.6
0.7
0.8

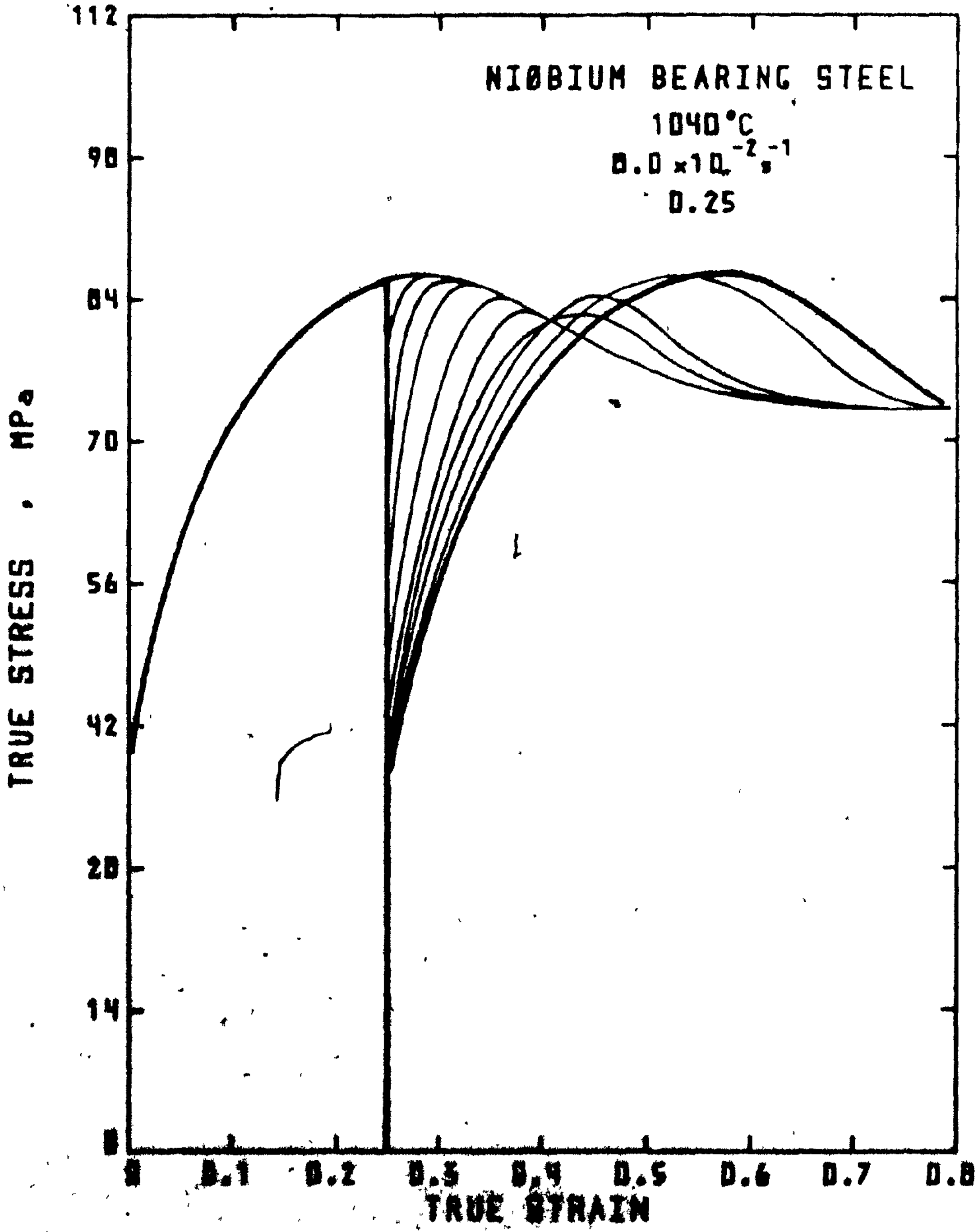
NIØBIUM BEARING STEEL
1040°C
8.0 ×10^{-2} s^{-1}
0.25
TRUE STRESS , MPa
112
98
84
70
56
42
28
14
0
TRUE STRAIN
0
0.1
0.2
0.3
0.4
0.5
0.6
0.7
0.8

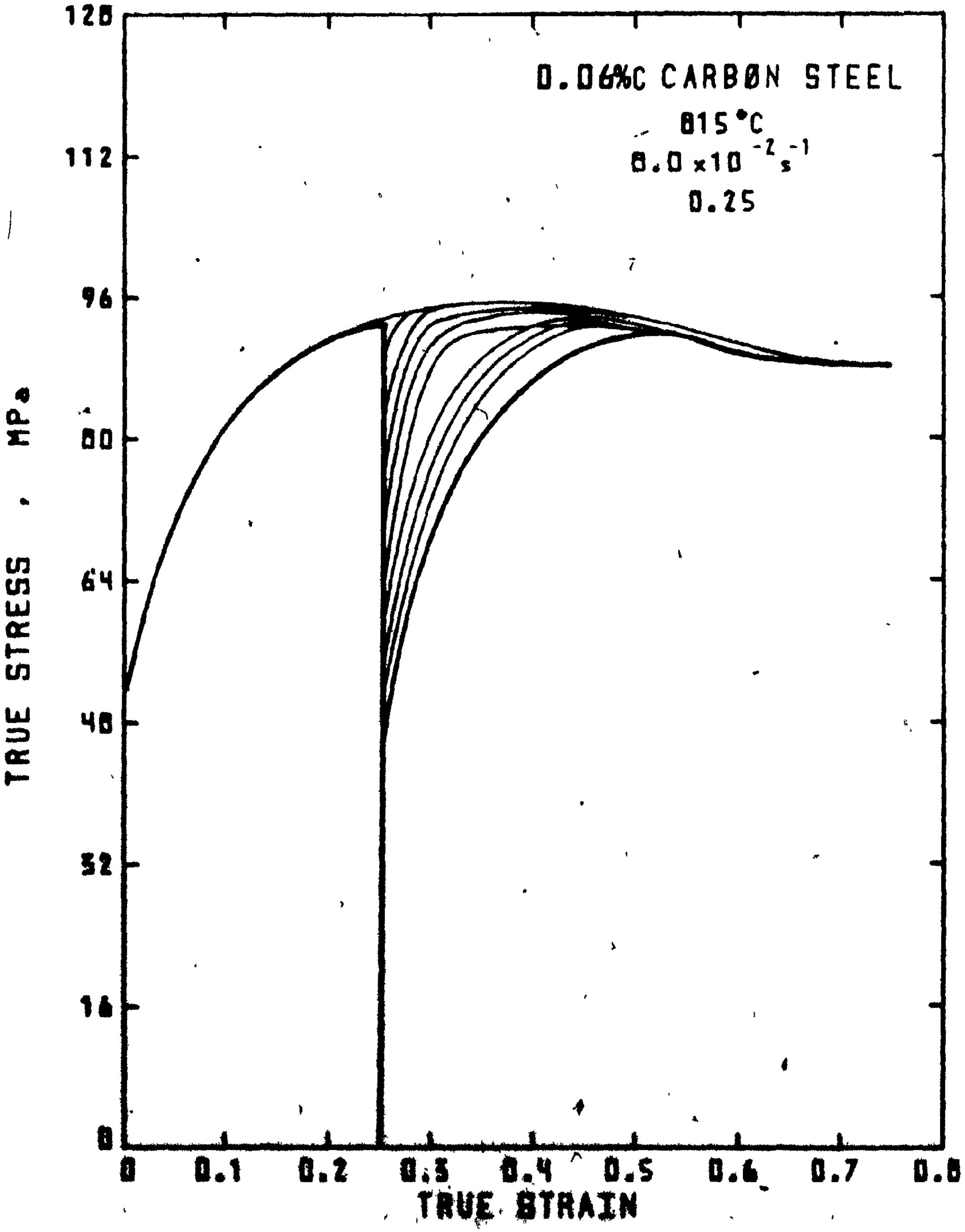
0.06%C CARBON STEEL
815 °C
8.0 x10⁻² s⁻¹
0.25
TRUE STRESS , MPa
TRUE STRAIN
0
16
32
48
64
80
96
112
128
0
0.1
0.2
0.3
0.4
0.5
0.6
0.7
0.8

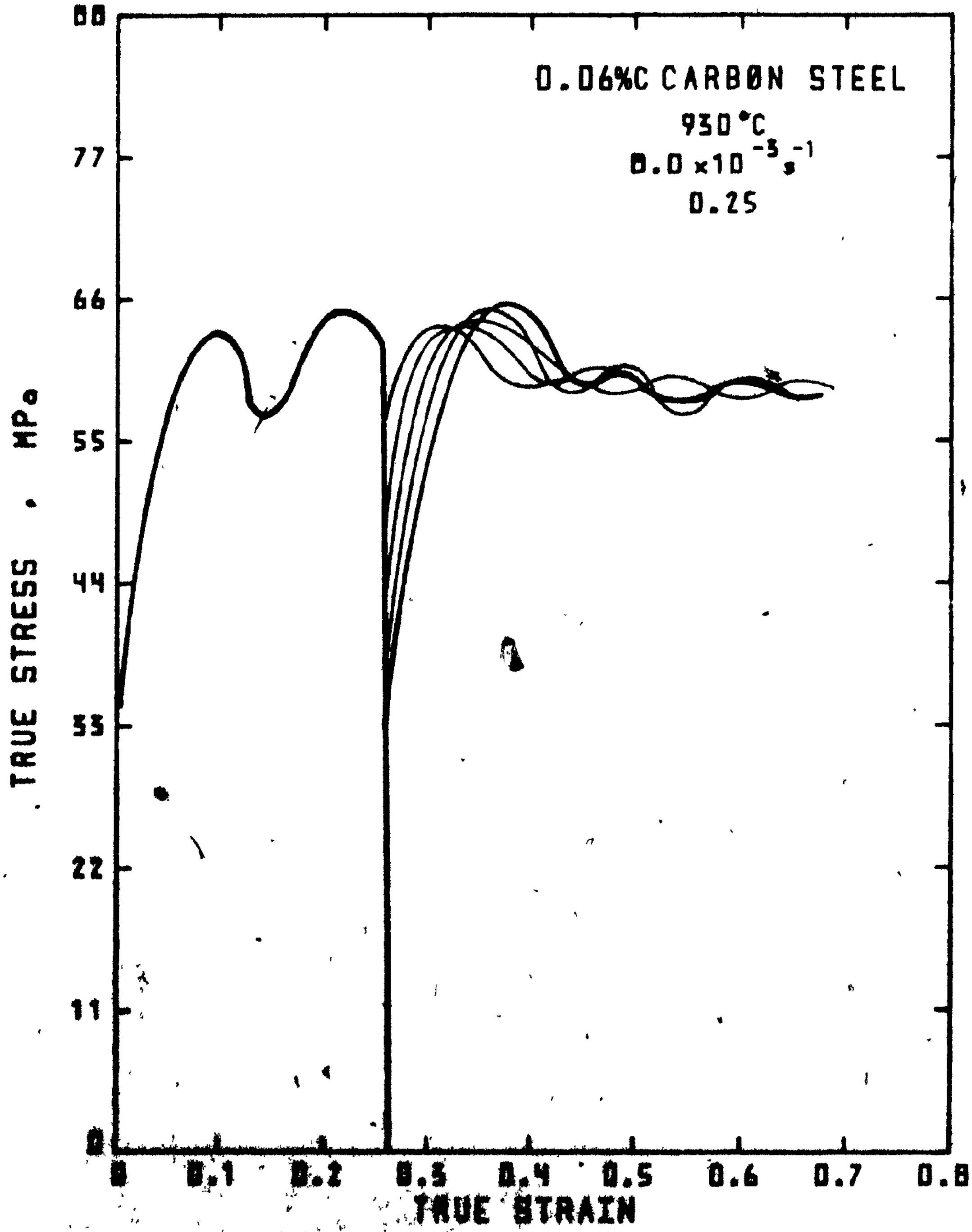
0.06%C CARBON STEEL
930°C
8.0 x10^{-3} s^{-1}
0.25
TRUE STRESS , MPa
88
77
66
55
44
33
22
11
0
TRUE STRAIN
0
0.1
0.2
0.3
0.4
0.5
0.6
0.7
0.8

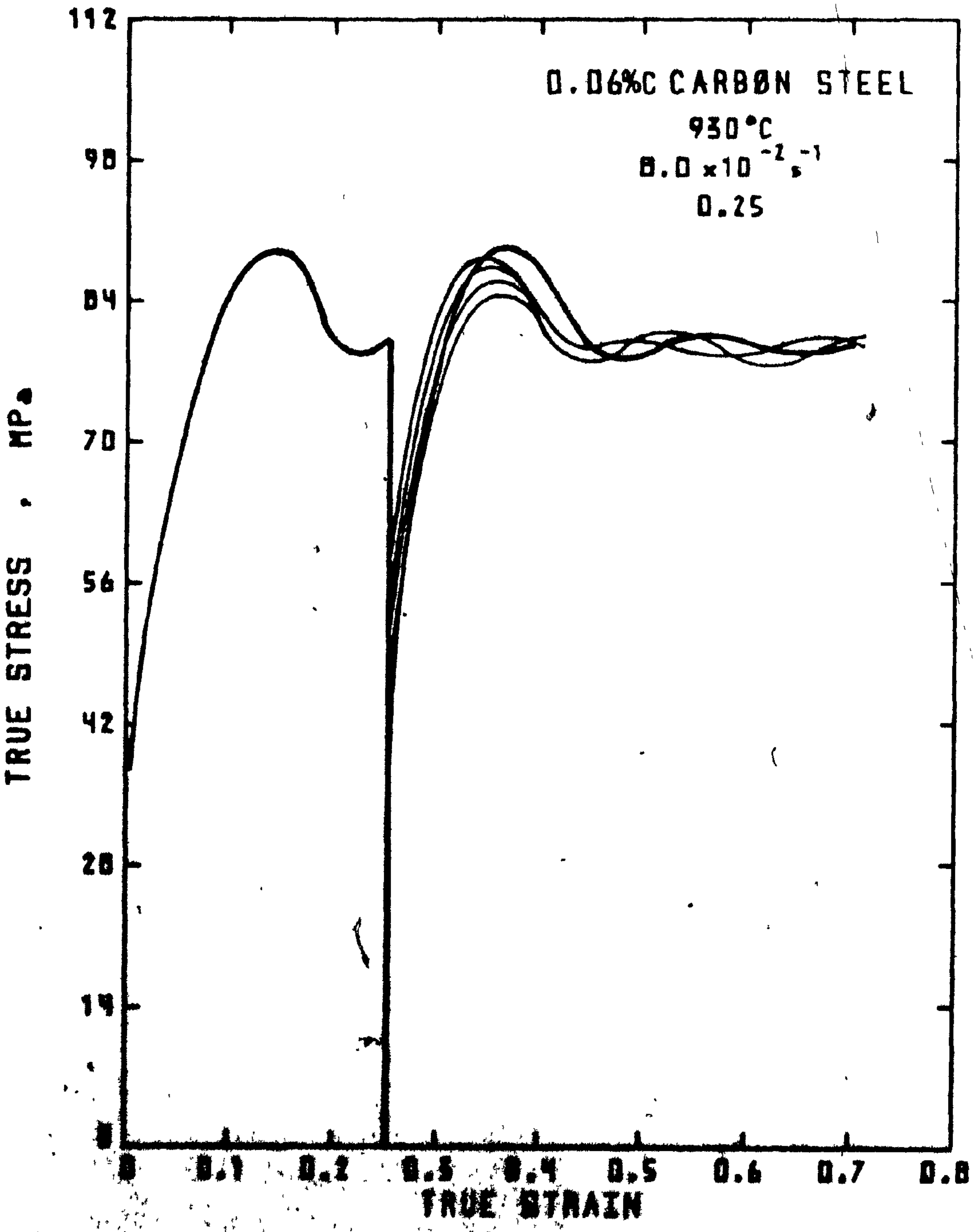
0.06%C CARBON STEEL
930°C
8.0 x10⁻² s⁻¹
0.25
TRUE STRESS , MPa
112
98
84
70
56
42
28
14
0
TRUE STRAIN
0
0.1
0.2
0.3
0.4
0.5
0.6
0.7
0.8

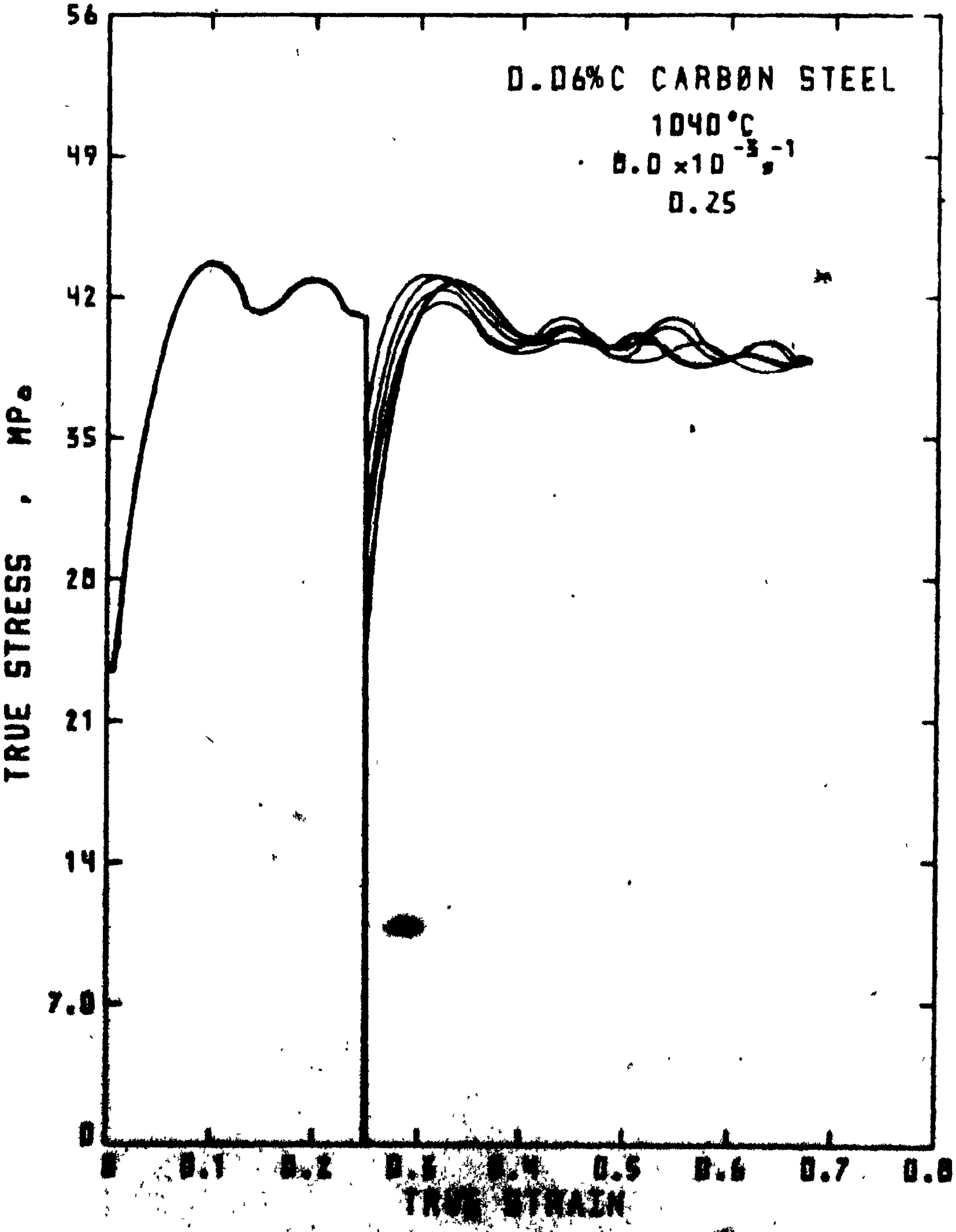
0.06%C CARBON STEEL
1040°C
8.0 ×10⁻³s⁻¹
0.25
TRUE STRESS , MPa
TRUE STRAIN
56
49
42
35
28
21
14
7.0
0
0
0.1
0.2
0.3
0.4
0.5
0.6
0.7
0.8

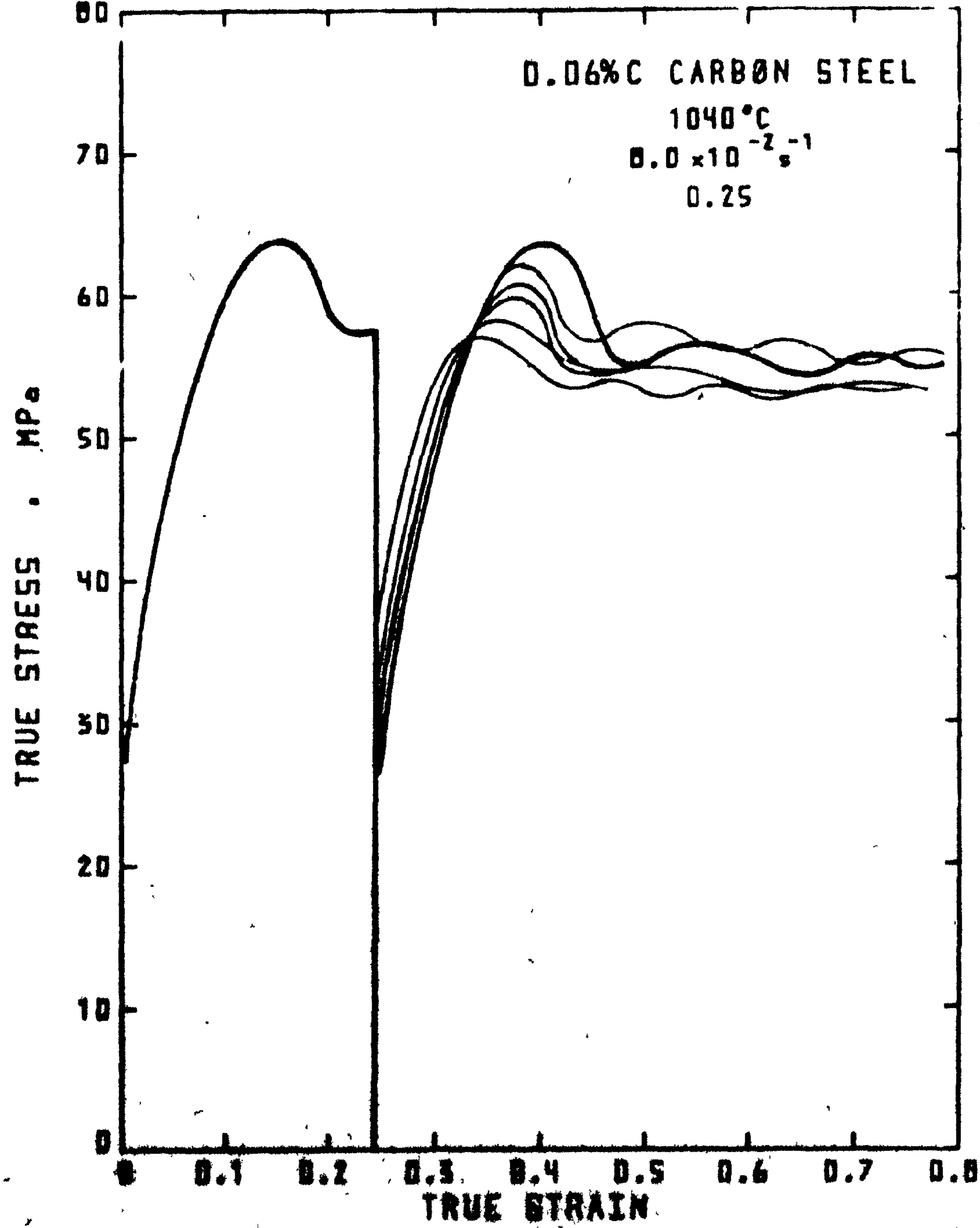
0.06%C CARBON STEEL
1040°C
8.0 x10^{-2} s^{-1}
0.25
TRUE STRESS , MPa
TRUE STRAIN
0
10
20
30
40
50
60
70
80
0
0.1
0.2
0.3
0.4
0.5
0.6
0.7
0.8

APPENDIX 3.1

Experimental Conditions Employed to Evaluate the Influence of Grain Size on the High Temperature Yield Stress of Copper

APPENDIX 3.1

Experimental Conditions Employed to Evaluate the Influence of Grain Size on the High Temperature Yield Stress of Copper

TOUGH PITCH COPPER, T = 540°C

Test No.	$\dot{\varepsilon}_L$ (s^{-1})	$\dot{\varepsilon}_{RL}$ (s^{-1})	t_D (s)	ε	σ_M (MPa)	σ_y (MPa)	σ_{RL} (MPa)	$\bar{d}$ (mm)
1	2	3	4	5	6	7	8	9
Cu 913	$3x10^{-2}$	$8x10^{-2}$	10	0.40	94	49	36	0.056
Cu 905		$1.8x10^{-2}$	12.2	0.41	93	50	34	
Cu 906		$1.8x10^{-2}$	12.2	0.41	92.9	48	34	
Cu 925		$3.7x10^{-3}$	15	0.40	94	48	32	
Cu 926		$3.7x10^{-3}$	15	0.40	94.5	48	32	
Cu 923		$7.5x10^{-4}$	35	0.41	94	48	30	
Cu 924		$7.5x10^{-4}$	36	0.41	94.6	48	30	
Cu 929	$1.8x10^{-2}$	$8x10^{-2}$	20	0.39	75	43	35	0.10
Cu 930		$8x10^{-2}$	20	0.40	76	45	35	
Cu 912		$1.8x10^{-2}$	20.5	0.40	77	46	33	
Cu 927		$3.7x10^{-3}$	23	0.39	77	42	31	
Cu 928		$3.7x10^{-3}$	23.1	0.40	76	43	31	
Cu 920		$7.5x10^{-4}$	39.8	0.40	77	43	29.5	
Cu 921		$7.5x10^{-4}$	38.7	0.41	76	43	29.5	
Cu 931	$3.7x10^{-3}$	$8x10^{-2}$	60.3	0.39	61.6	40.5	34	0.145
Cu 932		$8x10^{-2}$	60.4	0.40	60.2	39	34	
Cu 933		$1.8x10^{-2}$	60.7	0.40	62.8	38	32.5	
Cu 934		$1.8x10^{-2}$	60.7	0.39	60	39	32.5	
Cu 911		$3.7x10^{-3}$	68	0.39	61	41	30.5	
Cu 918		$7.5x10^{-4}$	77.6	0.40	62	40.9	28.5	
Cu 919		$7.5x10^{-4}$	78	0.40	61.9	41	28.5	

APPENDIX 3.1 (cont'd)

1	2	3	4	5	6	7	8	9
Cu 914	$7.5\text{x}10^{-4}$	$8\text{x}10^{-2}$	300	0.40	53	38.5	33.5	0.2
Cu 915		$8\text{x}10^{-2}$	300	0.40	53.3	36	33.5	
Cu 916		$1.8\text{x}10^{-2}$	301	0.41	52	36.6	32	
Cu 917		$1.8\text{x}10^{-2}$	301	0.40	52.9	33	32	
Cu 907		$3.7\text{x}10^{-3}$	302	0.39	52.8	43	30	
Cu 908		$3.7\text{x}10^{-3}$	302	0.39	53	38	30	
Cu 910		$7.5\text{x}10^{-4}$	314	0.40	54	38	28	

TOUGH PITCH COPPER, T = 600°C

1	2	3	4	5	6	7	8	9
Cu 261	$7.5\text{x}10^{-2}$	$7.5\text{x}10^{-2}$	1	0.40	63.5	41	34	0.16
Cu 260		$1.9\text{x}10^{-2}$			63	40.8	32	
Cu 259		$3.8\text{x}10^{-3}$			62.9	41	30	
Cu 258		$7.5\text{x}10^{-4}$			63.1	40.5	28	
Cu 257	$1.9\text{x}10^{-2}$	$7.5\text{x}10^{-2}$	5	0.40	54.5	31.5	33	0.26
Cu 256		$1.9\text{x}10^{-2}$			55	29.6	31	
Cu 255		$3.8\text{x}10^{-3}$			54.9	31.1	29.5	
Cu 254		$7.5\text{x}10^{-4}$			55.1	31.5	27.8	
Cu 253	$3.8\text{x}10^{-3}$	$7.5\text{x}10^{-2}$	22	0.40	41.1	29.5	33	0.32
Cu 252		$1.9\text{x}10^{-2}$			40.5	28.0	31	
Cu 251		$3.8\text{x}10^{-3}$			41.2	29.5	29	
Cu 250		$7.5\text{x}10^{-4}$			41.0	29	27	
Cu 266	$7.5\text{x}10^{-4}$	$7.5\text{x}10^{-2}$	90	0.40	33	28.4	31.6	0.51
Cu 248		$1.9\text{x}10^{-2}$			34.2	39	30.3	
Cu 247		$3.8\text{x}10^{-3}$			33.5	27	29	
Cu 245		$7.5\text{x}10^{-4}$			33.7	27.5	27	
Cu 245		7.5x10			33.7	27.5	27	

APPENDIX 3.2

The Amounts of Softening Occurring in each of the Materials under the Experimental Conditions Employed

APPENDIX 3.2

The Amounts of Softening Occurring in each of the Materials under the Experimental Conditions Employed

TOUGH PITCH COPPER

Testing Temperature 450^{o}C, Unloading Strain 0.05,
Strain Rate 1.8x10^{-3}s^{-1}

Delay Time s	σ_y (MPa)	σ_m (MPa)	σ_R (MPa)	Amount of Softening %
1	2	3	4	5
5,000	43	70	70	0
11,000			68.7	5.5
24,000			65.1	18
36,000			61.4	32
46,000			60.3	36
100,000			58.6	42

Testing Temperature 450^{o}C, Unloading Strain 0.10,
Strain Rate 1.8x10^{-3}s^{-1}

1	2	3	4	5
500	43	92	92	0
1,000			92	0
3,000			90.5	3
5,000			89.5	5
7,000			87.6	9
9,000			85	14
14,000			81	22
17,000			77.3	30
30,000			69.5	46
55,000			67.5	50
100,000			67.5	50

APPENDIX 3.2 (cont'd)

Testing Temperature 450°C, Unloading Strain 0.15,
Strain Rate $1.8\mathrm{x}10^{-3}\mathrm{s}^{-1}$

1	2	3	4	5
10	$\overline{43}$	$\overline{96}$	96	0
30			96	0
80			96	0
180			94.4	3
300			94	4
500			92.8	6
1,000			88.6	14
1,400			86	19
2,000			82.2	26
2,700			77.5	35
4,000			71.6	46
6,000			69.5	50
8,000			69.5	50
12,000			69.2	50.5
18,000			67.4	54
28,000			62.1	64
40,000			55	78
70,000			45.1	96
200,000			30.8	123

Testing Temperature 450°C, Unloading Strain 0.40,
Strain Rate $1.8\mathrm{x}10^{-3}\mathrm{s}^{-1}$

1	2	3	4	5
2	$\overline{43}$	$\overline{95}$	92.9	4
4.4			90.3	9
6.5			89.3	11
9			87.7	14
10			87	15
15			86.2	17
20			85	19
24			84	21

APPENDIX 3.2 (cont'd)

1	2	3	4	5
32	$\overline{43}$	$\overline{95}$	81.5	26
38			79.4	30
55			75.2	38
90			70.5	47
100			67.9	52
110			66.9	54
120			64.8	58
150			64.3	59
200			64.8	58
240			64.8	58
300			64.8	58
400			63	62
500			60	68
600			56	75
700			54.4	78
900			53	80
2,000			53	80
3,000			52.3	82
3,800			48	90
5,000			43	100
40,000			43	< 103

Testing Temperature 500°C, Unloading Strain 0.05,
Strain Rate $1.8\times10^{-2}s^{-1}$

1	2	3	4	5
6	$\overline{43}$	$\overline{69}$	69	0
40			69	0
60			68.5	2
80			68.2	3
100			68	4
150			67	8
200			66	11
251			65	16
400			[illegible]	22

APPENDIX 3.2 (cont'd)

1	2	3	4	5
500	$\overline{43}$	$\overline{69}$	61.5	29
700			59.9	35
1.200			58.5	40.5
2,000			58.1	42
4,000			58.3	41
7,500			58.1	42
500,000			58.1	42

Testing Temperature 500^{0}C, Unloading Strain 0.10,
Strain Rate 1.8x10^{-2}s^{-1}

1	2	3	4	5
5	$\overline{43}$	$\overline{90}$	90	0
10			90	0
15			90	0
20			88.6	3
24			88.1	4
30			87.2	6
40			87.2	6
45			85.3	10
60			84.4	12
70			83	15
85			81.5	18
130			78.7	24
160			76.8	28
180			75.9	30
200			74.5	33
240			73	36
300			69	45
400			67.4	48
500			66.5	50
600			66.5	50
700			66.5	50
900			65.1	53
1,500			66	51
4,000			66.5	50

APPENDIX 3.2 (cont'd)

Testing Temperature 500^{0}C, Unloading Strain 0.15,
Strain Rate 1.8x10^{-2}s^{-1}

1	2	3	4	5
1	$\overline{43}$	$\overline{96}$	96	0
2			96	0
3			94.4	3
5			93.8	4
7			93.4	5
10			90.7	10
15			88.1	15
20			85.4	20
30			80.1	30
40			74.8	40
42			71.6	46
50			71.6	46
60			68.4	52
70			64.2	60
100			55.2	77
106			51	85
150			48.3	90
260			45.1	96
460			43	100
1,500			43	100
21,000			34.5	116

Testing Temperature 500^{0}C, Unloading Strain 0.18,
Strain Rate 1.8x10^{-2}s^{-1}

1	2	3	4	5
0.7	$\overline{43}$	$\overline{108}$	108	.0
2			104.8	5
3.4			102.8	8
5			99.6	13
6			97.6	16
8			91.1	26
11			82	40

APPENDIX 3.2 (cont'd)

1	2	3	4	5
16	$\overline{43}$	$\overline{108}$	76.8	48
22			76.8	48
28			72.9	54
32			68.4	61
36			62.4	70
40			59.2	75
46			54.7	82
60			49.5	90
120			43	100
500			32	117

Testing Temperature 500°C, Unloading Strain 0.30, Strain Rate $1.8\text{x}10^{-2}\text{s}^{-1}$

1	2	3	4	5
0.55	$\overline{43}$	$\overline{105}$	93.8	18
0.8			89.5	25
1.35			83.3	35
1.5			82.1	37
1.7			80.2	40
2.4			76.5	46
3			74	50
4			71.5	54
4.6			70.3	56
5.1			70.3	56
6.5			67.2	61
7.5			61.6	70
8			60.4	72
10			56.6	78
10.1			56.6	78
10.3			56.6	78
10.5			55.4	80
19			54.1	82
24			50.4	88
31			45.4	96
60			43	100
500			34.8	113

APPENDIX 3.2 (cont'd)

Testing Temperature 500^{0}C, Unloading Strain 0.40,
Strain Rate 1.8x10^{-2}s^{-1}

1	2	3	4	5
1	$\overline{43}$	$\overline{95}$	78.4	32
1.8			72.1	44
2.2			69	50
2.8			68	52
3.6			66	56
4.4			64.8	58
5			63.8	60
6			61.2	65
8			55.5	76
10			53	81
12			52.4	82
17			51.3	84
24			46.6	93
30			44	98
40			43	100

Testing Temperature 500^{0}C, Unloading Strain 0.52,
Strain Rate 1.8x10^{-2}s^{-1}

1	2	3	4	5
0.9	$\overline{43}$	$\overline{95}$	76	37
1.25			73.2	42
2			68	52
2.4			66	56
3.3			63.3	61
4.8			61.2	65
5			58.6	70
6.5			53.4	80
8			51.8	83
10			50.8	85
10.3			49.8	87
10.7			48.7	89
20			45.1	96
24			43	100
100			38.8	108

APPENDIX 3.2 (cont'd)

Testing Temperature 540°C, Unloading Strain 0.05,
Strain Rate $8 \times 10^{-2} s^{-1}$

1	2	3	4	5
12	$\overline{43}$	$\overline{71}$	71	0
20			71	0
32			71	0
130			68.5	9
280			65.4	20
400			62.6	30
550			60.4	38
900			60	40
1,400			59.8	42
2,200			59.8	42
3,000			59.8	42
5,500			59.8	42
10,000			59.8	42
70,000			59.8	42

Testing Temperature 540°C, Unloading Strain 0.10,
Strain Rate $8 \times 10^{-2} s^{-1}$

1	2	3	4	5
1.8	$\overline{43}$	$\overline{90}$	90	0
2.8			90	0
10			88.6	3
20			87.2	6
42			82.5	16
65			78.3	25
90			75.9	30
110			74.0	34
150			72.1	38
220			67.9	47
320			67.4	48
420			66.5	50
700			66.5	50

APPENDIX 3.2 (cont'd)

1	2	3	4	5
900	$\overline{43}$	$\overline{90}$	64.6	54
1.300			61	62
1,600			57.1	70
2,100			51.5	82
3,600			45	96
5,500			43	100
8,000			43	100
11,000			43	100

Testing Temperature 540°C, Unloading Strain 0.15,
Strain Rate $8 \times 10^{-2} s^{-1}$

1	2	3	4	5
0.8	$\overline{43}$	$\overline{96}$	93.8	4
1.3			93	6
1.7			91	10
2.4			88.1	15
3			86.5	18
3.4			84.3	22
4.6			81.2	28
6			78	34
7			75	40
8			72.1	45
9			71.1	47
11			69.5	50
15			69.5	50
18			66.9	55
22			65.3	58
26			63.1	62
30			59.9	68
36			66.3	75
46			52	83
50			49.4	88
55			46.7	93
70			44.5	97
85			43	100
1,600			39.2	126

APPENDIX 3.2 (cont'd)

Testing Temperature 540°C, Unloading Strain 0.40, Strain Rate $8x10^{-2}s^{-1}$

1	2	3	4	5
1	43	95	73.2	42
1.5			70	48
1.8			68	52
2.5			63	62
2.8			60	68
3.2			57	73
3.5			53.4	80
3.5			50.3	86
4.6			50.3	86
5.5			49	88
6.5			50.3	86
7.5			48.2	90
8			46.1	94
9			44.6	97
12			43	100
17			43	100
1,000			32.6	120

0.06%C LOW CARBON STEEL

Testing Temperature 815°C, Unloading Strain 0.25, Strain Rate $8x10^{-2}s^{-1}$

1	2	3	4	5
1	45	85	74.2	27
2.8			68.6	41
5.5			68.6	41
10			68.6	41
15			68.2	42
18			67	45
22			61	60
30			[illegible].2	67
40			54.2	77
55			46.5	96
100			42.8	106

APPENDIX 3.2 (cont'd)

Testing Temperature 930°C, Unloading Strain 0.25, Strain Rate $8\times10^{-2}s^{-1}$

1	2	3	4	5
0.9	$\overline{40}$	$\overline{80}$	54.4	64
1.8			52.4	69
2			50	75
4			50	75
5.5			49.6	76
8			45.6	86
10			37.6	106
22			35.2	112

Testing Temperature 930°C, Unloading Strain 0.25, Strain Rate $8\times10^{-3}s^{-1}$

1	2	3	4	5
4.8	$\overline{33}$	$\overline{62}$	49.5	43
5.5			48.1	48
6.5			44.6	60
14			44.0	62
45			42.6	67
65			39.4	78
100			35.0	93
300			33	100
1,000			33	100

Testing Temperature 1040°C, Unloading Strain 0.25, Strain Rate $8\times10^{-2}s^{-1}$

1	2	3	4	5
1.5	$\overline{32}$	$\overline{57}$	38.2	75
1.8			38.2	75
2			38.2	75
3			38	76
3.8			33	96

APPENDIX 3.2 (cont'd)

1	2	3	4	5
6.5	$\overline{32}$	$\overline{57}$	29	112
20			29	112
30			29	112
40			29	112
60			29	112

Testing Temperature 1040°C, Unloading Strain 0.25,
Strain Rate $8x10^{-3}s^{-1}$

1	2	3	4	5
2	$\overline{25}$	$\overline{42}$	38.8	19
9.5			31.8	60
14			30.4	68
25			30.4	68

0.07%C + Nb STEEL

Testing Temperature 815°C, Unloading Strain 0.30,
Strain Rate $8x10^{-2}s^{-1}$

1	2	3	4	5
10	$\overline{62}$	$\overline{171}$	165.6	5
60			154.6	15
600			136.1	32
1,500			105.6	60
5,400			57.6	104
30,000			40.2	120

Testing Temperature 930°C, Unloading Strain 0.25,
Strain Rate $8x10^{-2}s^{-1}$

1	2	3	4	5
9	$\overline{55}$	$\overline{90}$	83.2	22
25			76.7	46
35			72.3	67
60			72.3	67
100			62.1	90

APPENDIX 3.2 (cont'd)

1	2	3	4	5
140	59	90	57.5	105
200			57.5	105
300			57.5	105
600			57.5	105
1,500			52.8	120

Testing Temperature 930°C, Unloading Strain 0.10,
Strain Rate $8\times10^{-3}s^{-1}$

1	2	3	4	5
30,000	45	70.5	66.7	15

Testing Temperature 930°C, Unloading Strain 0.25,
Strain Rate $8\times10^{-3}s^{-1}$

1	2	3	4	5
25	45	78	75.7	7
40			72.0	18
60			66.1	36
110			64.8	40
200			59.8	55
300			53.6	74
500			53.6	74
800			46.7	95
1,100			43.7	104
1,500			42.1	109

Testing Temperature 1040°C, Unloading Strain 0.10,
Strain Rate $8\times10^{-2}s^{-1}$

1	2	3	4	5
60	44	69	69	0
150			63.3	23
300			55.5	54
400			55.5	54
600			55.5	54
1,200			43	104

APPENDIX 3.2 (cont'd)

Testing Temperature 1040°C, Unloading Strain 0.25, Strain Rate $8 \times 10^{-2} s^{-1}$

1	2	3	4	5
1	$\overline{44}$	$\overline{84}$	82.4	4
4			72	30
5.4			58.4	64
10			48.8	88
15			48.8	88
26			44	100
40			44	100
60			42	105
200			40	110
800			40	110
1,200			40	110

Testing Temperature 1040°C, Unloading Strain 0.10, Strain Rate $8 \times 10^{-3} s^{-1}$

1	2	3	4	5
1,000	$\overline{32}$	$\overline{49}$	48.5	3
2,000			40	55
3,500			40	55
12,000			33	94
15,000			31	101
35,000			30.9	106
56,000			30.9	106

Testing Temperature 1040°C, Unloading Strain 0.25, Strain Rate $8 \times 10^{-3} s^{-1}$

1	2	3	4	5
2.5	$\overline{32}$	$\overline{56.3}$	55.6	3
5.6			51.4	20
14			44.2	50
24			36.2	87
36			36.2	87

APPENDIX 3.2 (cont'd)

1	2	3	4	5
50	32	56.3	32.2	99
60			31.5	102
105			31.5	102
350			30.3	107
1,200			30.3	107

APPENDIX 3.3

Specimen Preparation for Optical Metallography

APPENDIX 3.3

Specimen Preparation for Optical Metallography

The compression cylinders were sectioned and mounted in Scandiplast.[†] Mechanical polishing was performed on a series of emery papers, with water as lubricant, starting with 220-grit, and followed by 320, 400 and 600 grit papers. The polished slices were carefully washed in acetone, rinsed in methanol and dried. They were then electropolished in a solution containing:

133 ml. glacial acetic acid
25 gm chromium trioxide
7 ml H_2O

at 8.5V and 18°C in three-minute intervals. An alcoholic rinse was used between polishing intervals. The specimens subjected to grain size measurement were etched in a potassium dichromate solution for 20s. The solution contained

800 ml H_2O
65 ml H_2SO_4 (conc)
16 gm potassium dichromate
3 gm sodium chloride

and was used only once and discarded. It should be mentioned that a chemical polish containing 20 ml nitric acid, 55 ml orthophosphoric acid and 25 ml glacial acetic acid was also tried as a grain boundary etchant, but was not found to give satisfactory results.

Dislocation etch pits were produced with the aid of a solution containing 1 ml bromine, 15 ml glacial acetic acid, 25 ml HCl, 90 ml water, and 130 ml methanol(155). The etching time was kept constant. Individual pits were resolved readily with a Reichert optical microscope at ~2000 magnification, using an oil-immersion 140x objective lens.

[†] Olsen Scientific Instruments Inc., Long Island City, New York.

APPENDIX 3.4

Quantitative Evaluation of the Volume Fraction Recrystallized

APPENDIX 3.4

Quantitative Evaluation of the Volume Fraction Recrystallized

Four sets of grain intercept measurements were used to determine the progress of static recrystallization in tough pitch copper. The four sets of data were obtained on samples prestrained 0.05, 0.10, 0.15 and 0.40 at a strain rate of $1.8\times10^{-2}s^{-1}$. As described in the text, individual grain intercept measurements were made on samples held for various delay times following deformation prior to quenching. The individual intercept lengths were equally divided into 25 discrete size groups in the size range 0 to 0.2 mm, and in the range 0.2 to 2.0 mm. The relative frequency of intercepts within each size class is given by

$$f_i = \frac{n_i}{N}$$

where n_i is the number of intercepts within the ith group and N is the total number of intercepts. When N is large, the total length of line L^T measured is then given by

$$L^T = N\sum_{i=1}^{N} f_i\bar{d}_i$$

where $\bar{d}_i$ is the mean length of the intercepts within the ith class.

In the three sets of samples which had not undergone dynamic recrystallization during prestraining it was assumed that intercept lengths which fell in size classes greater than 0.2 mm were obtained from the population of unrecrystallized grains. If the size groups are indexed from the smallest to the largest, then the total length of line intersecting the recrystallized material is

$$L^R = N\sum_{i=1}^{25} f_i.\bar{d}_i \; .$$

similarly the unrecrystallized length L^U is given by

$$L^U = N\sum_{i=26}^{N} f_i.\bar{d}_i$$

The linear fraction recrystallized L_L^R is then

$$L_L^R = \frac{L^R}{L^T} = \frac{\sum_{i=1}^{25} f_i . \bar{d}_i}{\sum_{i=1}^{N} f_i . \bar{d}_i}$$

The discontinuous distribution curves in Figure 3.11 (a to d) show that, for samples strained beyond the peak, the grain size at the beginning of the delay is smaller than the original one. This arises because the material had undergone at least one cycle of dynamic recrystallization prior to interruption. In view of this, intercept lengths greater than 0.174 were considered to fall within the population of grains which were unrecrystallized *statically*. In this case L^R was defined as

$$L^R = \sum_{i=1}^{18} f_i . \bar{d}_i / \sum_{i=1}^{N} f_i \bar{d}_i$$

The values of L^R and L^U as well as L_L^R are given in the following tables for samples that were prestrained 0.15 and 0.40 at 500°C and $1.8 \times 10^{-2} s^{-1}$. Values are not given for the samples prestrained 0.05 and 0.10 under the same deformation condition as no static recrystallization took place (see Figure 3.11a and 3.11b).

APPENDIX 3.4

Quantitative Evaluation of the Recrystallization Parameters

TOUGH PITCH COPPER

$T = 500^{0}C$, $\dot{\varepsilon} = 1.8\times10^{-2}s^{-1}$, unloading strain 0.15

Sample No. 1	Time (s) 2	$\sum_{i=26}^{N} f_i \bar{d}_i$ 3	$\sum_{i=1}^{25} f_i \cdot \bar{d}_i$ 4	L_L^R (%) 5
Cu 555	1	0.945	0.0036	0.4
Cu 556	30	0.411	0.0135	3.2
Cu 566	60	0.204	0.0267	11.5
Cu 565	120	0.134	0.0460	26
Cu 567	180	0.083	0.0759	48
Cu 557	480	0	0.0748	100
Cu 976	12,000	0	0.0749	100

$T = 500^{0}C$, $\dot{\varepsilon} = 1.8\times10^{-2}s^{-1}$, unloading strain 0.40

1	2	3	4	5
Cu 558	1	0.055	0.018	24
Cu 564	3.8	0.055	0.032	36
Cu 563	4.8	0.051	0.039	44
Cu 560	6	0.036	0.036	50
Cu 561	13	0.036	0.039	53
Cu 562	20	0.018	0.045	71
Cu 966	40	0	0.052	100

APPENDIX 3.5

Cu-O Equilibrium Diagram

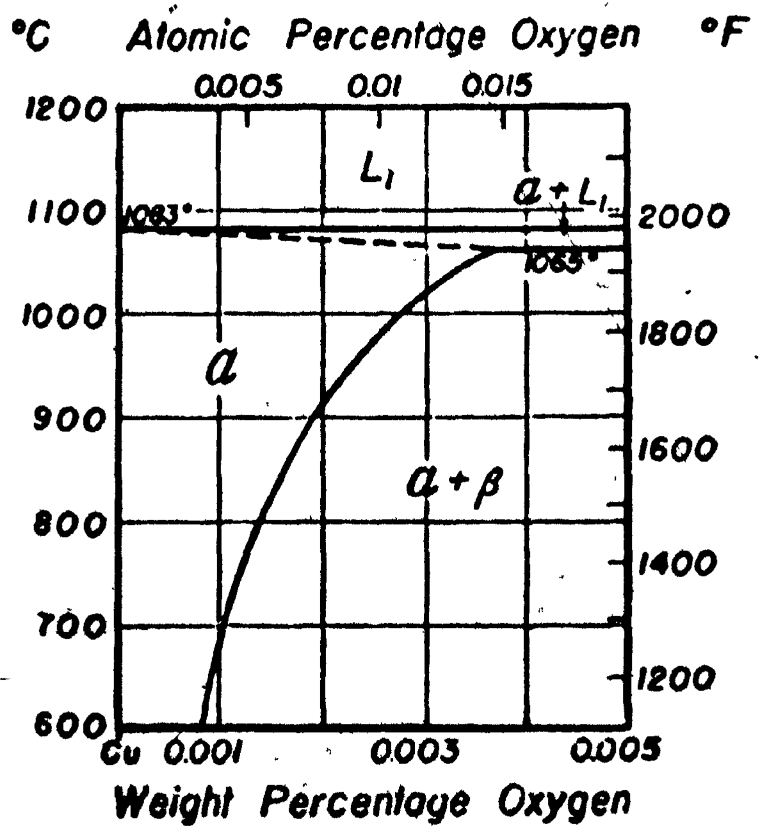
°C
Atomic Percentage Oxygen
°F
0.005
0.01
0.015
1200
1100
1000
900
800
700
600
L1
1083°
a + L1
2000
1065°
1800
a
1600
a + β
1400
1200
Cu
0.001
0.003
0.005
Weight Percentage Oxygen

APPENDIX 3.6

Flow Curves for Tough Pitch Copper used to Determine the Dependence of the High Temperature Yield Stress on the Grain Size

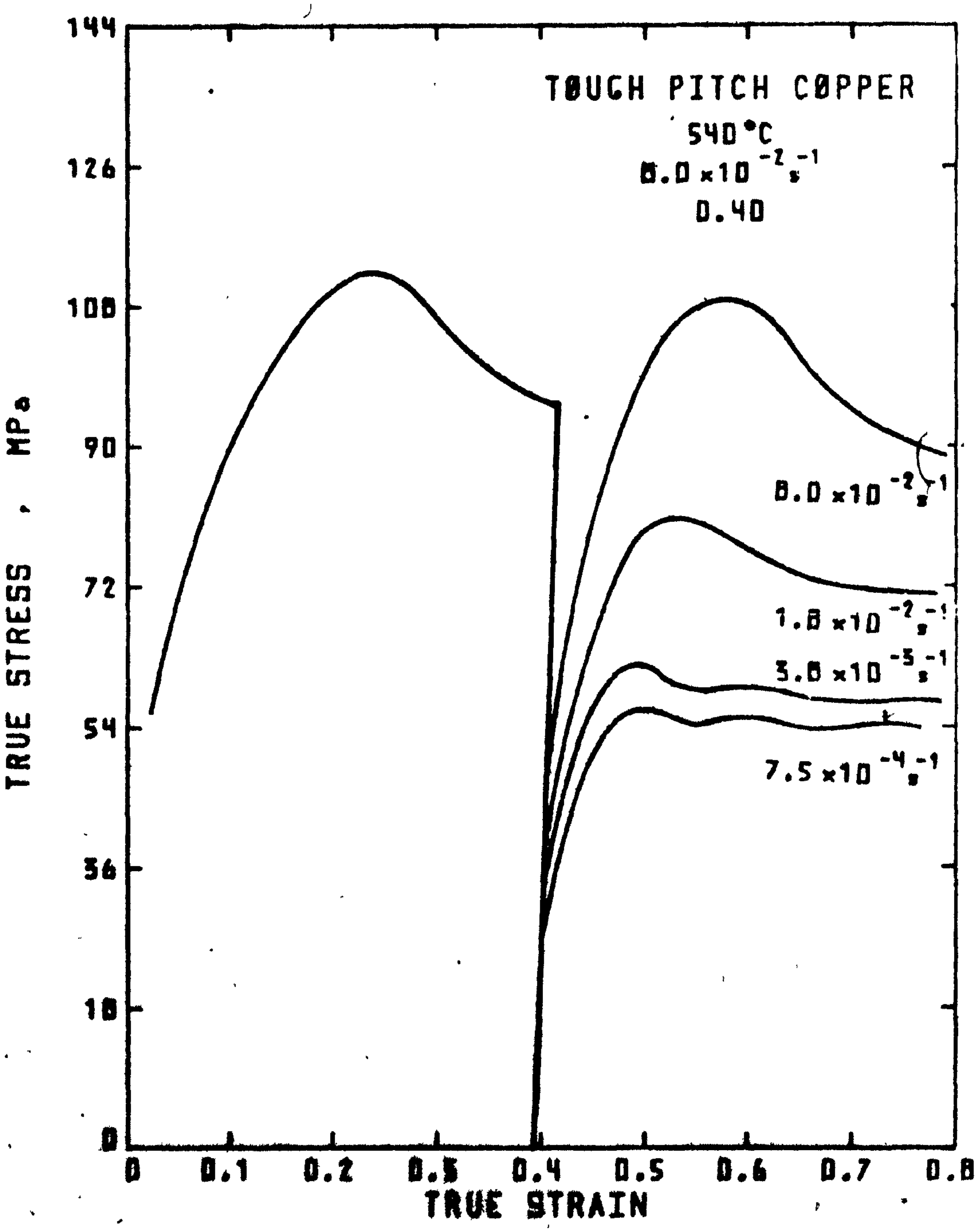
TOUGH PITCH COPPER
540°C
8.0×10^{-2} s^{-1}
0.40
TRUE STRESS , MPa
TRUE STRAIN
144
126
108
90
72
54
36
18
0
0
0.1
0.2
0.3
0.4
0.5
0.6
0.7
0.8
8.0 ×10^{-2} s^{-1}
1.8 ×10^{-2} s^{-1}
3.8 ×10^{-3} s^{-1}
7.5 ×10^{-4} s^{-1}

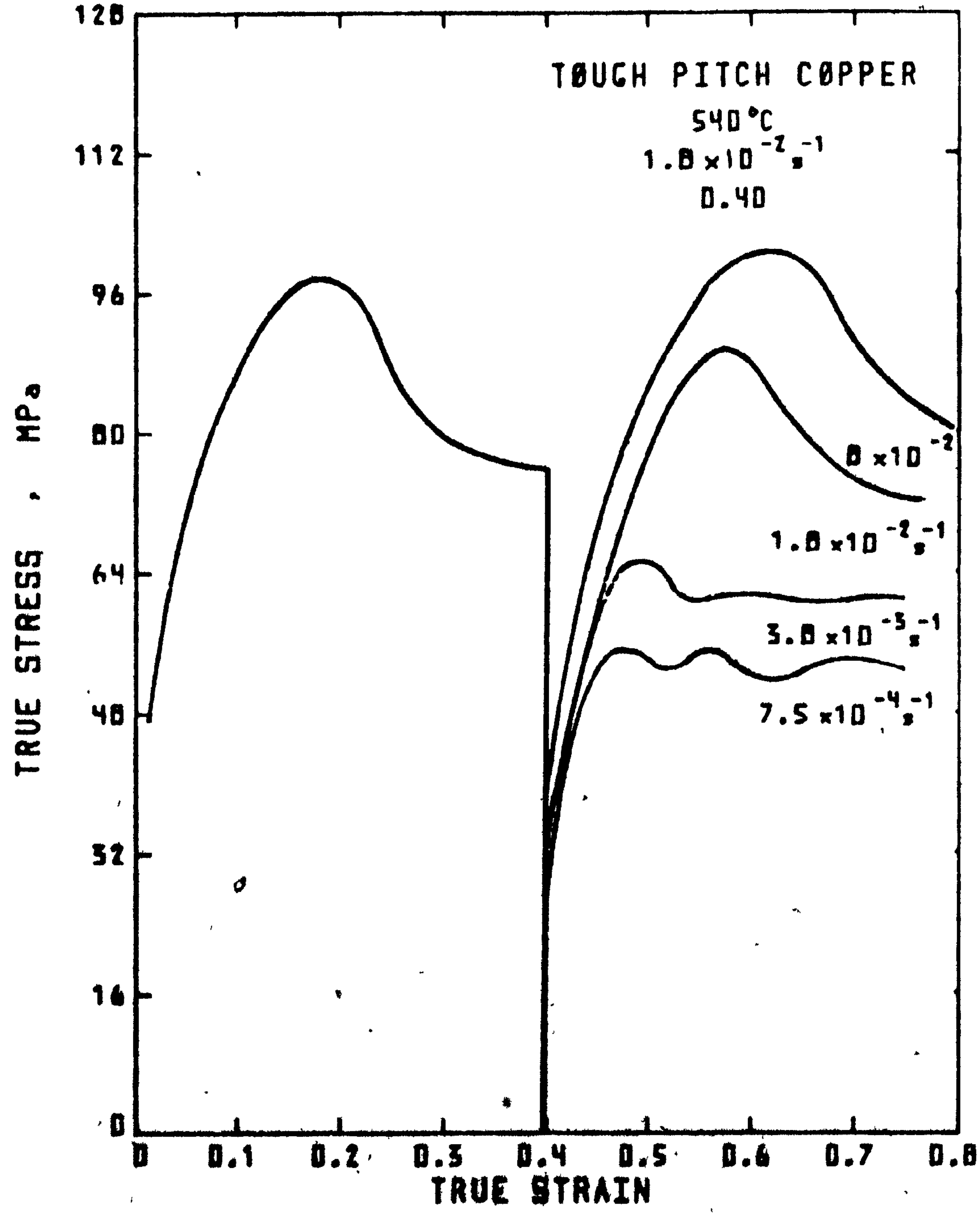
TØUGH PITCH CØPPER
540 °C
1.8 x 10^-2 s^-1
0.40
8 x 10^-2
1.8 x 10^-2 s^-1
3.8 x 10^-3 s^-1
7.5 x 10^-4 s^-1
TRUE STRESS , MPa
128
112
96
80
64
48
32
16
0
TRUE STRAIN
0
0.1
0.2
0.3
0.4
0.5
0.6
0.7
0.8

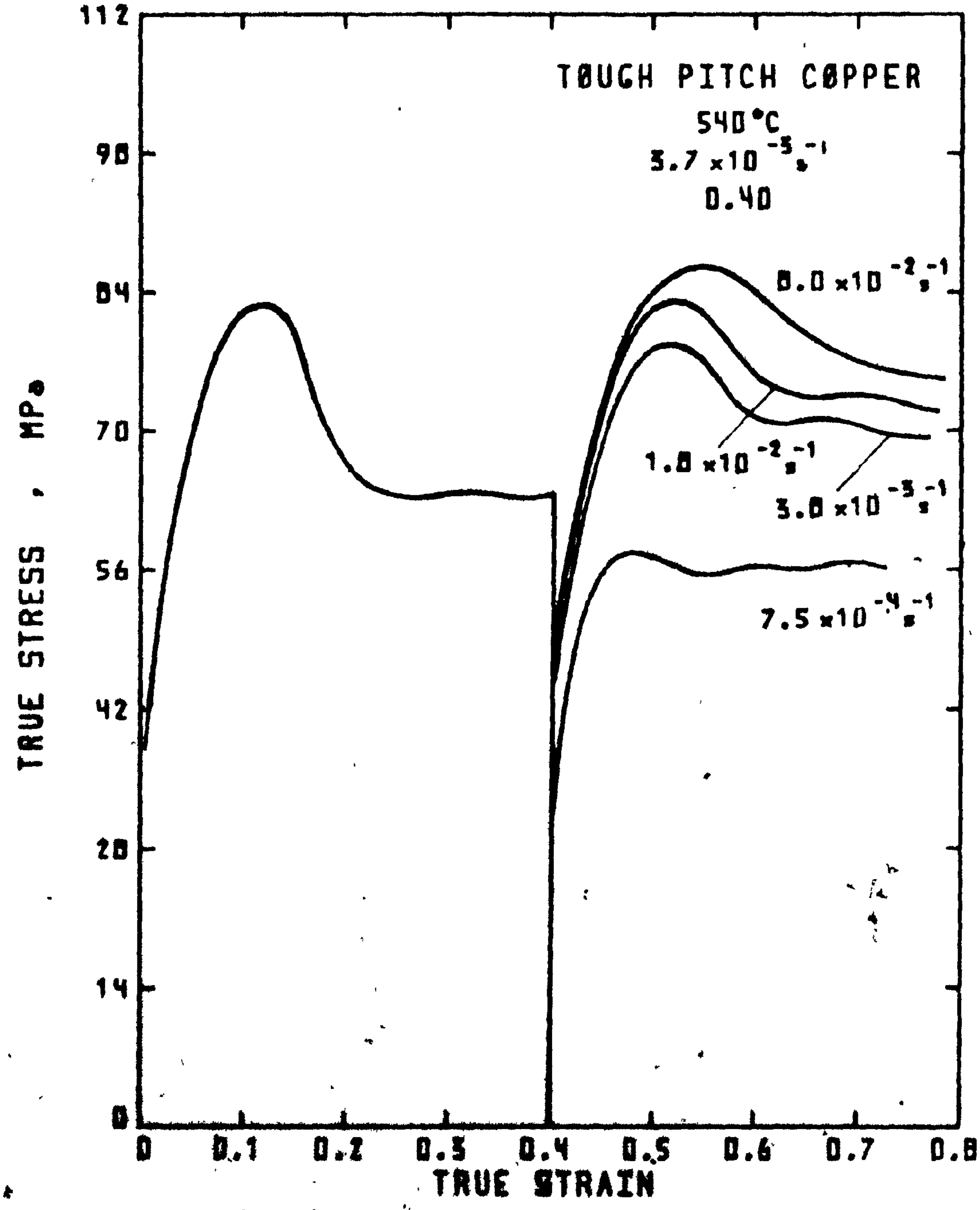
TOUGH PITCH COPPER
540°C
3.7×10⁻³ s⁻¹
0.40
8.0×10⁻² s⁻¹
1.8×10⁻² s⁻¹
3.8×10⁻³ s⁻¹
7.5×10⁻⁴ s⁻¹
TRUE STRESS , MPa
112
98
84
70
56
42
28
14
0
0
0.1
0.2
0.3
0.4
0.5
0.6
0.7
0.8
TRUE STRAIN

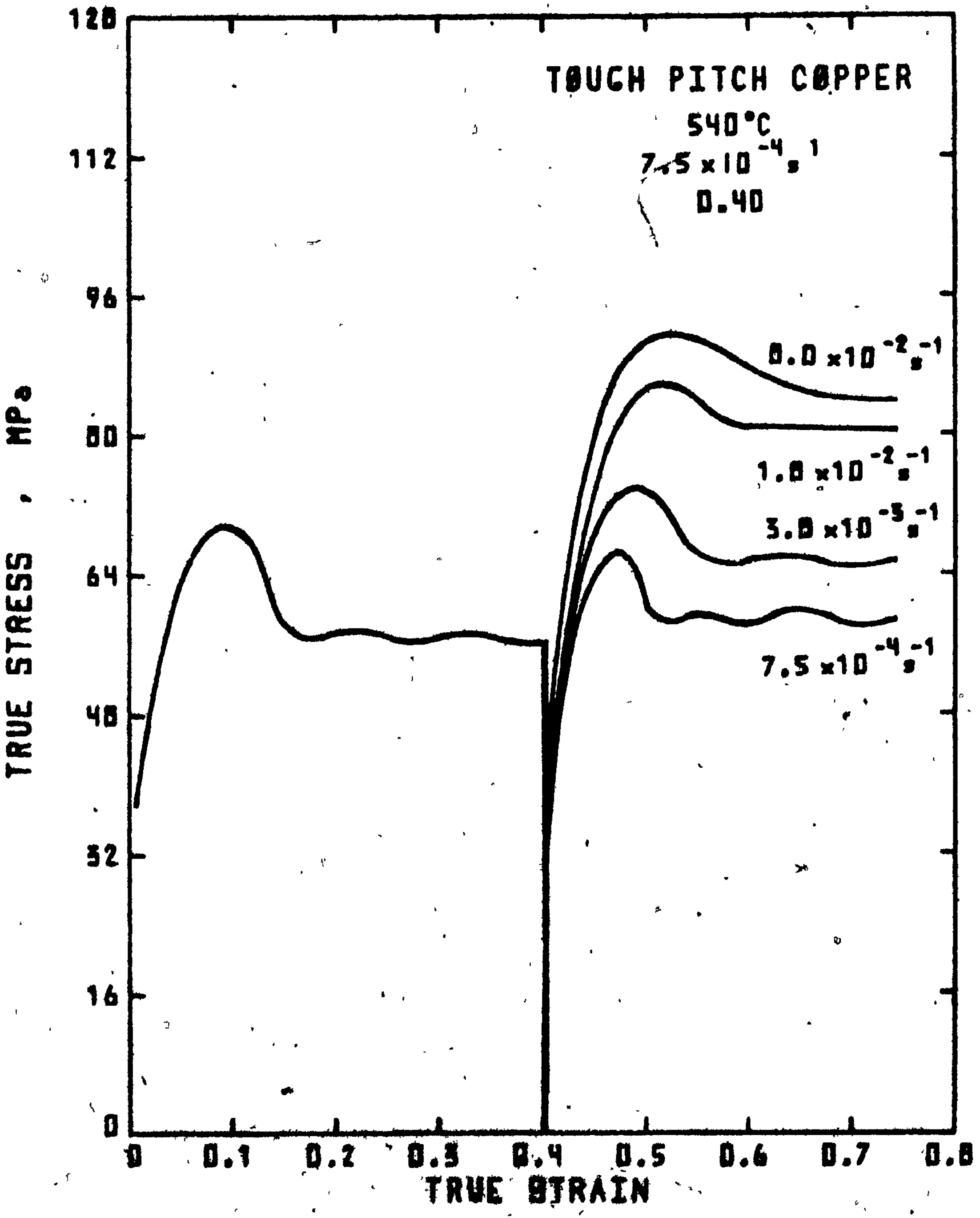
TOUCH PITCH COPPER
540°C
7.5 x 10-4 s 1
0.40
8.0 x10-2 s-1
1.8 x10-2 s-1
3.8 x10-3 s-1
7.5 x10-4 s-1
TRUE STRESS , MPa
TRUE STRAIN
128
112
96
80
64
48
32
16
0
0
0.1
0.2
0.3
0.4
0.5
0.6
0.7
0.8

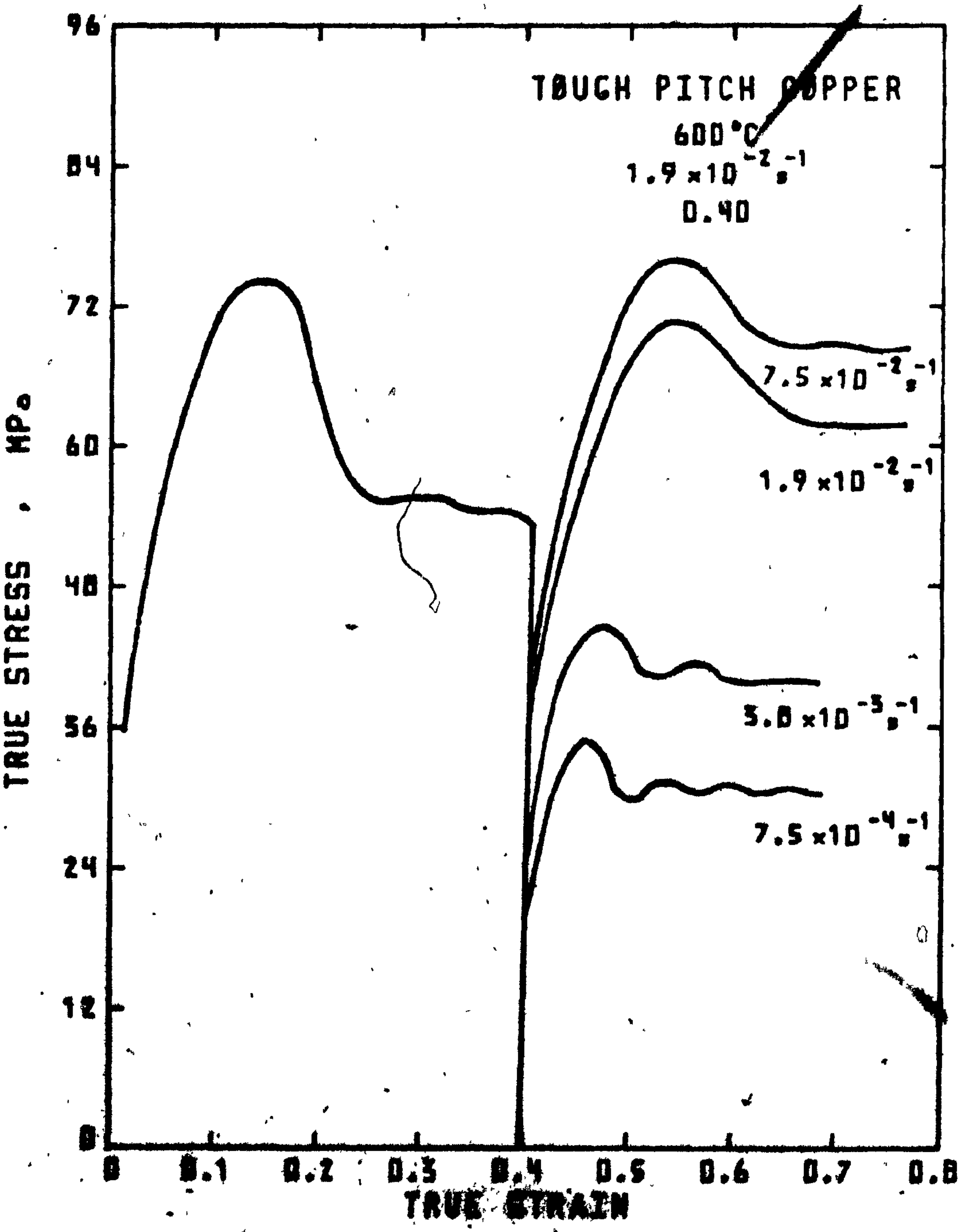
TOUGH PITCH COPPER
600 °C
1.9 × 10^{-2} s^{-1}
0.40
7.5 × 10^{-2} s^{-1}
1.9 × 10^{-2} s^{-1}
3.8 × 10^{-3} s^{-1}
7.5 × 10^{-4} s^{-1}
TRUE STRESS , MPa
96
84
72
60
48
36
24
12
0
0
0.1
0.2
0.3
0.4
0.5
0.6
0.7
0.8
TRUE STRAIN

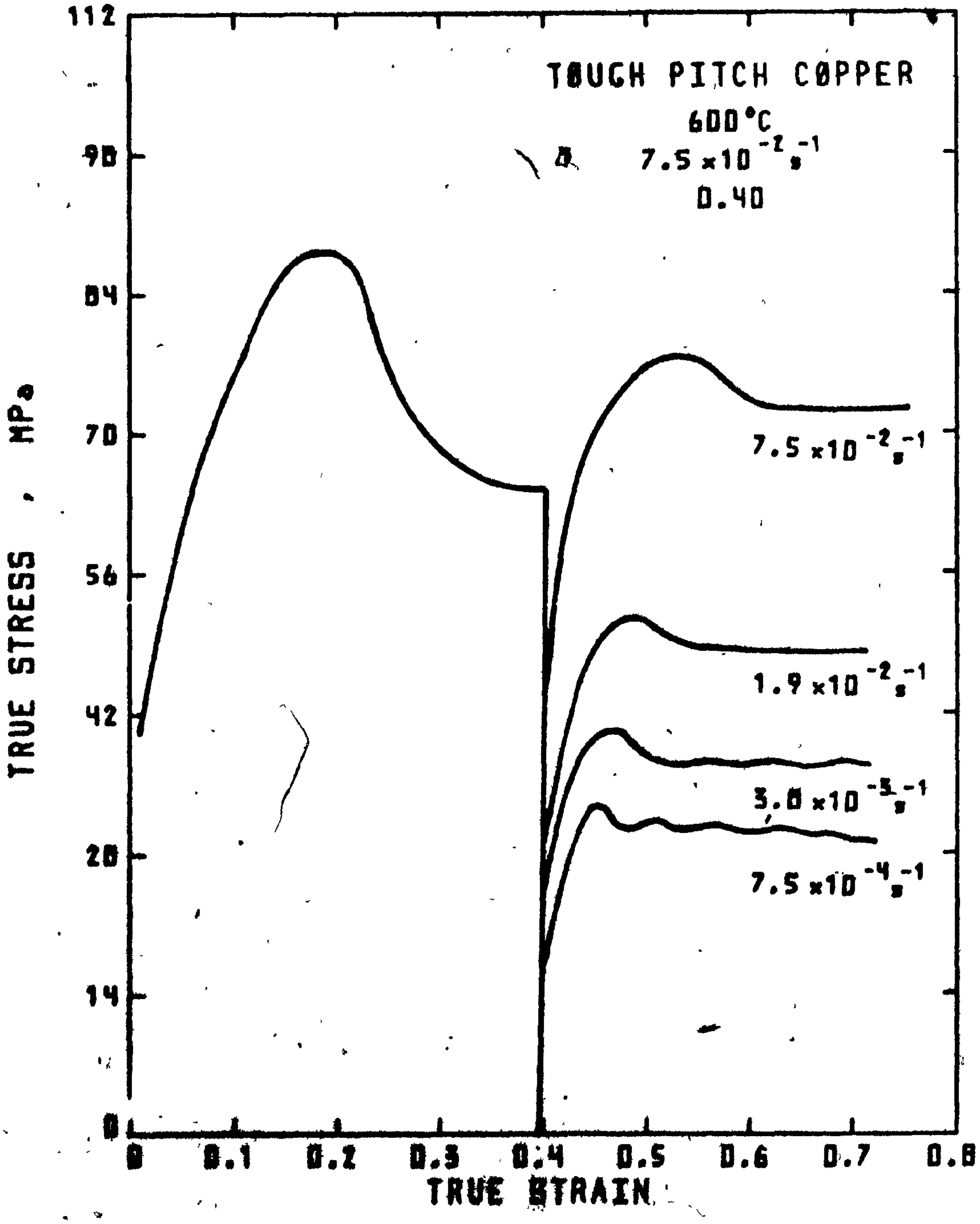
TOUGH PITCH COPPER
600°C
7.5 x10^-2 s^-1
0.40
7.5 x10^-2 s^-1
1.9 x10^-2 s^-1
3.8 x10^-3 s^-1
7.5 x10^-4 s^-1
TRUE STRESS , MPa
TRUE STRAIN
0
14
28
42
56
70
84
98
112
0
0.1
0.2
0.3
0.4
0.5
0.6
0.7
0.8

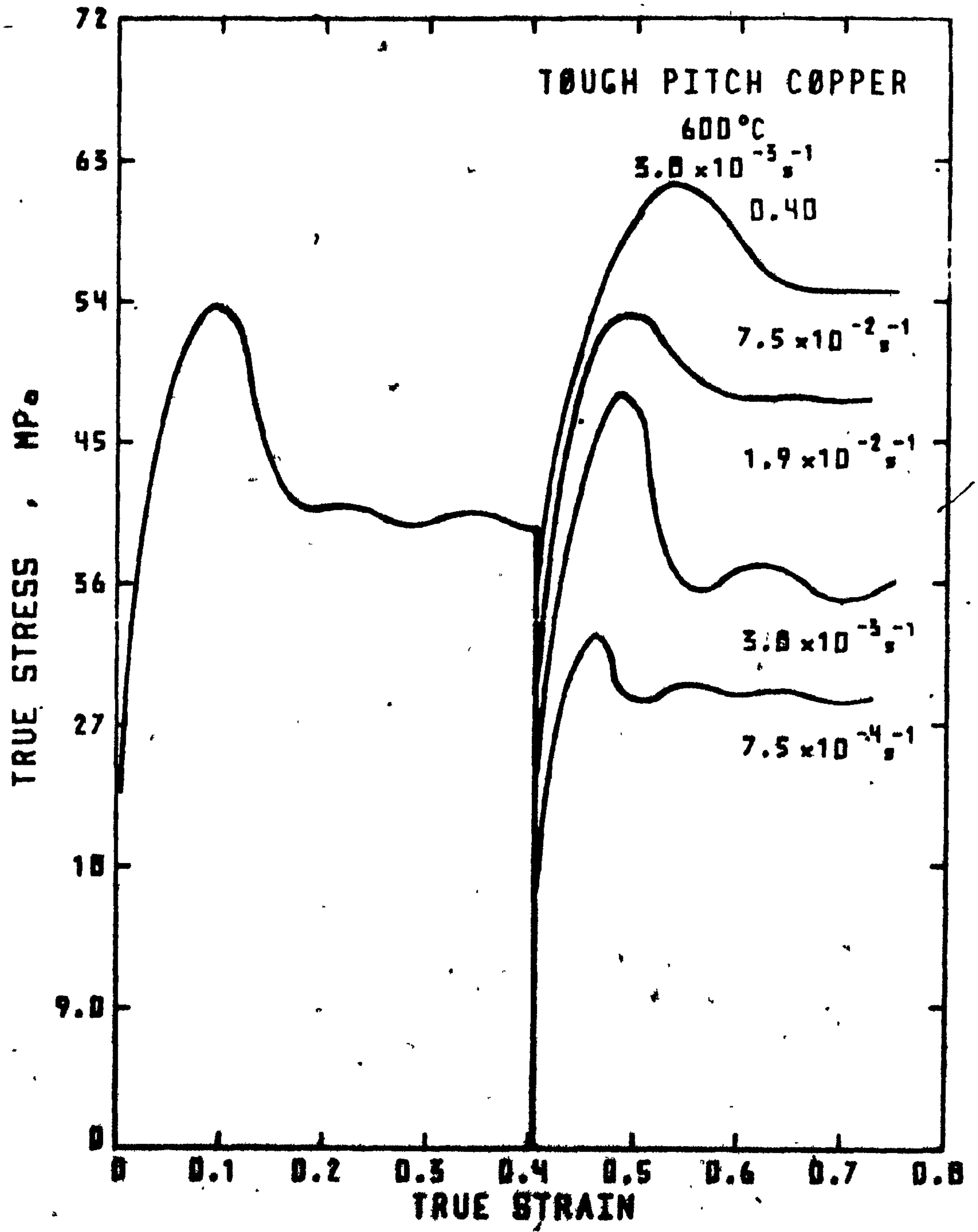
TOUGH PITCH COPPER
600°C
3.8 x10^-3 s^-1
0.40
7.5 x10^-2 s^-1
1.9 x10^-2 s^-1
3.8 x10^-3 s^-1
7.5 x10^-4 s^-1
TRUE STRESS , MPa
72
63
54
45
36
27
18
9.0
0
TRUE STRAIN
0
0.1
0.2
0.3
0.4
0.5
0.6
0.7
0.8

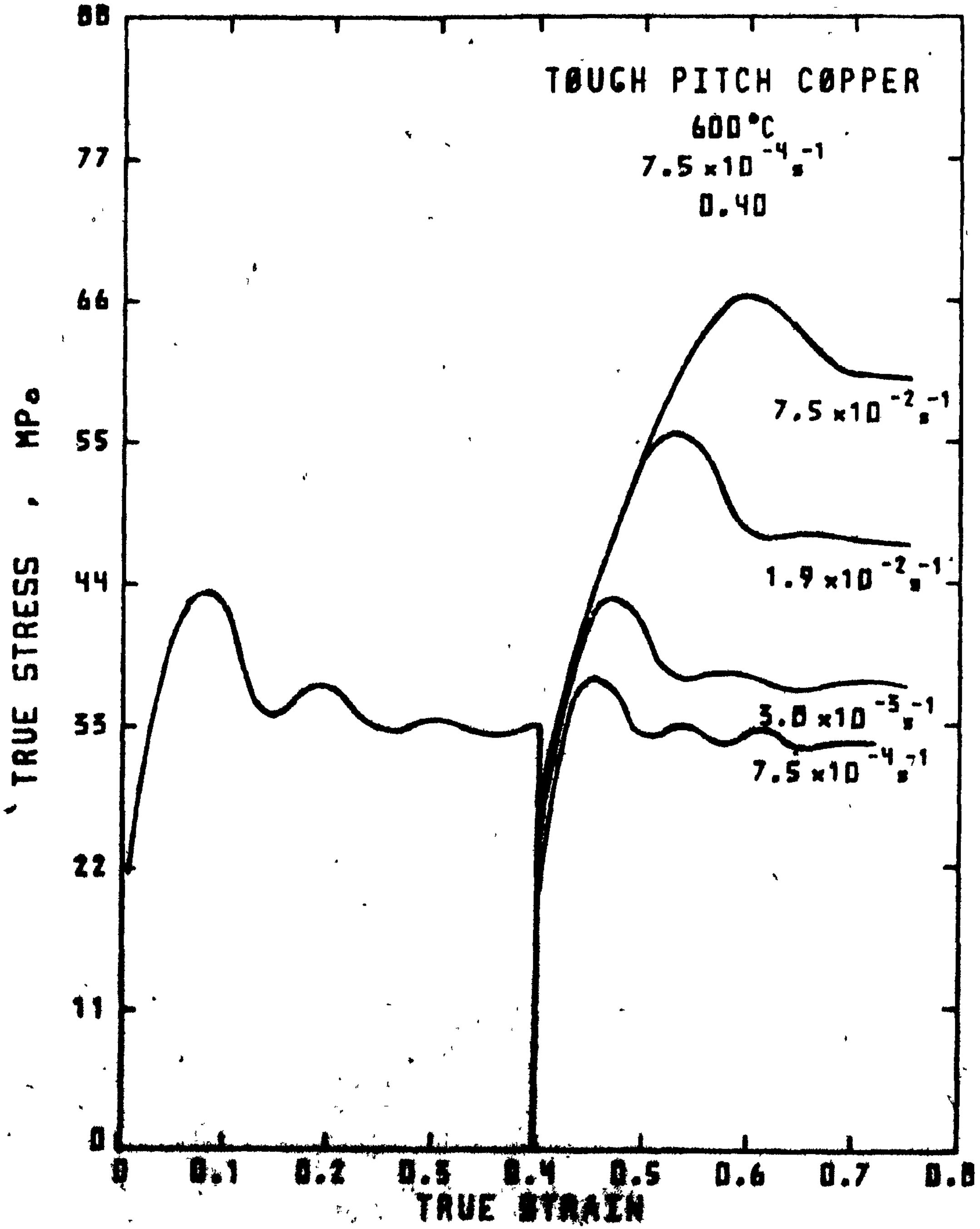
TØUGH PITCH CØPPER
600°C
7.5×10⁻⁴s⁻¹
0.40
7.5×10⁻²s⁻¹
1.9×10⁻²s⁻¹
3.0×10⁻³s⁻¹
7.5×10⁻⁴s⁻¹
TRUE STRESS , MPa
TRUE STRAIN
0
11
22
33
44
55
66
77
88
0
0.1
0.2
0.3
0.4
0.5
0.6
0.7
0.8

APPENDIX 4.1

Iterations used to Determine Saturation Levels for the Three Softening Mechanisms

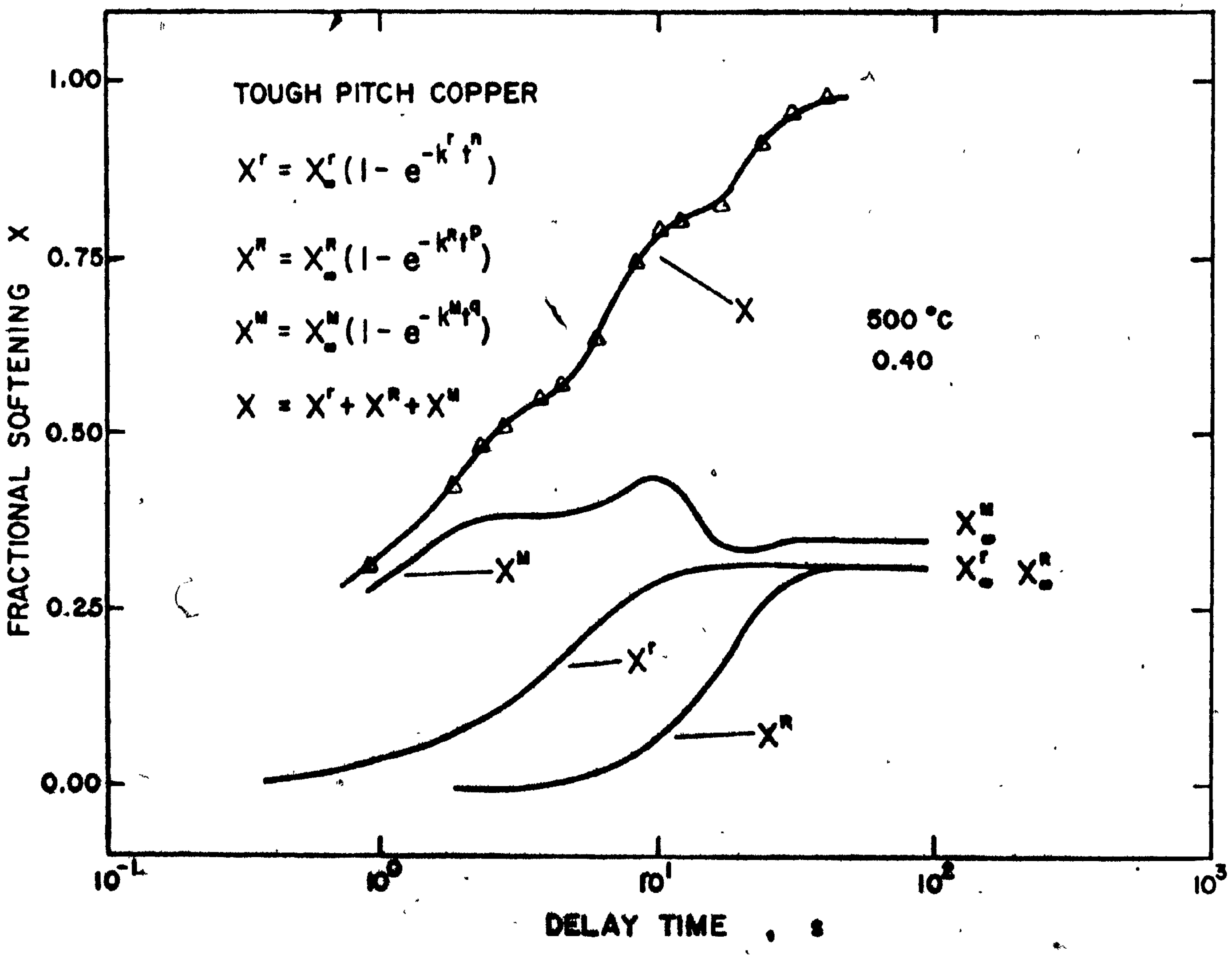

1. X^r_∞ - 0.32
X^R_∞ - 0.32
X^M_∞ - 0.36

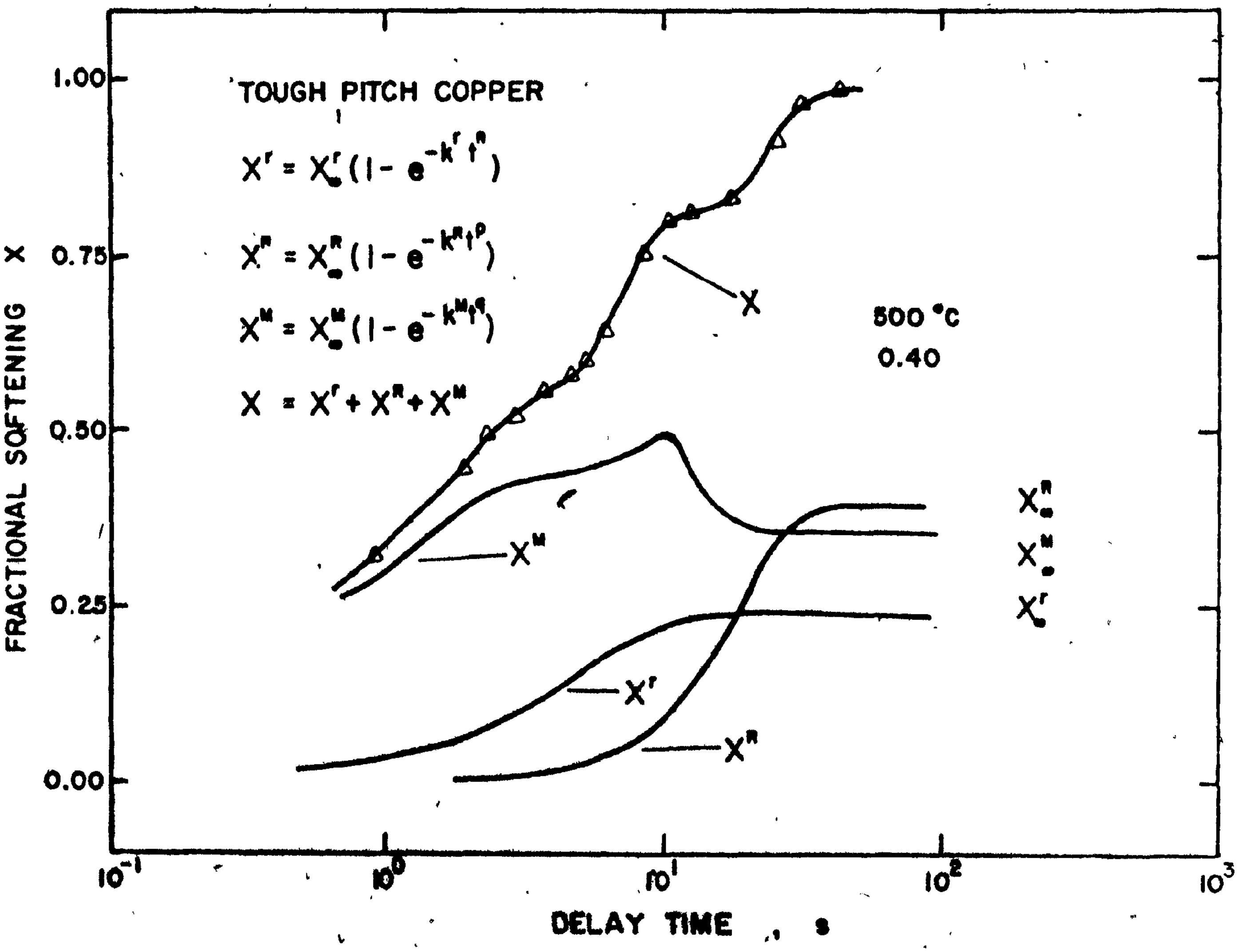

2. X_∞^r — 0.24

X_∞^R — 0.40

X_∞^M — 0.36

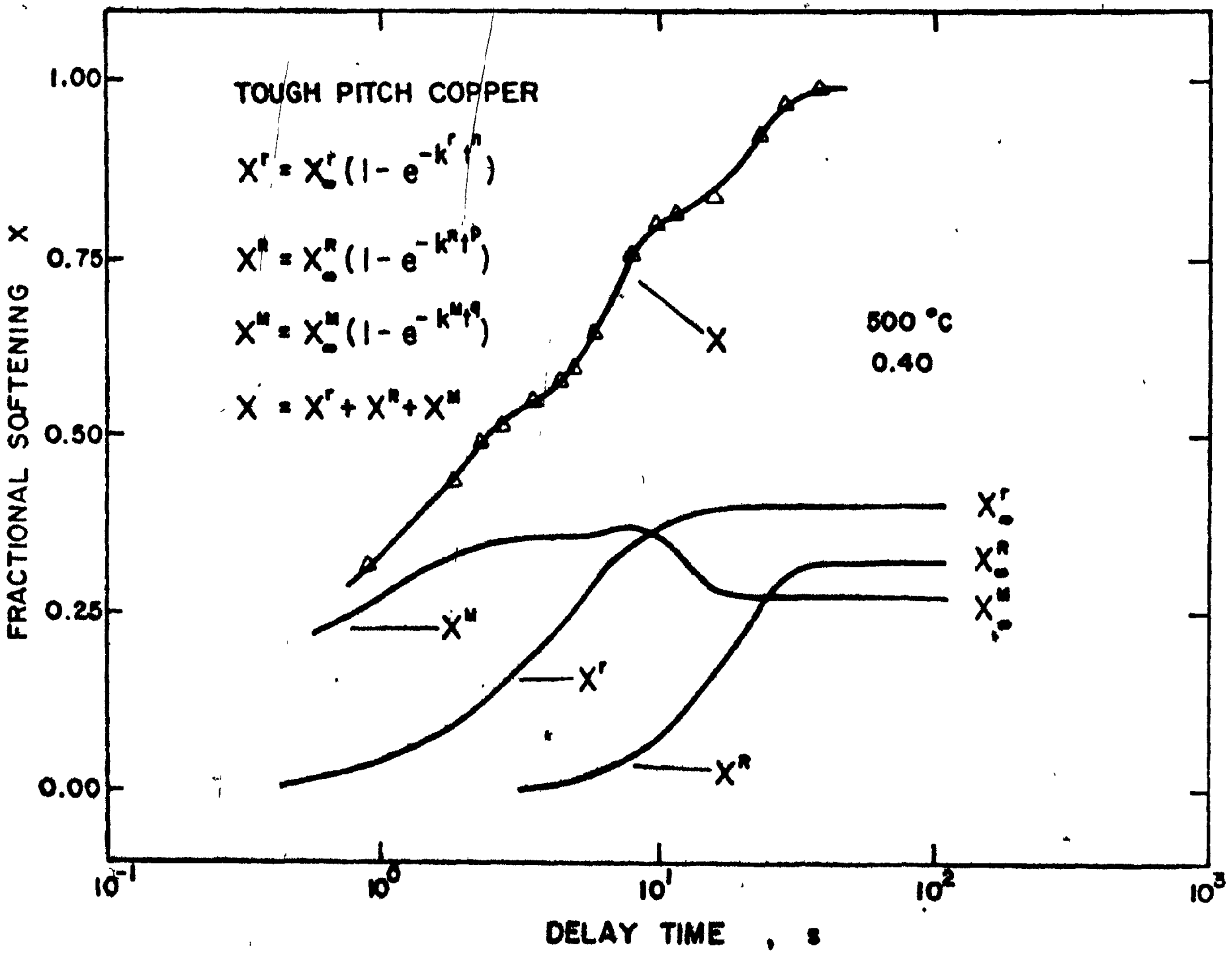

3. X^r_∞ — 0.40
X^R_∞ — 0.32
X^M_∞ — 0.28

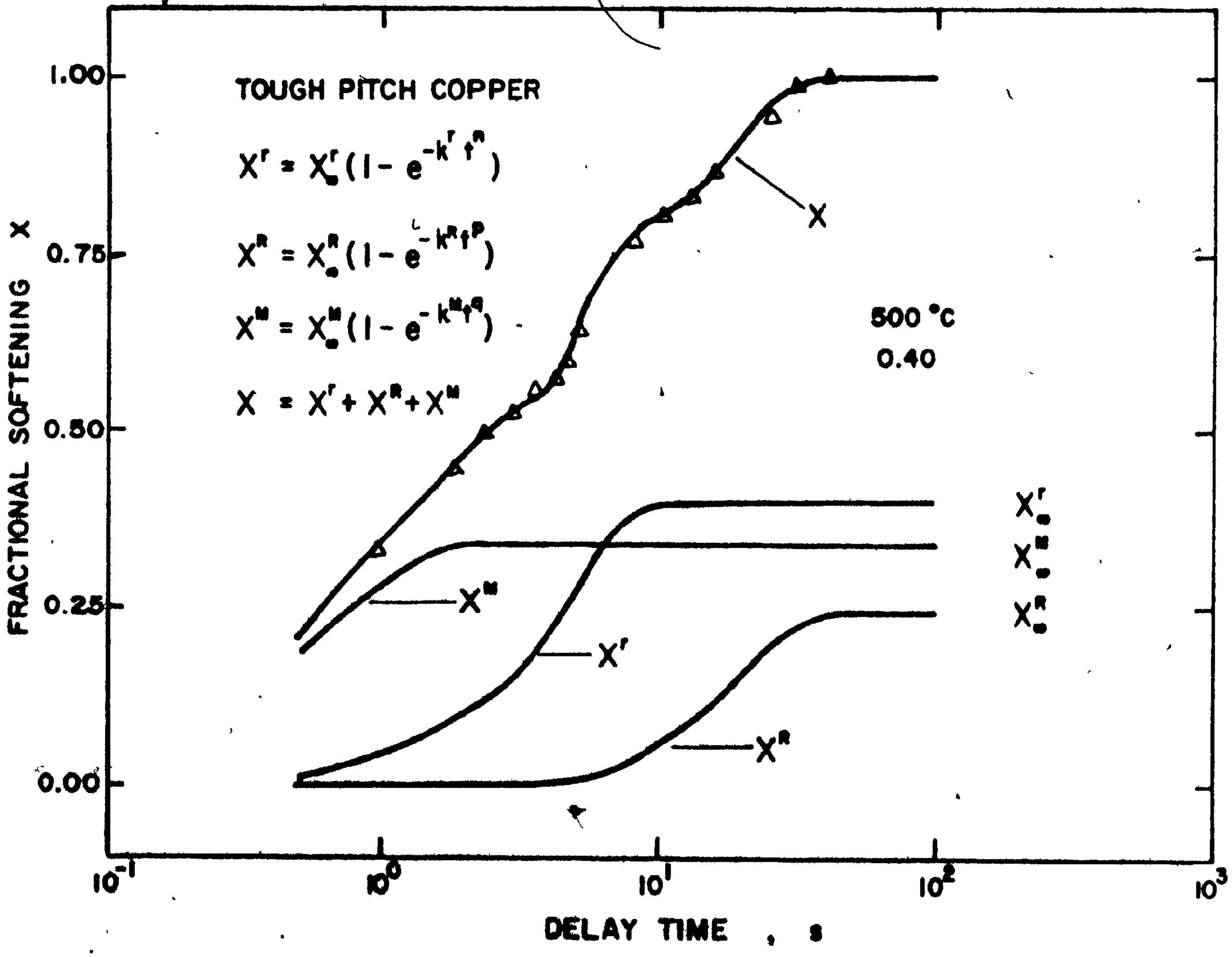

4. $X_\infty^r = 0.40$
$X_\infty^R = 0.24$
$X_\infty^M = 0.36$